

**INTENSIFICATION OF DUAL-PHASE OPERATIONS
USING LOW-FREQUENCY HIGH-POWER ULTRASOUND
IRRADIATION**

SEYED ALI ASGHARZADEHAHMADI

**FACULTY OF ENGINEERING
UNIVERSITY OF MALAYA
KUALA LUMPUR**

2017

**INTENSIFICATION OF DUAL-PHASE OPERATIONS
USING LOW-FREQUENCY HIGH-POWER
ULTRASOUND IRRADIATION**

SEYED ALI ASGHARZADEHAHMADI

**THESIS SUBMITTED IN FULFILLMENT OF THE
REQUIREMENTS FOR THE DEGREE OF DOCTOR OF
PHILOSOPHY**

**FACULTY OF ENGINEERING
UNIVERSITY OF MALAYA
KUALA LUMPUR**

2017

UNIVERSITY OF MALAYA
ORIGINAL LITERARY WORK DECLARATION

Name of Candidate: Seyed Ali Asgharzadehahmadi (Passport No: [REDACTED])

Registration/Matric No: KHA120088

Name of Degree: Doctor of Philosophy

Title of Thesis: Intensification of dual-phase operations using low-frequency high-power ultrasound irradiation

Field of Study: Health, Safety & Environment

I do solemnly and sincerely declare that:

- (1) I am the sole author/writer of this Work;
- (2) This Work is original;
- (3) Any use of any work in which copyright exists was done by way of fair dealing and for permitted purposes and any excerpt or extract from, or reference to or reproduction of any copyright work has been disclosed expressly and sufficiently and the title of the Work and its authorship have been acknowledged in this Work;
- (4) I do not have any actual knowledge nor do I ought reasonably to know that the making of this work constitutes an infringement of any copyright work;
- (5) I hereby assign all and every rights in the copyright to this Work to the University of Malaya ("UM"), who henceforth shall be owner of the copyright in this Work and that any reproduction or use in any form or by any means whatsoever is prohibited without the written consent of UM having been first had and obtained;
- (6) I am fully aware that if in the course of making this Work I have infringed any copyright whether intentionally or otherwise, I may be subject to legal action or any other action as may be determined by UM.

Candidate's Signature

Date:

Subscribed and solemnly declared before,

Witness's Signature

Date:

Name:

Designation:

ABSTRACT

Sonochemical reactors operate based on the release of high amount of energy from ultrasonic irradiations. Many applications in chemical processes are being developed using these reactors. However, the potential of their applications are still limited largely due to the lack of understanding about their design, operational and performance characteristics. More information about the effects of ultrasound irradiation on systems with different phases is also required in order to apply sonochemical reactors as a practical alternative for conventional stirred vessels. Accordingly, the aim in the present research is to study the effects of ultrasound irradiation on different dual-phase operations and intensify them using sonochemical reactors.

The effect of ultrasonication on a gas-liquid system was investigated first by determining the gas-liquid mass transfer of oxygen dissolution in water. The influence of ultrasound power, liquid rheological properties, gas flow rate, size of tank and position of ultrasonic horn on gas-liquid mass transfer in a sonochemical reactor was studied in separate sets of experiments. Computational analysis using 3D CFD simulation was carried out in order to compare the performance of sonoreactor with conventional stirred vessel and also to visualize the behaviour of ultrasound waves within the system, fluid flow pattern and velocity, turbulence and acoustic pressure layers within the liquid. The performance of sonochemical reactors in terms of reaction yield was then investigated in a liquid-liquid system for transesterification of *Jatropha curcas* oil to biodiesel. The effects of ultrasound power, catalyst concentration, methanol to oil molar ratio, reaction temperature and reaction time on biodiesel yield and conversion rate were analyzed. Subsequently, the effects of ultrasound irradiation in a solid-liquid operation were also studied by determining the biodiesel yield and conversion rate of *in situ* transesterification process. Besides, the individual and

interactive effects of other operating parameters on *in situ* transesterification of *J. curcas* seeds were investigated. Moreover, a separate set of experiments was also designed to compare the ultrasound-assisted transesterification and *in situ* transesterification with traditional method under mechanical stirring. Central Composite Design (CCD) was employed to design all of the experiments, develop regression models, optimize and evaluate different operating parameters.

Ultrasound power, size of tank and position of ultrasonic horn were found to significantly affect the gas-liquid mass transfer in the sonochemical reactor. In the CFD simulation part, the results were illustrated as a function of acoustic streaming, fluid flow pattern, gas-liquid volume fraction and turbulence in the gas-liquid system and it was found that additional turbulence created by ultrasound played the most important role on intensifying the mass transfer phenomena compared to that in stirred vessel. In transesterification of *J. curcas* oil for biodiesel production in liquid-liquid system, the maximum biodiesel yield of 94.23 % and conversion rate of 98.54 % were obtained under ultrasound irradiation. In the *in situ* transesterification experiments in solid-liquid system, methanol to seed ratio and ultrasonic power were found to exert more significant effects on the product yield compared to the other operating parameters while catalyst concentration was the most significant parameter on the conversion rate. The highest biodiesel yield of 93.45% and conversion rate of 99.26% were also achieved in solid-liquid system. In conclusion, this study proved that sonochemical reactors could be applied as a suitable alternative for conventional stirred vessels regarding to the significant process intensification obtained under ultrasound irradiations. The obtained results in this research are helpful for understanding the effective role of ultrasound as an energy source on intensifying different dual-phase operations.

ABSTRAK

Reaktor kimia sono beroperasi berdasarkan pembebasan jumlah tenaga yang tinggi daripada penyinaran ultrabunyi. Kebanyakan aplikasi di dalam proses kimia dibangunkan menggunakan reaktor ini. Walaubagaimanapun, potensi aplikasi ini masih lagi terhad disebabkan kekangan pemahaman terhadap rekabentuk, pengoperasian dan ciri-ciri prestasi. Lebih banyak maklumat mengenai kesan penyinaran ultrabunyi ke atas sistem berbeza fasa juga diperlukan bagi menggunakan reaktor kimia sono sebagai alternatif yang praktikal bagi tangki pengadukan konvensional. Maka, matlamat kajian ini adalah untuk mengkaji kesan-kesan penyinaran ultrabunyi ke atas operasi fasa berkembar yang berbeza dan memantapkannya menggunakan reaktor kimia sono.

Kesan penyinaran ultrabunyi ke atas sistem cecair-gas telah diselidik terlebih dahulu dengan menentukan pemindahan jisim cecair-gas bagi pelarutan oksigen di dalam air. Pengaruh kuasa ultrabunyi, kadar alir gas, saiz tangki, dan kedudukan corong ultrabunyi ke atas pemindahan jisim cecair-gas di dalam reaktor kimia sono telah dikaji di dalam set ujikaji yang berasingan dan membandingkannya dengan hasil kajian yang diperolehi daripada kajian pemindahan jisim di dalam tangki pengadukan. Analisis berkomputer menggunakan simulasi CFD 3D telah dijalankan untuk membandingkan pencapaian reaktor sono dengan tangki pengadukan konvensional dan juga untuk menggambarkan kelakuan gelombang ultrabunyi di dalam sistem, corak aliran bendalir dan halaju, aliran bergolak dan lapisan tekanan akustik dalam cecair. Seterusnya, prestasi reaktor kimia sono dari segi hasil tindakbalas telah diselidik di dalam sistem cecair-cecair bagi transesterifikasi minyak *Jatropha Curcas* kepada biodisel. Kesan kuasa ultrabunyi, kepekatan mangkin, nisbah molar metanol kepada minyak, suhu tindakbalas dan masa tindakbalas ke atas hasil biodisel dan kadar penukaran telah dianalisa. Kesan penyinaran ultrabunyi di dalam operasi pepejal-cecair juga telah dikaji bagi menentukan hasil biodisel dan kadar penukaran bagi proses transesterifikasi in situ.

Selain itu, kesan individu dan interaktif bagi parameter operasi ke atas transesterifikasi benih *J. Curcas* telah diselidik. Di samping itu, beberapa set ujikaji yang berasingan juga telah direkabentuk untuk membandingkan transesterifikasi dan transesterifikasi *in situ* ultrabunyi-terbantu dengan menggunakan pengadukan mekanikal. Central Composite Design (CCD) telah digunapakai untuk merekabentuk kesemua ujikaji, membangunkan model kemerosotan, mengoptima dan menilai parameter operasi yang berbeza.

Kuasa ultrabunyi, saiz tangki dan kedudukan corong ultrasonik didapati telah memberikan kesan yang ketara terhadap pemindahan jisim di dalam reaktor sonokimia. Di bahagian simulasi CFD, keputusan telah diilustrasikan sebagai fungsi aliran mantap akustik, corak aliran bendalir, pecahan isipadu cecair-gas dan aliran bergolak di dalam sistem cecair-gas. Di dapati bahawa, penambahan aliran bergolak yang dihasilkan oleh kuasa ultrabunyi memainkan peranan yang paling penting bagi memantapkan fenomena pemindahan jisim berbanding di dalam tangki pengadukkan. Bagi pentransesterifikasi minyak *J. Curcas* untuk penghasilan biodisel di dalam sistem cecair-cecair, hasil biodisel maksimum sebanyak 94.23% dan kadar penukaran sebanyak 98.54% telah diperolehi di bawah penyinaran ultrabunyi. Bagi ujikaji pentransesterifikasi *in situ* di dalam sistem pepejal-cecair, nisbah metanol kepada benih dan kuasa ultrabunyi didapati telah memberikan lebih banyak kesan yang ketara ke atas hasil produk, dibandingkan dengan parameter operasi lain, manakala kepekatan mangkin merupakan parameter yang paling ketara ke atas kadar penukaran. Hasil biodisel yang paling tinggi sebanyak 93.45% dan kadar penukaran sebanyak 99.26% juga telah dicapai di dalam sistem pepejal-cecair. Kesimpulannya, kajian ini membuktikan bahawa reaktor kimia sono boleh digunakan sebagai alternatif bagi tangki pengadukan konvensional berhubung kepada proses pentransesterifikasi yang diperolehi di bawah penyinaran ultrabunyi yang ketara. Hasil kajian ini adalah berguna untuk pemahaman mengenai peranan efektif bagi

ultrabunyi sebagai sumber tenaga ke atas pemantapan operasi fasa berkembar yang berbeza.

University of Malaya

ACKNOWLEDGEMENTS

Praises to Allah for giving me the strength, perseverance and intention to go through and complete my study.

My sincere gratitude goes to the University of Malaya, for granting me the opportunity to pursue my PhD programme, allowing access to laboratories, equipments, library resources and all other supports during the period of study.

I also am grateful to the University of Malaya High Impact Research Grant (HIR) from the Ministry of Higher Education Malaysia which financially supported this work.

I would like to express my sincere gratitude to my respected supervisor Prof. Abdul Aziz Abdul Raman for his help, support, and guidance. I owe him a lot for what he taught me during these years. I am also very thankful to Dr. Rajarathinam Parthasarathy for his guidance, advices and motivation.

Last but not least, I am grateful to my loving parents for their loves and supports.

TABLE OF CONTENTS

| | |
|--|----------|
| Abstract | iii |
| Abstrak | v |
| Acknowledgements | viii |
| Table of Contents | ix |
| List of Figures | xiv |
| List of Tables..... | xix |
| List of Abbreviations..... | xxi |
| CHAPTER 1: INTRODUCTION..... | 1 |
| 1.1 Background..... | 1 |
| 1.2 Problem Statement..... | 3 |
| 1.3 Research Aim and Objectives..... | 4 |
| 1.4 Research Scopes | 5 |
| 1.5 Outline of the Thesis..... | 5 |
| CHAPTER 2: LITERATURE REVIEW..... | 8 |
| 2.1 Sonochemical Reactors..... | 9 |
| 2.1.1 Type of Sonochemical Reactors | 9 |
| 2.2 Design of Sonochemical Reactors | 14 |
| 2.3 Main Operating Parameters in Sonochemical Reactors | 18 |
| 2.3.1 Frequency of Irradiation | 18 |
| 2.3.2 Ultrasonic Intensity | 21 |
| 2.4 Performance of Sonochemical Reactors | 23 |
| 2.4.1 Mass Transfer | 23 |
| 2.4.2 Mixing Time..... | 26 |

| | | |
|------------------------------------|---|-----------|
| 2.4.3 | Flow Pattern | 30 |
| 2.4.4 | Reaction Rate | 34 |
| 2.5 | Comparison between Sonochemical Reactors and Stirred Vessels..... | 34 |
| 2.5.1 | CFD Simulation of Fluid Flow..... | 40 |
| 2.6 | Gas-Liquid Systems..... | 43 |
| 2.7 | Liquid-Liquid Systems | 44 |
| 2.7.1 | Transesterification Reaction..... | 46 |
| 2.7.2 | Biodiesel Quality | 49 |
| 2.8 | Solid-Liquid Systems | 49 |
| 2.8.1 | <i>In Situ</i> Transesterification | 50 |
| 2.8.2 | Parameters in <i>In Situ</i> Transesterification..... | 51 |
| 2.8.3 | <i>Jatropha Curcas</i> | 56 |
| 2.9 | Summary of Literature Review | 61 |
| CHAPTER 3: METHODOLOGY..... | | 63 |
| 3.1 | Gas-Liquid Experiments; Mass Transfer in Air-Water System | 64 |
| 3.1.1 | Experimental Set Up | 65 |
| 3.1.2 | Volumetric Gas-Liquid Mass Transfer Coefficient (k_La) Measurement .. | 67 |
| 3.1.3 | Study of Main Parameters | 68 |
| 3.1.4 | Computational Fluid Dynamic Study..... | 70 |
| 3.1.4.1 | Theoretical Background | 70 |
| 3.1.5 | Geometry and Boundary Conditions..... | 73 |
| 3.1.5.1 | Simplification Assumptions and Justification..... | 75 |
| 3.1.5.2 | Numerical Solution of Equations | 76 |
| 3.2 | Liquid-Liquid Experiments; Transesterification Reaction | 77 |
| 3.2.1 | Materials | 78 |
| 3.2.2 | Experimental Set Up | 78 |

| | | |
|--|--|-----------|
| 3.2.3 | Biodiesel Synthesis..... | 79 |
| 3.2.4 | Operational Conditions in Transesterification Reaction | 80 |
| 3.2.4.1 | Interaction of Operating Parameter | 81 |
| 3.2.4.2 | Effect of Mechanical Mixing | 82 |
| 3.2.5 | Biodiesel Content Analysis | 82 |
| 3.3 | Solid-Liquid Experiments; <i>In Situ</i> Transesterification Reaction..... | 83 |
| 3.3.1 | Characterisation of the Oilseed | 83 |
| 3.3.1.1 | Oil Content Determination | 83 |
| 3.3.1.2 | Moisture Content..... | 85 |
| 3.3.2 | Experimental Set Up | 85 |
| 3.3.3 | Biodiesel Synthesis..... | 87 |
| 3.3.4 | Operational Conditions in <i>In Situ</i> Transesterification | 88 |
| 3.3.4.1 | Individual Effect of Each Parameter | 89 |
| 3.3.4.2 | Interaction of Operating Parameters..... | 90 |
| 3.3.4.3 | Effect of Mechanical Mixing | 90 |
| 3.3.5 | Biodiesel Content Analysis | 91 |
| CHAPTER 4: RESULTS AND DISCUSSION | | 92 |
| 4.1 | Experimental Analysis of Ultrasound effect on Gas-Liquid System..... | 93 |
| 4.1.1 | Effect of Liquid Volume on Mass Transfer under Sonication | 93 |
| 4.1.2 | Mass Transfer Coefficient in 2 L Liquid Volume | 94 |
| 4.1.2.1 | Effects of Ultrasound Power and Gas Flow Rate..... | 94 |
| 4.1.2.2 | Development of Regression Model..... | 94 |
| 4.1.2.3 | Interaction of Operating Parameters..... | 98 |
| 4.1.3 | Mass Transfer Coefficient in 200 mL Liquid Volume..... | 101 |
| 4.1.3.1 | Mass Transfer by Vertical Ultrasonic Probe | 102 |
| 4.1.3.2 | Mass Transfer by Horizontal Ultrasonic Probe..... | 106 |

| | | |
|---------|---|-----|
| 4.1.3.3 | Mass Transfer by Mechanical Stirring | 109 |
| 4.1.4 | Simulation Analysis of Ultrasonicator versus Stirred Vessel | 113 |
| 4.1.4.1 | Fluid Flow Pattern and Liquid Velocity..... | 113 |
| 4.1.4.2 | Turbulent Intensity Dissipation..... | 120 |
| 4.1.4.3 | Gas-liquid interfacial area | 121 |
| 4.1.4.4 | Volumetric Gas-Liquid Mass Transfer | 124 |
| 4.1.5 | Empirical Correlations for Gas-Liquid Mass Transfer..... | 129 |
| 4.2 | Experimental Analysis of Ultrasound Effects on Liquid-Liquid System..... | 136 |
| 4.2.1 | Effect of Operating Parameters on Transesterification Reaction | 136 |
| 4.2.1.1 | Reaction Temperature | 137 |
| 4.2.1.2 | Methanol to Oil Ratio..... | 139 |
| 4.2.1.3 | Catalyst Concentration | 139 |
| 4.2.1.4 | Ultrasound Power | 141 |
| 4.2.1.5 | Reaction Time | 142 |
| 4.2.2 | Transesterification Process Using Mechanical Stirring | 143 |
| 4.2.3 | Development of Regression Model | 148 |
| 4.2.3.1 | Biodiesel Yield..... | 148 |
| 4.2.3.2 | Conversion Rate | 148 |
| 4.3 | Experimental Analysis of Ultrasound Effects on Solid-Liquid System | 149 |
| 4.3.1 | <i>J. curcas</i> Characterisation | 149 |
| 4.3.2 | Effect of Operating Parameters on <i>In Situ</i> Transesterification..... | 150 |
| 4.3.2.1 | Catalyst Concentration | 151 |
| 4.3.2.2 | Reaction Time | 152 |
| 4.3.2.3 | Methanol to Seed Ratio | 153 |
| 4.3.2.4 | Reaction Temperature | 154 |
| 4.3.3 | Interaction of Operating Parameters on <i>In Situ</i> Transesterification | 155 |

| | | |
|---|--|------------|
| 4.3.3.1 | Biodiesel Yield | 155 |
| 4.3.3.2 | Conversion Rate | 160 |
| 4.3.4 | <i>In Situ</i> Transesterification Process Using Mechanical Stirring | 164 |
| 4.3.5 | Development of Regression Model | 166 |
| 4.3.5.1 | Biodiesel Yield | 166 |
| 4.3.5.2 | Conversion Rate | 167 |
| 4.3.6 | Process Optimization | 168 |
| 4.4 | Summary of Results and Discussion | 169 |
| CHAPTER 5: CONCLUSIONS AND FURTHER WORKS | | 171 |
| 5.1 | Conclusions | 171 |
| 5.2 | Further works | 174 |
| References | | 176 |
| Appendix | | 192 |

LIST OF FIGURES

| | |
|--|----|
| Figure 2.1: The general topics presented in chapter II..... | 8 |
| Figure 2.2: Ultrasonic horn reactor, adapted from Csoka et al. (Csoka et al., 2011)..... | 10 |
| Figure 2.3: Locations of boundary conditions (BC). 1 at $z=0.05H$, 2 at $z=0.32H$, 3 at $z = 0.71H$, 4 at $z = 0.94H$. The contours represent the mean velocity magnitude in ms^{-1} . (Kumar et al., 2006) | 11 |
| Figure 2.4: Ultrasonic longitudinal horn reactor (Csoka et al., 2011) | 12 |
| Figure 2.5: Simulation results of liquid velocity distributions in sonochemical reactors with input power of 50 W (Xu et al., 2013) | 13 |
| Figure 2.6: a) Cylindrical dual frequency flow reactor. b) Hexagonal triple frequency flow reactor (Gogate et al., 2003b; Gogate et al., 2004)..... | 16 |
| Figure 2.7: Effect of power dissipation on iodine yield (Henglein and Gutierrez, 1990; Gogate et al., 2011) | 22 |
| Figure 2.8: Comparison of mass-transfer coefficient in different reactors at constant power density of 11.71 kW.m^{-3} (Kumar et al., 2004; Linek et al., 1987) | 25 |
| Figure 2.9: The average velocity vectors field at 20 kHz – input power = 45W. The electrode/horn distance = 30 mm (a) and 10 mm (b) (Mandroyan et al., 2009) | 33 |
| Figure 2.10: Comparison between efficiency of piezoelectric transducer and Rushton turbine impeller. $T = 298 \text{ K}$, $P = 1 \text{ atm}$, $f = 1.7 \text{ MHz}$ (Parvizian et al., 2011)..... | 37 |
| Figure 2.11: Schematic representation of biodiesel production using transesterification process..... | 46 |
| Figure 2.12: Reaction route of transesterification with methanol..... | 47 |
| Figure 2.13: Structure of oleic acid..... | 48 |
| Figure 2.14: Side reaction of saponification in transesterification process | 48 |
| Figure 2.15: Side reaction of water with triglyceride in transesterification process..... | 49 |
| Figure 3.1: The arrangement of research methodology. | 64 |
| Figure 3.2: The details of experiments and studied parameters in section 3.1. | 65 |
| Figure 3.3: Experimental set up for gas-liquid mass transfer experiments..... | 66 |

| | |
|--|-----|
| Figure 3.4: Computational domains of (a) Stirred vessel (b) HP-ultrasonicator, (c) VP-ultrasonicator geometries. | 75 |
| Figure 3.5: Experimental setup of transesterification under ultrasonic irradiation. 1. Reaction Vessel, 2. Water bath jacket, 3. Ultrasound probe, 4. Thermometer, 5. Condenser..... | 79 |
| Figure 3.6: Schematic diagram of transesterification under ultrasonic irradiation..... | 80 |
| Figure 3.7: The details of experiments and studied parameters in this section 3.2.4..... | 81 |
| Figure 3.8: <i>J. curcas</i> seeds, the raw material in this research..... | 83 |
| Figure 3.9: Picture of Soxhlet extraction apparatus..... | 84 |
| Figure 3.10: Experimental set up for biodiesel synthesis by mechanical stirring..... | 86 |
| Figure 3.11: Schematic diagram of <i>in situ</i> transesterification under ultrasonic irradiation. | 88 |
| Figure 3.12: The details of experiments and studied parameters in this section 3.3.4.... | 89 |
| Figure 4.1: k_La versus liquid volume under ultrasound power of 400 W and gas flow rate of 5 L/min..... | 93 |
| Figure 4.2: k_La in 2 L liquid volume versus (a) ultrasound power (b) gas flow rate. | 95 |
| Figure 4.3: Predicted vs. actual value of k_La in 2 L. | 97 |
| Figure 4.4: Response surface plot showing the mutual effect of gas flow rate and temperature on k_La at ultrasonic power of 320 W..... | 99 |
| Figure 4.5: Response surface plot showing the mutual effect of the ultrasonic power and temperature on k_La at gas flow rate of 7.5 L/min..... | 99 |
| Figure 4.6: Response surface plot showing the mutual effect of ultrasonic power and temperature on k_La at temperature of 30 °C. | 100 |
| Figure 4.7: Schematic representation of the experimental setup: (a) vertical ultrasonic horn, (b) horizontal ultrasonic horn and (c) mechanically stirred vessel..... | 101 |
| Figure 4.8: Response surface plot showing the mutual effect of ultrasonic power and viscosity on k_La at superficial gas velocity of 2.35 m/s (VP). | 104 |
| Figure 4.9: Response surface plot showing the mutual effect of superficial gas velocity and viscosity on k_La at ultrasonic power of 300 W (VP)..... | 105 |

| | |
|--|-----|
| Figure 4.10: Response surface plot showing the mutual effect of superficial gas velocity and ultrasonic power on k_La at viscosity 3.5 cP (VP)..... | 105 |
| Figure 4.11: Response surface plot showing the mutual effect of ultrasonic power and viscosity on k_La at superficial gas velocity of 2.35 m/s (HP). | 108 |
| Figure 4.12: Response surface plot showing the mutual effect of ultrasonic power and superficial gas velocity on k_La at viscosity of 3.5 cP (HP). | 108 |
| Figure 4.13: Response surface plot showing the mutual effect of viscosity ultrasonic power and superficial gas velocity on k_La at ultrasonic power of 300 W (HP). | 109 |
| Figure 4.14: Response surface plot showing the mutual effect of viscosity and superficial gas velocity on k_La at stirrer speed of 300 rpm (SV). | 112 |
| Figure 4.15: Response surface plot showing the mutual effect of viscosity and stirrer speed on k_La at superficial gas velocity of 2.35 m/s (SV). | 112 |
| Figure 4.16: Response surface plot showing the mutual effect of stirrer speed and superficial gas velocity on k_La at viscosity of 3.5 cP (SV). | 113 |
| Figure 4.17: Distribution of pressure pulses inside the a) VP-Sonicator. b) HP-Sonicator, c) Stirred vessel under superficial gas velocity of 0.117 m/s. | 115 |
| Figure 4.18: Fluid flow pattern and velocity profiles induced by a) Vertical sonicator, b) Horizontal sonicator, c) Mechanically stirring (Sajjadi et al., 2017) | 117 |
| Figure 4.19: Velocity magnitude at 3cm elevation from the tank bottom induced by: a) VP-Sonicator, b) HP-Sonicator, c) mechanically Stirrer. Grey filled: Case 1, Black filled: Case 2, White filled: Case 3 Pattern filled: Case 4..... | 119 |
| Figure 4.20: Distribution of turbulence intensity at 3cm elevation from the tank bottom induced by ○) VP-Sonocation, Δ) HP-Sonocation, ◇) mechanically stirring. Grey filled: Case 1, Back filled: Case 2, White filled: Case 3 Pattern filled: Case 4. | 121 |
| Figure 4.21: Flow pattern of gas bubbles distribution within the a) VP-Sonocation, b) HP-Sonocation, c) mechanically stirring. | 123 |
| Figure 4.22: Gas hold up volume fraction within the a) VP-Sonocation, b) HP-Sonocation, c) mechanically stirring..... | 124 |
| Figure 4.23: Gas-liquid mass transfer coefficient within the a) Vertical sonicator, b) Horizontal sonicator, c) Mechanically stirrer (Sajjadi et al., 2017).. | 125 |

| | |
|---|-----|
| Figure 4.24: Volumetric mass transfer coefficient within the a) VP-Sonocation, b) HP-Sonocation, c) mechanically stirring. ●: Above sparger, ●: Middle of the reactor, ○: Close to the free surface..... | 127 |
| Figure 4.25: Volumetric mass transfer coefficient within the a) VP-Sonocation, b) HP-Sonocation, c) mechanically stirring..... | 128 |
| Figure 4.26: The correlated k_La versus k_La obtained from vertical ultrasonic horn experimental work..... | 134 |
| Figure 4.27: The correlated k_La versus k_La obtained from horizontal ultrasonic horn experimental work..... | 134 |
| Figure 4.28: The correlated k_La versus k_La obtained from stirred vessel experimental work. | 135 |
| Figure 4.29: Response surface plots showing the effects of reaction temperature and methanol to oil molar ratio on a) product yield, b) conversion rate..... | 138 |
| Figure 4.30: Response surface plots showing the effects of reaction temperature and catalyst concentration on a) product yield, b) conversion rate..... | 141 |
| Figure 4.31: Response surface plots showing the effects of reaction temperature and ultrasonic power on a) product yield, b) conversion rate..... | 142 |
| Figure 4.32: Response surface plots showing the effects of reaction temperature and reaction time on a) product yield, b) conversion rate..... | 143 |
| Figure 4.33: Percentages of biodiesel yield and conversion rate versus stirrer speed and ultrasound power. Methanol to oil molar ratio: 9:1, NaOH concentration: 1.5%wt, reaction time: 30 min and reaction temperature: 40 °C..... | 145 |
| Figure 4.34: Vertical fluid flow pattern induced by ultrasound irradiation with power of 400W (a) presented by velocity vectors (b) presented by pathlines (Sajjadi et al., 2015b). | 146 |
| Figure 4.35: Vertical fluid flow pattern induced by stirred vessel with impeller velocity of 600 RPM (a) presented by velocity vectors (b) presented by pathlines (Sajjadi et al., 2015b). | 146 |
| Figure 4.36: Plotted data for the effect of catalyst concentration on <i>in situ</i> transesterification of <i>J. curcas</i> . Ultrasound power = 300W; methanol to seed ratio = 9:1; reaction temperature = 40°C; reaction time = 30 min..... | 152 |
| Figure 4.37: Plotted data for the effect of catalyst concentration on <i>in situ</i> transesterification of <i>J. curcas</i> . Ultrasound power = 300W; methanol to seed ratio = 9:1; NaOH concentration = 0.1N; reaction temperature = 40°C..... | 153 |

| | |
|---|-----|
| Figure 4.38: Plotted data for the effect of catalyst concentration on <i>in situ</i> transesterification of <i>J. curcas</i> . Ultrasound power = 300W; NaOH concentration = 0.1N; reaction temperature = 40°C; reaction time = 30 min. | 154 |
| Figure 4.39: Plotted data for the effect of catalyst concentration on <i>in situ</i> transesterification of <i>J. curcas</i> . Ultrasound power = 300W; methanol to seed ratio = 9:1; NaOH concentration = 0.1N; reaction time = 30 min. | 155 |
| Figure 4.40: Response surface plots showing the mutual effects of ultrasonic power and methanol to seed ratio on product yield. | 157 |
| Figure 4.41: Response surface plots showing the mutual effects of catalyst concentration and reaction time on product yield. | 158 |
| Figure 4.42: Response surface plots showing the mutual effects of catalyst concentration and methanol to seed ratio on product yield. | 159 |
| Figure 4.43: Response surface plots showing the mutual effects of ultrasonic power and reaction temperature on product yield. | 159 |
| Figure 4.44: Response surface plots showing the mutual effects of ultrasonic power and methanol to seed ratio on conversion rate. | 162 |
| Figure 4.45: Response surface plots showing the mutual effects of catalyst concentration and reaction time on conversion rate. | 162 |
| Figure 4.46: Response surface plots showing the mutual effects of catalyst concentration and methanol to seed ratio on conversion rate. | 163 |
| Figure 4.47: Response surface plots showing the mutual effects of ultrasonic power and reaction temperature on conversion rate. | 163 |
| Figure 4.48: Percentages of biodiesel yield and conversion rate versus stirrer speed and ultrasound power. Methanol to seed ratio: 9:1, NaOH concentration: 0.1 mol/L, reaction time: 30 min and reaction temperature: 40 °C. | 164 |

LIST OF TABLES

| | |
|---|-----|
| Table 2.1: Comparison of cavitation yield in various types of sonochemical reactors (Gogate et al., 2003b; Gogate et al., 2004) | 17 |
| Table 2.2: Overview of some important works on mixing time. | 29 |
| Table 2.3: Overview of important works on comparison of sonochemical reactors and stirred vessels | 38 |
| Table 2.4: Overview of important works on coupling of sonication and stirring | 40 |
| Table 2.5: Fatty acid composition of <i>J. curcas</i> oil (Becker and Makkar, 2008)..... | 58 |
| Table 2.6: chemical and physical properties of <i>J. curcas</i> oil (Becker and Makkar, 2008; Achten et al., 2008) | 58 |
| Table 2.7: Composition of fatty acids in various non-edible oils (Azam et al., 2005). .. | 59 |
| Table 2.8: CN and IV for various inedible oils (Azam et al., 2005). | 60 |
| Table 3.1: Independent variables and their coded levels for the CCD for 2 L liquid volume experiments | 68 |
| Table 3.2: Independent variables and their coded levels for the CCD for 200 mL liquid volume experiments | 69 |
| Table 3.3: Defined boundary conditions in Low Frequency Sonicator and mechanical stirrer vessel. | 74 |
| Table 3.4: Experimental design matrix and the final Mass transfer results in V-US, H-US and MS. | 76 |
| Table 3.5: Independent variables and their coded levels for the CCD for transesterification experiments..... | 82 |
| Table 3.6: Independent variables and their coded levels for the CCD for <i>in situ</i> transesterification experiments..... | 90 |
| Table 4.1: Experimental design matrix and response results for k_{La} in 2 L. | 96 |
| Table 4.2: Analysis of variance of the quadratic model for the k_{La} | 98 |
| Table 4.3: Experimental design matrix and response results for vertical ultrasonic mixing. | 102 |

| | |
|--|-----|
| Table 4.4: Experimental design matrix and response results for horizontal ultrasonic mixing. | 106 |
| Table 4.5: Experimental design matrix and response results for mechanical mixing... 110 | |
| Table 4.6: k_La correlations based on the different operational parameters. | 130 |
| Table 4.7: Experimental design matrix and response results of biodiesel yield and conversion rate for transesterification reaction. | 136 |
| Table 4.8: Experimental design matrix and response results for mechanical mixing... 143 | |
| Table 4.9: Experimental design matrix and response results under ultrasonic power of 300 W | 150 |
| Table 4.10: Experimental design matrix and response results of biodiesel yield for <i>in situ</i> transesterification. | 156 |
| Table 4.11: Experimental design matrix and response results of conversion rate for <i>in situ</i> transesterification. | 160 |
| Table 4.12: Experimental design matrix and response results for mechanical mixing. 165 | |
| Table 4.13: FAME profiles of produced biodiesel under ultrasonication and mechanical stirring. | 166 |
| Table 4.14: Predicted and experimental values of the studied responses at optimum conditions. | 168 |

LIST OF ABBREVIATIONS

| | | |
|-------|---|---|
| ANOVA | : | Analysis of Variances |
| ASTM | : | American Standard Test Method |
| CCD | : | Central Composite Design |
| CFD | : | Computational Fluid Dynamic |
| CN | : | Cetane Number |
| FAME | : | Fatty Acid Methyl Ester |
| GC-MS | : | Gas Chromatography-Mass Spectrometry |
| HP | : | Horizontal Ultrasound Probe |
| IV | : | Iodine Value |
| LDA | : | Laser Doppler Anemometer |
| MAC | : | Mechanically Agitated Contactor |
| PIV | : | Particle Image Velocimetry |
| RSM | : | Response Surface Methodology |
| SV | : | Stirred Vessel |
| US | : | UltraSound (UltraSonicator) |
| VP | : | Vertical Ultrasound Probe |
| atm | : | Atmosphere |
| c | : | Sound speed (m/s) |
| cP | : | Centipoise |
| C^* | : | Saturated dissolved oxygen concentration (mmol.m^{-3}) |
| C_t | : | Dissolved oxygen concentration (mmol.m^{-3}) |
| d_b | : | Bubble diameter (m) |
| d_h | : | Diameter of horn (m) |
| D | : | Vessel diameter (m) |

| | |
|-----------|---|
| D_L | : Diffusion coefficient (m^2/s) |
| E | : Cumulative dissipated energy (m^2/s^3) |
| f | : Ultrasonic frequency (Hz) |
| F | : Force ($kg.m/s^2$) |
| g | : Acceleration due gravity (m/s^2) |
| $k_L a$ | : Volumetric mass transfer coefficient (s^{-1}) |
| K | : Proportional coefficient |
| Hz | : Hertz |
| I | : Irradiation intensity (W/cm^2) |
| K | : Kinetic rate constant ($dm^3/mol.min$) |
| L | : Liter |
| min | : Minute |
| N_c | : Critical agitator speed (rpm) |
| P | : Pressure ($kg/m.s^2$) |
| P_0 | : Static pressure ($kg/m.s^2$) |
| P_g | : Gas pressure inside the bubble ($kg/m.s^2$) |
| $P(t)$ | : Sinusoidal acoustic pressure ($kg/m.s^2$) |
| R | : Mass transfer Source ($kg/(m^2.s)$) |
| Re | : Reynolds number, $[Re = ND^2/\nu]$ |
| s | : Seconds |
| t | : Time (s) |
| t_m | : Micromixing time (s) |
| T | : Temperature ($^{\circ}C$) |
| u | : Liquid velocity (m/s) |
| u_i | : Instantaneous velocity (m/s) |
| \bar{u} | : Mean velocity (m/s) |

| | |
|----------------|--|
| v/w | : Volume/weight (mL/mg) |
| V | : Volume (m ³) |
| V_g | : Superficial gas velocity (m/s) |
| V_s | : Acoustic streaming velocity (cm/s) |
| W | : Watt |
| X_s | : Segregation index |
| $S\phi$ | : Source-sink term |
| α | : Volume fraction |
| ρ | : Density of liquid (kg/m ³) |
| ρ_c | : Density of continuous phase (kg/m ³) |
| ρ_d | : Density of dispersed phase (kg/m ³) |
| μ | : Viscosity of liquid (cP) |
| μ_c | : Viscosity of the continuous phase (cP) |
| $\mu^{(t)}$ | : Turbulent viscosity (kg/m s) |
| ε | : Turbulent dissipation rate (m ² /s ³) |
| ν | : Kinematic viscosity (m ² /s) |
| τ_s | : Surface stress (N/m ²) |
| τ_v | : Vicious stress (N/m ²) |
| ϕ_{SI} | : Source term for interfacial area density (1/m.s) |
| θ_{mix} | : Mixing time (s) |

CHAPTER 1: INTRODUCTION

1.1 Background

Sonochemical reactors, based on the use of ultrasound as a source of energy, are being used for various applications due to their special features (Priego-Capote and Luque de Castro, 2004; Csoka et al., 2011). The phenomenon of acoustic cavitation, as the most important feature of sonochemical reactors, can be defined as the generation, growth and violent collapse of microbubbles under ultrasonic irradiations which can release high amount of energy in a small location (Leighton, 1994; Ashokkumar and Mason, 2007; Gogate, 2008; Gogate et al., 2003a). This released energy causes a dramatic increase in temperature and pressure (few thousand Kelvin temperature and few hundred atmospheric pressure) near the ultrasonic transducer which can lead to great amount of process intensification (Gogate and Pandit, 2004; Suslick, 1989). In addition to this phenomenon, propagation of ultrasonic waves in the liquid medium generates local turbulence and micro-circulation in liquid which is known as acoustic streaming (Gogate, 2008). Acoustic streaming can mainly cause physical effects and also influence chemical processing limited by mass transfer (Gogate, 2008).

These two phenomena also lead to some other significant properties such as high shear stress near the bubble wall, free radical production, high rate of heating and cooling, formation of liquid jet, generation of shock waves and streaming of the liquid near the bubble (Mason and Phillip, 2002; Suslick and Price, 1999; Lifka et al., 2003; Ohl et al., 2006; González-García et al., 2010). Since conventional stirred vessels always suffer from the limitations in mass transfer of multi-phase operations, sonochemical reactors can be effectively applied for various chemical and physical processes such as chemical synthesis, biotechnology, wastewater treatment, polymers degradation, extraction, textile processing, crystallization, leaching, emulsification and petrochemical industries, etc. (Luche, 1998; Thompson and Doraiswamy, 1999; Gogate, 2002; Sutkar and

Gogate, 2009). Despite wide range applications of ultrasound and sonochemistry, this type of reactors mostly apply in laboratory scale and practical usage of sonochemical reactors for industrial scale will face with some difficulties due to the lack of understanding about their design, operational and performance characteristics.

Effects of ultrasound irradiation can be classified into three major categories based on their frequency and power amplitude. The conventional frequency range is within 20 to 100 kHz. Ultrasound with a frequency from 100 kHz to 2 MHz is named intermediate frequency or extended range for sono-chemistry within which bubbles generation becomes extremely difficult. Finally, at frequency above 2.5 MHz, cavitation does not happen. In the case of low-frequency high-power ultrasound, the main effect of sonication is mechanical and this effect is linked to interfacial transfer kinetics because of an increase in the interfacial area (Laugier et al., 2008). Basically, mechanical effects can improve multiphase transfer processes, increase movement and mixing of fluid and prevent clogging of samples. Accordingly, low-frequency high-power ultrasound is widely used in the industry whereas high-frequency or low-amplitude propagation is mostly used in chemical analyses and medical diagnoses. For this reason, further investigation on how ultrasound can influence mass transfer phenomena is important.

In this study, the effects of low-frequency high-power ultrasound irradiation on dual-phase operations and their intensifications were investigated separately. The influence of ultrasonication on gas-liquid system was studied first by determining the volumetric mass transfer coefficient of oxygen dissolution operation in different volumes and viscosities. A computational and comparative study was also conducted to investigate the complex structure of wave propagations of low-frequency ultrasound waves in liquid media in the presence of gas phase using Computational Fluid Dynamics (CFD). For studying the effect of ultrasound irradiation on liquid-liquid system a

transesterification process from *J. curcas* oil was considered and the biodiesel yield and conversion rate of reaction were determined. The effect of ultrasound irradiation on solid-liquid system was also investigated by determining the biodiesel yield and conversion rate of *in situ* transesterification of *J. curcas* seeds. In addition, for each part, the results were compared with those obtained by traditional mechanical mixing in stirred vessels. Response Surface Methodology (RSM) coupled with Central Composite Design (CCD) was used for design, statistical analysis and evaluation of the interaction between operational parameters in different experiments.

1.2 Problem Statement

Although it has been proved that ultrasound-assisted mixing is a feasible method to increase mass transfer, considerable effort is still required to fully understand the fundamental processes within the various operations. In addition, the effect of sonication on different phases needs to be investigated separately for further application of ultrasound irradiation in different processes. Moreover, dependency of mass transfer on different parameters is still a big issue in design and operation of sonochemical reactors which required more detailed information. On the other hand, determining the amount of mass transfer in some multi-phase system with reaction is not possible by using the common approaches, so the effect of sonication can be evaluated only by studying the obtained results such as determining the yield of reaction.

Therefore, in this study a comparative study on the effect of ultrasound irradiation on different dual-phase operations was carried out. Generally, the main questions that have tried to find the answer in this project are:

1. What is the effect of ultrasound irradiation on dual-phase operations in comparison with mechanical stirring?

2. What are the effects of other operating parameters on different dual-phase operations under ultrasound irradiation?

1.3 Research Aim and Objectives

The present study aims to investigate the effect of low-frequency high-power ultrasound irradiation on intensification of various dual-phase operations. To achieve this aim, the following objectives are defined:

1. To determine the performance of ultrasound irradiation on gas-liquid, liquid-liquid and solid-liquid operations. The operations conducted to achieve this objective are as follows:
 - i. For gas-liquid system: Oxygen dissolution in water.
 - ii. For liquid-liquid system: Transesterification of *J. curcas* oil.
 - iii. For solid-liquid system: *In situ* transesterification of *J. curcas* seed.
2. To determine the effects of various operating parameters on dual-phase operations under ultrasound irradiation. The operating parameters investigated to achieve this objective are as follows:
 - i. For gas-liquid system: Size of tank, temperature, gas flow rate, viscosity and position of ultrasonic horn.
 - ii. For liquid-liquid system: Catalyst concentration, methanol to oil molar ratio, reaction temperature and reaction time.
 - iii. For solid-liquid system: Catalyst concentration, methanol to seed ratio, reaction temperature and reaction time.
3. To compare the performance of sonoreactor with conventional stirred vessel in gas-liquid system using 3D Computational Fluid Dynamics (CFD) simulation.
4. To develop regression models based on ultrasound power and other operating parameters for different dual-phase systems.

1.4 Research Scopes

1. An ultrasonic horn with a maximum power dissipation of 400 W and fixed frequency of 24 kHz was used for intensifying different dual-phase operations.
2. In gas-liquid system, the intensification of the process was evaluated by determining the volumetric mass transfer coefficient.
3. In liquid-liquid system, the intensification of the process was evaluated by determining the product yield and conversion rate of transesterification reaction.
4. In solid-liquid system, the intensification of the process was evaluated by determining the product yield and conversion rate of *in situ* transesterification reaction.
5. The experiment was conducted in batch mode at room pressure.

1.5 Outline of the Thesis

This thesis deals with various aspects relevant to the topic and objectives of the research as mentioned in the following:

Chapter 1: Introduction

The first chapter includes a brief introduction to the problems and limitations of sonochemical reactors and also the approaches applied in this research to eliminate some of the explained issues. The objectives of the study are clarified and the outline of the thesis is mentioned.

Chapter 2: Literature Review

The first part of this chapter presents a comprehensive literature search about the sonochemical reactors which operate based on the release of high amount of energy from ultrasonic irradiations. Afterward, the performance of these reactors evaluated from different aspects and compared with stirred vessels. In the final part, some of the

application of sonochemical reactors in the gas-liquid system, liquid-liquid system and solid-liquid system are summarized and biodiesel production process using transesterification and *in situ* transesterification methods are also explained and their effective operating parameters are discussed individually.

Chapter 3: Methodology

The beginning of this chapter describes the experimental set up for study the effect of ultrasound irradiation on gas-liquid mass transfer for oxygen dissolution operation as well as how these have guided data collection. The essential background and fundamental equations, models and theories used for CFD simulation of fluid flow under ultrasound irradiation are provided. The chapter continues with explanation about the experiments which evaluate the effect of sonochemical reactor on liquid-liquid operation including the materials and experimental set up of biodiesel synthesis from *J. curcas* oil. In the final part, information about the solid-liquid experiments in sonochemical reactor is provided. The characterisation method for *J. curcas* and thereafter, the experimental set up together with the methods of *in situ* transesterification and analysis are presented in this part. It needs to be mentioned that a low-frequency high-power ultrasound horn was applied as a micro-mixer and some experiments under mechanical mixing were also performed in order to compare the effects of ultrasound mixing with conventional one.

Chapter 4: Results and Discussion

This chapter presents the results of all of the experiments carried out in this study. The effects of ultrasound irradiation on gas-liquid system, liquid-liquid system and solid-liquid system were investigated, respectively. The results obtained in gas-liquid part were further compared with that of stirred vessel using 3D CFD simulation. Besides, for

all three parts, the combined effects of different operating parameters are studied and regression models are developed using CCD and RSM.

Chapter 5: Conclusions and Further Works

The project results and findings conclude in this chapter, followed by a list of recommended areas for further research.

University of Malaya

CHAPTER 2: LITERATURE REVIEW

This review starts with a comprehensive summary of sonochemical reactors, their types and the most significant features of these reactors, followed by explanation of important parameters for evaluating the performance of them. Comparison between stirred vessel and sonochemical reactors is carried out according to the previous works from literature. Finally, the application of sonochemical reactors in the three different systems of gas-liquid, liquid-liquid and solid liquid are summarized. In addition, the process of biodiesel synthesis and its most influencing parameters discussed as one of the practical applications of sonochemical reactors. The arrangement of topics in this chapter is presented in Figure 2.1.

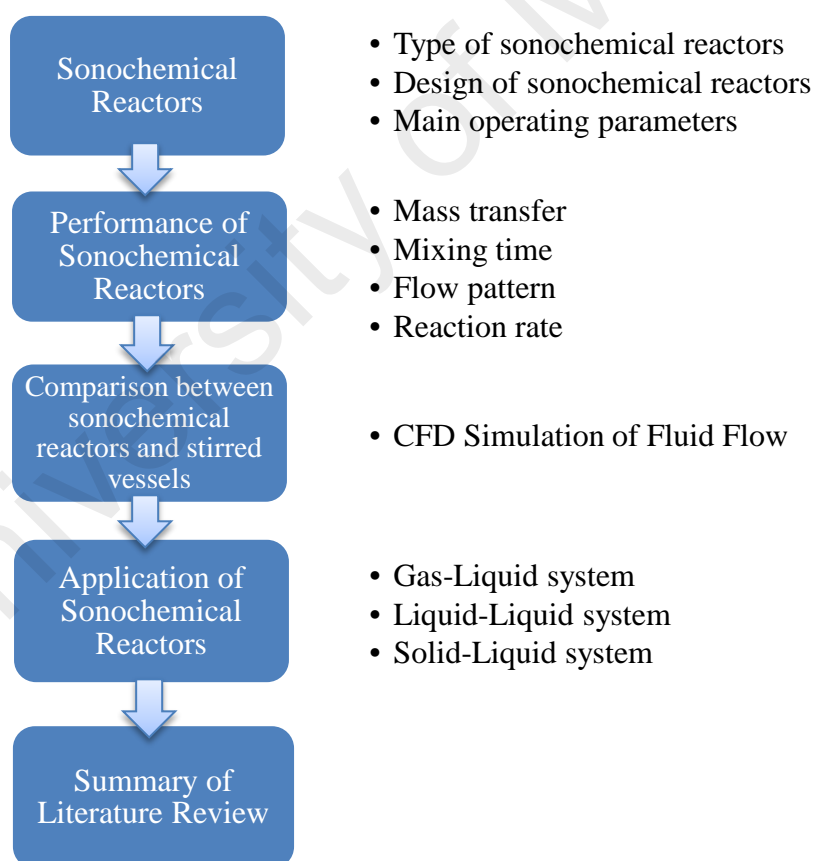


Figure 2.1: The general topics presented in chapter II.

2.1 Sonochemical Reactors

Sonochemical reactors operate based on the release of high amount of energy from ultrasonic irradiations. Having sufficient knowledge about features and characteristics of sonochemical reactors leads to appropriate design and obtainment of optimum operating parameters which plays a crucial role in process efficiency based on specific applications. Choosing the suitable type of transducer with proper frequency range and power intensity, number of transducers and their positions in the reactor can be extremely effective in optimizing the cavitation activity, acoustic streaming and enhancement of sonochemical reactor efficiency.

2.1.1 Type of Sonochemical Reactors

There are a few types of sonochemical reactors with different ultrasonic transducers which are usually applied in laboratory scale applications. Ultrasonic horn is the most common type of sonochemical reactor which is applied in many experimental studies such as micromixing, transesterification of biodiesel, saccharification, microfiltration, etc. (Monnier et al., 1999b; Ji et al., 2006; Singh et al., 2007; Li et al., 2005; Liu et al., 2013a; Sutkar and Gogate, 2009; Worapun et al., 2012; Badday et al., 2012).

A schematic picture of ultrasonic horn reactor is illustrated in Figure 2.1. The ultrasonic horn involves a cylindrical probe which submerges in the liquid and transmits the wave into the medium directly. According to the literature, the diameter of this probe is usually between 5 mm to 1.5 cm and it is usually made of transition metals such as titanium (Goyat et al., 2011; Faïd et al., 1998). Ultrasonic horn can generate a high magnitude of intensity close to the probe and they can be beneficial for vigorous stirring in small scale operations (Gole and Gogate, 2012b).

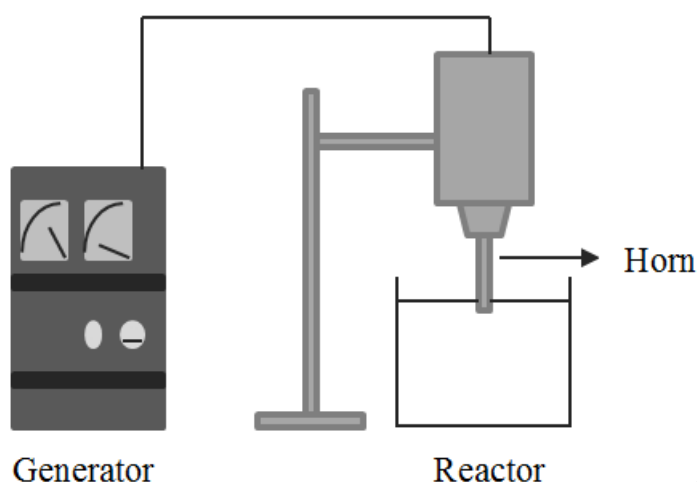


Figure 2.2: Ultrasonic horn reactor, adapted from Csoka et al. (Csoka et al., 2011)

The immersion depth of probe into the medium and the ratio of probe diameter to vessel diameter are the parameters that should be considered in designing horn ultrasonic reactors (Kumar et al., 2006). Kumar et al. (Kumar et al., 2006) analyzed the effect of this ratio on mixing time by modifying the size of vessels and claimed that an optimum diameter for vessel could be found in order to gain a uniform mixing. They also studied the fluid velocity in axial, radial and tangential direction and obtained high axial and radial velocity close to the horn and lower at the vessel wall.

In another study, Faïd et al. (Faïd et al., 1998) analyzed the effect of three types of sonochemical reactor and mentioned that the number of cavitation bubble near the transducer was much higher than other positions in ultrasonic horn reactor. Figure 2.2 shows distribution of the mean velocity and locations of boundary conditions for CFD simulation in the vessel (Kumar et al., 2006). It can be seen from Figure 2.2 that ultrasonic horn can provide significant cavitation in the medium by focusing its energy on a specific zone of sample.

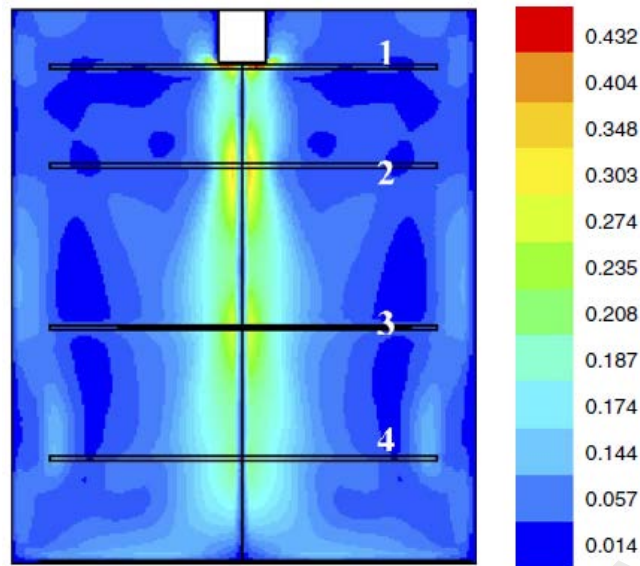


Figure 2.3: Locations of boundary conditions (BC). 1 at $z=0.05H$, 2 at $z=0.32H$, 3 at $z=0.71H$, 4 at $z=0.94H$. The contours represent the mean velocity magnitude in ms^{-1} . (Kumar et al., 2006)

Ultrasonic horn can also be used longitudinally in the vessel for different applications. Bhirud et al. (Bhirud et al., 2004) applied a longitudinal horn in a batch reactor for wastewater treatment application and concluded that this type of transducer was more effective for degradation of formic acid in this process. The longitudinal horns usually have higher surface area of irradiation in the medium and therefore the magnitude of energy efficiency in this type of ultrasonic is higher than the conventional one (Csoka et al., 2011). Furthermore, the large irradiation area of longitudinal ultrasonic horn leads to uniform distribution of cavitation activity in the whole reactor volume which can be more beneficial in pilot scale in comparison with simple ultrasonic horn (Kumar et al., 2007; Csoka et al., 2011). Figure 2.3 shows a typical ultrasonic longitudinal horn reactor.

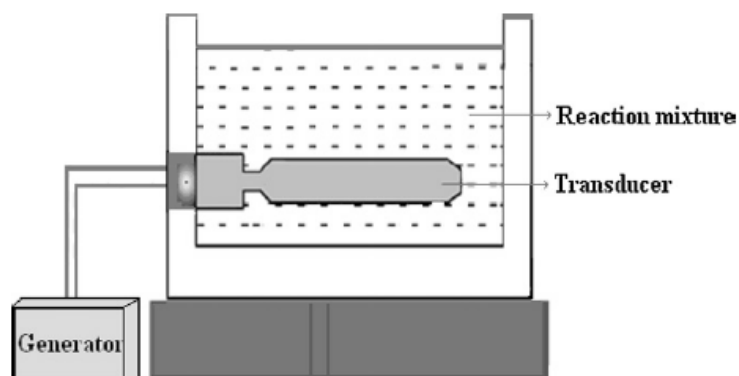


Figure 2.4: Ultrasonic longitudinal horn reactor (Csoka et al., 2011)

Despite common applications of ultrasonic horn in laboratory scale, the reactor is not powerful enough for scale up prospects because of slightly weak capacity for transition of acoustic energy into the big tank volume. In addition, cavitation blocking (acoustic decoupling), particle shedding and erosion of ultrasonic probe are some of the other challenges for industrial usage of ultrasonic horn reactors (Sutkar and Gogate, 2009; Chivate and Pandit, 1995; Horst et al., 1996). As a result, another type of ultrasonic system called ultrasonic bath is usually applied in scaled up systems.

Ultrasonic bath (or cup-horn) is a type of sonochemical reactors in which transducers are located at the bottom of the reactor (Gogate et al., 2004) and ultrasound irradiations transmit into the system indirectly (Gole and Gogate, 2012b). However, some authors have considered the sonochemical reactors in which transducers have a direct contact with fluid as ultrasonic bath reactor (Gogate and Katekhaye, 2012). One of the most recent numerical studies on acoustic streaming in ultrasonic bath was carried out by Xu et al. (Xu et al., 2013) and compared with experimental data provided by Kojima et al. (Kojima et al., 2010). They investigated the influence of input power, liquid height and plate radius in the system. Figure 2.4 illustrates the fluid velocity distribution in the right half of the sonochemical reactor with high input power of 50 W. As observed in

the figure there are two circulations in the tank and a fountain at the center of the liquid surface which are due to high magnitude of input power.

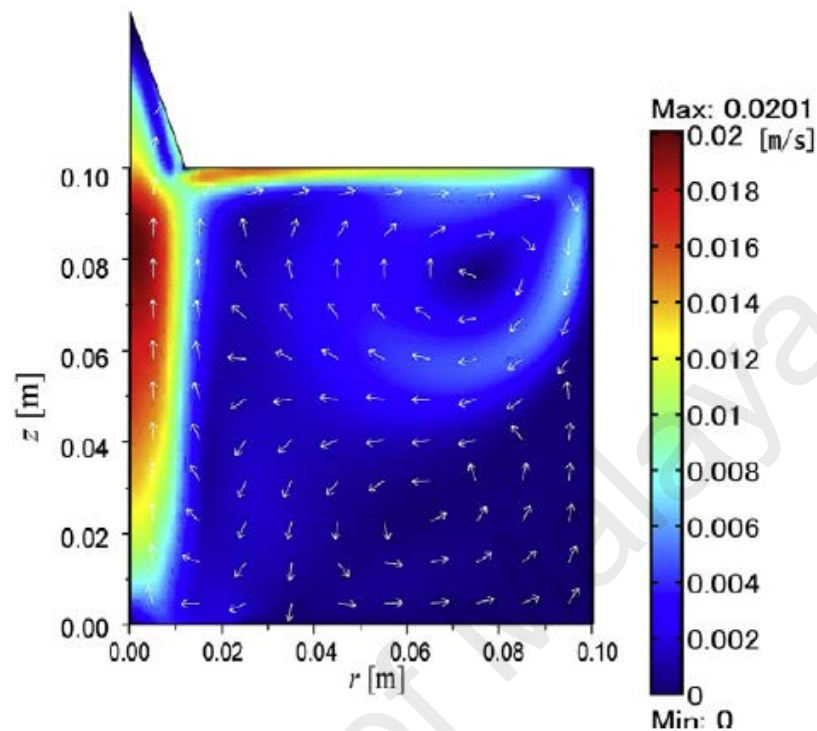


Figure 2.5: Simulation results of liquid velocity distributions in sonochemical reactors with input power of 50 W (Xu et al., 2013)

Monnier et al. (Monnier et al., 1999a) studied the differences between probe-horn and cup-horn for micromixing in order to study the effects of propagation direction and performances of two transducers in sonochemical reactors. They measured micromixing time by modifying the acoustic intensity and noticed that cop-horn needed more energy cost in comparison with probe-horn.

Another comparative study among ultrasonic horn, bath and longitudinal horn was accomplished by Csoka et al. (Csoka et al., 2011) in which the magnitude of frequency for these three reactors were 20, 204 and 36 kHz and the amount of rated power output were 240, 220 and 150 W, respectively. They mentioned that higher area of irradiation

had a considerable role in efficiency of transducers. As a result, they reported that the reactor equipped by ultrasonic longitudinal horn has a more uniform distribution of cavitation activity in comparison with the other sonoreactors.

Generally, ultrasonic bath should be used where a specific power number or ultrasonic intensity is not required, because ultrasonic power does not change in this type of sonochemical reactors (Priego-Capote and Luque de Castro, 2004). In addition, a significant disadvantage of ultrasonic bath is decline of power with time (Priego-Capote and Luque de Castro, 2004). Besides that, it is not easy to obtain a uniform distribution of ultrasonic energy with ultrasonic bath, so ultrasonic horn are preferable in situations that a localized energy is required (Pugin, 1987). Overall, choosing the suitable sonochemical reactor should be carried out considering a particular application. However, the use of more than one transducer is mandatory for large scale applications.

2.2 Design of Sonochemical Reactors

Most of the sonochemical reactors mentioned in the previous sections were applicable in laboratory scale due to generation of small cavitation zone which is usually close to the transducer. Such problem leads to sonochemical reactors with multiple irradiating transducers which can be applied in large scale operations (Sutkar and Gogate, 2009). These transducers can work with different or same frequency and cause an increase in cavitation zones in reactors (Sutkar and Gogate, 2009). Parvizian et al. (Parvizian et al., 2011) designed a new sonochemical reactor that include four piezoelectric transducers with high frequency of 1.7 MHz at the bottom of the reactor which were in direct contact with fluid. Diameter of tank was 15 cm and diameter of each transducer was 2.5 cm. One transducer was located in the center of the tank and three others were placed around it with 120° circumferential space. They studied macro- and micromixing

in their novel sonochemical reactors and cited the effective roles number of transducers play on mixing efficiency.

The location of transducers is another factor for modifying the direction of ultrasonic irradiations into the fluid and achieving a uniform and maximum cavitation zone in sonochemical reactor (Sutkar and Gogate, 2009). Finding the optimum position of the transducers with multiple frequencies has a key role in geometrical design of the reactor, hence many studies have been carried out with different numbers and positions of transducers in order to reach higher efficiency of reactor for different applications (Hatanaka et al., 2006; Gogate et al., 2004; Loranger et al., 2011; Memoli et al., 2012; Gonze et al., 1998).

In 2001, Sivakumar and Pandit (Sivakumar and Pandit, 2001) accomplished an investigation on degradation of reactive dye, Rhodamine B, for wastewater treatment using three different laboratory scale sonochemical reactors. They studied the efficiency of an ultrasonic horn reactor (with different probe size), an ultrasonic bath reactor (with two transducers at the bottom of the vessel) and a dual frequency batch reactor including six transducers with different frequencies. Consequently, Gogate et al. (Gogate et al., 2003b) used these three reactors for degradation of formic acid and also designed a novel triple frequency hexagonal flow cell in large scale involving eighteen transducers with multiple frequencies in order to compare it with the three mentioned reactors. They found out that the hexagonal sonochemical reactor causes a much uniform distribution of cavitation activity in both axial and radial directions. As a result, it had higher cavitation yields and energy efficiencies in comparison with conventional sonochemical reactors. Figure 2.5 depicts the arrangement of transducers in dual and triple frequency flow reactor.

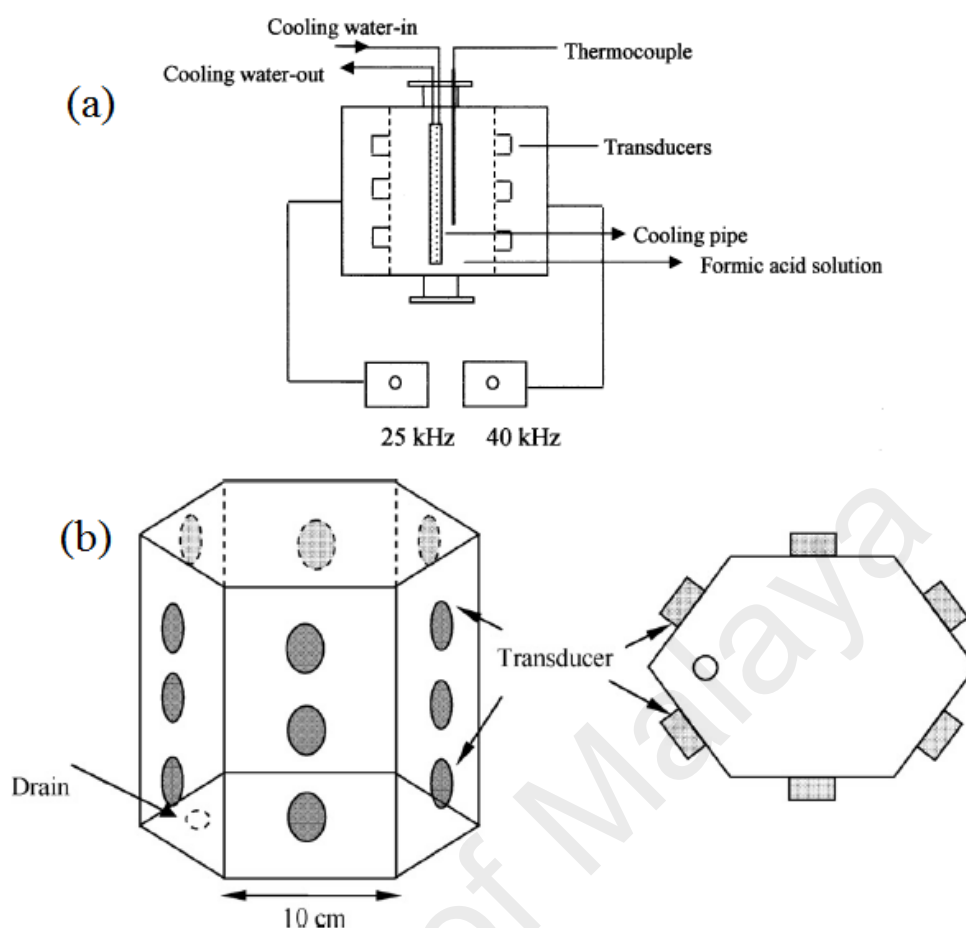


Figure 2.6: a) Cylindrical dual frequency flow reactor. b) Hexagonal triple frequency flow reactor (Gogate et al., 2003b; Gogate et al., 2004)

In another study, Bhirud et al. (Bhirud et al., 2004) applied their new sonochemical reactor using a longitudinal horn with ultrasonic frequency of 36 kHz and maximum power input of 150 W for formic acid degradation in wastewater treatment and obtained the highest amount of cavitation yield among these five sonochemical reactors (Table 2.1). As mentioned before, such results show that high irradiation area of longitudinal horn has a considerable effect on uniform distribution of cavitation zone. Consequently, it can supply energy into the reactor better than other configuration.

Table 2.1: Comparison of cavitation yield in various types of sonochemical reactors (Gogate et al., 2003b; Gogate et al., 2004)

| Type of Reactor | Cavitation yield (mol/W) |
|----------------------------------|--------------------------|
| Ultrasonic horn | 0.0005 |
| Ultrasonic bath | 0.01 |
| Dual frequency flow cell | 0.011 |
| Triple frequency flow cell | 0.018 |
| Longitudinally vibrating reactor | 0.077 |

Hatanaka et al. (Hatanaka et al., 2006) measured the intensity of sonoluminescence in a rectangular sonochemical reactor equipped with four transducers installed to the bottom and two to the facing side of the vessel. Considering the cavitation bubbles movement generated by six transducers, they analyzed the effect of ultrasonic frequency and power on the process yield and obtained an increase in sonoluminescence intensity by increase in flow speed induced by high power transducers.

Generally, the position and number of transducers should be designed based on the reactor diameter and liquid height. The transducer in the reactors, on the basis of many transducer arrangement (with perhaps many frequency operation), should be positioned in such a way that constant and maximum cavitation activity is acquired. Cavitation activity distribution's theoretical analysis helps to reach the most favorable position of the transducers. The more proper arrangement for large scale operation is typically flow cell kind of arrangements. This is due to the fact that, this certainly provides flexibility regarding the continuous operation. Moreover, it provides a choice of arranging the transducers on the wall of the reactor on opposite faces. In this way, standing wave pattern can be produced.

Rectangular cross-sections or hexagonal have been typically announced to provide very good distribution of the cavitation activity. They are suggested for the large scale operation. In the reactor system, the effective cavitation intensity will be increased by the establishment of the standing wave patterns. It also helps to increase the processing rates of particular applications. The mixing characteristics and the hydrodynamic behavior in the reactor which can be the most important particularly for the physical processing applications are affected by the location and number of transducers. For the purpose of achieving the desired objectives, it is significant to keep similar conditions of mixing characteristics and hydrodynamics in the reactor while keeping the geometric likeness for the design of large scale sonochemical reactors (Sutkar and Gogate, 2009; Gogate et al., 2011).

Moreover, an increase in the immersion transducer's diameter concerning the reactor diameter will lead to an increase in the cavitation activity till the most favorable ratio which usually is contingent upon application. The level of turbulent dissipation of energy is mainly affected by the ratio. Moreover, the ratio affects the intensity of the acoustic streaming, so it would be more essential in the applications where physical influences are more significant (Sutkar and Gogate, 2009; Gogate et al., 2011). Therefore, it could be concluded that the position, number and diameter of ultrasound transducer are the most important parameters in design of sonoreactors which should be determined based on different applications, reactor size and liquid height in the reactor.

2.3 Main Operating Parameters in Sonochemical Reactors

2.3.1 Frequency of Irradiation

Choosing the suitable frequency of irradiation is one of the most significant parameters in sonochemical reactors. According to the literature, in order to cause a physical effect in the system, a low irradiation frequency of 10-100 kHz can be appropriate. This range

of frequency usually applies in biodiesel synthesis, polymer degradation and extraction, textile processing, etc. (Gole and Gogate, 2012b; Gogate et al., 2011; Pejin et al., 2012; Ramachandran et al., 2013). Higher range of frequencies can be used where intense chemical effect is required in usages such as chemical synthesis and wastewater treatment (Gole and Gogate, 2012b; Gogate et al., 2011).

Koda et al. (Koda et al., 2003) analyzed the sonochemical efficiency for potassium iodide oxidation using seven different sonochemical reactors in order to investigate the effect of frequency of irradiation in the range of 19.5 kHz to 1.2 MHz. They reported that in the range of 19.5 to 200 kHz, increase in the frequency leads to an increase in sonochemical efficiency. However, a reverse influence was observed at high frequency due to low energy dissipation of ultrasound. Furthermore, the same results were obtained for Fricke solution with maximum sonochemical efficiency at 130 kHz. Wayment and Casadonte (Wayment and Casadonte Jr, 2002) studied the decomposition of potassium iodide under different frequency between 20 to 500 kHz and reported the maximum oxidation rate at 300 kHz. The existence of optimum frequency of irradiation in sonochemical reactors has also been reported by some other researchers (Mark et al., 1998; Hung and Hoffmann, 1999; Kang et al., 1999; Beckett and Hua, 2001).

On the other hand, there are some other disadvantages using high frequency of irradiation such as erosion of the transducers surface in continuous operations and high magnitude of power consumption (Sutkar and Gogate, 2009). In order to eliminate these problems, single high frequency operation can be replaced with dual or multiple low frequencies where high cavitation intensities are required. In addition, more uniform distribution of cavitation activity and superior acoustic streaming can be obtained using dual or multiple frequency operation (Feng et al., 2002; Servant et al., 2003; Yasui et al., 2005). Feng et al. (Feng et al., 2002) investigated potassium iodide

decomposition by combination of low frequency of 28 kHz from an ultrasonic horn with some high frequency transducers in the frequency range of 0.75 to 1.06 MHz. They reported that combination of low frequencies led to higher efficacy as compared to a high single frequency.

Servant et al. (Servant et al., 2003) also reported higher cavitation bubble volume fractions induced by dual frequency sonochemical reactor in comparison with the one under single frequency operation. There are also many other reports indicating higher efficiency of dual or multiple frequency operation as compared to single frequency sonochemical reactors (Tatake and Pandit, 2002; Barati et al., 2007; Zhao et al., 2002; Prabhu et al., 2004).

For any scale of operation, the frequency selection criterion is determined and it is also determined for single frequency operation. However, based on literature, multi-frequency operation (combination of different or same frequency) increases the overall cavitation activity (Servant et al., 2003; Sivakumar and Pandit, 2001; Gogate et al., 2004; Tatake and Pandit, 2002; Feng et al., 2002). Moreover, it generates intensities proper for chemical processing applications at higher energy effectiveness.

The cavitation medium is strongly disturbed because of the combination of frequencies causing overall higher cavitation activity. This is because of generating more cavities and stronger bubble-bubble, bubble-sound field interaction as a result of secondary and primary Bjerkens forces. In another theoretical examination, dual frequency system's modeling with an objective of comprehending the reliance of temperature, collapse pressure, time of collapse and the degree of bubble on different combinations of frequencies was carried out by Tatake and Pandit (Tatake and Pandit, 2002). Based on the reports, it could be concluded that multiple frequency operation leads to higher

intensity of cavitation collapse. However, using multi-frequency sonoreactor also suffer from disadvantages such as less energy efficiency and high operation costs.

2.3.2 Ultrasonic Intensity

Another critical operating parameter in sonochemical reactor design is the ultrasonic intensity which is defined as amount of power dissipation in the fluid per unit area of irradiating surface. The power dissipation rate will affect number, size and life time of bubbles in the liquid medium and also temperature rise which is directly related to gas solubility and vapor pressure (Gogate et al., 2011). Calorimetric method is generally applied to get the power based on the first law of thermodynamics (Gogate et al., 2011). Löning et al (Löning et al., 2002) carried out an investigation on energy transformation in an ultrasonic horn system applying calorimetry and electrical power measurement technique and observed that the amount of power dissipation was considerably affected by properties of liquid medium i.e. power transfer decrease in high volatile and high viscosity medium which results in increase in power consumption.

Kumar et al. (Kumar et al., 2005) studied the mass transfer for a gas-liquid system in a horn ultrasonic reactor and reported that mass transfer coefficient of air into the liquid increased by increasing the power intensity of the system. Feng et al. (Feng et al., 2002) also investigated the effects of ultrasonic intensity on iodine liberation with different ultrasonic frequencies and they observed that the cavitation activity and liberation of iodine increased by increasing the intensity of irradiation.

On the other hand, Henglein and Gutierrez (Henglein and Gutierrez, 1990) investigated the effects of power dissipation on iodine yield of potassium iodide oxidation in constant frequency of 20 kHz and obtained an optimum value of 50 W for power dissipation as shown in Figure 2.7. The existence of optimum ultrasonic intensity has also been reported by many other researchers (Contamine et al., 1995; Whillock and

Harvey, 1997; Hodnett et al., 2007; Nanzai et al., 2009). As a result, it can be summarized that choosing appropriate power rating does not only increase the efficiency of operation but also lead to decrease in operating cost for a given process.

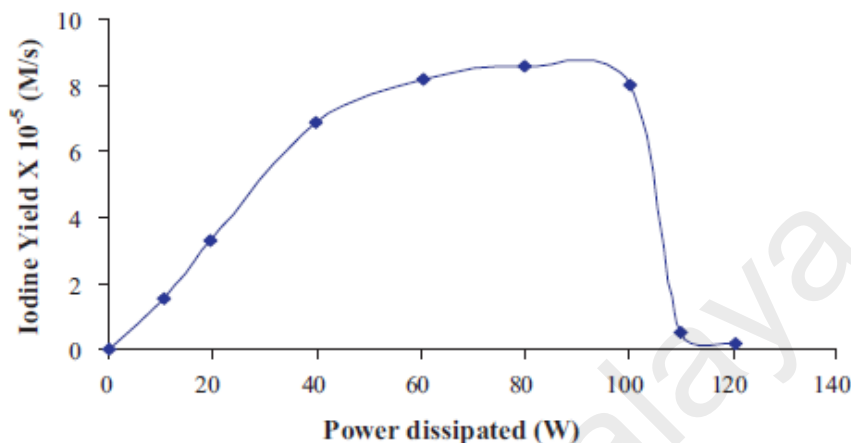


Figure 2.7: Effect of power dissipation on iodine yield (Henglein and Gutierrez, 1990; Gogate et al., 2011)

In addition, in bulk of liquid, the degree of temperature increase can be described as the rate of power dissipation's function which finally leads to change gas solubility and vapor pressure influencing the ease of producing cavitation events and final collapse intensity. It is of great importance to possess the knowledge of hydrodynamic behavior such as mixing time which is contingent upon the power density in the development of continuous scale sonochemical reactors. Therefore, it is significant to express the quantity of the actual power disappeared in the bulk of liquid and available for generating cavitating conditions (Gogate et al., 2011).

Generally, it is very difficult to dissipate the whole power in the specified reactor volume utilizing single transducer with excellent efficacy as a result of restrictions in the construction materials, vibrating piezoelectric crystal, in large scale operation with operating volume in the range of few to few hundred liters. Moreover, in sonochemical

reactors, active zones with preferred minimum cavitation activity concentrate close to irradiating surface (2-3 cm away). Therefore, more than one irradiating surface will be needed for attaining constant distribution of the cavitation activity. Furthermore, the arrangement of these transducers at different places must be optimized. The power demand for specified application, the dimensions of each transducer and the operating volume decide the exact number. The normal range of irradiation's optimum intensity (power dissipated per unit area of irradiating surface, W/cm²) is 5–20 W/cm². In addition, it depends on the final application and actual reactor system (Gogate et al., 2011).

2.4 Performance of Sonochemical Reactors

The performance of reactors can be analyzed in different aspects. In this study, an attempt has been made to investigate the performance of sonochemical reactors in terms of mass transfer, mixing time, flow pattern and reaction rate, based on the previous works in the literature.

2.4.1 Mass Transfer

Effects of ultrasonic irradiation on mass transfer characteristics were firstly investigated by Cadwell and Fogler (Cadwell and Fogler, 1971) in a batch reactor. They quantified the absorption rate of carbon dioxide by glycerol with and without ultrasonication and obtained higher rate of absorption in presence of ultrasonic irradiation which was due to the influence of acoustic streaming and the associated turbulence (Lighthill, 1978). For gas-liquid mass transfer analysis in sonochemical reactors, the dissolved oxygen concentration in the liquid can be predicted by using the following equation (Gogate et al., 2011):

$$k_L a V (C_{O_2}^* - C_{O_2}) = V \frac{d(C_{O_2})}{dt} \quad (2.1)$$

where $k_L a$ is the volumetric mass transfer coefficient (1/s), V is the volume of the liquid in the reactor (m^3), $C_{\text{O}_2}^*$ is the saturation concentration of dissolved oxygen (mmol.m^{-3}) and C_{O_2} is the concentration of dissolved oxygen in the reactor at any time t (mmol.m^{-3}). However, dependency of this equation on the operating temperature should be considered during the experimental tests in order to obtain accurate measurements.

Kumar et al. (Kumar et al., 2004) quantified the overall volumetric mass transfer coefficient ($K_L a$) in ultrasonic horn and bath reactors for transfer of oxygen gas from air into water. The liquid volume in conventional horn reactor was fixed at 500 mL and operated with ultrasonic frequency of 20 kHz and maximum power dissipation of 65 W while the ultrasonic bath reactor (with capacity of 3.3 L and equipped by three transducers at the bottom of the reactor) operated with ultrasonic frequency and power input of 20 kHz and 120 W. They developed two mathematical correlations for ultrasonic horn and bath reactors as follows:

$$\text{Ultrasonic horn: } K_L a = 0.029(P/V)^{0.17}(V_g)^{0.37} \quad (2.2)$$

$$\text{Ultrasonic bath: } K_L a = 0.0039(P/V)^{0.4}(V_g)^{0.6} \quad (2.3)$$

where (P/V) is the power dissipated per unit volume (W/m^3) and V_g is superficial gas velocity (m/s). In addition, they compared the mass transfer coefficient in the two mentioned reactors with a mechanically agitated contactor (MAC). Figure 2.7 shows the MAC data estimated from equation reported by Linek et al. (Linek et al., 1987).

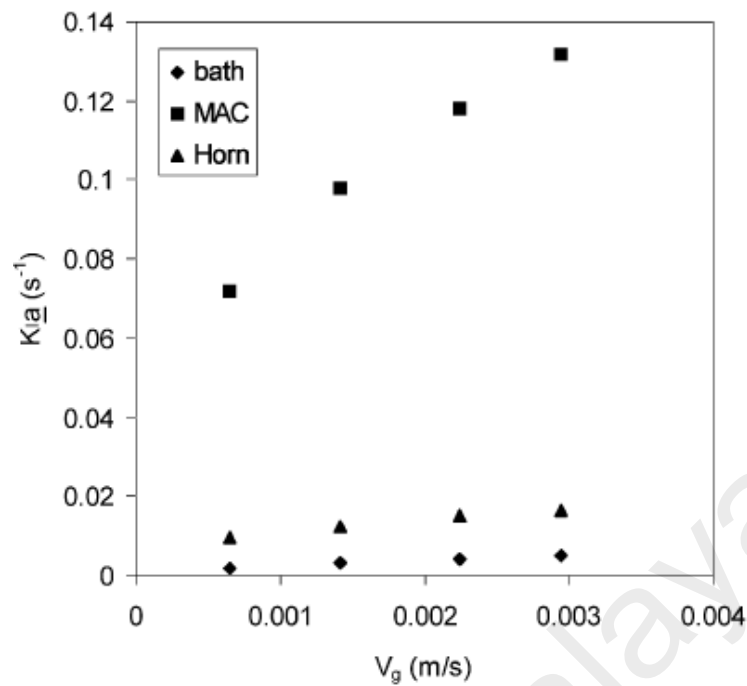


Figure 2.8: Comparison of mass-transfer coefficient in different reactors at constant power density of 11.71 kW.m^{-3} (Kumar et al., 2004; Linek et al., 1987)

This figure demonstrates high difference between mass transfer value of the mechanically agitated contactor and the ultrasonic reactors. This difference shows the significant role of convective fluid motion on overall mass transfer coefficient. Furthermore, the location of sparger to release gas into the liquid is one of the other important parameters that should be considered in design of gas-liquid systems (Kumar et al., 2004).

In another study, Kumar et al. (Kumar et al., 2005) investigated the induction of air into the sonochemical reactor by locating the ultrasonic horn just above the liquid surface and quantified the gas-liquid mass transfer coefficient using dynamic method. They reported that mass transfer coefficient increased by increasing the power density (W/m^3). However, they mentioned that this mechanism for the induction of air into the liquid was not beneficial compared to surface aerators.

Laugier et al. (Laugier et al., 2008) analyzed the solubility and mass transfer in a 1 liter stainless steel ultrasonic autoclave reactor with irradiating frequency of 20 kHz and input power of 200 W. This reactor was also equipped with a Rushton turbine with maximum stirring speed of 3000 rpm and power dissipation of 16.7 W. They reported that although solubility was not significantly improved using ultrasonic irradiation in a stirred tank (due to increase in temperature), the gas-liquid mass transfer greatly increased. They mentioned that the mass transfer coefficient would be increased by 11 times by combining ultrasonic irradiation with mechanical agitation at temperature of 323 K, stirring speed of 110 rpm and absolute pressure of 10 bars. They also reported that mass transfer coefficient depended highly on the operating pressure and temperature in the reactor.

2.4.2 Mixing Time

Mixing time is one of the most significant factors in designing sonochemical reactors and it generally depends on the discussed operating parameters in previous sections. The knowledge of mixing time is very important when a chemical reaction occurs in the sonochemical reactor. Reaction time must be higher than mixing time in order to achieve the effective reaction rate, although it is very difficult to obtain for fast reactions (Bakłdyga et al., 1995; Baldyga et al., 1995; Monnier et al., 1999b).

Many different methods have been applied for mixing time measurement in conventional reactors, but only few of them can be used for sonochemical reactors such as measurement of pH, dissolved oxygen, conductivity, particle image velocimetry and computational fluid dynamics (Gogate et al., 2011). The variation of the mixing time in different sonochemical reactors and dependency of the mixing time on reactor size, ultrasonic frequency and power has been discussed in this section.

Monnier et al. (Monnier et al., 1999b; Monnier et al., 1999a; Monnier et al., 2000) investigated the effects of operating parameters on micromixing of batch and semi-batch sonochemical reactor and measured the mixing time for a model reaction of iodide and iodate called Dushman Reaction. They reported that the mixing time decreased by increasing the ultrasonic intensity and also by increasing the Reynolds number. They obtained the mixing time of 0.015 s for intensity of 10 W.cm⁻². However, they also reported that the effect of power on mixing time reduced after this amount of intensity. In addition, Monnier et al. (Monnier et al., 2000) developed a correlation between micromixing time and segregation index (segregation index is equal to zero for complete mixing) based on the continuous model as follows:

$$t_m = 0.31X_S^{1.02} \approx 0.3X_S \quad (2.4)$$

where t_m is micromixing time (s) and X_S is segregation index. Vichare et al. (Vichare et al., 2001) studied the mixing time variation in an ultrasonic horn reactor with frequency of 22.7 kHz and power dissipation of 24.5 W. They found that the mixing time for horn type reactor strongly depends on geometrical design of the vessel, horn position and diameter of horn tip. They also developed a correlation for the prediction of mixing time as follows:

$$\theta_{mix} = 7 \times 10^6 d^{-0.235} \left[\frac{Z^{3/2} T^3 (T+2Z)^{-2} d_h^{-4}}{v_h^2 g^{1/2} \mu^{-2} \rho_l^2} \right] \quad (2.5)$$

where θ_{mix} is mixing time (s), d is distance between horn and bottom of reactor, Z is height of liquid in reactor (m), T is diameter of vessel (m), d_h is diameter of horn (m), v_h is velocity of horn (m/s) (amplitude of oscillation in m \times frequency in Hz), g is gravity constant=988 m/s², μ is viscosity of liquid (N s/m²) and ρ_l is bulk density of liquid (kg/m³).

Kumar et al. (Kumar et al., 2006) also studied the effects of power density and reactor geometry on mixing time. They reported that mixing time decreased by increasing the power density and measured the mixing time value of 131 to 17 s for power density of 15 to 35 kW/m³. In addition, they analyzed the effects of D/T ratio (where D is horn diameter and T is reactor diameter) on mixing time variation by changing the reactor diameter in constant horn diameter of 0.013 m and power density of 35 kW/m³. Mixing time of 62 and 12 s were obtained for reactor diameters of 0.11 and 0.14 m respectively which were attributed to the fact that average turbulent kinetic energy (TKE) was lower for the larger vessel. Yusaf and Buttsworth (Yusaf and Buttsworth, 2007) also investigated the mixing time variation in a sonochemical batch reactor and discussed the dependency of mixing time on applied ultrasonic power.

In 2008, Deshpande et al. (Deshpande et al., 2008) developed a new correlation for mixing time based on the flow structure pattern which could be used for different types of chemical reactors. They considered the operating and geometrical conditions of the reactor and also the statistical parameters in developing this unified correlation. However, one of the most recent investigations on macro- and micromixing in sonochemical reactors were carried out by Parvizian et al. (Parvizian et al., 2012a; Parvizian et al., 2012b) in which mixing time was also measured using Monnier et al. (Monnier et al., 2000) correlation. The obtained micromixing time values were in the range of 0.001-0.01 s. This low range of micromixing time could be due to high ultrasonic frequency and generated jet streams which assisted the local micro agitation and micromixing. Table 2 depicts some representative studies on mixing time. The presented table provides information about the variation of mixing time in different sonochemical reactor with different operating parameters. This information can be used in design of new sonochemical reactors with similar conditions.

Table 2.2: Overview of some important works on mixing time.

| Sr. No | Details of sonochemical reactor and operating parameters | Other variable parameters | Mixing time (s) | Ref. |
|--------|--|---|-----------------|---------------------------|
| 1 | The experiments were performed in three cylindrical glass vessels with different volume. Ultrasonic horn with diameter of 5 mm, dissipated power of 30 W/kg and frequency of 20 kHz were used. | Reactor capacity of 100 mL | 0.1 | (Monnier et al., 1999b) |
| | | Reactor capacity of 500 mL | 0.01 | |
| | | Reactor capacity of 3750 ml and Reynolds number of 100,000. | 0.005 | |
| 2 | The experiments were performed in a cylindrical sonochemical reactor with diameter of 40 mm and height of 56 mm. Ultrasonic horn with diameter of 13 mm and frequency of 20 kHz were used. | Coupling with Rushton turbine, Reynolds number of 100,000 | 0.01 | (Monnier et al., 1999a) |
| | | Ultrasonic intensity of 10 W/cm ² | 0.015 | |
| 3 | An ultrasonic horn with irradiation frequency of 22.7 kHz and energy dissipation of 24.5 W and different cross sectional area of the horn tip were used. | Reactor capacity of 1 L | 4-6 | (Vichare et al., 2001) |
| | | Reactor capacity of 2 L | 5-8.5 | |
| 4 | The experiments were performed in a cylindrical sonochemical reactor with diameter of 0.135 m and volume of 2000 ml. | Power density range of 15-35 kW/m ³ (experimental) | 17-131 | (Kumar et al., 2006) |
| | | Power density range of 15-35 kW/m ³ (predicted by CFD) | 16.8-139.21 | |
| 5 | A cylindrical sonochemical reactor with high frequency of 1.7 MHz was used. T = 298 K, P = 1 atm, f = 1.7 MHz. | - | 0.028 | (Parvizian et al., 2011) |
| 6 | A new continuous tubular sonochemical reactor with capacity of 370 ml and irradiation frequency of 1.7 MHz was applied. | - | 0.001–0.01 | (Parvizian et al., 2012a) |

2.4.3 Flow Pattern

Using ultrasonic waves in medium generates acoustic streaming in liquid phase which causes an increment in the mass and heat transfer (Kumar et al., 2006). Rayleigh (Rayleigh, 1945) carried out the first analysis about acoustic streaming and many investigations were accomplished after that in order to measure the fluid velocity and increase it by applying various approaches. Cadwell and Fogler (Cadwell and Fogler, 1971) calculated the acoustic streaming velocity generated by low frequency of 20 kHz in the range of 0.7-1.0 m/s and high frequency of 800 kHz near the ultrasound horn in the range of 0.3-0.5 m/s. Some other investigations have also been carried out in high frequency (500 kHz) to analyze the effects of power on flow velocity.

Gondrexon et al. (Gondrexon et al., 1998) found the velocity value of 0.01-0.03 m/s and 0.05-0.10 m/s for electrical powers of 40 W and 100 W respectively in a PVC cylindrical body with diameter of 0.10 m and height of 0.10 m. Another point mentioned in this paper was that experimental outlet response of the system did not change by increasing the ultrasonic power and there was an ideal flow in the sonochemical reactors under ultrasonic irradiation.

Another investigation in frequency of 500 kHz was accomplished by Chouvellon et al. (Chouvellon et al., 2000). They measured the flow velocity in different situations by modifying the electrical power, the water height and the fluid viscosity using laser tomography technique. The velocity calculated was in the range of 0.005-0.033 m/s for the electrical power range of 12.5-150 W. However, the maximum rate of velocity achieved was until 100 W after which the flow velocity increased slowly. They also reported that the average velocity decreased in a linear way by increasing the water height. Furthermore, they observed that the flow velocity increased by increasing the liquid viscosity until it reached the threshold.

In 1998, Laborde et al. (Laborde et al., 1998) utilized Particle Image Velocimetry (PIV) to measure the amount of velocity in a sonochemical reactor. PIV is an optical method for studying fluid dynamic, flow velocity measurement, flow structure, etc. by determining particle displacement over time using a double-pulsed laser technique (Adrian, 1991; Xia et al., 2003). The liquid media needs to be seeded by tracers in PIV (Mandroyan et al., 2009). Laborde et al. (Laborde et al., 1998) took cavitation bubbles as tracer for measuring the flow velocity by PIV at low and high frequencies. Although the cavitation bubbles were considerably stable and a velocity vector around 1 cm/s were reported, the measurement of velocity could be more inaccurate at low frequency due to increment in number of cavitation bubbles. The velocity vectors reported in this paper were in the range of 50-85 cm/s which were not so reliable due to non-uniform distribution and difference in kinds of cavitation bubbles.

Dahlem et al. (Dahlem et al., 1999) measured the velocity of acoustic streaming with frequency of 20 kHz in two different sonochemical reactors applying PIV technique. The average velocity of an ultrasound reactor with volume of 3.5 l and equipped with the telsonic horn (radial horn) was about 0.05 m/s while for the other sonochemical reactor with the laboratory stepped horn (Longitudinal horn) and volume of 0.3 l, the velocity was measured to be around 0.35 m/s. Frankel et al. (Frenkel et al., 2001) used PIV technique to measure the amount of flow velocity in a 6 l glass tank with dimensions of 0.25*0.17*0.14 m and ultrasonic frequency of 3 MHz. They obtained a linear relationship as follows:

$$V_S = 0.0992 \times I \quad (2.6)$$

where V_S is acoustic streaming velocity in cm/s and I is the irradiation intensity in W/cm^2 . Another investigation on acoustic streaming in frequency of 40 kHz was carried out by Kumar et al. (Kumar et al., 2006) for measuring the mean flow and turbulence

parameters applying laser Doppler anemometer (LDA) in a cylindrical vessel with diameter of 0.135 m and volume of 2000 ml. Maximum magnitude which they determined for axial velocity near the ultrasound horn was 1.6, 1.3 and 0.57 m/s for dissipated power density of 35, 25 and 15 kW/m³ and intensities of 527.6, 376.8 and 226.1 kW/m², respectively. Axial velocity increases with power and decreases with axial and radial distance but increases near the wall. Radial and tangential velocities are almost in the same range but lower than axial velocity and they also increase with power. Moreover, the effect of vessel size on flow behavior has been investigated and observed that the optimum diameter of vessel and power intensity should be determined in order to obtain a uniform mixing in sonochemical reactor.

In 2009, Mandroyan et al. (Mandroyan et al., 2009) also used PIV to study the velocity distribution induced by ultrasonic irradiation at frequencies of 20 and 40 KHz, taking fluorescent seeds as tracer which could not be disturbed by cavitation bubble. For both frequencies, the axial flow velocity presents a greater magnitude in comparison with the recirculation velocity and it exceeded 1 m/s in some specific situations.

In addition, Mandroyan et al. (Mandroyan et al., 2009) added an electrode in front of the transducer, which could reflect the ultrasonic waves in order to analyze the new hydrodynamic behavior of the fluid within the sonochemical reactor and also investigated the influence of electrode distance from transducer on ultrasonic system. This electrode generated a new flow on its both sides correspond to tangential flow. Figure 2.8 demonstrates the effects of electrode distance on average velocity vectors at frequency of 20 KHz and input power of 45 W.

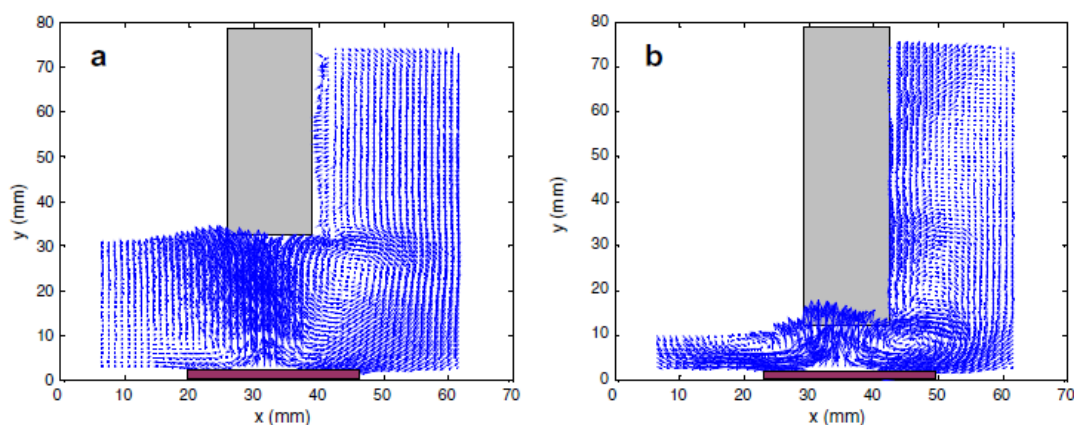


Figure 2.9: The average velocity vectors field at 20 kHz – input power = 45W. The electrode/horn distance = 30 mm (a) and 10 mm (b) (Mandroyan et al., 2009)

One of the recent studies on flow velocity was carried out by Kojima et al. (Kojima et al., 2010) in a rectangular parallelepiped sonochemical reactor under 490 KHz ultrasonic frequency. They concluded that the average flow velocity increases by increasing the electric power after analyzing the effect of electric input power. However, the efficiency of reactor diminished up to a particular amount of electric power due to the lack of active bubbles per unit volume.

In addition, Kojima et al. (Kojima et al., 2010) enhanced the efficiency of sonochemical reactor about 100 % by adding a stirrer to the sonochemical reactor and combining the mechanical flow with acoustic streaming. On the other hand, Xu et al. (Xu et al., 2013) accomplished a numerical study on liquid velocity distribution in an ultrasonic reactor and compared their results with experimental ones obtained by Kojima et al. (Kojima et al., 2010) at the same ultrasound frequency. They investigated the effect of acoustic power at 10, 30 and 50 W in a cylindrical vessel with radius and height of 0.1 m filled with water. They demonstrated that for the high and middle input power the experimental results agreed well with simulation results. However, the results were not completely similar to the experimental ones for the low acoustic power of 10 W. Xu et

al. (Xu et al., 2013) concluded that experimental test couldn't measure the low fluid velocity and as a result the circulation was not depicted in experimental results. They also mentioned that the thermal convection could influence the experimental results.

2.4.4 Reaction Rate

Reaction rate is another important factor for evaluating the performance of sonochemical reactors. Ultrasonic irradiation has been used in many chemical reactions in order to enhance the kinetics and selectivity (Priego-Capote and Luque de Castro, 2004; Priego-López and de Castro, 2003; Hsiao et al., 2010; Stavarache et al., 2005; Gogate and Katekhaye, 2012; Son et al., 2012; Wang et al., 2012). A comprehensive review is carried out by Gogate on application of cavitational reactors including sonochemical reactors for intensification of chemical processes (Gogate, 2008).

One of the most significant applications of sonochemical reactors is through the process of biodiesel production. Gole and Gogate (Gole and Gogate, 2012b) investigated the performance of sonochemical reactors on intensification of biodiesel synthesis from sustainable feedstock in a review paper. Sonochemical reactors based on the use of cavitational effects can improve the synthesis of biodiesel by causing physical effects and increasing the mass transfer.

2.5 Comparison between Sonochemical Reactors and Stirred Vessels

Ultrasound irradiation could be used in diversity of application for intensification of chemical and physical processes. In this section, the performance of sonochemical reactors was compared with different types of stirred vessels in terms of energy efficiency and mixing patterns. In 2000, Simon et al (Simon et al., 2000) carried out a comparative study between classical mechanical stirrer and ultrasonic-assisted mixing for a dead-end ultrafiltration process. They changed the classical stirrer speed and ultrasonic power at constant frequency of 20 kHz for the purpose of the study. The

maximum electrical power of ultrasonic was 40 W. They demonstrated that increment of ultrasonic power as well as increment of stirrer speed led to an increment in volumetric permeate flux and enhancement in dead-end ultrafiltration efficiency. However, they did not distinguish which one could be more effective for this process.

Guo et al. (Guo et al., 2007) also compared the ultrasound mixing with the stirring type applying a Kodak motion analyzer to observe the dispersion of ink in the ethanol and to trace of sugar crystals in a 55 mm diameter jacketed vessel. The power and frequency of ultrasonic processor were 750 W and 20 KHz, respectively and the stirred vessel were equipped with a 4-blade impeller. For the amplitude of 41% of maximum power and the stirring rate of 400 rpm they found that the movement of particles in the stirring vessel was more orderly in comparison with the vessel equipped by ultrasound. The particles in the ultrasonic vessel moved erratically and the collision rate between them increased in the system due to their chaotic movements. As a result, a uniform distribution of sugar crystals was obtained in the vessel with ultrasound while for the stirring vessel the particles were not dispersed in the whole vessel as well as in the ultrasonic one and the majority of sugar crystals were precipitated in the bottom of the vessel. In addition, velocity variance was applied in order to show the difference of turbulence between ultrasound and stirring and it was indicated that the velocity variance of particles in the vessel with ultrasound was much higher than in the stirred vessel.

Another comparative investigation on ultrasonic and impeller mixing was accomplished by Wu et al. (Wu et al., 2007) for producing biodiesel during the Alkali-catalyzed transesterification process. The parameter investigated in this paper using both mixing method was the droplet size distribution. The experiments were carried out in a 1 gallon tank with diameter and height of 17 and 20 cm, respectively. The ultrasonic frequency was 24 kHz and the impeller was a flat blade turbine with six blades with diameter of 5

cm. They also used a critical agitator speed for the impeller in order to diminish a separated layer of two immiscible liquids (Nagata, 1975) and presented the below empirical equation:

$$N_c = KD^{-2/3} \left(\frac{\mu_c}{\rho_c} \right)^{1/9} \left(\frac{\rho_c - \rho_d}{\rho_c} \right)^{0.26} \quad (2.7)$$

where N_c is the critical agitator speed, K is a proportional coefficient, D is the vessel diameter ρ_c and ρ_d are the densities of the continuous and dispersed phases, respectively and μ_c is the viscosity of the continuous phase. Taking K as 750 at the center of the vessel, the amount of N_c obtained was 493 rpm and by comparing it with the highest rate of impeller at 1000 rpm and ultrasonic power of 30 W, Wu et al. (Wu et al., 2007) found that the mean droplet size obtained by impeller mixing was 2.4 times larger than the ultrasonic type, so ultrasonic reactor was a more efficient tool for breaking methanol into small droplets at equivalent power input.

In 2011, Parvizian et al. (Parvizian et al., 2011) analyzed the macro- and micromixing of a new type of sonochemical reactor with four piezoelectric transducers (with diameter of 2 cm and high frequency of 1.7 MHz) and they compared the new sonochemical reactor mixing efficiency and power consumption with Rushton turbine impeller in a brief part of this work. Macromixing investigations was analyzed visually while micromixing was studied by using Dushman reaction (iodide–iodate) coupled with a neutralization reaction. Fig. 2.10 demonstrates the comparison between the power consumption of these two mixing vessels versus increase in micromixing efficiency which is defined as below:

$$\text{Increase in micromixing efficiency} = \left(\frac{t_{m0} - t_m}{t_{m0}} \right) \times 100 \quad (2.8)$$

where t_{m0} is mixing time without power input and t_m is mixing time in different power inputs. Figure 2.10 presents that the ultrasonic reactor can reduce the micromixing time more effectively in comparison with the stirring type by increasing the power input. Furthermore, it can be concluded from this figure that the differences in efficiencies of these two setups decrease at higher power inputs.

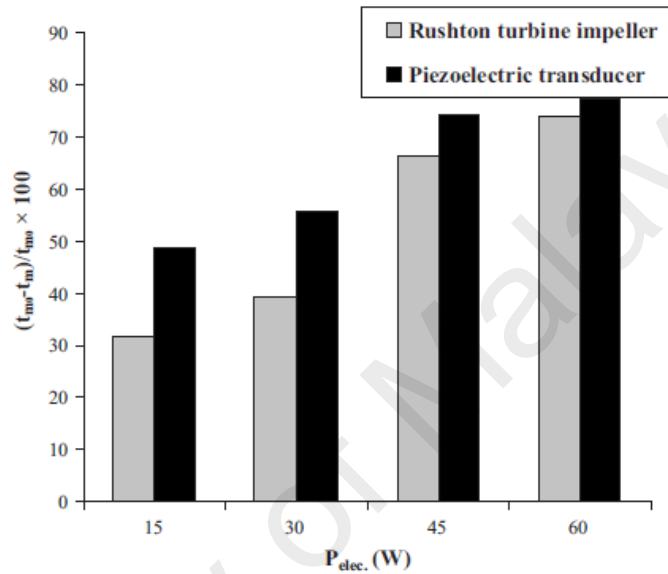


Figure 2.10: Comparison between efficiency of piezoelectric transducer and Rushton turbine impeller. $T = 298\text{ K}$, $P = 1\text{ atm}$, $f = 1.7\text{ MHz}$ (Parvizian et al., 2011)

Consequently, they have investigated the mechanical mixing in same stirred tank and sonochemical reactor by focusing on the velocity distribution and mixing time in a liquid medium in another study (Parvizian et al., 2012b). Parvizian et al. (Parvizian et al., 2012b) studied only mechanical mixing in both systems without any chemical reactions and the Computational Fluid Dynamics (CFD) modeling was applied in order to report the results. The predicted results related to the stirred tank with Rushton turbine impeller were compared with the experimental results reported by Ranade and Joshi (Ranade and Joshi, 1990), Vlaev et al. (VLAEV et al., 2007), Ranade et al. (Ranade et al., 2002) and Wang et al. (Wang et al., 2006) for validation. The obtained

results were compared with the Frenkel et al. (Frenkel et al., 2001) works for the ultrasonic reactor. Considering the reasonable agreement between the CFD modeling results and experimental data, they compared the operation of two setups and reported a higher and more uniform velocity distribution in the sonochemical reactor.

Furthermore, they obtained the average axial circulation time of 7.12 and 1.3695 s for the stirred tank and sonochemical reactor, respectively, which was another reason for efficacious of sonochemical reactor in comparison with the stirred tank reactor. Some of the most important representative works on comparison of sonication with stirring for different applications are depicted in Table 2.3 In addition, the combination of ultrasonic irradiation with mechanical stirring has been studied by some researchers in order to achieve more uniform agitation. Table 2.4 depicts some important studies on combination of sonication and stirring.

Table 2.3: Overview of important works on comparison of sonochemical reactors and stirred vessels

| Ultrasonic properties | Impeller properties | Tank properties | Investigated parameters | Comments/ results | Ref. |
|---------------------------------------|----------------------------|--------------------------------|--|--|-------------------------|
| 20-540-1000 kHz / 67 W | - | 50 mm in diameter, 100 ml | micromixing times / viscosity | Ultrasound (US) may be as effective as classic stirring. | (Monnier et al., 1999a) |
| 20 kHz / 40 W | classical stirrer | - | volumetric permeate flux / dead-end ultrafiltration efficiency | Increment of US power as well as increment of stirrer speed leads to increase in efficiency. | (Simon et al., 2000) |
| 20 kHz / 750 W (41% of maximum power) | 4-blade impeller / 400 rpm | 55 mm diameter jacketed vessel | velocity of ink and sugar crystals | Uniform distribution of sugar crystals obtained in the vessel with | (Guo et al., 2007) |

Table 2.3: Continued

| | | | | | |
|------------------------------------|--|---|---|---|---------------------------|
| | | | | US / higher velocity variance with US. | |
| 24 kHz | Flat blade turbine with six blades (d = 5 cm, height of the blade/diameter = 0.2) / 300 – 1000 rpm | 1 gallon tank (Dinside = 17 cm, H = 20 cm, liquid fill level = 10 cm) with 4 baffles (width = 1.7 cm) | droplet size in Alkali Transesterification | The mean droplet size obtained by impeller mixing is 2.4 times larger than the US one. | (Wu et al., 2007) |
| 1.7 MHz | Rushton turbine impeller, diameter of 7.5 cm and bottom clearance of 4 cm | 2 L, diameter of 15 cm and height of 15 cm | Macromixing visualizing / micromixing characterizing and time / viscosity | By increasing the power input, the US reactor can reduce the micromixing time more effectively in comparison with the stirring one. | (Parvizian et al., 2011) |
| 1.7 MHz | Rushton turbine impeller, diameter of 7.5 cm and bottom clearance of 3 cm | diameter of 14 cm and height of 14 cm | Velocity distribution by CFD / Mixing time | More uniform velocity distribution in the sonochemical reactor / the average axial circulation time is 7.12 and 1.3695 s for the stirred tank and sonochemical reactor, respectively. | (Parvizian et al., 2012b) |
| 24 kHz / 400 W / The amplitude are | adjustable from 0 to 2000 rpm. | - | Flux enhancement, power dissipated by stirrer and ultrasonic | Flux enhancement is much higher for the US-assisted | (Liu et al., 2013a) |

Table 2.3: Continued

| | |
|------------------------------------|------------------|
| adjustable from 20% to 100%. | microfiltration. |
|------------------------------------|------------------|

Table 2.4: Overview of important works on coupling of sonication and stirring

| Ultrasonic properties | Impeller properties | Tank properties | Investigated parameters | Comments/ results | Ref. |
|--------------------------------|-------------------------------|---|-------------------------------------|--|-------------------------|
| 20 kHz / 50-100- 150 W | Rushton turbine | Three cylindrical glass vessel 100, 500, 3750 ml (semi-batch reactor) | micromixing time | Coupling of Rushton turbine to ultrasound was not efficient. More interesting was the coupling of a propeller (at low velocity) with ultrasound. | (Monnier et al., 1999b) |
| 1 MHz / 2 W/cm ² | Motor driven plastic stirrer, | - | Acceleration of enzymatic plasma | If ultrasound was applied together with stirring, only 30% acceleration by ultrasound was documented. | (Sakharov et al., 2000) |
| 20 kHz / 30-60-250 W | 6-blade impeller / 300 rpm | continuously irradiated stirred tanks / 3.2 and 6.4 l | Kinetic and time | This reactor was efficient in enzymatic saccharification of various waste papers. | (Li et al., 2005) |
| 20 kHz / max 500 W | Simple impeller | - | Nanoparticle distribution in system | Nanoparticle dispersion improved. | (Goyat et al., 2011) |

2.5.1 CFD Simulation of Fluid Flow

Since, it is impossible to cover all unknown parameters experimentally or mathematically and regarding the lack of numerical studies on investigating the effects

of power ultrasound waves on micromixing efficiency, Computational Fluid Dynamics (CFD) was employed as an opportunity to compare the behaviours of fluid flow in sonoreactor and stirred vessel (Patel et al., 2010). CFD can provide useful information for regions with intense or mild turbulence zones, Reynolds stresses, vortex structures, circulation patterns, flow behaviour and many other parameters (Ding et al., 2010). The system such as high power sonoreactors that was employed in this research is categorized as the turbulent flow system. This system is complex to model because of the occurrence and interaction of turbulence, local dispersed concentration and distribution and fluid flow (Leng and Calabrese, 2004). In order to optimise and control these systems, exact understanding on dispersed phase distribution and its transient behaviour under different practical operations is of major importance. In addition, these concepts are the key parameters for mass, momentum and energy transfer between dispersed and continuous phases (Bouyatiotis and Thornton, 1967).

Dahnke and Keil (Dahnke and Keil, 1999) presented the first numerical study of ultrasound wave irradiation by considering three-dimensional time-dependent wave equations through finite differences approach. They investigated homogenous and non-homogenous distribution of cavitation bubbles, the impact of ultrasound pressure on bubble generation and their volume fraction. Osterman et al (Osterman et al., 2009) studied the shape and collapse of a single bubble in a 33 kHz-ultrasound pressure field using a 2D finite-volume modelling. They reported a good agreement between the experimental observation and simulation results. Few studies also have been conducted on prediction of cavitation position using CFD modeling (Laborde et al., 2000; Servant et al., 2000). Laborde et al. (2000) studied the initiation of acoustic cavitation and bubble behaviour under ultrasound irradiation with a frequency range of 20–800 kHz in a cylindrical sonoreactor using CFD simulation combined with a mathematical modelling. They investigated the influence of the acoustic fountain on the wave

propagation. In the other work done by Jamshidi et al. (Jamshidi et al., 2012), the authors analysed the effect of chamber configurations on acoustic streaming generation and propagation of ultrasound waves with frequency of 20kHz and power of 200Watt. They investigated the attenuation of pressure caused by generation of cavitation bubbles. The acoustic pressure distribution, acoustic fountain shape and sound absorption coefficient in a sono-reactor with an acoustic amplitude of 10, 30 and 50 W, and frequency of 490 kHz were numerically simulated by Xu et al (Xu et al., 2013). CFD was also successfully employed in analysing the effect of ultrasound irradiation on heat transfer. Wan and kuznetsov (Wan and Kuznetsov, 2003) studied the efficiency of sound waves (with frequency of 160 Hz) for enhancing heat transfer between two parallel beams. Lin and Farouk (Lin and Farouk, 2008) also studied the effects of a vibrating sidewall on heat transfer in a rectangular chamber with heated horizontal walls.

A series of works have been carried out by Abolhasani et al (Abolhasani et al., 2012) for high-frequency (1.7MHz) and low-power ultrasound. They studied the micro mixing and heat transfer in this range by employing the ultrasound waves as the input sinusoidal pressures. In two other works, Parvizian et al. (Parvizian et al., 2012b) and Liu et al. (Liu et al., 2013b) used a similar model to investigate acoustic streaming in a high-frequency sono-reactor and an airlift sonobioreactor by using CFD simulation respectively. Both substituted the plane form of sound pressure waves using the Helmholtz equation with compressible Navier-Stocks equations along with the Rayleigh-Plesset equation. Recently, Jiao et al (Jiao et al., 2014) have investigated the influence of ultrasound irradiation on mass transfer coefficient by using the same model along with the inhomogeneous Helmholtz equation. They reported that mass transfer coefficient increased with temperature, ultrasound power and frequency but decreased with decreasing transducer diameters and distance between the reactors and ultrasound

sources. However, application of ultrasound energy still suffers from the lack of knowledge in this area. Optimizing design, scaling up, temperature controlling and working with stable condition are the main obstacles due to complexity of the interactions between the ultrasound energy with liquid media. Besides, analyzing the ultrasonic wave distribution in liquid media and the generation of cavitation bubbles (cavitation) is still a challenge since not all phenomena are quantified and well understood.

The use of ultrasonic in laboratory scale and industrial areas has increased in recent years. Acoustic cavitation is the most significant characteristics of sonochemical reactors leading to high effective temperature and pressure locally, high shear stress near the bubble wall, creation of microjets, etc. which can provide an appropriate situation for numerous applications (Gogate et al., 2011). The three main systems where sonoreactors can be applied effectively are presented as following subsections.

2.6 Gas-Liquid Systems

About 25% of chemical processes such as wastewater treatment, aerobic fermentations and biological production (organic acids, alcohols, antifoams, alkaloids, antibiotics, proteins) occur between gas phase and liquid phase (Cachaza et al., 2009) Ultrasound irradiation has been used in many of these processes in order to enhance the kinetics or selectivity.

A literature review on the effects of type and concentration of different gases on ultrasonic cavitation processes was carried out by Rooze et al (Rooze et al., 2012).

Petrier et al (Pétrier et al., 2007) applied the ultrasound irradiation for eliminating volatile and non-volatile aromatic compounds from water by inducing oxygen. They reported that hydroxyl radicals can be produced by cavitation bubbles in the

sonochemical reactor and as a result these hydroxyl radicals react with organic compounds in the water shell around the bubble. Gogate and Katekhaye (Gogate and Katekhaye, 2012) also studied the effect of introduction of air as an additive to a model reaction of potassium iodide oxidation in ultrasonic horn and ultrasonic bath reactors. Their experiments show that presence of air in the system generates more numbers of gas bubbles which can improve the cavitational activity.

In addition, the use of sonochemical reactors can be beneficial in filtration process. The process of filtration is generally carried out by using a porous medium for separating two phases (gas-liquid or solid-liquid) (Gallego-Juárez et al., 2003). Ultrasonic irradiation can assist the performance of membrane-based filtration devices by countering their disadvantages such as membrane fouling, short lifetime, high costs and mechanical complexity.

2.7 Liquid-Liquid Systems

Sonochemical reactors have been applied in many of chemical reactions and processes at the liquid-liquid phase. Under suitable operating parameters, ultrasonic can considerably decrease the time of reactions and also increase the reaction yield (Gogate, 2008). Determination of the oxidative stability of edible oils is a typical example of oxidation which is significantly accelerated by ultrasonic (Canizares-Macias et al., 2004; Priego-Capote and Luque de Castro, 2004). In environmental area, the ultrasonic decomposition of toxic organic compound such as phenolic compounds, aromatic compounds, esters and textile dyes into the short chain organic acid, inorganic ions or carbon dioxide can be carried out 10,000 times faster than natural oxidation (Adewuyi, 2001; Chitra et al., 2004).

Dissolution process is another application of sonochemical reactors. Dissolution of soluble sample is generally accomplished by mechanical or manual stirring, which is

usually time-consuming and it leads to random error as a result of manipulation. Ultrasonic energy can be applied to assist the dissolution process with the purpose of saving time and accelerating the dissolution of great variety of samples (Yebra et al., 2004). Furthermore, low frequency irradiation of ultrasonic with high intensity can be combined with fibrinolytic therapy for dissolving clots in pharmacological thrombolysis in order to reduce the treatment time (Birnbaum et al., 1998).

Recently, one of the most important application of sonochemical reactors is in biodiesel production (Choudhury et al., 2013; Kumar et al., 2011; Gole and Gogate, 2012a). Biodiesel can be defined as an alternative fuel that is produced from animal fats or vegetable oils. It, chemically, includes mono alkyl esters of long chain acids existed in the animal fats or vegetable oils' triglycerides. Biodiesel can be regarded as a renewable fuel due to the fact that the feedstock is plant or animal derived. It also consists of less amounts of polycyclic aromatic hydrocarbons, sulfur or metals compared to petrodiesel (Vasudevan and Briggs, 2008).

The properties of biodiesel are similar to those of petrodiesel. However, the diesel index, cetane number and also the flashpoint of biodiesel is higher than those of diesel oil. Therefore, it is easier to operate and handle. The diesel index and cetane number of biodiesel is higher. The lower ash content and sulphur content of biodiesel made it more environmentally friendly in comparison with fossil fuels (Agarwal and Das, 2001).

Nowadays, most biodiesel is made through procedures which are on the basis of transesterification reaction. Figure 2.10 demonstrates the fundamental procedure of this reaction. The raw materials usually include refined vegetable or seed oil. This oil reacts with alcohol together with suitable catalysts in order to produce glycerol and biodiesel. Crude glycerol and crude biodiesel's layers are later set apart and improved to yield

glycerol and biodiesel. The alcohol can be recovered during the process get recycle in to the tank.

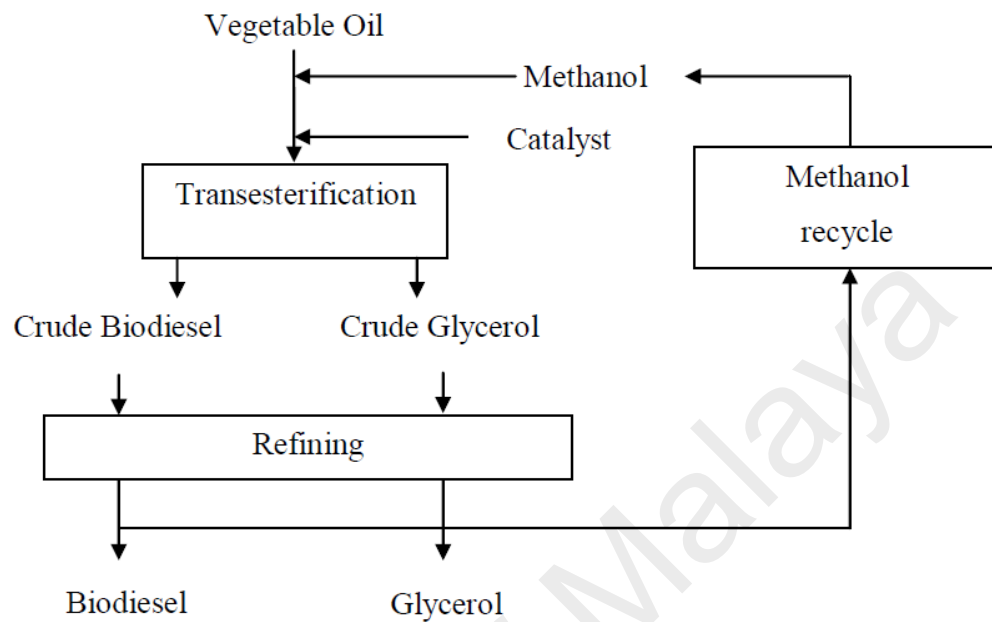


Figure 2.11: Schematic representation of biodiesel production using transesterification process

2.7.1 Transesterification Reaction

Transesterification refers to a reaction between an alkyl alcohol and a triglyceride. The products of this reaction are glycerol as the side product and fatty acids alkyl esters or biodiesel as the main product. Figure 2.12 shows the transesterification reaction using methanol.

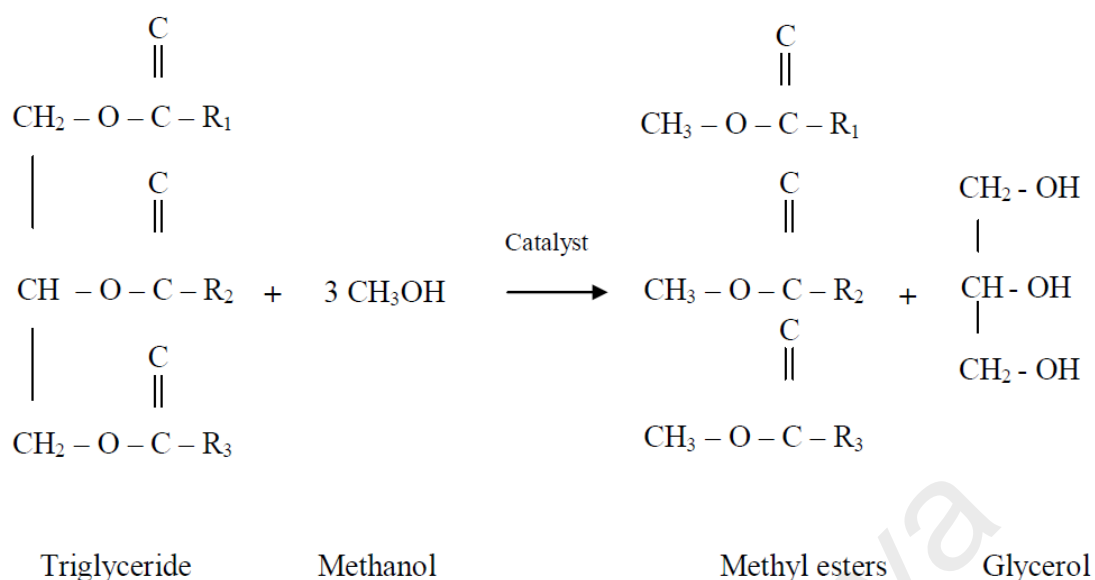


Figure 2.12: Reaction route of transesterification with methanol

In the above equation, R_1 , R_2 and R_3 are long fatty acid chains. An excess amount of alcohol is usually utilized for the purpose of increasing in the conversion rate. The transesterification reaction can be accomplished by using three moles of methanol for each mole of triglycerides. Different types of catalysts also can be utilized in order to increase the reaction time.

The presence of water as well as fatty acids in the oil can cause side reactions that influence the final conversion rate. By disconnecting carbon chains from the glycerol backbone, the free fatty acid will form. Some of the most common free fatty acids in vegetable oils and animal fats are palmitic, stearic, oleic, linoleic and linolenic acid (Van Gerpen, 2005). The structure of oleic acid as an example of a common free fatty acid in vegetable oils is shown in Fig. 2.13.

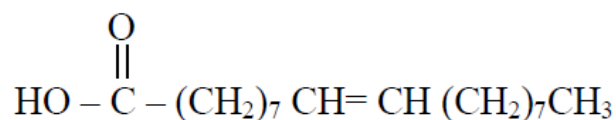


Figure 2.13: Structure of oleic acid

Saponification reaction as shown in Figure 2.14, is one of the side reactions of transesterification, i.e. the soap is produced through the reaction of free fatty acids and alkali catalysts such as sodium hydroxide or potassium hydroxide. As a result, saponification reaction will reduce the yield of main reaction by consuming the catalyst.

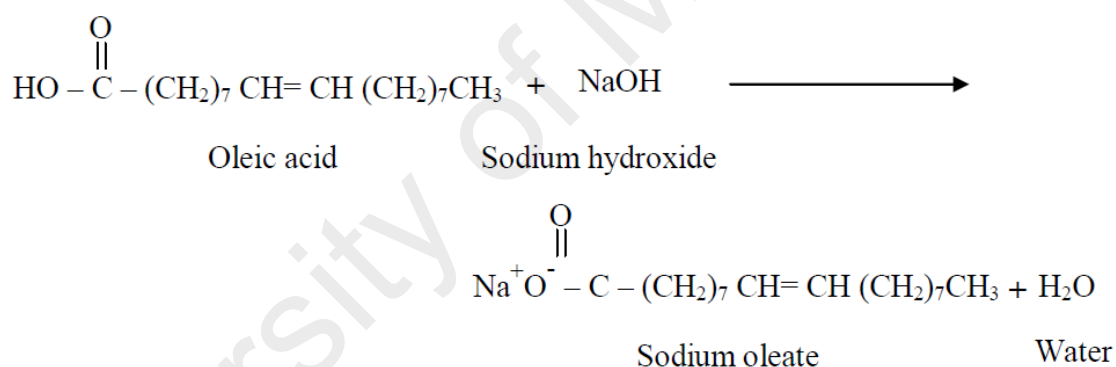


Figure 2.14: Side reaction of saponification in transesterification process

For the purpose of forming free fatty acids, water reacts with triglyceride in oil and hydrolyses it. Saponification happens in the presence of free fatty acids and soap will produce in the system as well as the biodiesel. The produced soap will reform to solid in the room temperature and as a result the mixture of reaction cannot be recovered easily (Van Gerpen, 2005). The reaction between water and triglyceride that lead to the production of fatty acid and diglyceride is shown in Figure 2.15.

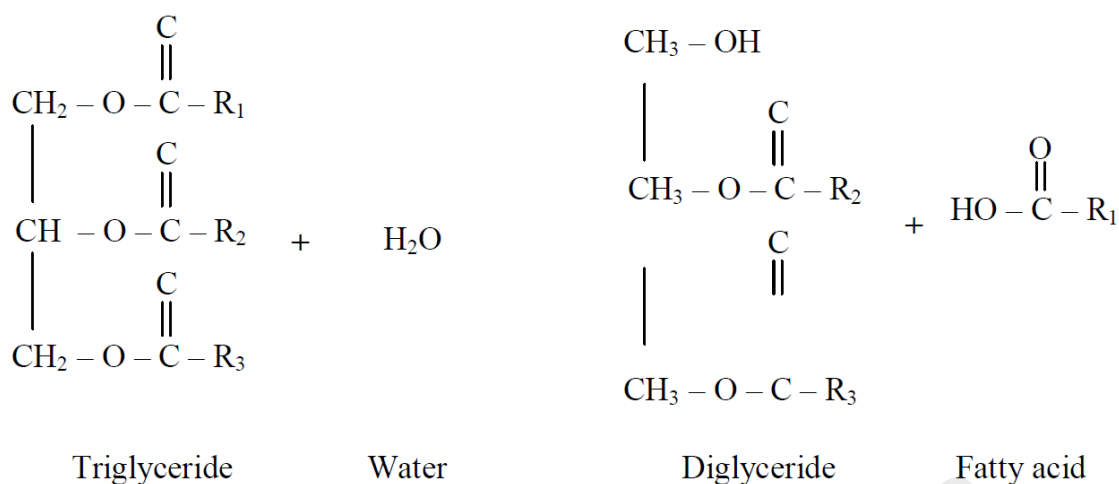


Figure 2.15: Side reaction of water with triglyceride in transesterification process

2.7.2 Biodiesel Quality

One of the most significant elements in the development of *in situ* transesterification that needs to be considered is that if the process is capable of supplying the market with biodiesel of adequate quality to fulfill the requirement of governing bodies. ASTM D6751 and EN 14214 are the two most important standards. Haas and Scott (Haas and Scott, 2007) compared the biodiesel obtained from the *in situ* transesterification of soybean flakes with the ASTM D6751 standard and they cited that excluding the acid number test, their produced biodiesel passed all the other tests.

2.8 Solid-Liquid Systems

Solid-liquid system also is a significant part of chemical industries and mineral processing which contains leaching, adsorption, digestion, precipitation, etc (Bong et al., 2015). Ultrasound irradiation can greatly promote the solid-liquid processes as well as gas-liquid and liquid-liquid processes.

Ultrasonic-assisted extraction has usually been accomplished in terms of solid-liquid extraction and liquid-liquid extraction in order to remove a number of analytes from

various types of samples (Capelo et al., 2004; Huang et al., 2003; Miege et al., 2003). Sonochemical reactors can be effectively applied for various extraction operations due to high temperature and pressure which enhance solubility and penetration between different phase interface, and oxidative energy of the radicals released by sonication of the solvent (Chu et al., 2003; Romdhane and Gourdon, 2002; Rostagno et al., 2003).

Priego-Capote and Luque de Castro (Priego-Capote and Luque de Castro, 2004) reviewed about sixty experimental studies on continuous and discontinuous ultrasonic-assisted leaching applications and concluded that in many cases, using ultrasonic-assisted leaching was more beneficial compared with conventional or microwave-assisted leaching due to higher efficiency and kinetics. *In situ* transesterification is also another application of sonochemical reactors in solid-liquid phase. During *in situ* transesterification the grinded seeds contact directly with alcohol and as a result oil extraction and transesterification carry out in one step.

In solid-liquid filtration process ultrasonic-based devices can enhance the membrane permeability by increasing the diffusion of a solute in membrane barrier for electrolyte membrane dialysis and also by removing particles from the filters (Wang et al., 2000). Ultrasonic irradiations is not only used for analytical laboratory applications, but also for analyzing the raw samples by dissolving the minerals in metallurgical industries (St Slaczka, 1986). The most significant advantage of ultrasonic in comparison with other equipment is that it needs only the presence of liquid medium for transmission of energy.

2.8.1 *In Situ* Transesterification

In situ transesterification process refers to the direct transesterification of oil bearing seeds. In this method, biodiesel is produced from the direct contact of grinded seed with alcohol and as a result oil extraction and transesterification carry out in one step.

However, in the traditional transesterification process the seeds must go through several processes after grinding. These processes include: mechanical pressing, solvent extraction, degumming and esterification. These four steps can be reduced to one by using *in situ* transesterification (Georgogianni et al., 2008b; Amalia Kartika et al., 2013). Using fewer unit operations is the most significant advantage of *in situ* transesterification which can reduce the major cost and also time of process.

The other difference of *in situ* transesterification process with the conventional one is the outputs. The output of conventional transesterification includes alkyl esters, alcohol, glycerol and unused catalyst while in *in situ* transesterification, the solid meal from the grinded seeds also will remain after the reaction. This meal need to be separated from the other products by using a simple filtering process. However, the other purification steps for conventional and *in situ* transesterification are similar, including recycling of alcohol, washing and separating the biodiesel from the other products.

2.8.2 Parameters in *In Situ* Transesterification

(a) *Raw Materials*

From the literature, different kinds of oil bearing materials such as sunflower seed, rapeseed, soybean, palm oil pulp and wastewater sludge have been investigated by researchers in order to apply as raw materials for *in situ* transesterification process (Harrington and D'Arcy-Evans, 1985; Kildiran et al., 1996; Mondala et al., 2009). The amount of fatty acids of the oils extracted from each seed is different, thereby the yield of reaction is different for each feedstock (Ramos et al., 2009).

Haas et al. (Haas et al., 2007) studied the *in situ* transesterification for other oil bearing materials such as distillers dried grains with soluble (DDGS) and meat/bone meal (MBM). Although these materials bear low percentages of oil, however high conversion rates of 91% and 93% to biodiesel was achieved for DDGS and MBM, respectively. In

another study, Dufreche et al. (Dufreche et al., 2007) were carried out *in situ* transesterification by using sewage sludge as feedstock and they converted 6.23% of dried sludge to biodiesel.

(b) *Type of Catalyst*

Based on the literature, *in situ* transesterification cannot be carried out without using catalyst (Kildiran et al., 1996; Qian et al., 2008). Presence of catalyst assists in crashing the cell wall of the seed and as a result alcohol can contact with oil in the cotyledon cell. Acid catalyst like sulphuric acid has been used for *in situ* transesterification firstly by Harrington and D'Arcy-Evans (Harrington and D'Arcy-Evans, 1985). They could successfully convert 98% of oil from sunflower seeds to biodiesel by utilizing methanol and sulphuric acid as catalyst.

Acid catalysts are mostly suitable for transesterification of feedstocks with high amount of free fatty acids. Alkaline catalyst will be consumed rapidly by contacting with high amount of free fatty acids due to the saponification reaction. The produced soap also will emulsify the final products and make the separation process of glycerol from biodiesel more difficult. Mondala et al. (Mondala et al., 2009) utilized acid catalyst for transesterification of wastewater sludge which include 65% free fatty acids by weight.

On the other hand, the reaction time is longer when utilizing acid catalyst compared to alkaline one. Normal reaction time, based on the literature, for *in situ* transesterification by acid catalyst is between 12 to 24 hours, however the same conversion level can be obtained by using alkaline catalyst in less than one hour. In 2004, Haas et al. (Haas et al., 2004) successfully used alkaline catalyst for *in situ* transesterification of soybean for the first time. However, the amount of methanol that they consumed in their process was much more than the one that was used in a conventional transesterification process such as the work was carried out by Freedman et al (Freedman et al., 1984).

(c) **Catalyst Concentration**

Catalyst concentration can be considered as the most significant parameter for specifying the conversion rate in transesterification process (Yuan et al., 2008; Vicente et al., 2007). Zeng et al. (Zeng et al., 2008) calculated the biodiesel yield and conversion rate for various concentration of alkaline catalyst in *in situ* transesterification. They reported that the effect of catalyst concentration on biodiesel yield was negligible, however the conversion rate of methyl esters was influenced by this parameter significantly. In low concentration of sodium hydroxide they obtained 93% of biodiesel yield with only 30% of conversion rate, while in higher catalyst concentration they achieved biodiesel yield and conversion rate of 95% and 98%, respectively.

However, in another study, Qian et al. (Qian et al., 2008) cited that the biodiesel yield for *in situ* transesterification of cottonseed increased from 33% to 97% by increasing the catalyst concentration from 0.05 mol/L to 0.1 mol/L. The observed contrast in the results could be due to the difference in the raw materials of each study, since the various seeds demonstrate various features in the process.

(d) **Moisture Content**

The presence of moisture in the feedstock causes saponification reaction in transesterification process. This reaction reduces the yield of products and makes the separation process of biodiesel from glycerol more difficult. In addition, Haas et al. (Haas and Scott, 2007) mentioned that less moisture content in the feedstock can decrease the required amount of alcohol and catalyst in *in situ* transesterification process.

They reduced the amount of methanol and sodium hydroxide required up to 40% and 33%, respectively, by drying the feedstock in a convection oven and reducing the moisture content to 2.6%. They also reported that the required amount of methanol and

sodium hydroxide can be reduced to 60% and 56%, respectively, by reducing the water content in feedstock to zero.

(e) ***Mixing Intensity***

Georgogianni et al., studied the effects of mechanical stirring and sonication mixing on *in situ* transesterification of cottonseed and sunflower in two different research (Georgogianni et al., 2008b; Georgogianni et al., 2008a). Experiments were carried out under stirrer speed of 600 rpm and ultrasonic frequency of 24 kHz. No considerable variation in the reaction yield was reported for *in situ* transesterification with methanol, whereas by using ethanol, the conversion rate was higher under ultrasound irradiation compared to mechanical mixing. Ultrasonication resulted in high yield of 98% in 40 min, however lower conversion rate of 88% was obtained under mechanical mixing for both cottonseed and sunflower. They also claimed that ultrasonic mixing causes less saponification reaction because no stirring is needed.

(f) ***Molar Ratio of Alcohol to Seed***

The cost of products in *in situ* transesterification mostly determines by the amount of alcohol consumed in this process (Core, 2005). Amalia Kartika et al. (Amalia Kartika et al., 2013) studied the methanol to seed ratio between 2 ml/g to 6 ml/g in their work with alkali catalyst, while Shuit et al. (Shuit et al., 2010) examined the ratio of 7.5 ml/g with acid catalyst. However, the typical range of alcohol to oil ratio in *in situ* transesterification process is from 100:1 to 800:1 which is extremely higher than this ratio in conventional transesterification (Siler-Marinkovic and Tomasevic, 1998; Haas et al., 2004).

Many researches have been carried out in order to reduce the amount of required alcohol in transesterification process. Using co-solvent in conventional transesterification causes an improvement in alcohol solubility and as a result an

increment in product yield (Boocock et al., 1996). Qian et al. (Qian et al., 2008) investigated the possibility of utilizing petroleum ether as co-solvent in their study and they could increase the rate of oil extraction up to 3%. Zeng et al. (Zeng et al., 2008) studied the effect of diethoxymethane (DEM) as co-solvent in *in situ* transesterification and reported a reduction in the amount of required methanol.

(g) Temperature

In conventional transesterification process, temperature effects on mass transfer, thereby the conversion rate increases by increasing the temperature (Noureddini and Zhu, 1997). In addition, high temperature can reduce the required alcohol to oil ratio (Haas et al., 2004). However, in *in situ* transesterification some researchers reported that temperature cannot effect on reaction rate significantly (Haas and Scott, 2007) and some others claimed that increasing temperature can considerably effect on biodiesel yield (Liu and Zhao, 2007). The contrast in obtained results could be due to the difference in the feedstocks and also in other operating parameters such as type of catalyst and mixing method. Moreover, an optimal point for temperature based on the feedstock can be reached.

(h) Particle Size

The size of seeds' particles has a significant effect on *in situ* transesterification process, since they had a great importance role in conventional oil extraction process as well (Snyder et al., 1984). Ren et al (Ren et al., 2009) analyzed the influence of particle size on *in situ* transesterification of rapeseeds using SEM and light microscopy. They observed that all the oil was extracted from smallest size of particles in 60 min, but in the larger particle size, extraction was not carried out completely. By decreasing the particle size from 1000-1400 μm to 500 – 850 μm , and then to 300 – 500 μm , the conversion rate in 60 min increased from 43% to 65% and then to 86%. However,

Kildiran et al. (Kildiran et al., 1996) reported that oil extraction is higher for larger particle size in reaction time of 60 min, while increasing the reaction time led to increase in the yield for smaller particle sizes.

2.8.3 *Jatropha Curcas*

In this study *Jatropha curcas* (*J. curcas*) seed was chosen as feedstock due to the fact that it is uneatable and its oil properties are much the same as that of rapeseed. Moreover, growing on nearly all kind of soil is another advantage of this seed. The focus of studies on biodiesel is presently on using inedible oils and one of the most promising inedible oils that can be utilized for this purpose is *J. curcas*. Based on reports, in 2014, *J. curcas* was planted five million globally in the whole world and Asia is the majority of its planted areas.

(a) *General Background*

The word *Jatropha* came from two Greek words of *jatros* and *trophe* which mean doctor and food, respectively. The literal meaning of this word shows that *Jatropha* had medicinal applications in the past. *Jatropha* species are large shrubs or small trees from *Euphorbiaceae* family. The plants are capable of surviving in harsh condition. They can grow up to seven meters. Becker and Makkar (Becker and Makkar, 2008), tried to grow *J. curcas* on degraded lands and they could successfully obtain fruit after 9 months. The plant also fruited on coastal sand dunes in which the level of organic carbon, nitrogen and phosphate are very low in comparison with fertile lands.

The greatest numbers of *Jatropha* species are toxic due to containing phorbol esters, lectins and curcin. The toxic feature of this plant provides a protection against different diseases and pests. It also protects the plant from being consumed as a food source of ruminant animals. The *Jatropha* seed contains two parts; the shell and kernel. Crude protein and crude fat are the two most important components of kernel while shell

consists of different kinds of fibre. The amount of moisture in shell is higher than kernel while kernel contains more gross energy compared to shell.

J. curcas is the most often cited *Jatropha* species in literature among over 170 known *Jatropha* species. Central America is where genus *Jatropha* originally came from. However, it has spread throughout the globe and nowadays it can be found mostly in countries such as Nigeria, India, Malaysia, Thailand and Mozambique.

(b) *Jatropha* as a Fuel Source

Different scholars examined *Jatropha* as a fuel source. Banerji et. al., (Banerji et al., 1985) carried out a comparative study on the fatty acid profile of four various *Jatropha* species; *J. curcas*, *J. glandulifera*, *J. gossypifolia* and *J. multifida*. They reported that all of the four different species of *Jatropha* are appropriate for producing methyl ester, while *J. curcas* contained 48% of oil which was the highest among the four species. *J. multifida* was also found to have the highest value of energy.

Among the *Jatropha* species, *J. curcas* is the most common species, specifically due to its high oil content. It has been applied in engines directly (Kumar et al., 2003) or used in transesterification processes (Foidl et al., 1996; Chhetri et al., 2008; de Oliveira et al., 2009).

(c) *Characteristics and Composition of J. curcas*

An important role is played by the characteristics and composition of *J. curcas* in order to determine the suitability of the oil as a fuel source. The fatty acid composition of *J. curcas* oil is shown in Table 2.5 (Becker and Makkar, 2008). In general, the oil is mostly constituted by oleic acid (C18:1) and linoleic acid (C18:2). The other majority of fatty acid contains palmitic acid (C16:0) and stearic acid (C18:0). The chemical and physical properties of *J. curcas* oil are also presented in Table 2.6.

Table 2.5: Fatty acid composition of *J. curcas* oil (Becker and Makkar, 2008)

| Systematic name | C:D | Scientific name | Percentage (%) |
|-----------------|------|----------------------------------|----------------|
| Myristic | 14:0 | Tetradecanoic | 0.1 |
| Palmitic | 16:0 | Hexadecanoic | 15.3 |
| Heptadecanoic | 17:0 | Heptadecanoic | 0.1 |
| Palmitoleic | 16:1 | 9-hexadecanoic | 0.9 |
| Stearic | 18:0 | Octadecanoic | 6.6 |
| Oleic | 18:1 | <i>cis</i> -9-octadecanoic | 41 |
| Linoleic | 18:2 | <i>cis</i> -9-12-octadecadienoic | 35.3 |
| Linolenic | 18:3 | 9,12,15- octadecatrienoic | 0.3 |
| Arachidic | 20:0 | Eicosanoic | 0.2 |
| Behenic | 22:0 | Docosanoic | trace |
| Lignoceleric | 24:0 | Tetracosanoic | 0.1 |

C:D = carbon chain: no. of double bond.

Table 2.6: chemical and physical properties of *J. curcas* oil (Becker and Makkar, 2008; Achten et al., 2008)

| | Range |
|---------------------------------------|---------------|
| Specific gravity (g/cm ³) | 0.860-0.933 |
| Calorific value (MJ/ kg) | 37.83 – 42.05 |
| Pour point (°C) | -3 |
| Cloud point (°C) | 2 |
| Flash point (°C) | 210 – 240 |
| Cetane value | 38.0 – 51.0 |
| Iodine value | 102 |
| Saponification number (mg/g) | 102.9 – 209.0 |
| Viscosity at 30°C (cSt) | 37.00 – 54.80 |
| FFA % (kg/kg *100) | 0.18 – 3.40 |
| Unsaponifiable % (kg/kg *100) | 0.79 – 3.80 |

Table 2.6: Continued

| | |
|-------------------------------|------------------|
| Iodine Number (mg iodine/g) | 92 – 112 |
| Acid number (mg KOH/g) | 0.96 – 6.16 |
| Monoglycerides % (kg/kg *100) | nd – 1.7 |
| Diglycerides % (kg/kg *100) | 2.50 – 2.70 |
| Triglycerides % (kg/kg *100) | 88.20 – 97.30 |
| Carbon residue % (kg/kg *100) | 0.07 – 0.64 |
| Sulfur content % (kg/kg *100) | 0 – 0.13 |
| Cetane value Iodine value | 38.0 – 51.0 102* |
| nd = not detected | |

(d) *J. Curcas* versus other Inedible Oils

Composition of fatty acids is the most significant parameter for recognizing biodiesel properties. There are different kinds of compositions in plant oils. Four various non-edible oils' fatty acid compositions are listed in Table 2.7 (Azam et al., 2005). These plants can be considered as the most investigated non-edible plant in biodiesel research.

Table 2.7: Composition of fatty acids in various non-edible oils (Azam et al., 2005).

| Fatty acid | C:D | <i>J. curcas</i> | <i>P. pinnata</i> | <i>S. oleidis</i> | <i>A. indica</i> |
|------------|------|------------------|-------------------|-------------------|------------------|
| (%) | | | | | |
| Capric | 10:0 | | | 0.8 | |
| Lauric | 12:0 | | | 35.6 | |
| Myristic | 14:0 | 1.4 | | 50.7 | |
| Palmitic | 16:0 | 15.6 | 10.6 | 4.5 | 14.9 |
| Stearic | 18:0 | 9.7 | 6.8 | | 14.4 |
| Oleic | 18:1 | 40.8 | 49.4 | 8.3 | 61.9 |
| Linoleic | 18:2 | 32.1 | 19 | 0.1 | 7.5 |

Table 2.7: Continued

| | | | | |
|------------|------|-----|-----|-----|
| Arachidic | 20:0 | 0.4 | 4.1 | 1.3 |
| Eicosenoic | 20:1 | | 2.4 | |
| Behenic | 22:0 | | 5.3 | |
| Lignoceric | 24:0 | | 2.4 | |

Cetane number (CN) and iodine value (IV) are two of the most significant parameters in biodiesel properties. CN refers to a measure of the ignition properties of fuel and IV uses for measuring the amount of unsaturation in the fatty acids. Higher CN causes shorter ignition delay in the engine and results in premier performance as fuel. While, high IV levels in oil can cause different problems including polymerisation of the oil which results in deposits to be formed on engine parts (Van Hoed, 2010). Based on the EN 14214 standard, the biodiesel CN should be more than 51 and the IV should be less than 120 gI₂/100g. The CN and IV for the four mentioned inedible oils are presented in Table 2.8.

Table 2.8: CN and IV for various inedible oils (Azam et al., 2005).

| Property | Unit | <i>J. curcas</i> | <i>P. pinnata</i> | <i>S. oleidis</i> | <i>A. indica</i> |
|----------|-----------------------|------------------|-------------------|-------------------|------------------|
| CN | - | 52.31 | 55.84 | 7.6 | 57.83 |
| IV | gI ₂ /100g | 93 | 80.9 | 66.13 | 69.3 |

Muniyappa et al. (Muniyappa et al., 1996) studied the relationship of the viscosity, density and cloud point of biodiesels from beef tallow oil and soybean. Based on their findings, the high cloud point achieved for methyl ester from beef tallow oil was because of saturated fatty esters' high concentration. *J. curcas*, *P. pinnata* and *A. indica* are three of non-edible oils with high percentage of unsaturated fatty acids. Therefore,

there is a low possibility that they face this problem. *J. curcas* includes 72.9% of unsaturated fatty acid, however *A. indica* and *P. pinnata* both include both include 68.4%.

Among the four non-edible oils mentioned above, *J. curcas* is the best choice to be used as feedstock for biodiesel production. Though the CN of the *J. curcas* is the lowest among the four, it is still in the EN 14214 minimum range. Oleic (18:1) and linoleic (18:2) acids constitute the most fatty acid composition of *J. curcas* oil which both are unsaturated fatty acids. Therefore, oil's high cloud point with high percentage of saturated fatty acids will be avoided.

Animals cannot eat *J. curcas*, since it is a toxic plant. Furthermore, it is capable of growing on even non-fertilize lands. The plant can also resist for a long time without water and is resistant to disease (Becker and Makkar, 2008). Since *J. curcas* can be grown in arid land, its cultivation would not decrease the amount of available fertile land for food crops. The current tropical forest, savannah or grassland environments which are significant for the carbon cycle will not be affected by *J. curcas*. Little or no carbon debt would be involved through using arid, semi-arid, degraded and barren farm land. This would provide benefits concerning managing greenhouse gas emissions and helping countries such as India with wide areas of wasteland (Fargione et al., 2008; Searchinger et al., 2008). Francis et al. (Francis et al., 2005) discussed the issues in the reclamation of such wastelands. Moreover, they carried out a detailed study on the possibility of increasing the socio-economic profiles related to degrade areas from the planting of *J. curcas*.

2.9 Summary of Literature Review

On the basis of the literature review, sonochemical reactors are gaining attention from researchers and the industries. Ultrasound energy has appeared as a promising way to

overcome transfer limitations and enhance mass transfer compared to the same process in the absence of ultrasonication. However, they are still not widely used industrially due to unavailability of information about their features and performance. Frequency of irradiation and ultrasonic power are the most significant operating parameters in sonochemical reactors. Lower frequencies (<100 kHz) are suitable where the physical effects are required and higher frequency can be used for chemical effects.

Mass transfer, mixing time, flow pattern and reaction yield can be considered as the most important factors for evaluating the performance of sonochemical reactors. The knowledge of hydrodynamic characteristics and mixing behavior is important for selecting the reactor dimensions and position of ultrasonic transducers.

Uniform distribution of cavitation activity in reactor is one of the most important challenges in scale up design of sonochemical reactors. However, it should be considered that in spite of higher operating costs of these reactors in comparison with the conventional stirred vessels, sonochemical reactor can be economically beneficial due to their special features such as acoustic cavitation and acoustic streaming. In addition, CFD simulation presented as a computational method for comparing sonoreactors with stirred vessels by visualizing fluid flow patterns in different systems.

Ultrasound irradiation also can successfully improve the transesterification process which is the main synthesis method for biodiesel production. Transesterification can be defined as the reaction of refined, bleached vegetable oil with alcohol in the presence of alkali or acid catalysts. However, the refining and bleaching of the vegetable oils for using as the raw material in this process cost around 75% of overall expenditure (Haas et al., 2006). In order to reduce the costs and time of this reaction, the possibility of applying another approach, called *in situ* transesterification, has been investigated.

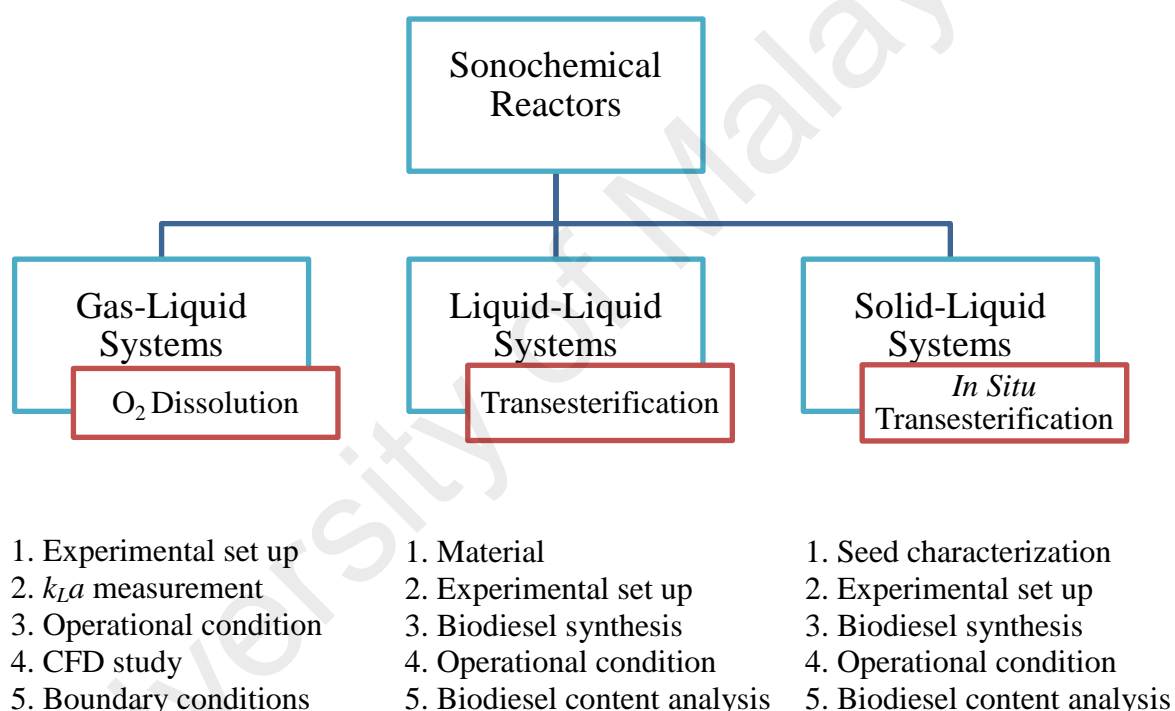
CHAPTER 3: METHODOLOGY

As it is mentioned, this research conducted by three parts including the effects of ultrasound irradiation on: i) Gas-liquid system. ii) Liquid-liquid system. iii) Solid-liquid system. Thereby, for the first part, experiments were design based on the dissolution of oxygen in water and determining the volumetric gas-liquid mass transfer coefficient. The first experiments investigated the effect of ultrasound irradiation on mass transfer in different liquid volumes. From this study, the appropriate size of tank was chosen and applied throughout the study. The other parameters such as viscosity, superficial gas velocity, temperature, stirrer speed and ultrasonic horn position also were studied using a design of experiments-based matrix.

In the second part design of experiment was used to design the experiments on transesterification of *J. curcas* oil for biodiesel synthesis and response surface methodology was used to study the effects of the independent variables that affect the biodiesel yield and conversion rate. The variables considered for the studying of this liquid-liquid operation including ultrasonic power, methanol to oil molar ratio, catalyst concentration, reaction time and reaction temperature. In addition, in another set of experiment, the obtained biodiesel yield and conversion rate in sonochemical reactor were compared with the results of conventional transesterification under mechanical mixing. The analytical studies of produced biodiesel were also performed using gas chromatography-mass spectroscopy (GC-MS).

Investigating the effects of ultrasonication on solid-liquid system starts with the characterisations of the oilseeds as the solid phase by determining the amounts of oil and moisture content. Five main parameters involved in *in situ* transesterification process were then analyzed individually, including ultrasonic power, methanol to seed ratio, catalyst concentration, reaction time and reaction temperature. This was followed

by studying the mutual effects of operating parameters on biodiesel production. Response Surface Methodology (RSM) coupled with Central Composite Design (CCD) was used for the design, statistical analysis and evaluation of the interaction between operating parameters. A comparison between traditional *in situ* transesterification using mechanical stirring and that under ultrasound energy was also carried out. The relationship between different parts of this chapter is presented in Figure 3.1.



3.1 Gas-Liquid Experiments; Mass Transfer in Air-Water System

Air-water mass transfer experiments were carried out in two reactors with different liquid volume in order to investigate the effect of ultrasound irradiation on gas-liquid systems. In the first set of experiments mass transfer was studied under ultrasonication in 2 L liquid volume and the second set of experiments were carried out in 200 mL liquid volume. Figure 3.2 presents the details of experiments and studied parameters in this section.

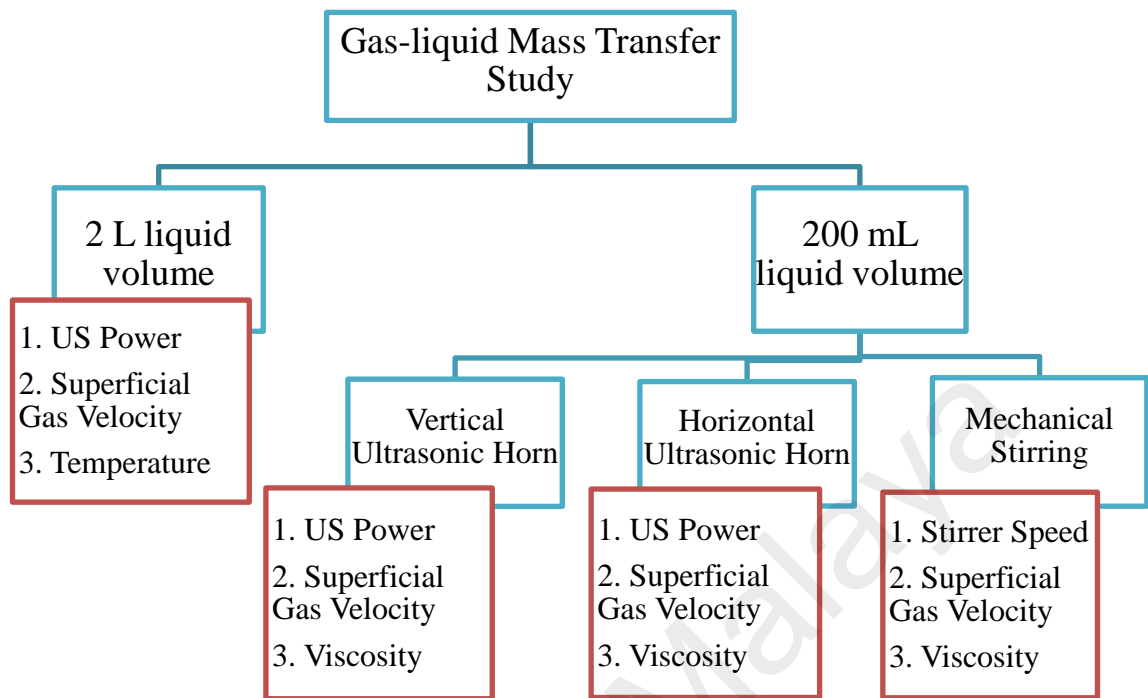


Figure 3.2: The details of experiments and studied parameters in section 3.1.

3.1.1 Experimental Set Up

The first part of experiments were carried out in a 0.15 m diameter Perspex tank using an ultrasonic horn with variable amplitudes and cycles (Ultrasonic Processor model UP400S; Dr. Hielscher GmbH, Stuttgart, Germany). The ultrasonic equipment used operated with a maximum intensity of 400 W and fixed frequency of 24 kHz. Air was directed into the medium using a Tubing stainless steel gas sparger with a diameter of 0.05 m and equipped with 19 holes with a diameter of 0.001 m. The liquid volume was 2 L in all experiments and the temperature of the liquid was kept constant with an error of ± 2 °C using a recirculating chiller and a cube Perspex jacket. Figure 3.3 shows the experimental setup for the experiment.

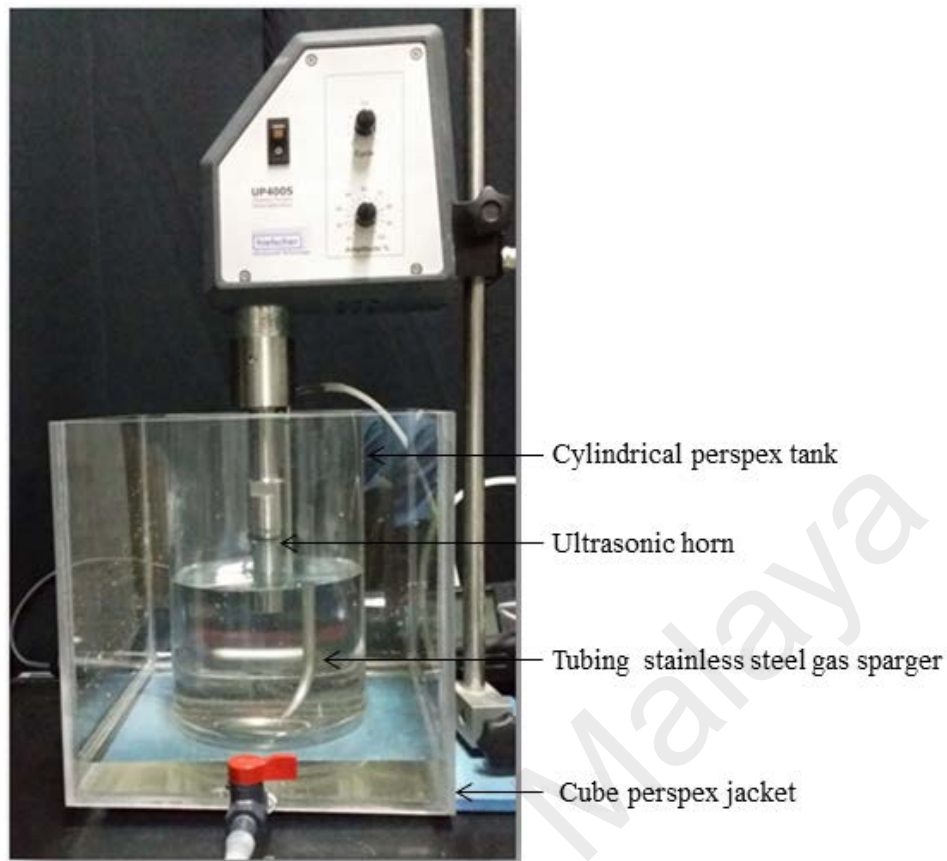


Figure 3.3: Experimental set up for gas-liquid mass transfer experiments.

The second part of experiment was carried out in a 0.1 m diameter glass tank using the same ultrasonic horn. Air was directed into the 200 mL of liquid medium at 25 °C using a porous rubber sparger. The effect of ultrasonic irradiation on temperature can be considered negligible in these sets of experiments due to the short time of each experiment. In addition, different percentages of glycerol (10-50 %) were added into the water in order to investigate the effect of viscosity on gas-liquid mass transfer coefficient.

Three different sets of experiments were carried out in 200 mL liquid volume setup. In the first set, ultrasonic horn was submerged into the liquid phase vertically from the top of the vessel and dipped 10 mm inside the medium. In the second set of experiments, ultrasonic horn tip was located into the system horizontally in order to investigate the

effect of horn position on k_La . The distance of ultrasonic horn from the bottom of the tank was 15 mm. Last set of experiment have been done using a magnet stirrer instead of ultrasonication in order to compare the efficiency of mechanical and ultrasonic mixing.

3.1.2 Volumetric Gas-Liquid Mass Transfer Coefficient (k_La) Measurement

Dynamic gassing-in method have been used for measurement of volumetric gas-liquid mass transfer coefficient (k_La) which is known as a fast and experimentally simple method for various systems (Gogate and Pandit, 1999). In this method, the dissolved oxygen concentration in the water is initially reduced to zero by sparging nitrogen gas. The system is then kept stationary for a few minutes so that all the nitrogen bubbles are allowed to escape from the liquid. The ultrasonic horn is then turned on and oxygen gas is added into the system. The difference of dissolved oxygen concentration with time is recorded by a dissolved oxygen meter every 5 seconds until the liquid is almost saturated by oxygen. The overall volumetric gas-liquid mass transfer coefficient in transient state in the reactor can be measured using the following equation (Kumar et al., 2005):

$$k_La \cdot V(C^* - C_t) = V \cdot \frac{dC_t}{dt} \quad (3.1)$$

Where, V is the liquid volume in the reactor, C^* is the saturated dissolved oxygen concentration, C_t is the dissolved oxygen concentration at any time t in the reactor.

After integration, Equation (3.1) transforms into below:

$$\ln \left(\frac{C^* - C_0}{C^* - C_t} \right) = k_La \cdot t \quad (3.2)$$

A plot of the left-hand side of Equation (3.2) and time provides a straight line with a slope of k_La . This procedure was used for all experiments in this study.

3.1.3 Study of Main Parameters

Response Surface Methodology (RSM) coupled with Central Composite Design (CCD) was used for design, statistical analysis and evaluation of the interaction between operational parameters. Central Composite Design (CCD) is one of the most frequently applied designs for RSM to create a second order model for the responses (Sakkas et al., 2010). CCD is a factorial or fractional factorial design with centre points, enhanced with a group of axial points. In this research, Design-Expert 8.0.5 software was employed for experimental design, model development and statistical analysis.

For each set of experiments, a three-level full factorial design of experiments with six replicates at the center point was employed to prepare a regression model to correlate the three independent experimental variables with the gas-liquid mass transfer. For the experiments in 2 L liquid volume, the range and level of the three independent variables comprised temperature, X_1 , gas flow rate, X_2 and ultrasonic power, X_3 . Their coded levels for CCD are displayed in Table 3.1. The studied range was 240-400 W for ultrasonic intensity; 5-10 L/min for gas flow rate, and 10-50 °C for temperature. The required number of experiments that consisted of 8 factorial runs, 6 fixed axial runs and 6 replications of centre points were carried out in randomized sequence to reduce the effects of uncontrolled parameters (Shafeeyan et al., 2012). The value of “ α ” which shows the distance of the axial point from the centre was fixed at 0.5.

Table 3.1: Independent variables and their coded levels for the CCD for 2 L liquid volume experiments

| Variables | Code | Coded variable level | | |
|-----------------------|-------|----------------------|--------|--------|
| | | -1 | 0 | 1 |
| Temperature (°C) | X_1 | 10.00 | 30.00 | 50.00 |
| Gas Flow Rate (L/min) | X_2 | 5.00 | 7.50 | 10.00 |
| Ultrasonic Power (W) | X_3 | 240.00 | 320.00 | 400.00 |

For the experiments in 200 mL liquid volume, The range and level of the three independent variables comprised viscosity, X_1 , superficial gas velocity, X_2 and ultrasonic power (Impeller speed for last set of experiment), X_3 , and their coded levels for CCD are displayed in Table 3.2 The studied range was 200-400 W for ultrasonic intensity; 1.17-3.53 m/s for superficial gas velocity, and 1-6 cP for viscosity.

Table 3.2: Independent variables and their coded levels for the CCD for 200 mL liquid volume experiments

| Variables | Code | Coded variable level | | |
|--------------------------------|--------|----------------------|--------|--------|
| | | -1 | 0 | 1 |
| Viscosity (cP) | X_1 | 1 | 3.5 | 6 |
| Superficial Gas Velocity (m/s) | X_2 | 1.17 | 2.35 | 3.53 |
| Ultrasonic Power (W) | X_3 | 200.00 | 300.00 | 400.00 |
| Impeller Speed (rpm) | X_3' | 300.00 | 420.00 | 540.00 |

Response Surface Methodology (RSM) method has been verified as a reliable statistical tool in the analysis of chemical processes (Arami-Niya et al., 2012; Ghotli et al., 2013). RSM has been proposed to reduce the number of experiments and analyze the interaction between variables (Myers et al., 1989; Shafeeyan et al., 2012).

The predicted responses were fit into the following quadratic polynomial regression model according to the independent variables and their interactions:

$$Y = \beta_0 + \sum_{i=1}^n \beta_i x_i + \sum_{i=1}^n \beta_{ii} x_i^2 + \sum_{i=1}^n \sum_{j>1}^n \beta_{ij} x_i x_j \quad (3.3)$$

where Y is the predicted response; x_i and x_j are the coded values; β_0 , β_i , β_{ij} and β_{ii} are the constant, linear, interaction and quadratic coefficients, respectively (Arami-Niya et al., 2012; Sahu et al., 2009). The significance of the models, factors, coefficients and regression were assessed statistically through the variance analysis (ANOVA).

3.1.4 Computational Fluid Dynamic Study

3.1.4.1 Theoretical Background

Continuity: Euler-Euler multiphase model was used in this study. In this model, the dispersed phase is described as the interpenetrating continua and the equations for conservation of mass and momentum are solved for both gas and liquid phases. In our previous study, Mixture model which could be combined with Keller-Miksis or Rayleigh model in order to investigate the cavitation generation and measure the total cavity volume fraction was employed (Sajjadi et al., 2015a; Sajjadi et al., 2015b). However, the focus of this study is on the interactive effects of acoustic jet-like streaming and mass transfer in a bubble. Therefore, the Eulerian scheme was more reliable. Accordingly, the mass conservation equation for each phase is defined as follows:

$$\frac{\partial}{\partial t}(\rho_i \alpha_i) + \nabla \cdot (\alpha_i \rho_i \vec{U}_i) = 0.0 \quad (3.4)$$

In this equation, ρ_i represents the density; α_i denotes the volume fraction and \vec{U}_i stands for the mean velocity for phase i (Gas or Liquid). The total volume fractions of the liquid and gas phases equals to unity in the cells domain since they are assumed to share space in proportion to their volume.

$$\alpha_L + \alpha_G = 1.0 \quad (3.5)$$

Gas-Liquid Mass transfer: The volumetric mass transfer coefficient was calculated based on the liquid mass transfer coefficient k_L and the interfacial area a , using Higbie's penetration theory:

$$k_L = \frac{2}{\sqrt{\pi}} \sqrt{D_{O_2}} \left(\frac{k \rho_L}{\mu_L} \right)^{1/4} \quad (3.6)$$

Where, D_{O_2} is oxygen diffusion coefficient ($2.01 \times 10^{-9} \text{ m}^2/\text{s}$) and k is the turbulence kinetic energy. ρ_l and μ_l denote the liquid density and viscosity, respectively. The interfacial area a , is also defined as a function of the local Sauter mean diameter (d_{32}) and local gas volume fraction (α_G):

$$a = \frac{6\alpha_G}{d_{32}} \quad (3.7)$$

Momentum: The momentum conservation equation for phase i is defined as:

$$\frac{\partial}{\partial t} (\rho_i \alpha_i \bar{U}_i) + \nabla \cdot (\alpha_i \rho_i \bar{U}_i \bar{U}_i) = -\alpha_i \nabla p + \nabla \cdot \bar{\tau}_{effi} + \bar{R}_i + \bar{F}_i + \alpha_i \rho_i \bar{g} \quad (3.8)$$

Where, the terms p , R_i and g denote the pressure shared by the two phases, interphase momentum exchange and gravity acceleration, respectively.

The term $\bar{\tau}_{effi}$ on the right hand-side of Equation (3.8) represents Reynolds stress tensor related to the mean velocity gradients using Boussinesq hypothesis which is defined as

$$\bar{\tau}_{effi} = \alpha_i (\mu_{lam,i} + \mu_{t,i}) (\nabla \bar{U}_i + \nabla \bar{U}_i^T) - \frac{2}{3} \alpha_i (\rho_i k_i + (\mu_{lam,i} + \mu_{t,i}) \nabla \cdot \bar{U}_i) \bar{I} \quad (3.9)$$

Turbulence model equations: In Equation (3.10), $\mu_{t,L}$ represents the turbulent liquid viscosity which is formulated through $\mu_{t,L} = \rho_L C \mu (k_L^2 / \varepsilon_L)$. In this study, standard k - ε turbulence model was employed for prediction of k_L and ε_L through:

$$\frac{\partial}{\partial t} (\rho_L \alpha_L k_L) + \nabla \cdot (\rho_L \alpha_L \bar{U}_L k_L) = \nabla \cdot \left(\alpha_L \frac{\mu_{t,L}}{\alpha_k} \nabla k_L \right) + \alpha_L G_{kL} - \alpha_L \rho_L \varepsilon_L + \alpha_L \rho_L \Pi_{kL} \quad (3.10)$$

$$\frac{\partial}{\partial t}(\rho_L \alpha_L \varepsilon_L) + \nabla \cdot (\rho_L \alpha_L \vec{U}_L \varepsilon_L) = \nabla \cdot \left(\alpha_L \frac{\mu_{t,L}}{\alpha_k} \nabla \varepsilon_L \right) + \alpha_L (C_{1\varepsilon} G_{kL} - C_{2\varepsilon} \rho_L \varepsilon_L) + \alpha_L \rho_L \Pi_{\varepsilon L} \quad (3.11)$$

$C_{1\varepsilon} = 1.44, C_{2\varepsilon} = 1.92, C_{3\varepsilon} = 0.09, \sigma_k = 1.0$ and $\sigma_\varepsilon = 1.3$ are the turbulent constants according to the recommendations of (Launder and Spalding, 1974).

Interfacial momentum exchange: Among different interphase forces, drag force plays an important role in the hydrodynamic studies. Drag force refers to the resistance experienced by a body moving in a liquid resulted from the mean relative velocity between two phases and turbulent fluctuations. In other words, viscous stress generates skin drag and viscous friction around the moving body is generated from drag. Drag force is proportional to the squared velocity of a turbulent flow. Accordingly, formulation of drag force is a key in simulation of multiphase flows.

Generally, interphase force is written as:

$$\vec{R}_L = -\vec{R}_G = K(\vec{U}_G - \vec{U}_L) \quad (3.12)$$

Where, K is the liquid-gas exchange coefficient which can be defined by Equation (12):

$$K = \frac{3}{4} \rho_L \alpha_L \alpha_G \frac{C_D}{d} |\vec{U}_G - \vec{U}_L| \quad (3.13)$$

In this Equation, d denotes the bubble diameter and C_D is the drag coefficient. In this study, drag coefficient was formulated through the Schiller-Neumann model as follows:

$$C_D = \begin{cases} \frac{24(1 + 0.15 \text{Re}^{0.687})}{\text{Re}} & \text{Re} \leq 1000 \\ 0.44 & \text{Re} > 1000 \end{cases} \quad (3.14)$$

where, Re is the relative Reynolds number for the dispersed phase (G) and the continuous phase (L).

In order to study the effect of ultrasound irradiation on mass transfer, Cai's model (Cai et al., 2009) was employed for defining ultrasound waves as acoustic pressure in the media:

$$P(t) = -P_a \sin \omega t \quad (3.15)$$

Here, $\omega = (2\pi f)$, c and $P_a = \sqrt{2\rho I_{US}}$ denote angular frequency, sound speed and intensity of ultrasound source. I_{US} refers to the ultrasound intensity. In doing so, acoustic pressure was written in a User Defined Function UDF and compiled in FLUENT to simulate the ultrasound waves and their interactive effect with the surrounding gas and liquid in this study. The programming codes were generated in Visual C++ (Version 6.0, Mathworks, Natick, MA).

3.1.5 Geometry and Boundary Conditions

As mentioned earlier, acoustic pressure was introduced through an inlet pressure with two different power amplitudes on piezoelectric transducer surface which was settled vertically in one geometry and horizontally in the other. Since the flow was axisymmetric in both sonicators, only half of the contactors were simulated and so a symmetrical boundary condition was considered. In the stirred tank, rotation of the pitched blade impeller was modeled with the Sliding Mesh (SM) method in which almost 20% of the vessel was considered stationary and the remaining (about 80%) was considered as the rotating region. The other boundary conditions defined for these geometries consisted of pressure outlet for the outlets, velocity inlet for sparger with the gas volume fraction equal to 1 and no-slip wall conditions for the lateral boundaries. More details about the boundary conditions of all the three systems are summarized in

Table 3.3 and Figure 3.4 (a, b, c). Besides, the initial gas holdups and the velocities of the fluids in all the three systems were set to zero.

Table 3.3: Defined boundary conditions in Low Frequency Sonicator and mechanical stirrer vessel.

| Ultra-Sono Reactor | | | | |
|---------------------------|--------|-----------------|-------|--|
| Boundary zone | Number | Type | Phase | Applied condition |
| Vessel | - | Fluid | Fluid | Stationary |
| Vessel top | 1 | Pressure Outlet | - | $P_{\text{gauge}}=0$ (pa) |
| Vessel bottom | 2 | Wall | - | Stationary, No slip |
| Vessel bottom center | | Velocity Inlet | Gas | Flow=0.117-0.353 m/s |
| Vessel wall | 3 , 4 | Wall | - | Stationary, No slip |
| | 5 | Symmetry | | Symmetry |
| Transducer | 6 | Pressure inlet | - | $P = P_A \cdot \sin[\omega(t)]$ Power=200-400Watt |
| Mechanical Stirrer Vessel | | | | |
| Vessel | - | Stationary | Fluid | Stationary |
| Vessel top | 1 | Pressure Outlet | - | $P_{\text{gauge}}=0$ (pa) |
| Vessel bottom | 2 | Wall | - | Stationary, No slip |
| Vessel bottom center | 2 | Velocity Inlet | Gas | Flow=0.117-0.353 m/s |
| Vessel wall | 3 | Wall | - | Stationary, No slip |
| Pitched blade impeller | | Wall | - | Stationary, No slip |
| Impeller motion model | 4 | SM | Fluid | Rotational velocity Rate=180-300RPM |

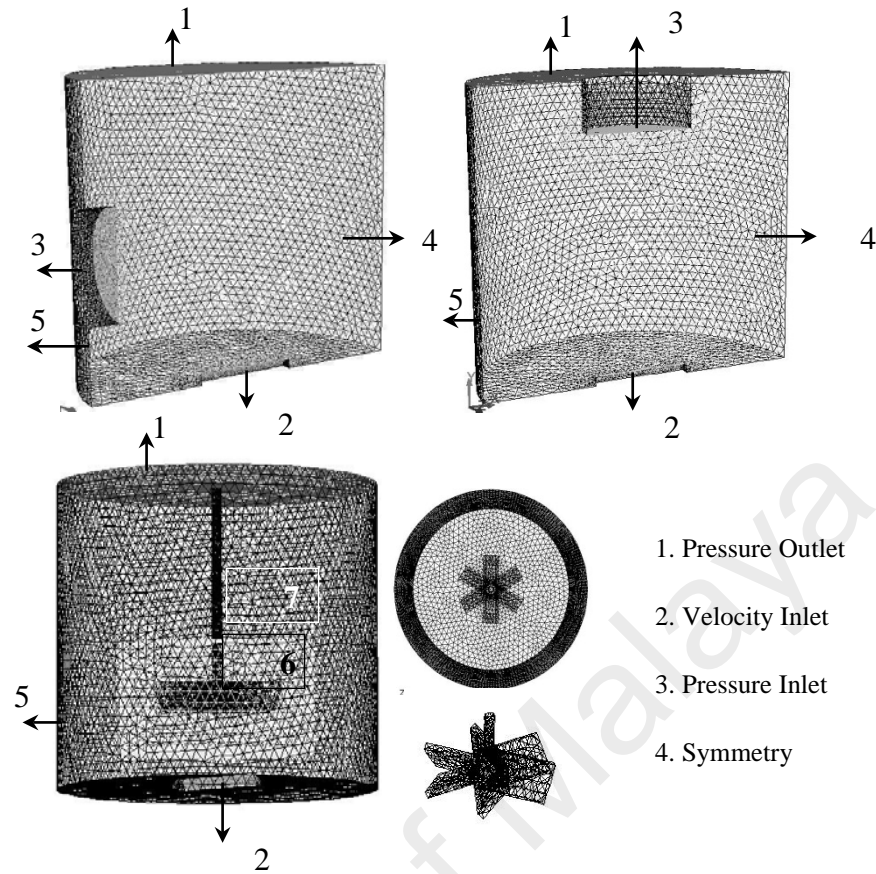


Figure 3.4: Computational domains of (a) Stirred vessel (b) HP-ultrasonicator, (c) VP-ultrasonicator geometries.

3.1.5.1 Simplification Assumptions and Justification

Table 3.4 lists the experimental tests selected for CFD simulation along with the responses of mass transfer for vertical ultrasound horn (V-US), horizontal ultrasound horn (H-US) and mechanically stirring (MS). It should also be noted that the mass transfer data were collected within 80 sec in experimental tests. However, it was not possible to simulate this duration. Therefore, the results related to the duration of 5 sec of experimental data were considered for the CFD simulation.

Table 3.4: Experimental design matrix and the final Mass transfer results in V-US, H-US and MS.

| Run | Type | Viscosity ($\text{kgm}^{-1}.\text{s}^{-1}$) | V_{gas} (m/s) | Mixing Intensity |
|-----|------|---|------------------------|------------------|
| | | | | US-Power |
| a1 | V-US | 0.001 | 0.117 | 200 |
| a2 | V-US | 0.001 | 0.117 | 400 |
| a3 | V-US | 0.001 | 0.353 | 200 |
| a4 | V-US | 0.006 | 0.117 | 200 |
| b1 | H-US | 0.001 | 0.117 | 200 |
| b2 | H-US | 0.001 | 0.117 | 400 |
| b3 | H-US | 0.001 | 0.353 | 200 |
| b4 | H-US | 0.006 | 0.117 | 200 |
| | | | | MS-Rotating rate |
| c1 | MS | 0.001 | 0.117 | 180 |
| c2 | MS | 0.001 | 0.117 | 300 |
| c3 | MS | 0.001 | 0.353 | 180 |
| c4 | MS | 0.006 | 0.117 | 180 |

In the present study, the fluid flow in all systems was assumed adiabatic, turbulent and transient with the initial velocity of zero. The liquid properties were set as pure water for glycerol 0%, $\rho_L=1083.7 \text{ kgm}^{-3}$ and $\rho_L=1123.6 \text{ kgm}^{-3}$, $\mu_L=0.006 \text{ kgm}^{-1}.\text{s}^{-1}$ for glycerol 50%. The properties of air was also set as $\rho_G=1.225 \text{ kgm}^{-3}$, $\mu_G=1.789 \cdot 10^{-5} \text{ kgm}^{-1}.\text{s}^{-1}$. Constant density was assumed since the pressure was almost the same throughout the vessel. Moreover, cavitation bubbles that may occur under high power ultrasound and their interaction with the liquid media were ignored and the effects of acoustic jet-like streaming and turbulent intensity on mass transfer were considered.

3.1.5.2 Numerical Solution of Equations

The solution domains investigated in this study are presented in Figure 3.4. ANSYS FLUENT (version 13.5) was used for geometry and mesh generating as well as combining and solving equations (3.4) to (3.15) numerically. The tanks' domains were discretized by an unstructured finite volume method, in order to convert the governing equations to algebraic equations that could be solved numerically (Sajjadi et al., 2013).

The SIMPLE pressure-velocity coupling algorithm along with the second-order upwind discretization scheme was used for all discretized terms. The solutions were considered to be converged when the normalized residuals of all the variables were less than 1×10^{-4} . Among different grid types and sizes tested in all the three systems, tetrahedral cells provided the best results. It was also found that pressure distribution was dramatically influenced by the grid size in all the three systems. Accordingly, 144488, 154223 and 330700 tetrahedral cells were generated for VP-Ultrasonicator, HP-Ultrasonicator and stirred vessel, respectively; consisting of the minimum and maximum of 0.3 and 1.5 mm for the elements quality. Finer grids were settled for in the vicinity of the probe in the ultrasonicator and the rotating region in the stirred vessel to obtain stable and reliable results. The quality of the meshes was presented in Figure 3.4 (a, b, c).

In unsteady-state simulations of the wave motion in the liquid, the time period of the sound wave should be considered bigger than the time step ($\tau_s = 1/f$). Accordingly, the value was set to quarter period of the ultrasound frequency (time step = $1e^{-6}$). Although higher time step could be used in the stirred vessel, the stability of the solution mainly depended on the time step at the starting point. Therefore, the calculation started with a very small time step size ($1e^{-7}$) followed by increment to $1e^{-5}$ to speed up the computation.

3.2 Liquid-Liquid Experiments; Transesterification Reaction

Transesterification reaction of *Jatropha curcas* oil for biodiesel synthesis was carried out under ultrasound irradiation in order to study the performance of sonochemical reactor for a liquid-liquid system.

3.2.1 Materials

RBD (Refined, Bleached and Deodorized) *J. curcas* oil was used as the triglyceride source. The oil was purchased from BATC (Bionas Agropolitan Technology Corridor) development Bhd, Malaysia. Methanol (99.9%) and n-hexane (99%) were provided from Sigma Aldrich and NaOH pellets as catalyst were provided from Merck companies, Malaysia.

3.2.2 Experimental Set Up

Transesterification experiments under ultrasound irradiation were carried out in a 400 ml stainless steel. A water bath was used for the vessel in order to control the temperature; a water condenser to reflux evaporated alcohol into the vessel and a thermometer to record the system temperature. The ultrasonication was done using an ultrasonic horn with various amplitudes and cycles (Ultrasonic Processor model UP400S; Dr. Hielscher GmbH, Stuttgart, Germany). It was operated with a fixed frequency of 24 kHz and maximum intensity of 200-400 W.

Transesterification under mechanical mixing was accomplished in a 500 ml glass flask as the reaction vessels. Mechanical stirring was carried out using a magnet stirrer. A water condenser and a thermometer were also used to reflux evaporated alcohol into the flask and to record the system temperature, respectively, as well as the sonochemical reactor. Figure 3.5 depicts the experimental set up for biodiesel synthesis under ultrasonic irradiation.

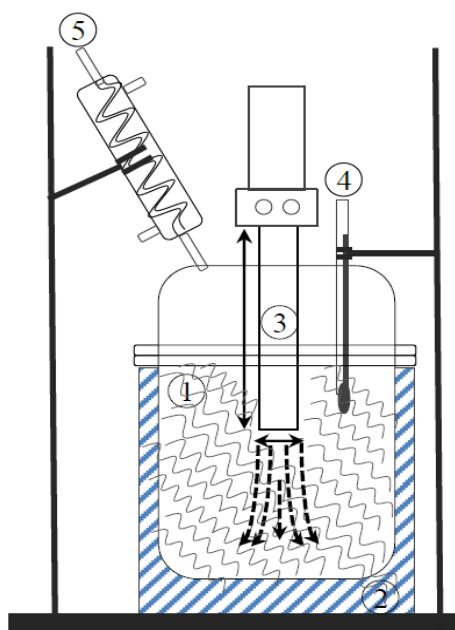


Figure 3.5: Experimental setup of transesterification under ultrasonic irradiation. 1. Reaction Vessel, 2. Water bath jacket, 3. Ultrasound probe, 4. Thermometer, 5. Condenser.

3.2.3 Biodiesel Synthesis

The reactors were initially filled with predetermined amount of *J. curcas* oil and heated to reaction temperature. Then, a pre-provided and pre-heated solution of methanol and sodium hydroxide was fed into the reactor. The sonication/stirring of the mixture was then started immediately with the specified sonication power/mixing intensity. After a sufficient duration of sonication/ stirring, glacial acetic acid (Fisher Scientific, UK) was added to the mixture to neutralize the catalyst and ensuring that the transesterification reaction had completely stopped. The product was then transferred into a separatory funnel for gravitational separation for 24 hours. Afterward, the obtained biodiesel was washed by distilled water and the excessive water and methanol were separated from the biodiesel by drying at 70 °C for 60 min. Figure 3.6 demonstrates schematic diagram of biodiesel production through transesterification process under ultrasonic irradiation.

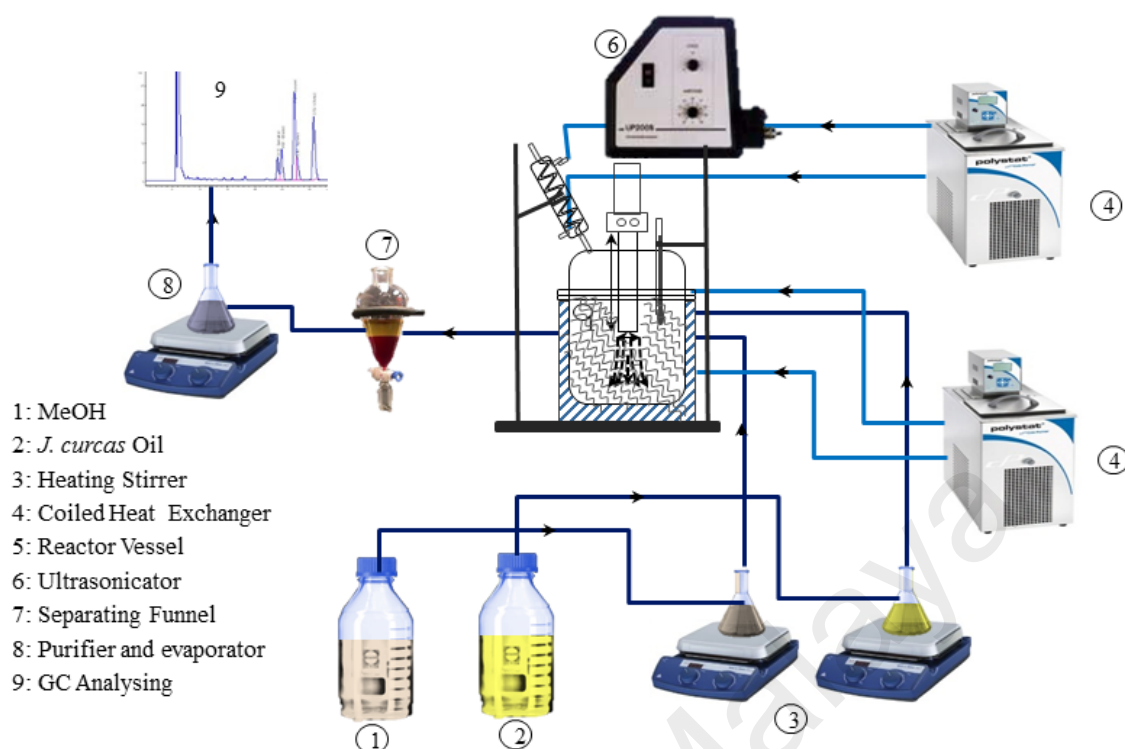


Figure 3.6: Schematic diagram of transesterification under ultrasonic irradiation.

3.2.4 Operational Conditions in Transesterification Reaction

In this section, two sets of experiments were considered to provide a deep insight into the transesterification of *J. curcas* oil into fatty acid methyl esters (FAME). The effects of reaction time, catalyst concentration, methanol to oil ratio, reaction temperature, mixing intensity and ultrasonic power on product yield and conversion rate were examined. The details of experiments and studied parameters in this section are presented in Figure 3.7.

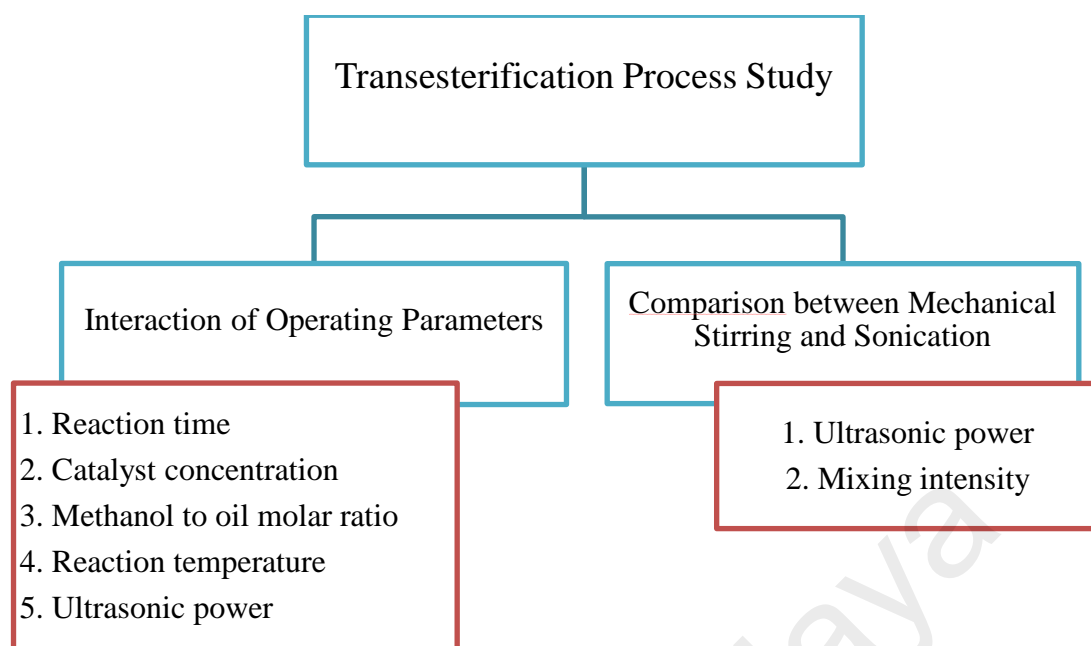


Figure 3.7: The details of experiments and studied parameters in this section 3.2.4.

3.2.4.1 Interaction of Operating Parameter

This set of experiments was designed by Response Surface Methodology (RSM) coupled with Central Composite Design (CCD) in order to statistically analyze the interactive effects of operating parameters, develop regression model and optimize the operating parameters.

The level and range of the five independent variables included reaction time, X_1 , catalyst concentration, X_2 , methanol to oil molar ratio, X_3 , reaction temperature, X_4 and ultrasonic power, X_5 , and their coded levels for CCD is shown in Table 3.5. The required number of experiments consisted of 10 fixed axial runs, 32 factorial runs and 8 replications of centre points which were carried out in a randomized sequence to reduce the effects of uncontrolled parameters.

Table 3.5: Independent variables and their coded levels for the CCD for transesterification experiments.

| Variables | Code | Coded variable level | | |
|-----------------------------------|----------------|----------------------|--------|--------|
| | | -1 | 0 | 1 |
| Reaction Time (min) | X ₁ | 10.00 | 30.00 | 50.00 |
| Catalyst Concentration (wt%) | X ₂ | 1 | 1.5 | 2 |
| Methanol to oil molar ratio (v/v) | X ₃ | 6 | 9 | 12 |
| Temperature (°C) | X ₄ | 30.00 | 40.00 | 50.00 |
| Ultrasonic Power (W) | X ₅ | 200.00 | 300.00 | 400.00 |

3.2.4.2 Effect of Mechanical Mixing

This set of experiments was carried out in order to compare the traditional transesterification of *J. curcas* oil under mechanical stirring with this novel one under ultrasound irradiation. One basic test with the condition of Catalyst: 1.5 wt%, methanol to oil molar ratio: 9, mixing intensity: 100 RPM, reaction temperature: 40 °C and reaction time of 30 min was considered in which the mixing intensity gradually increased up to 850 RPM. The study ranges of operating parameters in this work were according to the literature values

3.2.5 Biodiesel Content Analysis

The conversion rate of FAME in crude biodiesel product were determined using a GC-MS Ultra QP2010 (Shimadzu Scientific Instruments) with auto injector. The GC-MS was equipped with RTX5 column and helium was used as carrier gas. The initial temperature was held at 100 °C for 5 min, then increased at a rate of 10 °C/min to 250 °C and maintained at this temperature for 5 min. The standard test approach based on American Standard Test Method (ASTM) were used to determine the conversion rate in biodiesel (Knothe, 2006).

The biodiesel yield of transesterification process was determined according to following equation:

$$\text{Biodiesel Yield (\%)} = \frac{\text{Weight of obtained biodiesel (g)}}{\text{Weight of oil (g)}} \times 100 \quad (3.16)$$

3.3 Solid-Liquid Experiments; *In Situ* Transesterification Reaction

In situ transesterification reaction of *Jatropha curcas* seed for biodiesel synthesis was carried out under ultrasound irradiation in order to study the performance of sonochemical reactor for a solid-liquid system.

3.3.1 Characterisation of the Oilseed

Since *Jatropha curcas* (*J. curcas*) seeds, Figure 3.8, are used as feedstock in this work, this is essential to understand and confirm its properties. Therefore, characteristic studies on kernel oil and moisture were carried out in this section.



Figure 3.8: *J. curcas* seeds, the raw material in this research.

3.3.1.1 Oil Content Determination

J. curcas seeds were purchased from BATC (Bionas Agropolitan Technology Corridor) development Bhd, Malaysia, and stored in a dark and dry place. The oil content determination was performed based on the procedure described by the standard NF V

03-908. The *J. curcas* seeds placed in an oven at 100 °C for 24 hours and then the kernels were separated from the shells manually. The seeds then were ground for 5 min by a Kenwood blender (BL220 series, UK) for reducing the particle size and sieved until their size was not greater than 2 mm.

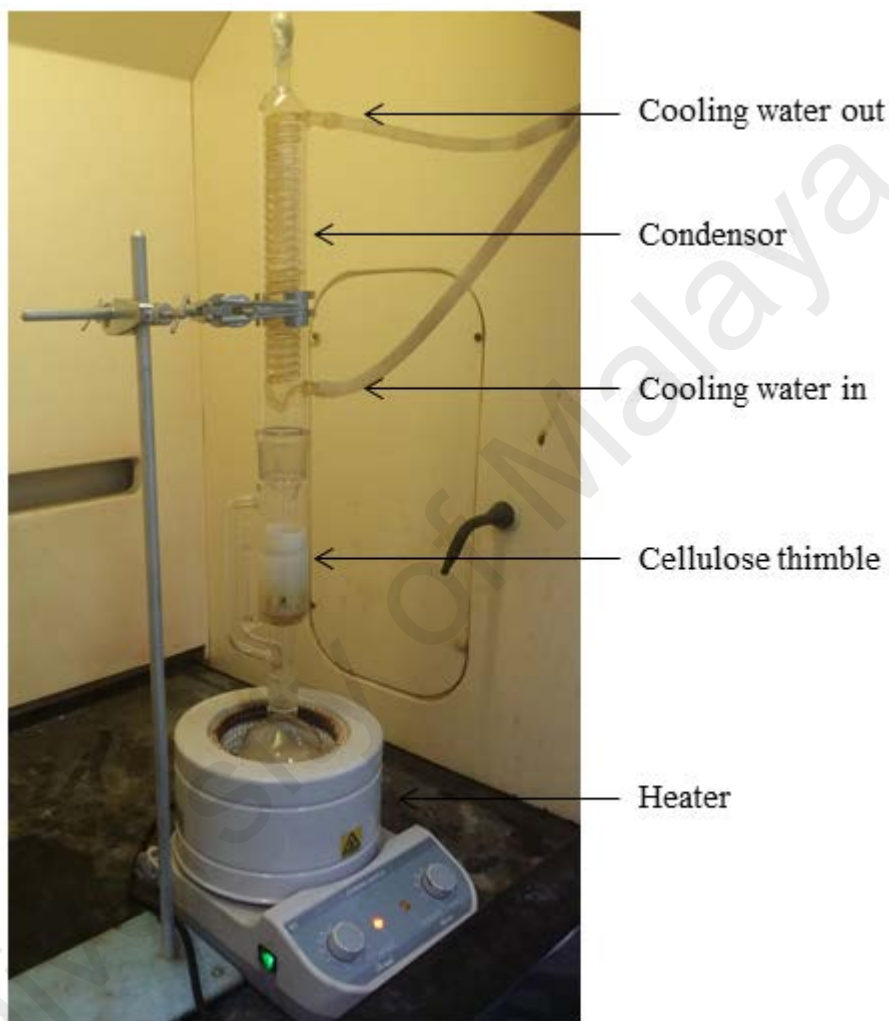


Figure 3.9: Picture of Soxhlet extraction apparatus.

Ten grams of grinded seeds were put into an extraction thimble and plugged using cotton wool. The thimble was placed in the Soxhlet extraction apparatus and hexane was used as solvent. The extraction was performed for 4 hours and then the extracted seeds were removed from the thimble and dried. The dried seeds were ground again and

extracted for another 2 hours. The solvent was then removed by using a rotary vacuum evaporator and the remaining oil was weighed. The amount of oil content was presented as percent by mass of the dry seed. Figure 3.9 shows the picture of Soxhlet extraction apparatus.

3.3.1.2 Moisture Content

The amount of moisture and volatile matter in the seeds were determined based on the method described by the British Standards Institution (BS EN ISO 665:2000). A flat-bottomed vessel was dried at 100 °C and weighted after 90 minutes, giving m_0 . Five grams of grinded oilseed (with particle size of less than 2 mm) were placed in the vessel and weighted, m_1 . The vessel was then put in an oven at 100 °C for 3 hours and weighted after it was cooled in room temperature, giving m_2 . The following equation was used in order to determine the mass percentage of moisture and volatile matter in the seeds.

$$w_m = \frac{m_1 - m_2}{m_1 - m_0} \times 100 \quad (3.17)$$

Where m_0 is mass of the vessel, m_1 is mass of the vessel and seed before drying and m_2 is mass of the vessel and seed after drying.

3.3.2 Experimental Set Up

In situ transesterification experiments under ultrasound irradiation were carried out in a 400 ml stainless steel as well as transesterification experiments. A water bath was used for the vessel in order to control the temperature; a water condenser to reflux evaporated alcohol into the vessel and a thermometer to record the system temperature. The ultrasonication was done using an ultrasonic horn with various amplitudes and cycles (Ultrasonic Processor model UP400S; Dr. Hielscher GmbH, Stuttgart, Germany). It was operated with a fixed frequency of 24 kHz and maximum intensity of 400 W.

In situ transesterification under mechanical mixing was accomplished in a 500 ml glass flask as the reaction vessels. Mechanical stirring was carried out using a magnet stirrer. A water condenser and a thermometer were also used to reflux evaporated alcohol into the flask and to record the system temperature, respectively, as well as the sonochemical reactor. Figure 3.10 depicts the experimental set up for biodiesel synthesis under mechanical mixing.

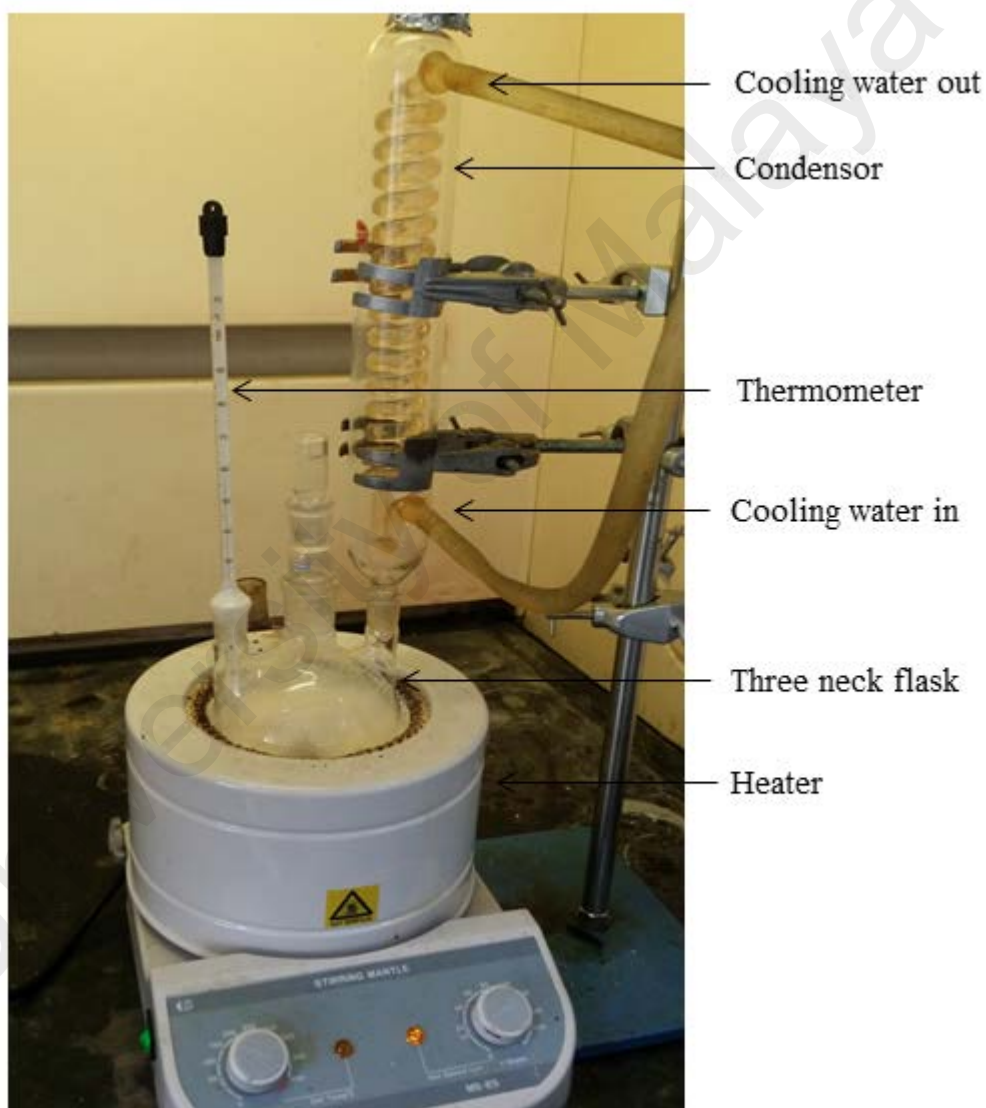


Figure 3.10: Experimental set up for biodiesel synthesis by mechanical stirring.

3.3.3 Biodiesel Synthesis

The *Jatropha curcas* seeds placed in an oven at 100 °C for 24 hours and then the kernels were separated from the shells manually. The seeds then were ground for 5 min by a Kenwood blender (BL220 series, UK) for reducing the particle size. The grinded seeds were sieved until their size was not greater than 2 mm.

In each experimental test, initially, a predetermined amount of methanol and sodium hydroxide which had been prepared earlier was transfer to the reaction vessel and heated to reach a favorable temperature. Then, the crushed seeds were fed into the reactor. In order to prevent the temperature drop caused by adding the crushed seeds, an extra heat was considered for the solution of methanol and sodium hydroxide to reach a higher temperature. Afterwards, a predetermined amount n-hexane (n-hexane to seed ratio (v/w) of 1:1) as co-solvent was then added in order to increase the oil solubility in the mixture.

The sonication of the mixture was then started immediately. After a sufficient duration of sonication, the product was cooled and filtered in order to separate the cake from the liquid mixture. The methanol and n-hexane were then recovered from the filtrate by a rotary evaporator and finally after the settlement two separate liquid layers were obtained. The upper layer which was yellow in color contained crude biodiesel and unreacted glycerides, while the lower layer which was dark brown contained glycerol. The mass of obtained biodiesel was measured after washing with warm water and drying at 70 °C for 60 min. Figure 3.11 demonstrates schematic diagram of biodiesel production under ultrasonic irradiation.

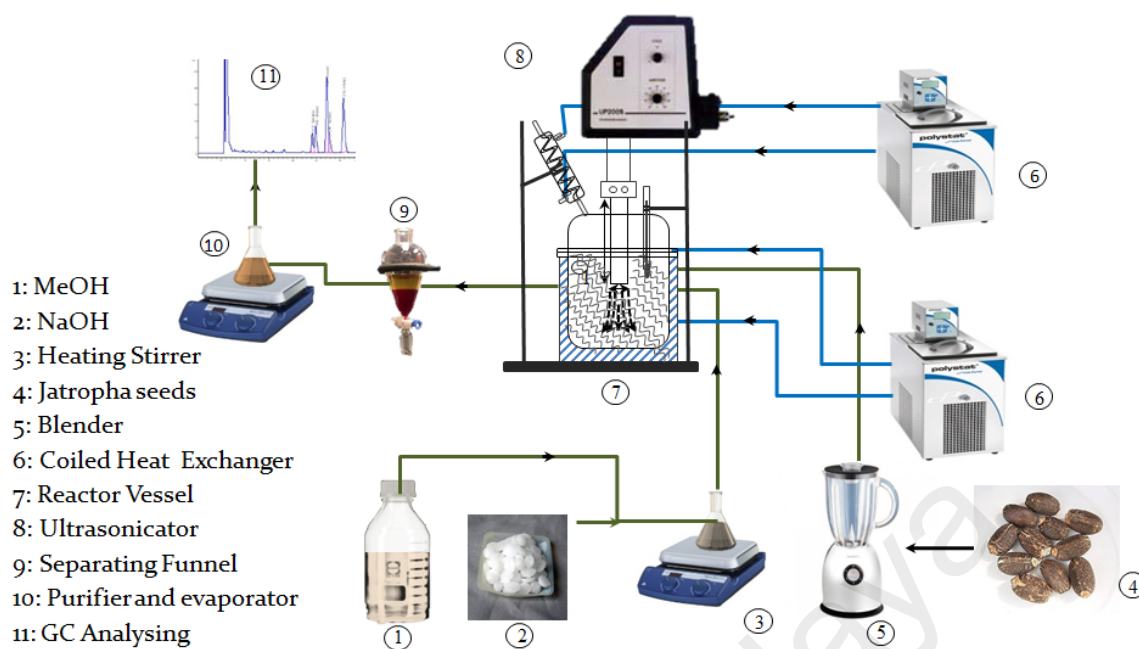


Figure 3.11: Schematic diagram of *in situ* transesterification under ultrasonic irradiation.

The effect of mechanical mixing on product yield and conversion rate was studied under the operating conditions of Catalyst: 0.1 mol/L in methanol, methanol:seed: 9:1, reaction temperature: 40 °C and reaction time of 30 min. Mixing intensity started from 100 RPM and gradually increased to 850 RPM in different tests. The same procedure as for ultrasound *in situ* transesterification was employed here except that mechanical mixing was applied instead of ultrasonication.

3.3.4 Operational Conditions in *In Situ* Transesterification

In this section, three different sets of experiments were considered to provide a deep insight into *in situ* transesterification of *J. curcas* seed into fatty acid methyl esters (FAME). The effects of reaction time, catalyst concentration, methanol to seed ratio, reaction temperature, mixing intensity and ultrasonic power on product yield and conversion rate were examined. The details of experiments and studied parameters in this section are presented in Figure 3.12.

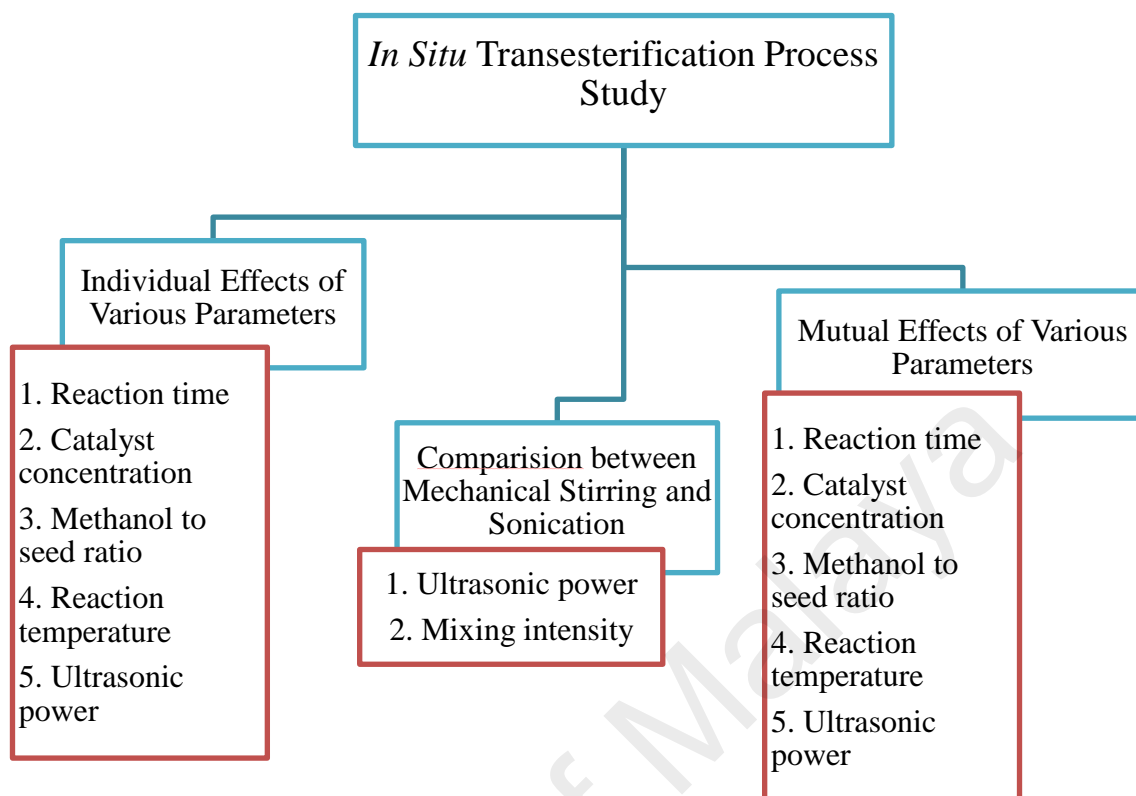


Figure 3.12: The details of experiments and studied parameters in this section 3.3.4.

3.3.4.1 Individual Effect of Each Parameter

The first set was designed manually to investigate the gradual increasing effect of operating parameters on *in situ* transesterification. Toward this objective, one basic test with the condition of Catalyst: 0.1 mol/L in methanol, ultrasound power: 300 W, methanol to seed ratio: 9:1 (v/w) reaction temperature: 40 °C and reaction time of 30 min was selected. By considering the basic test as the initial point, 7, 7, 6 and 5 tests were considered to analyse the effects of catalyst increment ranging from 0.025 to 0.175 mol/L, methanol to seed oil ratio ranging from 6:1 to 13.5:1 (v/w), reaction temperature ranging from 20 to 60 °C and reaction time ranging from 10 to 70 min, respectively.

3.3.4.2 Interaction of Operating Parameters

The second set of experiments was designed by Response Surface Methodology (RSM) coupled with Central Composite Design (CCD) in order to statistically analyze the interactive effects of operating parameters, develop regression model and optimize the operating parameters.

The level and range of the five independent variables included reaction time, X_1 , catalyst concentration, X_2 , methanol to seed ratio, X_3 , reaction temperature, X_4 and ultrasonic power, X_5 , and their coded levels for CCD is shown in Table 3.6. The required number of experiments consisted of 10 fixed axial runs, 32 factorial runs and 8 replications of centre points which were carried out in a randomized sequence to reduce the effects of uncontrolled parameters.

Table 3.6: Independent variables and their coded levels for the CCD for *in situ* transesterification experiments.

| Variables | Code | Coded variable level | | |
|------------------------------|-------|----------------------|--------|-------|
| | | -1 | 0 | 1 |
| Reaction Time (min) | X_1 | 10.00 | 30.00 | 50.00 |
| Catalyst Conc. (mol/L) | X_2 | 0.05 | 0.1 | 0.15 |
| Methanol to seed ratio (v/w) | X_3 | 6:1 | 9:1 | 12:1 |
| Temperature (°C) | X_4 | 30.00 | 40.00 | 50.00 |
| Ultrasonic Power (W) | X_5 | 200.00 | 300.00 | 400.0 |

3.3.4.3 Effect of Mechanical Mixing

This set of experiments was carried out in order to compare the traditional *in situ* transesterification of *J. curcas* under mechanical stirring with this novel one under ultrasound irradiation. One basic test with the condition of Catalyst: 0.1 mol/L in

methanol, methanol:seed: 9:1 (v/w), mixing intensity: 100 RPM, reaction temperature: 40 °C and reaction time of 30 min was considered in which the mixing intensity gradually increased up to 850 RPM. The study ranges of operating parameters in this work were according to the literature values (Mondala et al., 2009; Qian et al., 2008; Amalia Kartika et al., 2013; Shuit et al., 2010).

3.3.5 Biodiesel Content Analysis

The biodiesel content analysis is the same as explained in section 3.2.5 (Knothe, 2006).

The biodiesel yield of *in situ* transesterification process was determined according to following equation:

$$\text{Biodiesel Yield (\%)} = \frac{\text{Weight of obtained biodiesel (g)}}{\text{Weight of oil in Jatropha seed (g)}} \times 100 \quad (3.18)$$

where the obtained biodiesel mass is the weight of crude biodiesel after washing and drying, while the weight of oil in *J. curcas* seeds has been determined by the Soxhlet method.

CHAPTER 4: RESULTS AND DISCUSSION

The results of all of the experiments carried out in this study are presented and discussed in this chapter. On the basis of the objectives and methodology, this chapter is divided to three main parts. The first part, which presents the effects of ultrasound irradiation on gas-liquid system, starts with the results for influence of liquid volume on mass transfer of oxygen dissolution in water under ultrasound irradiation and followed by studying the effects of other parameters on k_La . The influence of mechanical mixing on k_La was then investigated and compared with the effect of ultrasonication. Empirical correlations were also presented from the performed experiments and compared with the existing correlation from literature.

In the second part, the performance of sonochemical reactor in a liquid-liquid system was studied by presenting the results of transesterification of *J. curcas* oil to biodiesel and determining the biodiesel yield and conversion rate of this reaction. The effects of other parameters on transesterification process were also investigated and a comparison was then carried out between the influence of ultrasound irradiation and mechanical mixing on biodiesel yield and conversion rate.

Finally, in the last part, for evaluating the performance of sonochemical reactor in solid-liquid system, a deep insight into the effect of ultrasound irradiation on the *in situ* transesterification process was carried out. The results for characterization of *J. curcas* were presented first and then the gradual increasing effect of each operating parameters on biodiesel production were studied. Besides, a separate set of experiments was also designed to analyze the mutual effect of different parameters and develop regression models for biodiesel yield and conversion rate. The next set of experiment was accomplished to compare the ultrasound-assisted *in situ* transesterification with traditional *in situ* transesterification under mechanical stirring. The chapter ends with

optimization of operational factor levels based on the experiments done for both transesterification yield and its conversion rate and the quadratic models obtained.

4.1 Experimental Analysis of Ultrasound effect on Gas-Liquid System

4.1.1 Effect of Liquid Volume on Mass Transfer under Sonication

Effect of liquid volume on gas-liquid mass transfer under ultrasound power of 400 W and gas flow rate of 5 L/min is demonstrated in Figure 4.1. This experiment was carried out in an air-water system under sonication in order to analyze the influence of ultrasonication on mass transfer in different volumes and to determine suitable volume for biodiesel production experiments. As shown in this figure, the amount of k_La decreases with increasing liquid volume. Therefore, ultrasound irradiation with power of 400 W and frequency of 24 kHz cannot make a significant effect on mass transfer in the liquid volume above 500 mL. However, effects of other parameters together with sonication in 2 L liquid volume were investigated in the following section in order to understand the combination effects of operating parameters on k_La .

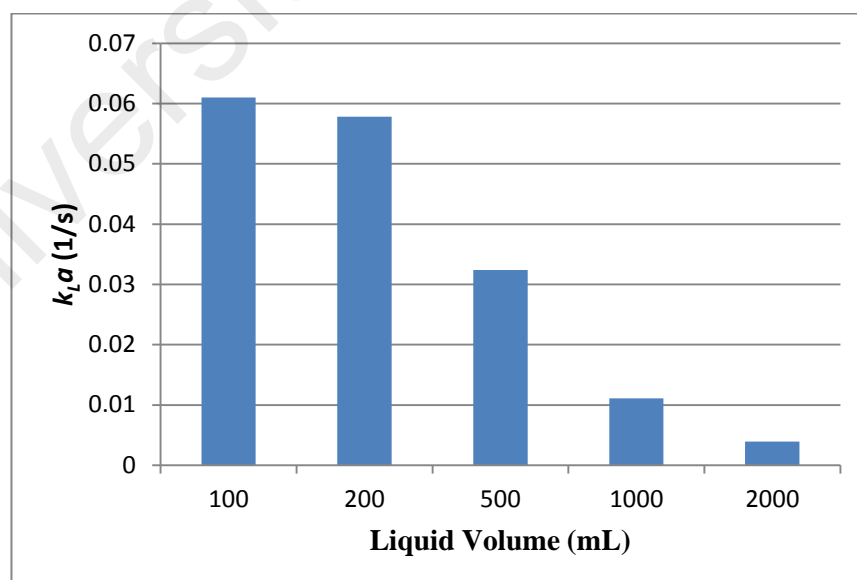


Figure 4.1: k_La versus liquid volume under ultrasound power of 400 W and gas flow rate of 5 L/min.

4.1.2 Mass Transfer Coefficient in 2 L Liquid Volume

4.1.2.1 Effects of Ultrasound Power and Gas Flow Rate

The effects of ultrasound power and gas flow rate on gas-liquid mass transfer coefficient in 2 L liquid volume were investigated separately in this section. As shown in Figure 4.2 (a), ultrasonic irradiation cannot make a considerable effect on the k_La in high liquid volume and the mass transfer is mostly controlled by gas flow rate. Even with no ultrasound power, the amount of k_La with gas flow rate of 5 L/min is 0.0028 s^{-1} which is only due to the mixing caused by gas flow rate. However, ultrasonication with power of 400 W can only increase it to 0.0039 s^{-1} . From Figure 4.2 (b) can also be observed that k_La depends on gas flow rate more than ultrasonic intensity.

4.1.2.2 Development of Regression Model

The relationship between responses (k_La) and three independent parameters (temperature, gas flow rate and ultrasonic power) were studied through CCD. Six runs were carried out at the centre point to determine the experimental inaccuracies. Sequential model sums of squares were selected as the highest order polynomial where the additional terms were significant and the model was not aliased (Afshar Ghotli et al., 2013). The complete design matrices of the experiments, together with the results obtained, are shown in Table 4.1.

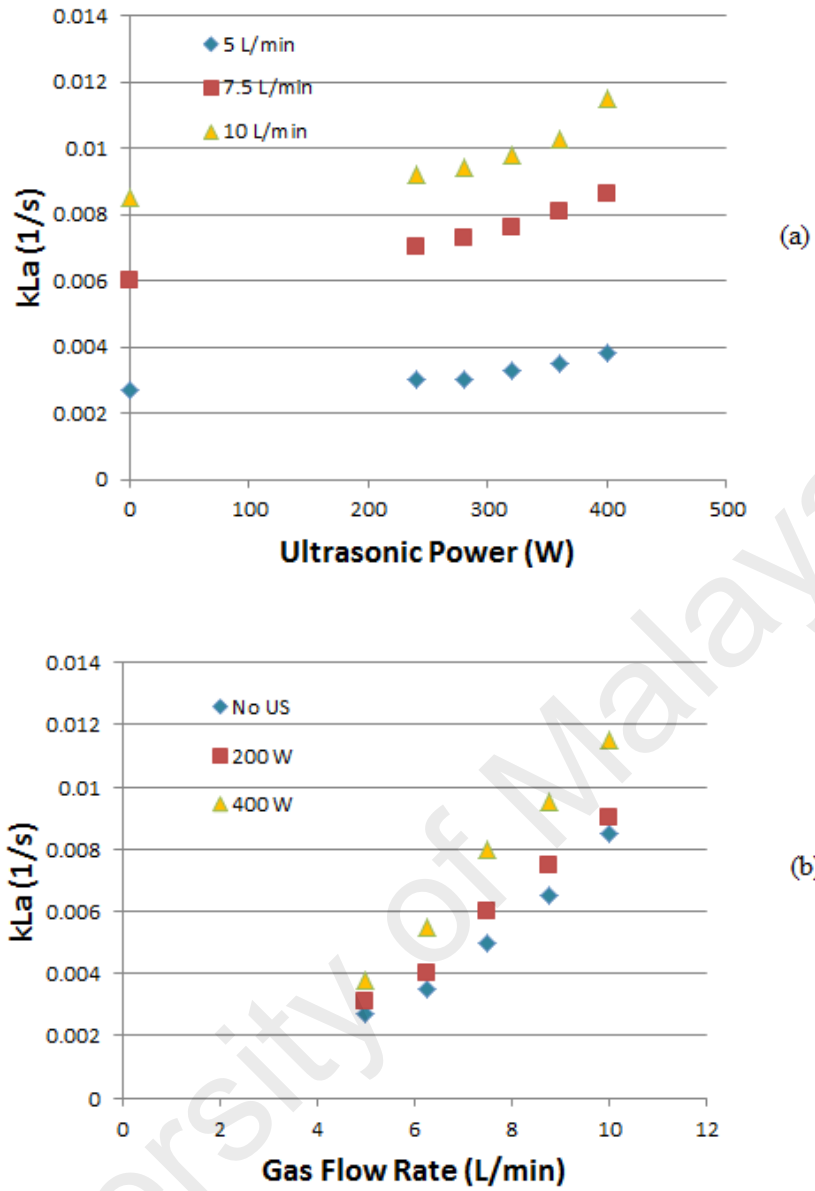


Figure 4.2: k_La in 2 L liquid volume versus (a) ultrasound power (b) gas flow rate.

A quadratic polynomial model was suggested by the software and the following model was developed in terms of coded factors to predict the mass transfer coefficient:

$$k_La = 7.427E^{-3} - 5.941E^{-4}X_1 + 3.388E^{-3}X_2 + 6.765E^{-4}X_3 \quad (4.1)$$

The positive and negatives term indicates synergistic and antagonistic effects, respectively (Ahmad et al., 2009). The lower standard deviation and higher R-squared is led to select the quadratic model.

Table 4.1: Experimental design matrix and response results for k_La in 2 L.

| Run | Type | Temperature, X_1 | Gas Flow rate , X_2 | Ultrasonic Power, X_3 | k_La , Y_1 |
|-----|-----------|-----------------------|--------------------------|----------------------------|----------------|
| 1 | Axial | 30.00 | 7.50 | 360.00 | 0.0081 |
| 2 | Factorial | 50.00 | 5.00 | 240.00 | 0.0024 |
| 3 | Factorial | 10.00 | 10.00 | 240.00 | 0.0106 |
| 4 | Axial | 20.00 | 7.50 | 320.00 | 0.0079 |
| 5 | Centre | 30.00 | 7.50 | 320.00 | 0.0071 |
| 6 | Factorial | 10.00 | 5.00 | 400.00 | 0.0039 |
| 7 | Centre | 30.00 | 7.50 | 320.00 | 0.0074 |
| 8 | Factorial | 50.00 | 5.00 | 400.00 | 0.0036 |
| 9 | Factorial | 50.00 | 10.00 | 240.00 | 0.0081 |
| 10 | Factorial | 10.00 | 10.00 | 400.00 | 0.0112 |
| 11 | Axial | 40.00 | 7.50 | 320.00 | 0.0068 |
| 12 | Factorial | 50.00 | 10.00 | 400.00 | 0.0102 |
| 13 | Axial | 30.00 | 7.50 | 280.00 | 0.006 |
| 14 | Factorial | 10.00 | 5.00 | 240.00 | 0.0031 |
| 15 | Axial | 30.00 | 6.25 | 320.00 | 0.0058 |
| 16 | Centre | 30.00 | 7.50 | 320.00 | 0.0075 |
| 17 | Centre | 30.00 | 7.50 | 320.00 | 0.0075 |
| 18 | Centre | 30.00 | 7.50 | 320.00 | 0.0077 |
| 19 | Centre | 30.00 | 7.50 | 320.00 | 0.0077 |
| 20 | Axial | 30.00 | 8.75 | 320.00 | 0.0092 |

The value of R-squared for Y was 0.9715. High R-squared values indicate a good agreement between the predicted and experimental values (Houshmand et al., 2011; Lee et al., 2006). The adequacy of the developed model was also verified with the close

position of points to the line in Figure 4.3. This figure reveals the predicted values (k_{La}) in terms of experimental results.

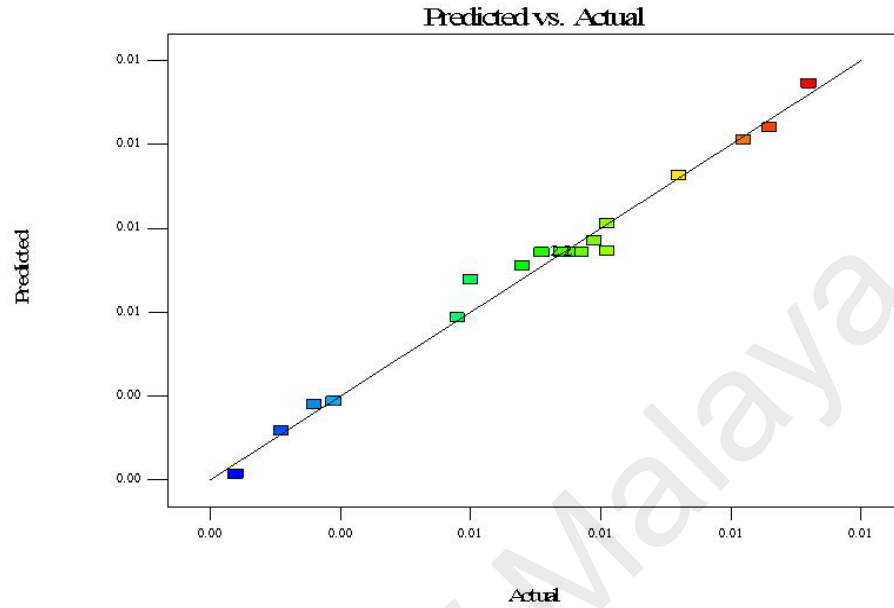


Figure 4.3: Predicted vs. actual value of k_{La} in 2 L.

The adequacy of the suggested model was justified through the analysis of variance (ANOVA). The statistical significance of the quadratic model is presented in Table 4.2 and the significance of the model was verified with F-Value of 73.08. There was only a 0.01% chance that a “Model F-Value” this large might happen due to noise. It was further justified based on the reasonable agreement between the predicted R-Squared of 0.8708 and adjusted R-square value of 0.9715. Moreover, P-value less than 0.05 indicate that the model terms were significant. Therefore, the three independent variables: temperature (X_1), gas flow rate (X_2) and ultrasonic power (X_3) were significant terms while the interaction between temperature and gas flow rate (X_1X_2), temperature and ultrasonic power (X_1X_3), gas flow rate and ultrasonic power (X_2X_3), X_1^2 , X_2^2 , and X_3^2 were not found to be significant terms as their P-values were more than 0.05.

Table 4.2: Analysis of variance of the quadratic model for the k_{La} .

| Source | Sum of squares | Degree of freedom (dF) | Mean of square | F-Value | p-value (Prob > F) | Remarks |
|-------------------------------|-----------------------|------------------------|-----------------------|--------------------|--------------------|-------------|
| Model | 1.088E ⁻⁴ | 9 | 1.208E ⁻⁵ | 73.08 | < 0.0001 | significant |
| X ₁ | 3.000E ⁻⁶ | 1 | 3.000E ⁻⁶ | 18.14 | 0.0017 | significant |
| X ₂ | 9.758E ⁻⁵ | 1 | 9.758E ⁻⁵ | 590.13 | < 0.0001 | significant |
| X ₃ | 3.890E ⁻⁶ | 1 | 3.890E ⁻⁶ | 23.52 | 0.0007 | significant |
| X ₁ X ₂ | 7.812E ⁻⁷ | 1 | 7.812E ⁻⁷ | 4.72 | 0.0548 | |
| X ₁ X ₃ | 4.513E ⁻⁷ | 1 | 4.513E ⁻⁷ | 2.73 | 0.1296 | |
| X ₂ X ₃ | 6.125E ⁻⁸ | 1 | 6.125E ⁻⁸ | 0.37 | 0.5564 | |
| X ₁₂ | 7.772E ⁻¹⁰ | 1 | 7.772E ⁻¹⁰ | 4.7E ⁻³ | 0.9467 | |
| X ₂₂ | 5.351E ⁻⁸ | 1 | 5.351E ⁻⁸ | 0.32 | 0.5820 | |
| X ₃₂ | 2.984E ⁻⁷ | 1 | 2.984E ⁻⁷ | 1.80 | 0.2088 | |
| Residual | 1.654E ⁻⁶ | 10 | 1.654E ⁻⁷ | | | |
| Lack of fit | 1.405E ⁻⁶ | 5 | 2.810E ⁻⁷ | 5.66 | 0.0401 | |
| Pure error | 2.483E ⁻⁷ | 5 | 4.967E ⁻⁸ | | | |
| Cor total | 1.104E ⁻⁴ | 19 | | | | |
| R-Squared | 0.9850 | | | | | |

4.1.2.3 Interaction of Operating Parameters

Response surface plots (Figure 4.4, 4.5 and 4.6) which graphically represent of the regression equation (3.3), are prepared by using design expert software. The influence of varying gas flow rates and temperatures on k_{La} at ultrasonic power of 320 W is shown in Figure 4.4. As presented in this figure, continuous increase in k_{La} was achieved with increase in gas flow rate and temperature, but the effect of gas flow rate was more significant. This result is in contrast with the statement of Sainz Herrán et al.

(Sainz Herrán et al., 2012) who reported there was no significant variation in k_La by changing temperature.

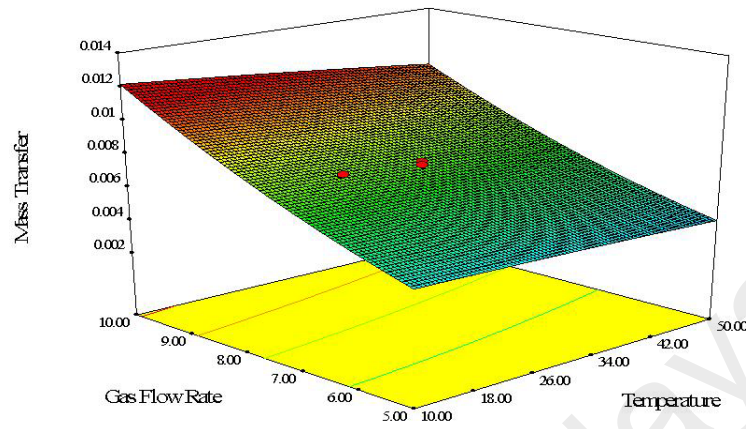


Figure 4.4: Response surface plot showing the mutual effect of gas flow rate and temperature on k_La at ultrasonic power of 320 W.

Figure 4.5 depicts the effect of ultrasonic power, temperature and their combined interaction on k_La at a gas flow rate of 7.5 L/min. In this figure, the value of k_La increased with increasing ultrasonic power and reached a maximum value in between 320 and 360 W. Beyond this range, k_La slightly decreased, possibly due to temperature rise caused by high ultrasonic amplitude.

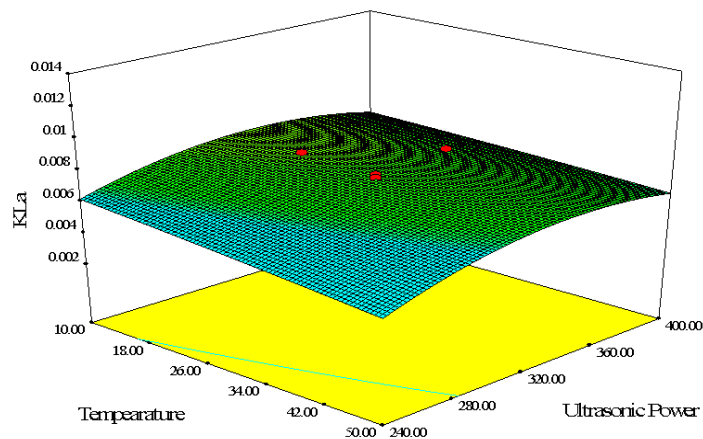


Figure 4.5: Response surface plot showing the mutual effect of the ultrasonic power and temperature on k_La at gas flow rate of 7.5 L/min.

Figure 4.6 presents the effect of ultrasonic power, gas flow rate and their mutual interaction on k_{La} at 30 °C. The velocity of sound waves in liquid is faster than in gas, since sound vibrational energy passes from molecule to molecule and the distance between gases molecules is more than liquid molecules (Sainz Herrán et al., 2012). Therefore, the performance of ultrasonic energy is related to the amount of gas holdup in the system, which usually increases in high gas flow rate (Soong et al., 1997; Stolojanu and Prakash, 1997). As a result, more ultrasonic energy is lost and the effect of ultrasonication on mass transfer is reduced by increasing gas flow rate. On the other hand, higher gas holdup leads to higher interfacial area and increase in the overall mass transfer. Accordingly, considerable effect of gas flow rate can be observed from Figure 4.6, although the effect of ultrasonic irradiation was insignificant.

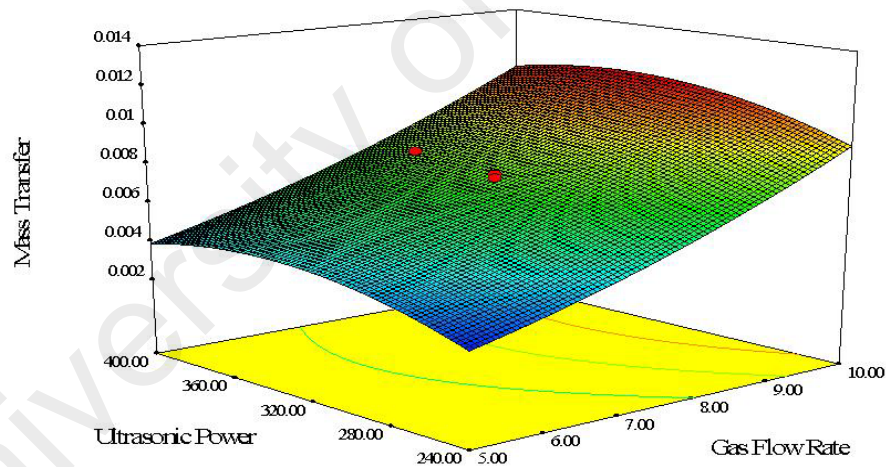


Figure 4.6: Response surface plot showing the mutual effect of ultrasonic power and temperature on k_{La} at temperature of 30 °C.

The obtained results demonstrate that low-frequency ultrasound irradiation with maximum power of 400 W cannot intensify the k_{La} in 2 L liquid volume significantly and gas flow rate is the most effective parameter on gas-liquid mass transfer in this situation.

4.1.3 Mass Transfer Coefficient in 200 mL Liquid Volume

In this part, three glass batch reactors with a diameter of 6 cm were used for the experiments in three different situation; using vertical ultrasonic probe (VP), using horizontal ultrasonic probe (HP) and by mechanical mixing in stirred vessel (SV). The first reactor was an ultrasonicator equipped with a central-down ward horn. The second was equipped with a side ward horn placed within 15 mm from the vessel bottom to investigate and clarify the possible influence that ultrasound might have on the mass transfer. The third reactor was a stirred vessel equipped with 45 pitched-blade impellers with 6 blades (Diameter: 25 mm) mounted on a shaft with a diameter of 4 mm placed at the centerline of the contactor and located 15 mm from the bottom of the contactor. Experiments were conducted using three different solutions of glycerol (0, 25 and 50 wt%) in water in order to investigate the effect of viscosity on gas-liquid mass transfer coefficient. Fig. 4.7 presents a schematic diagram of the experimental set up for: (a) vertical ultrasonic horn, (b) horizontal ultrasonic horn and (c) mechanically stirred vessel.

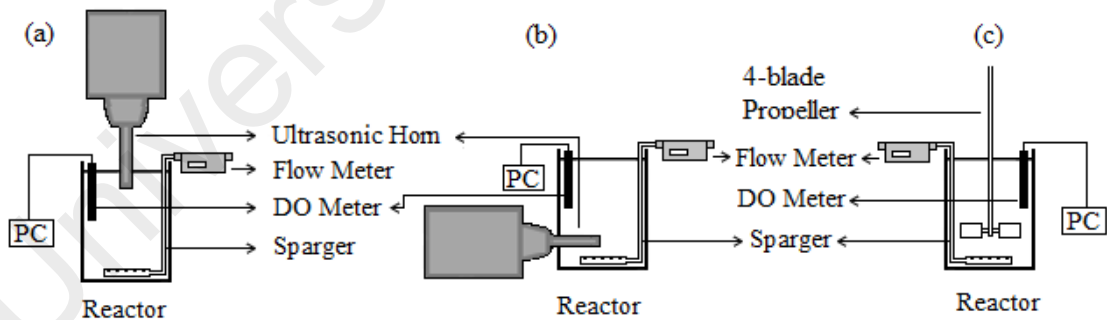


Figure 4.7: Schematic representation of the experimental setup: (a) vertical ultrasonic horn, (b) horizontal ultrasonic horn and (c) mechanically stirred vessel.

The relationship between responses (k_La) and three independent parameters for each set of experiments were studied through CCD, same as previous section. Six runs were

carried out at the centre point to determine the experimental inaccuracies. Sequential model sums of squares were selected as the highest order polynomial where the additional terms were significant and the model was not aliased.

4.1.3.1 Mass Transfer by Vertical Ultrasonic Probe

In this set of experiment, ultrasonic horn was submerged into the liquid phase vertically from the top of the vessel and dipped 10 mm inside the medium. The effects of viscosity, superficial gas velocity and ultrasonic power on k_La were studied and the complete design matrices of the experiments, together with the results obtained, are shown in Table 4.3.

Table 4.3: Experimental design matrix and response results for vertical ultrasonic mixing.

| Run | Type | Viscosity, X_1 | Superficial Gas Velocity, X_2 | Ultrasonic Power, X_3 | k_La , Y_1 |
|-----|-----------|---------------------|------------------------------------|----------------------------|----------------|
| 1 | Factorial | 1 | 1.17 | 200 | 0.025 |
| 2 | Factorial | 6 | 1.17 | 200 | 0.0144 |
| 3 | Factorial | 1 | 3.53 | 200 | 0.032 |
| 4 | Factorial | 6 | 3.53 | 200 | 0.0176 |
| 5 | Factorial | 1 | 1.17 | 400 | 0.0513 |
| 6 | Factorial | 6 | 1.17 | 400 | 0.0186 |
| 7 | Factorial | 1 | 3.53 | 400 | 0.0714 |
| 8 | Factorial | 6 | 3.53 | 400 | 0.0375 |
| 9 | Axial | 1 | 2.35 | 300 | 0.0319 |
| 10 | Axial | 6 | 2.35 | 300 | 0.0155 |
| 11 | Axial | 3.5 | 1.17 | 300 | 0.0208 |
| 12 | Axial | 3.5 | 3.53 | 300 | 0.036 |
| 13 | Axial | 3.5 | 2.35 | 200 | 0.0196 |
| 14 | Axial | 3.5 | 2.35 | 400 | 0.0555 |
| 15 | Center | 3.5 | 2.35 | 300 | 0.028 |
| 16 | Center | 3.5 | 2.35 | 300 | 0.0243 |
| 17 | Center | 3.5 | 2.35 | 300 | 0.0221 |

| | | | | | |
|----|--------|-----|------|-----|--------|
| 18 | Center | 3.5 | 2.35 | 300 | 0.0178 |
| 19 | Center | 3.5 | 2.35 | 300 | 0.0259 |
| 20 | Center | 3.5 | 2.35 | 300 | 0.0265 |

Three following models were developed in terms of coded factors to predict the mass transfer coefficient for vertical ultrasonic horn:

$$k_L a = 0.0794 + 3.956E^{-3}X_1 - 4.439E^{-3}X_2 - 4.726E^{-4}X_3 + 9.932E^{-7}X_3^2 \quad (4.2)$$

The positive and negatives term indicates synergistic and antagonistic effects, respectively. The lower standard deviation and higher R-squared is led to select the quadratic model. The value of R-squared for Y was 0.9137. High R-squared values indicate a good agreement between the predicted and experimental values.

The adequacy of the suggested model was justified through the analysis variance (ANOVA). P-value less than 0.05 indicate that the model terms were significant. Therefore, for mass transfer using vertical horn the three independent variables: viscosity (X_1), superficial gas velocity (X_2), ultrasonic power (X_3) and X_3^2 were significant terms while the interaction between viscosity and superficial gas velocity (X_1X_2), viscosity and ultrasonic power (X_1X_3), superficial gas velocity and ultrasonic power (X_2X_3), X_1^2 and X_2^2 were not found to be significant terms as their P-values were more than 0.05.

Response surface plots (Figure 4.7, 4.8 and 4.9) which graphically represent of the regression equation (3.3), are prepared by using design expert software. Figure 4.7 depicts the effect of ultrasonic power, viscosity and their combined interaction on $k_L a$ at a superficial gas velocity of 2.35 m/s for vertical ultrasonic horn system. In this figure, the value of $k_L a$ increased with increasing ultrasonic power and decrease with increasing liquid viscosity. The reverse effect of viscosity on $k_L a$ was expected due to reduction of

liquid diffusivity and also because of making bigger and more stable bubble in the system which led to reduce the value of $k_L a$. In high ultrasonic power, the diverse effect of viscosity is also more which could be due to acoustic cavitation and bigger size of bubbles.

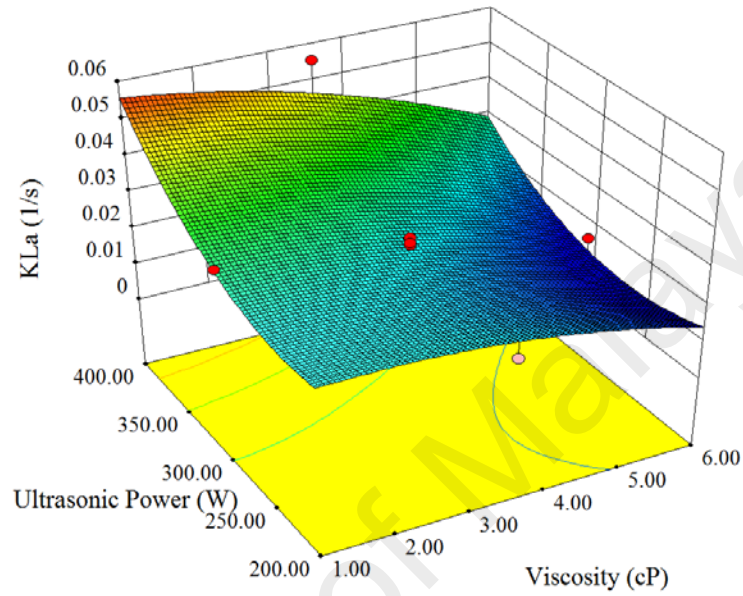


Figure 4.8: Response surface plot showing the mutual effect of ultrasonic power and viscosity on $k_L a$ at superficial gas velocity of 2.35 m/s (VP).

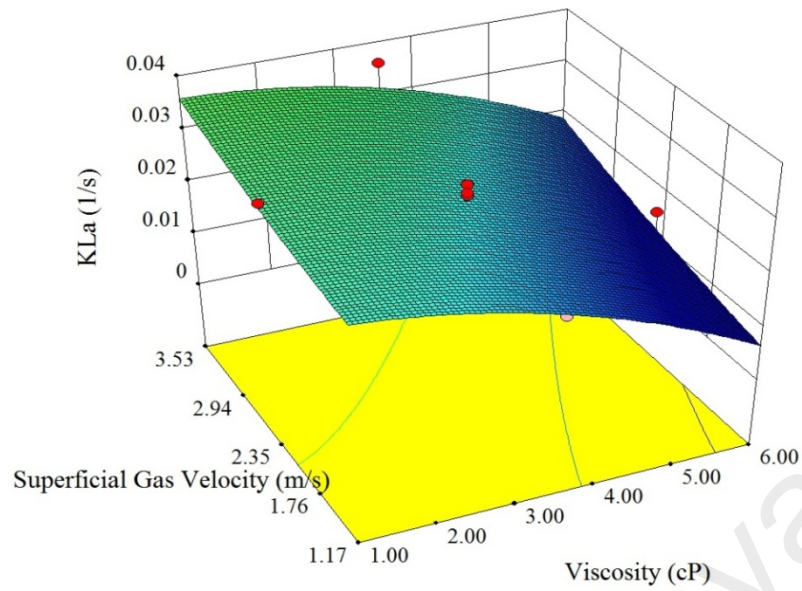


Figure 4.9: Response surface plot showing the mutual effect of superficial gas velocity and viscosity on k_{La} at ultrasonic power of 300 W (VP).

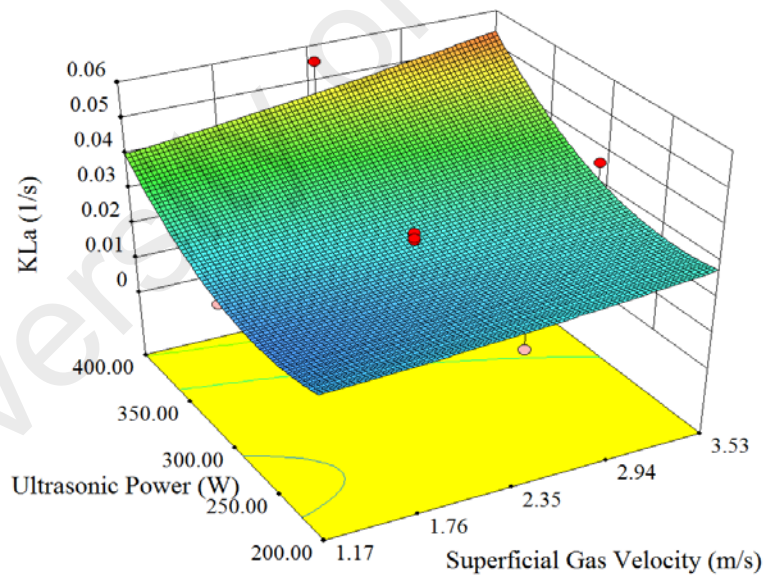


Figure 4.10: Response surface plot showing the mutual effect of superficial gas velocity and ultrasonic power on k_{La} at viscosity 3.5 cP (VP).

Figure 4.8 presents the effect of viscosity and superficial gas velocity and their mutual interaction on k_{La} . The diverse effect of viscosity on k_{La} can be also observed in this figure. In addition, the combined effect of ultrasonic power and superficial gas velocity

on k_La is demonstrated in Figure 4.9. As presented in these figures, the effect of superficial gas velocity on k_La is also considerable; however ultrasonic power is the most significant parameter in this experiment.

4.1.3.2 Mass Transfer by Horizontal Ultrasonic Probe

In the second set of experiments, ultrasonic horn tip was located into the system horizontally in order to investigate the effect of horn position on k_La . The distance of ultrasonic horn from the bottom of the tank was 15 mm. The complete design matrices of the experiments, together with the results obtained, are shown in Table 4.4.

Table 4.4: Experimental design matrix and response results for horizontal ultrasonic mixing.

| Run | Type | Viscosity, X_1 | Superficial Gas Velocity, X_2 | Ultrasonic Power, X_3 | k_La , Y_1 |
|-----|-----------|---------------------|------------------------------------|----------------------------|----------------|
| 1 | Factorial | 1 | 1.17 | 200 | 0.0316 |
| 2 | Factorial | 6 | 1.17 | 200 | 0.0193 |
| 3 | Factorial | 1 | 3.53 | 200 | 0.0405 |
| 4 | Factorial | 6 | 3.53 | 200 | 0.0224 |
| 5 | Factorial | 1 | 1.17 | 400 | 0.058 |
| 6 | Factorial | 6 | 1.17 | 400 | 0.026 |
| 7 | Factorial | 1 | 3.53 | 400 | 0.0578 |
| 8 | Factorial | 6 | 3.53 | 400 | 0.0462 |
| 9 | Axial | 1 | 2.35 | 300 | 0.043 |
| 10 | Axial | 6 | 2.35 | 300 | 0.0285 |
| 11 | Axial | 3.5 | 1.17 | 300 | 0.0325 |
| 12 | Axial | 3.5 | 3.53 | 300 | 0.0473 |
| 13 | Axial | 3.5 | 2.35 | 200 | 0.0309 |
| 14 | Axial | 3.5 | 2.35 | 400 | 0.0644 |
| 15 | Center | 3.5 | 2.35 | 300 | 0.0415 |
| 16 | Center | 3.5 | 2.35 | 300 | 0.0436 |
| 17 | Center | 3.5 | 2.35 | 300 | 0.0408 |

| | | | | | |
|----|--------|-----|------|-----|--------|
| 18 | Center | 3.5 | 2.35 | 300 | 0.0422 |
| 19 | Center | 3.5 | 2.35 | 300 | 0.0419 |
| 20 | Center | 3.5 | 2.35 | 300 | 0.041 |

Three following models were developed in terms of coded factors to predict the mass transfer coefficient for mass transfer using horizontal ultrasonic horn:

$$k_L a = 0.0417 + 6.734E^{-3}X_1 + 4.887E^{-3}X_2 - 2.3E^{-4}X_3 - 1.34E^{-5}X_1X_3 + 2.288E^{-5}X_2X_3 - 9.854E^{-4}X_1^2 + 5.74E^{-7}X_3^2 \quad (4.3)$$

The positive and negatives term indicates synergistic and antagonistic effects, respectively. The lower standard deviation and higher R-squared is led to select the quadratic model. The value of R-squared for Y was 0.9682. High R-squared values indicate a good agreement between the predicted and experimental values.

The adequacy of the suggested model was justified through the analysis of variance (ANOVA). P-value less than 0.05 indicate that the model terms were significant. Therefore, for mass transfer using horizontal horn the three independent variables: viscosity (X_1), superficial gas velocity (X_2), ultrasonic power (X_3) and also the interaction between viscosity and ultrasonic power (X_1X_3), superficial gas velocity and ultrasonic power (X_2X_3), X_1^2 and X_3^2 were significant terms while the other terms were not found to be significant as their P-values were more than 0.05.

For this set of experiments also response surface plots (Figure 4.10, 4.11 and 4.12) are prepared by using design expert software. As presented in Figure 4.10, the effect of ultrasonic power and viscosity on $k_L a$ in horizontal ultrasonic horn system is same as vertical system, however the overall value of $k_L a$ is lower in this situation..

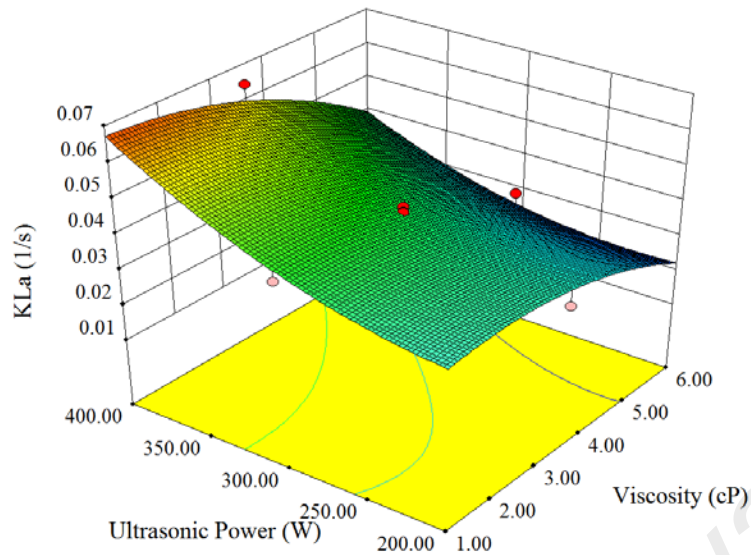


Figure 4.11: Response surface plot showing the mutual effect of ultrasonic power and viscosity on k_{La} at superficial gas velocity of 2.35 m/s (HP).

The effect of varying superficial gas velocity and ultrasonic power at viscosity of 3.5 cP on k_{La} for horizontal ultrasonic horn system is shown in Figure 4.11. At a lower superficial gas velocity, k_{La} increased with increase in ultrasonic power. A similar pattern was followed by increasing the superficial gas velocity. Therefore, a combined increase in ultrasonic power and superficial gas velocity enhance the k_{La} .

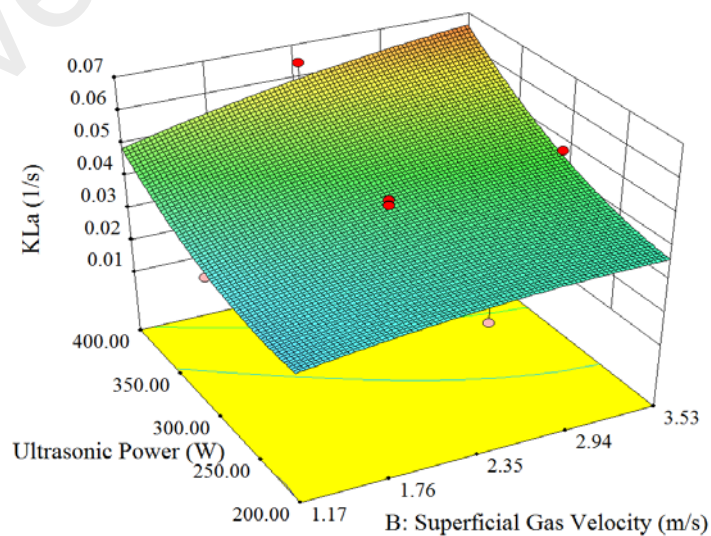


Figure 4.12: Response surface plot showing the mutual effect of ultrasonic power and superficial gas velocity on k_{La} at viscosity of 3.5 cP (HP).

In addition, a higher dependency of k_La on superficial gas velocity is observed in the case of horizontal ultrasonic horn which is due to the short distance of gas sparger and ultrasonic horn. In this case, the sparger located very close to the ultrasonic horn and all the sparged gas comes under the effect of ultrasonic irradiation and acoustic cavitation. Since, in the vertical ultrasonic horn the distance of gas sparger and horn is more and not all the sparged gas comes under the impact of cavitational activity. Furthermore, Figure 4.12 shows the mutual effect of viscosity ultrasonic power and superficial gas velocity on k_La at ultrasonic power of 300 W.

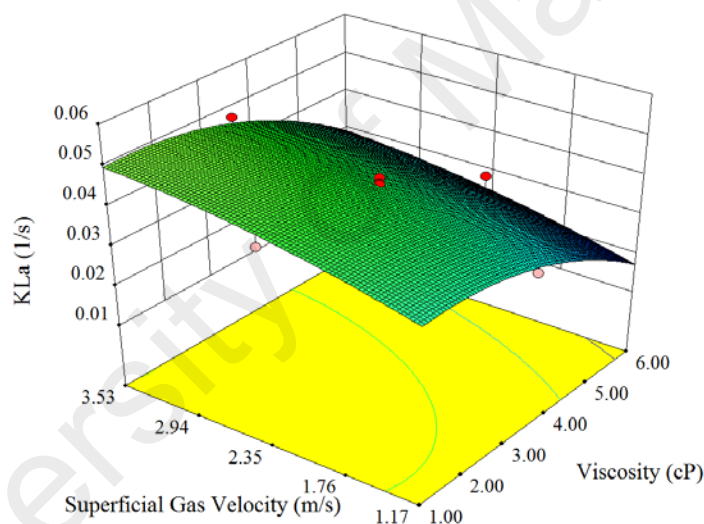


Figure 4.13: Response surface plot showing the mutual effect of viscosity ultrasonic power and superficial gas velocity on k_La at ultrasonic power of 300 W (HP).

4.1.3.3 Mass Transfer by Mechanical Stirring

Last set of gas-liquid mass transfer experiment have been done using a 45 pitched-blade impellers with 6 blades instead of ultrasonication in order to compare the efficiency of mechanical and ultrasonic-assisted mixing. The complete design matrices of the experiments, together with the results obtained, are shown in Table 4.5.

Three following models were developed in terms of coded factors to predict the mass transfer coefficient for the mass transfer by magnetic stirrer:

$$k_L a = 0.0121 - 2.713E^{-3}X_1 - 2.757E^{-5}X_3 - 1.191E^{-5}X_1X_3 + 7.549E^{-4}X_1^2 \quad (4.4)$$

The positive and negatives term indicates synergistic and antagonistic effects, respectively. The lower standard deviation and higher R-squared is led to select the quadratic model. The value of R-squared for Y was 0.9792. High R-squared values indicate a good agreement between the predicted and experimental values.

Table 4.5: Experimental design matrix and response results for mechanical mixing.

| Run | Type | Viscosity, X ₁ | Superficial Gas Velocity, X ₂ | Stirrer Speed, X ₃ | k _L a, Y ₁ |
|-----|-----------|------------------------------|---|----------------------------------|----------------------------------|
| 1 | Factorial | 1 | 1.17 | 200 | 0.0086 |
| 2 | Factorial | 6 | 1.17 | 200 | 0.001 |
| 3 | Factorial | 1 | 3.53 | 200 | 0.0112 |
| 4 | Factorial | 6 | 3.53 | 200 | 0.0013 |
| 5 | Factorial | 1 | 1.17 | 400 | 0.0231 |
| 6 | Factorial | 6 | 1.17 | 400 | 0.0015 |
| 7 | Factorial | 1 | 3.53 | 400 | 0.0275 |
| 8 | Factorial | 6 | 3.53 | 400 | 0.003 |
| 9 | Axial | 1 | 2.35 | 300 | 0.0123 |
| 10 | Axial | 6 | 2.35 | 300 | 0.0021 |
| 11 | Axial | 3.5 | 1.17 | 300 | 0.0026 |
| 12 | Axial | 3.5 | 3.53 | 300 | 0.0032 |
| 13 | Axial | 3.5 | 2.35 | 200 | 0.0018 |
| 14 | Axial | 3.5 | 2.35 | 400 | 0.0064 |
| 15 | Center | 3.5 | 2.35 | 300 | 0.0034 |
| 16 | Center | 3.5 | 2.35 | 300 | 0.0034 |
| 17 | Center | 3.5 | 2.35 | 300 | 0.0025 |
| 18 | Center | 3.5 | 2.35 | 300 | 0.0031 |

| | | | | | |
|----|--------|-----|------|-----|--------|
| 19 | Center | 3.5 | 2.35 | 300 | 0.0028 |
| 20 | Center | 3.5 | 2.35 | 300 | 0.0265 |

The adequacy of the suggested model was justified through the analysis of variance (ANOVA). P-value less than 0.05 indicate that the model terms were significant. Therefore, for mass transfer by mechanical mixing, the two independent variables: viscosity (X_1), ultrasonic power (X_3) and only two other terms of X_1^2 and X_1X_3 were significant while the other interaction terms were not found to be significant as their P-values were more than 0.05.

Figure 4.13, 4.14 and 4.15 are response surface plots for mechanical mixing mass transfer experiments. Figure 4.13 demonstrates the effect of viscosity, superficial gas velocity and their mutual interaction on k_La at stirrer speed of 300 rpm for the mechanical mixing situation. Continuous decrease in the k_La was obtained with the increase in liquid viscosity in the range considered. However, the superficial gas velocity was not a significant parameter in this system as reported before in equation 4.4. Generally, higher range of k_La value can be observed in all figures of ultrasonic mixing in comparison with mechanical agitation which is attributed to the high ability of ultrasound irradiation in increasing the interfacial surface and turbulent intensity.

Analysis of the effect of operating parameters on mass transfer depicted that they did not follow a similar pattern in the three systems and the intensity of their influence on each system was quite different. As observed, superficial gas velocity critically affected the mass transfer in VP-S, whereas, ultrasound power played the most important role in HP-S. In other words, in SV and HP-S in which circular fellow pattern dominated the system, the power or rotating rate are the most important parameters clarifying the impact of gas bubbles residence time. While in VP-Sonoreactor in which gas bubbles

directly came toward acoustic jet like streaming, superficial gas velocity is the key which was attributed to the ability of ultrasound in breaking gas bubbles and increasing the mass driving force using higher turbulence intensity.

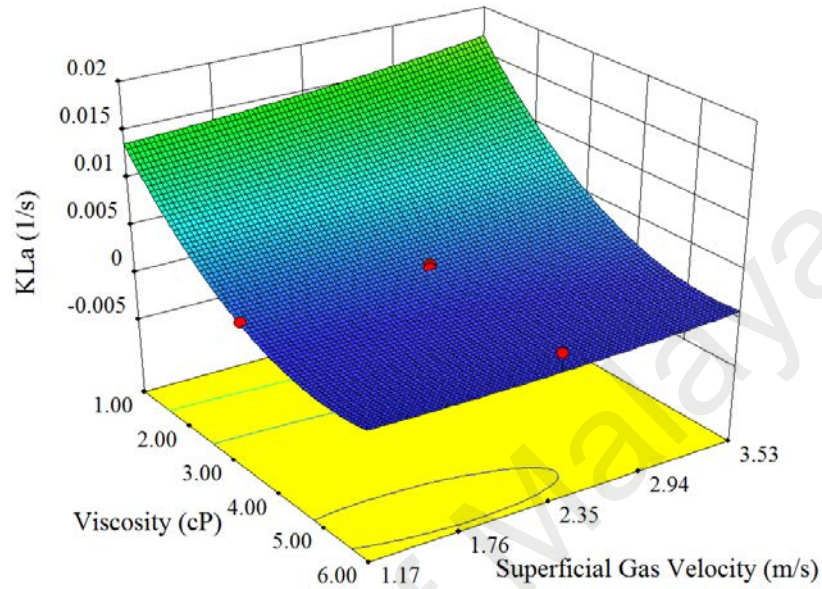


Figure 4.14: Response surface plot showing the mutual effect of viscosity and superficial gas velocity on k_{La} at stirrer speed of 300 rpm (SV).

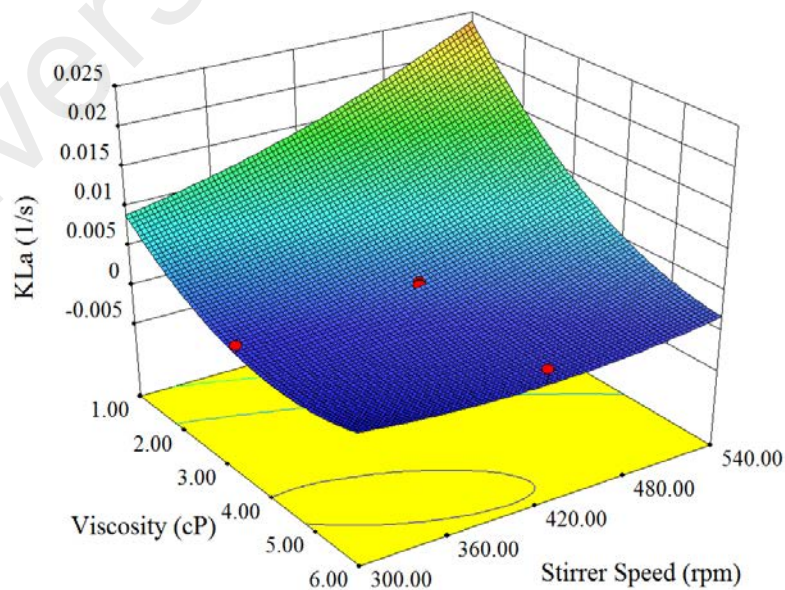


Figure 4.15: Response surface plot showing the mutual effect of viscosity and stirrer speed on k_{La} at superficial gas velocity of 2.35 m/s (SV).

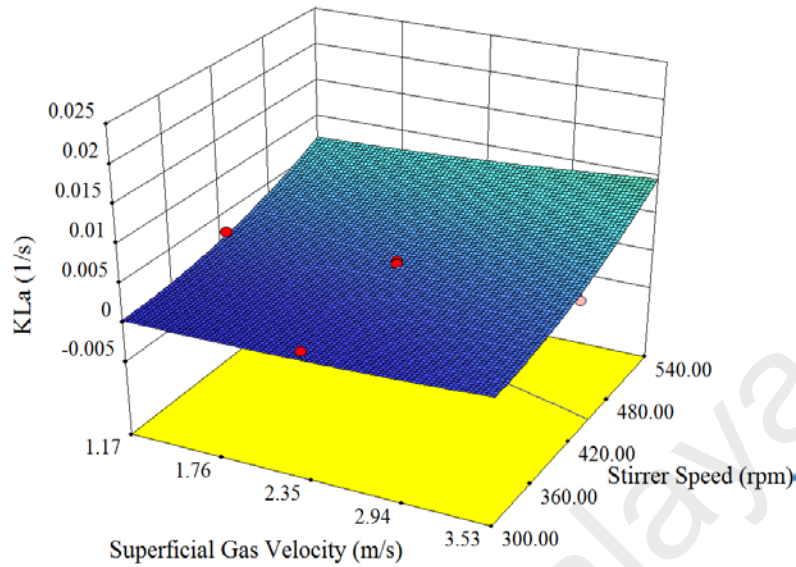


Figure 4.16: Response surface plot showing the mutual effect of stirrer speed and superficial gas velocity on k_{La} at viscosity of 3.5 cP (SV).

4.1.4 Simulation Analysis of Ultrasonicator versus Stirred Vessel

4.1.4.1 Fluid Flow Pattern and Liquid Velocity

Dynamic pressure is the kinetic energy per unit volume of a fluid that represents fluid kinetic energy, while static pressure represents hydrostatic effects ($P_{\text{total}} = P_{\text{dynamic}} + P_{\text{static}}$), which were presented in Figure 4.16. As observed in this figure, pressure pulses generated by the transducer started dispersing from surface of the ultrasound probe. It should be considered that ultrasound energy distributes in a fluid through mechanical pressure waves. In other words, ultrasound waves are sinusoidal mechanistic waves consisting of both expansion (negative) and compression (positive) pressure waves. Hence, irradiation of ultrasound waves affects the static pressure value in the liquid. Accordingly, the static pressure under ultrasound energy provided in Figure 4.16 a and b are not equal to ambient pressure.

However, in the system containing mechanical stirring, the surface static pressure represents the value, which is equal to the ambient static pressure. In regions below and above the impeller, the static pressure was affected by the impeller rotating motion, which leads to pulling and pushing the liquid, creating suction and discharge section and influencing the balance of pressure in those regions. It should be noted that, all values are gage pressure. The quality of these pressure waves determined the turbulence energy dissipation within the system, which subsequently intensified the mass transfer phenomenon. These positive and negative pressure pulses were converted to each other in turn, multiplying the turbulent energy within the system. Figure 4.16 clearly shows the magnitude and propagation of static pressure within the system and its interaction with the dynamic pressure in ultra-sonicators and stirred vessels. Considering the pressure distribution within the systems, different fluid flow patterns were imposed to the surrounding.

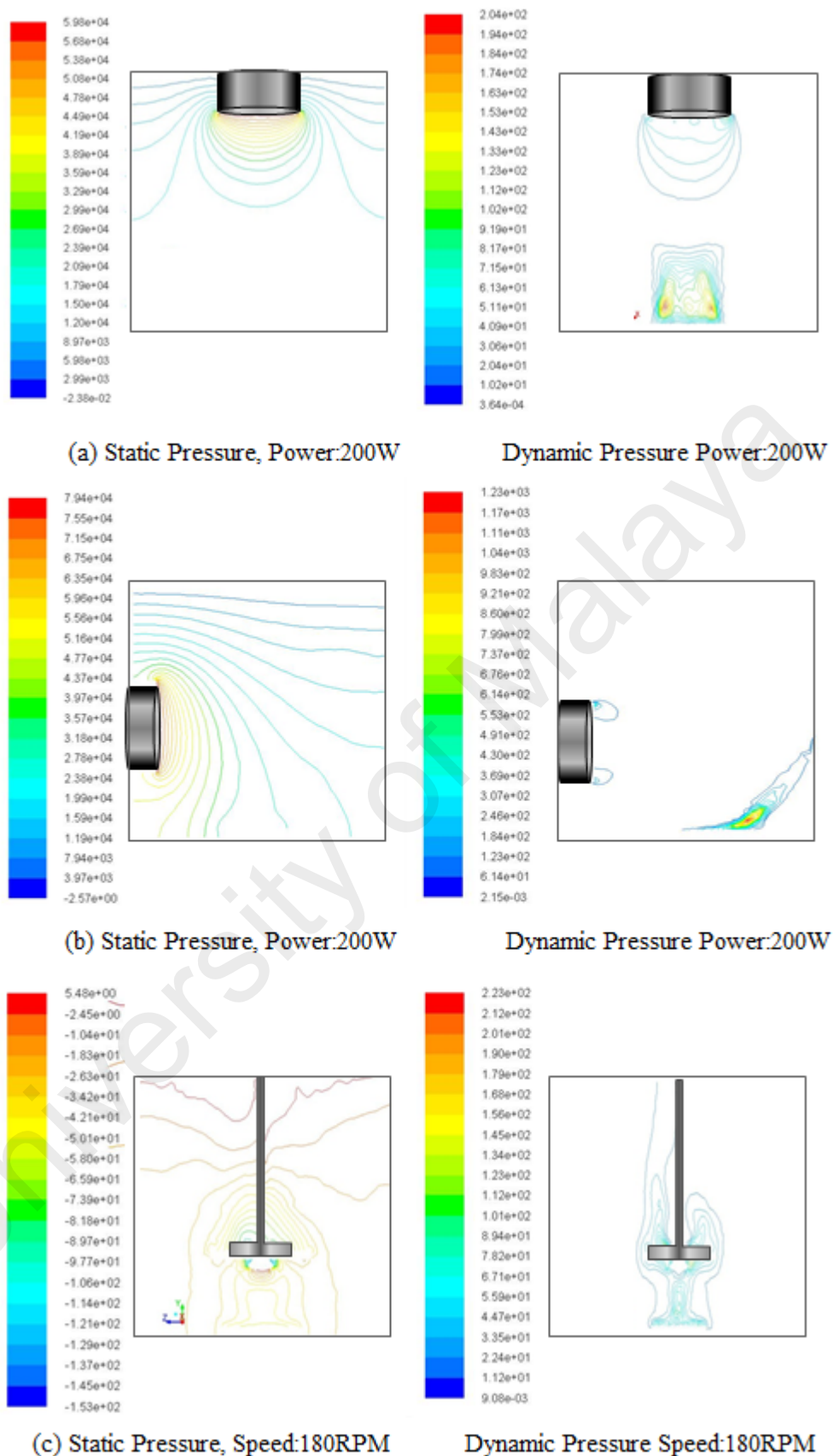


Figure 4.17: Distribution of pressure pulses inside the a) VP-Sonicator, b) HP-Sonicator, c) Stirred vessel under superficial gas velocity of 0.117 m/s.

Figure 4.17 shows the fluid flow pattern dominating the two ultra-sonicators compared to that in the mechanically stirred vessel. The corresponding velocity magnitude versus contactor radius is presented in Figure 4.18. Generally, the rotating impeller generated a strong convective flow in the mechanically agitated contactor, whereas ultrasound energy mostly produced oscillatory (vibratory) flow. This type of flow pattern was also observed in the CFD simulation by following the fluid flow in sequential time-steps with very short durations (in the level of 10^{-7} s). However, an overall fluid movement dominated the systems (as presented in Figure 4.17). In other words, acoustic streaming caused by high-power generated strong convective flow in both ultra-sonicators. Although the streamlines were deformed by gas injection, the flow in the vertical sonicators was mainly axial.

Besides, acoustic streaming conducted a strong recirculation flow from the probe surface toward the bottom of the contactor and then to the surface of the contactor. This type of flow pattern dragged the gas bubbles toward the wall of the contactors, which increased gas bubbles spreading while speeding up the release of bubbles from the system. The same flow pattern, although in horizontal direction, dominated in the system of the horizontal sonicator, generating a circulating flow which kept gas bubbles in the horizontal sonicator for a longer residence time and increased the gas-liquid contact time and mass transfer eventually.

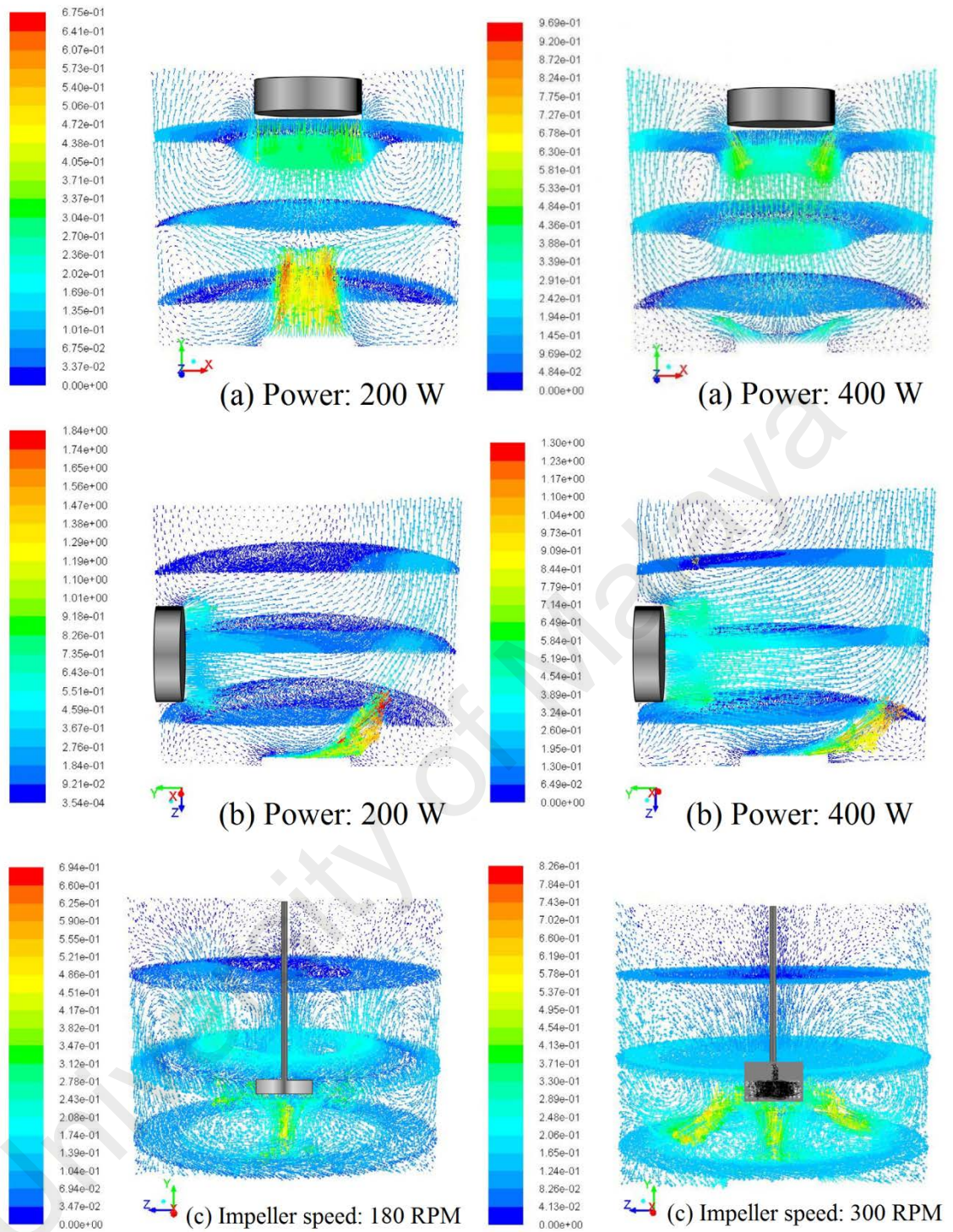


Figure 4.18: Fluid flow pattern and velocity profiles induced by a) Vertical sonicator, b) Horizontal sonicator, c) Mechanically stirring (Sajjadi et al., 2017)

However, the increment of mass transfer in this flow pattern depends on the number of bubbles imprisoned in the circulating flow. The numerical simulation showed that the

liquid velocity varied within the range of 4–47 and 9–52 cm/s in the vertical sonicator and horizontal sonicator, respectively. Furthermore, the maximum velocity magnitudes were observed in the acoustic streaming direction. The liquid velocity magnitude and fluid flow profiles were measured and validated in the non-aerated vertical sonicator using PIV analyses (Sajjadi et al., 2015b). There was only a marginal difference in the simulation results with those of PIV analyses.

On the other hand, a strong spiral and circulating flow was caused by agitation in the mechanically stirring contactor. The characteristics of the path-lines illustrated in Figure 4.18 clarify two different flow patterns induced by the impeller rotating at 180 and 300 RPM. In the former, the flow was upward among the impeller blades and it was downward along the vessel walls, assisting the gas bubbles to leave the system easier. In the latter, the direction of the central flow was downward (below the impeller), pulling the bubbles into the vicinity of the impeller to experience the highest turbulence value. However, the fluid flow pattern was not affected by the variation in ultrasound amplitude in both sonicators. It can be concluded that, the flow was discharged both axially and radially in the stirred vessel, with the highest value of 45.1 and 61.9cm/s (Figure 4.17) at impeller rotating speed of 180 and 300 RPM (below impeller).

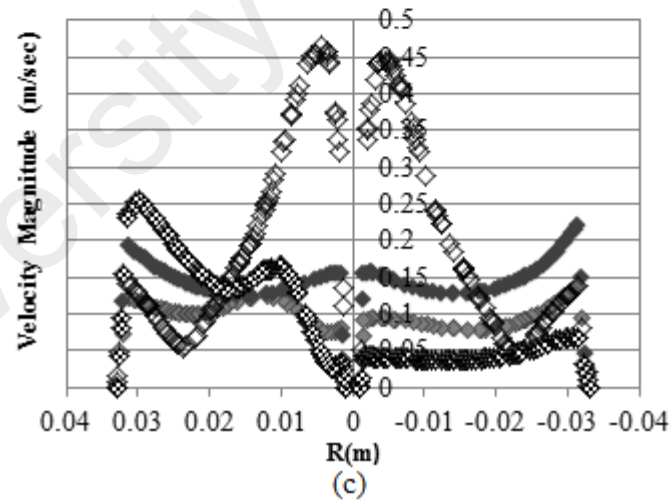
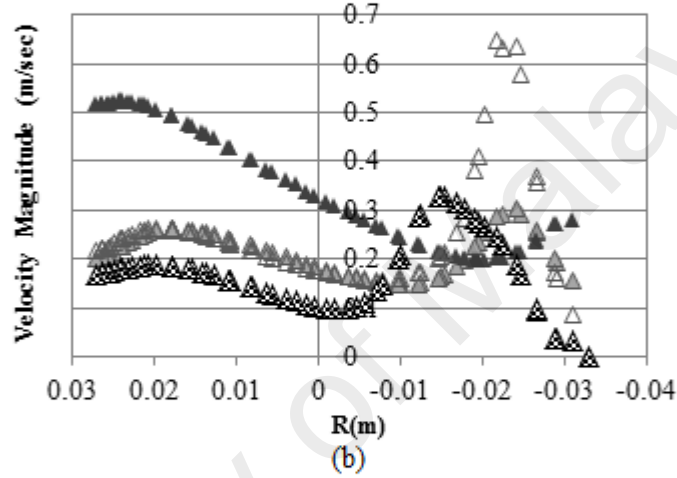
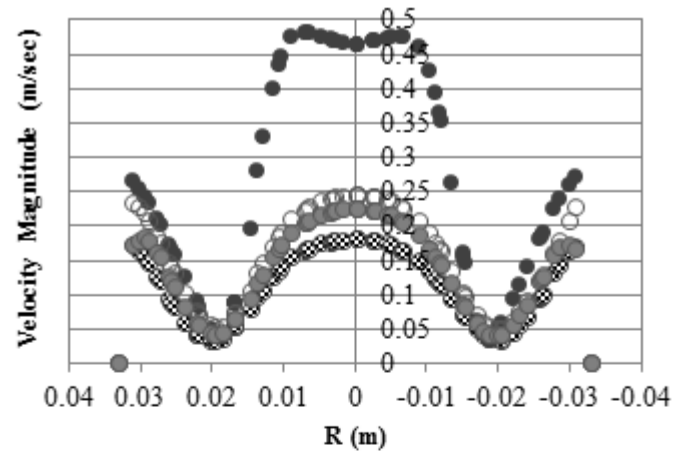


Figure 4.19: Velocity magnitude at 3cm elevation from the tank bottom induced by: a) VP-Sonocator, b) HP-Sonocator, c) mechanically Stirrer. Grey filled: Case 1, Black filled: Case 2, White filled: Case 3 Pattern filled: Case 4.

Note that the values presented in Figure 4.18c relate to the velocity magnitude above the impeller. A point should be considered in this figure. Velocity magnitude related to case 3 (with highest gas injection) and case 4 (with highest viscosity) demonstrate highest velocity magnitude in center and left side of the figure which is caused by the accumulation of gas bubbles. In other words the gas bubbles in some regions accumulate and go toward liquid surface, which affect the symmetrical distribution of velocity. This challenge is more intensive in liquid with higher viscosity as it is observed in Figures 4.18c and 4.20c and affected on the mass transfer profile as observed in Figure 4.22c, which will be discussed in next parts.

4.1.4.2 Turbulent Intensity Dissipation

The results obtained for turbulent intensity dissipated into the system are shown in Figure 4.19. As observed, the turbulent intensity dissipation values in the HP-sonicator and VP-sonicator were almost three times greater than that in the stirred vessel, where the systems contained liquid with a viscosity of $0.001\text{kgm}^{-1}\cdot\text{s}^{-1}$. The maximum turbulent intensity dissipation rate was observed in the direction of acoustic jet streaming starting from the transducer's surface in sonicators and in vicinity of the impellers in the stirred vessel. Increasing the liquid viscosity in sonicators limited the jet-like motion of acoustic streaming, resulting in lower turbulent intensity dissipation. The same happened in stirred vessel. In other words, higher turbulence observed in regions near the impeller. However, turbulence dissipation into regions away from the impeller was limited and reduced. Although, no significant increase in the turbulent intensity dissipation in HP-S and SV was observed with increased superficial gas velocity, the presence of entrapped air slightly altered the turbulent intensity dissipation in some regions. In term of input power, higher turbulent intensity dissipation was observed in the HP-sonicator, VP-sonicator and stirred vessel, respectively. It should be noted that, the values presented in Figure 4.17 are the exact turbulence intensity at 3cm elevation

from the tank bottom which is in the direction of horizontal probe sonoreactor. However, greater increment in turbulent intensity (as the average value in whole contactor) with ultrasound power was obtained by placing the horn tip vertically instead of horizontally.

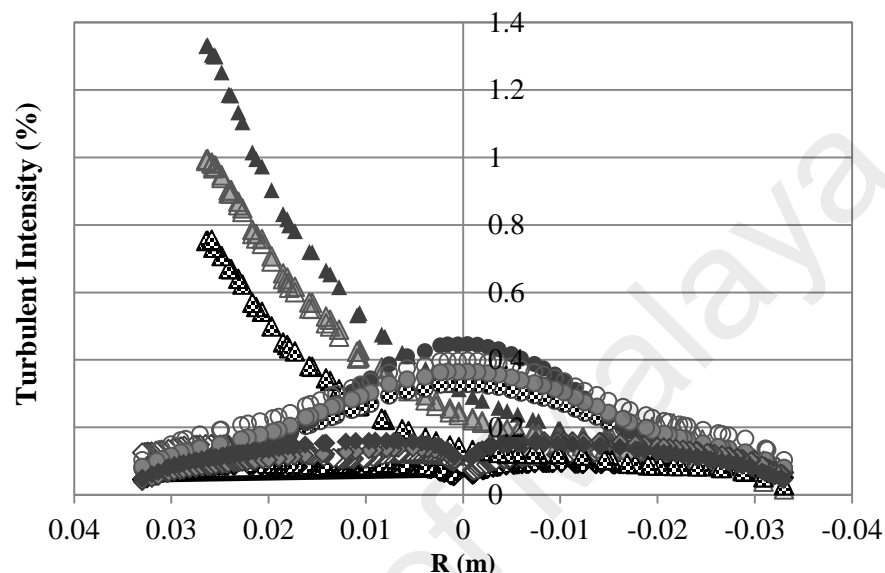


Figure 4.20: Distribution of turbulence intensity at 3cm elevation from the tank bottom induced by ○) VP-Sonocation, Δ) HP-Sonocation, ◇) mechanically stirring. Grey filled: Case 1, Back filled: Case 2, White filled: Case 3 Pattern filled: Case 4.

4.1.4.3 Gas-liquid interfacial area

The CFD results of the flow patterns in the investigated system are demonstrated in Figure 4.20. As observed, in the system of VP-sonicator, acoustic jet improved the gas volume fraction by creating a flow pattern in which gas bubbles were significantly spread along the wall. In parallel, this flow pattern had an antagonistic effect through which the gas bubbles were directly conducted to the free surface of the system. In contrast, HP-sonicator exploited of two advantage: i. acoustic jet-like streaming imprisoned the gas bubbles in the HP-sonicator (Figure 4.20 b₂ and b₃), which increased the residence time and subsequent mass transfer, ii) a section of the bubbles followed

the flow pattern circulating within the system. However, this flow pattern suffered from the weak spreading of the gas bubbles in the system and most of which got rid of the acoustic jet streaming and moved to the free surface of the system. The results related to the average volume fraction of air in the systems are provided in Figure 4.21. As observed, increasing the ultrasound power in the VP-sonicator (a2) had a negative effect on the presence of gas bubbles in that system. In this case, higher power helped the bubbles leave the system sooner. However, increment of gas hold up with ultrasound power in the HP-sonicator (b2) indicated that more bubbles were imprisoned under the acoustic jet or in the circulating flow induced by higher-powered jet streaming. The same situation happened by increasing the impeller rotating rate (c2). The figure also indicates that an increase in the superficial gas velocity led to an obvious increment in the value of the gas volume fraction with a linear trend. These changes were up to 90.2% (a3), 65.4% (b3) and 28.1% (c3) in the system of VP-sonicator, HP-sonicator and stirred vessel, respectively. Higher increments in sonoreactors corresponded to the homogeneous regime induced in these systems. But as observed in Figure 4.20 (c3), the impeller rotating rate of 180RPM is not sufficient to imprison the bubbles in the flow pattern dominated in the system and most of the bubbles easily leave the stirred vessel. The simulation results suggest that the increment of liquid viscosity from 0.001 to 0.006 cP slightly increased the gas hold up in the sonicators (a4 and b4) due to the increment of residence time. However, reduction of gas hold-up with viscosity in the stirred vessel related to the accumulated bubbles which leave the system faster as shown in case c4 (in Figure 4.21). Generally, Figure 4.21 shows that there was an average increment of 97.7% in the gas hold-up in the sonicators by changing the geometrical conditions (horizontal position of the probe to vertical position) under the same operating conditions.

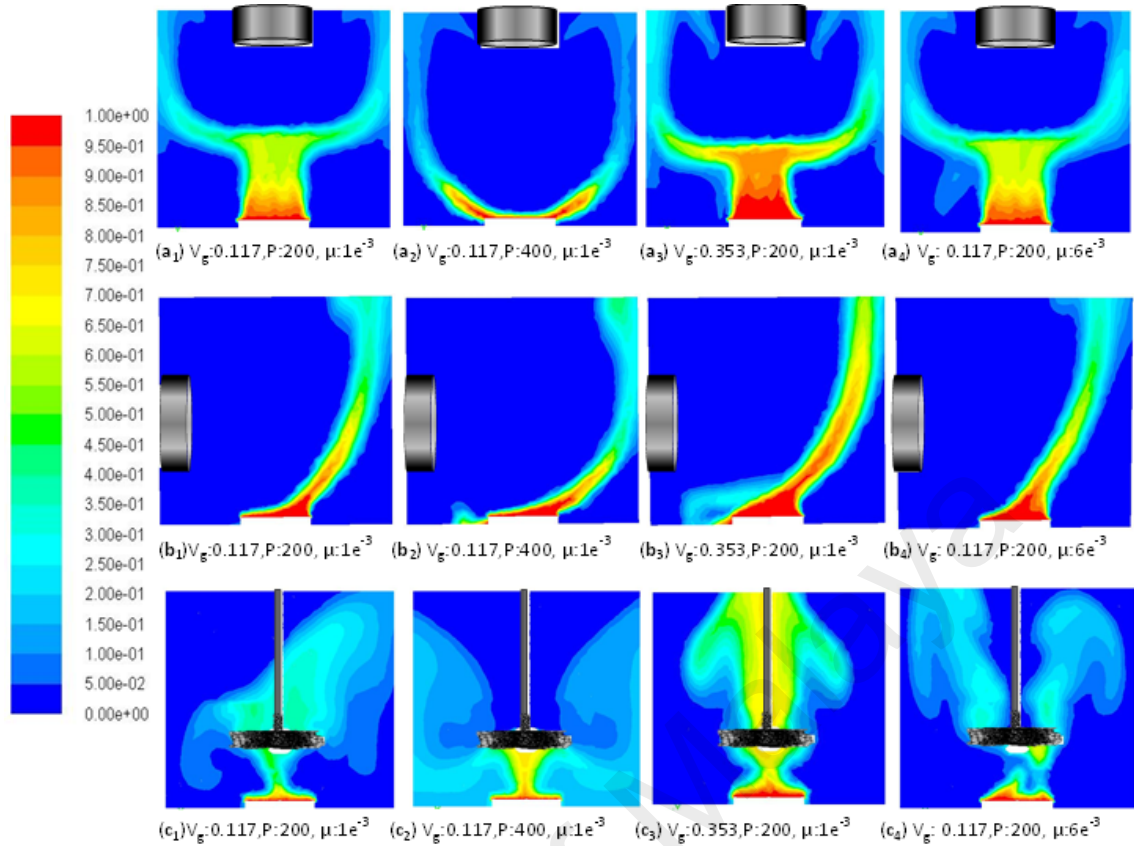


Figure 4.21: Flow pattern of gas bubbles distribution within the a) VP-Sonocation, b) HP-Sonocation, c) mechanically stirring.

The same difference was observed in the stirred vessel due to the circular liquid flow pattern that dominated in this system. Accordingly, the highest gas bubbles volume fraction with the values of 9.7% and 12% were observed in two cases: VP-sonoreactor with the gas injection of 0.353 m/s (a_3) and stirred vessel with the impeller rotating rate of 300RPM (c_2). The differences in terms of velocity magnitude and turbulent intensity dissipation appeared to be the main reasons for the observed variation in the mass transfer rate in these reactors.

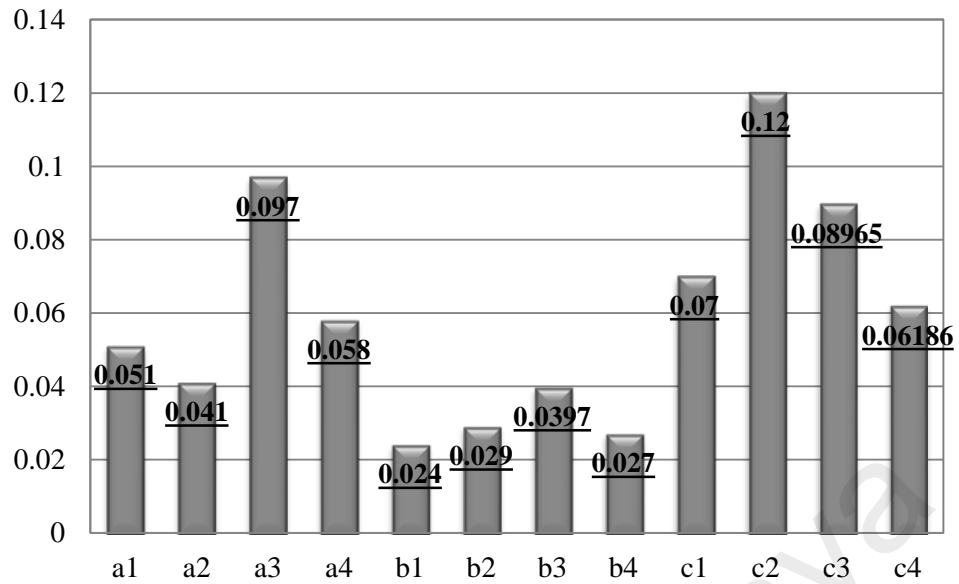
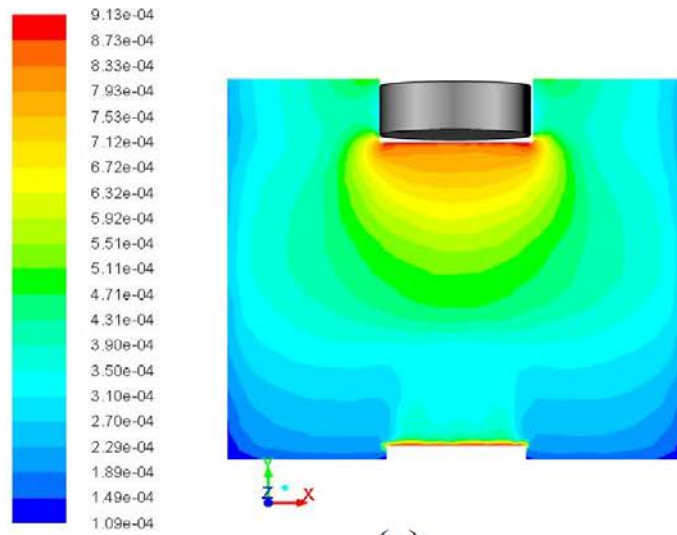


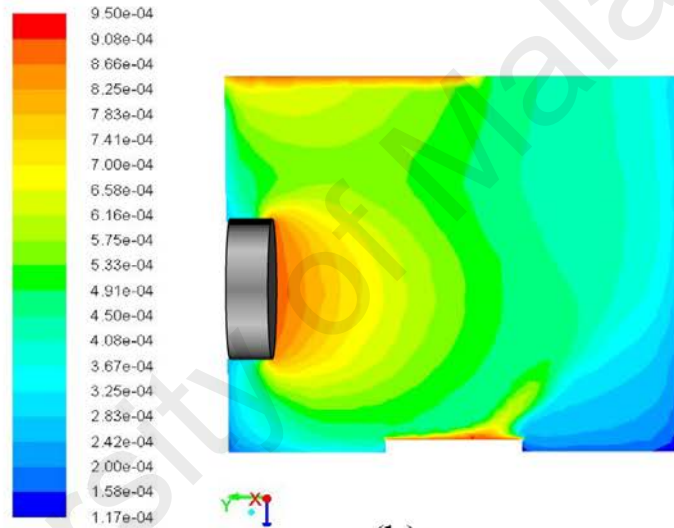
Figure 4.22: Gas hold up volume fraction within the a) VP-Sonocation, b) HP-Sonocation, c) mechanically stirring.

4.1.4.4 Volumetric Gas-Liquid Mass Transfer

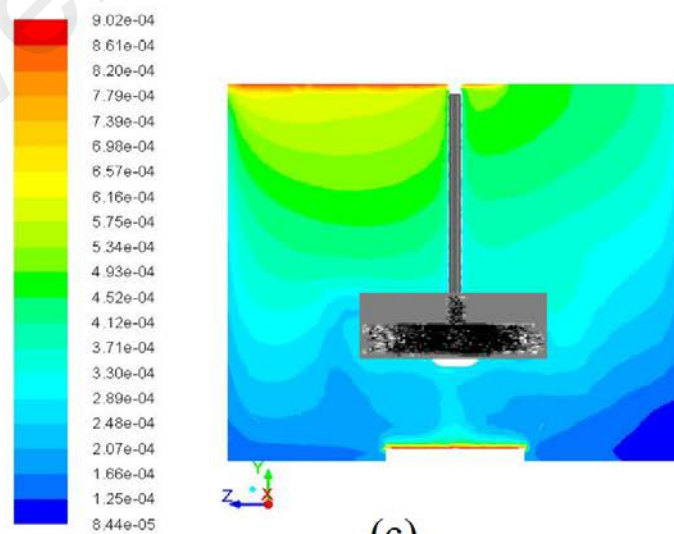
The momentary gas-liquid mass transfer coefficient (k_L) after 5 sec is presented in Figure 4.22. As observed, the maximum potential points of the liquid mass transfer coefficient in the VP-sonicator and HP-sonicator were observed in two regions i) in vicinity of the sparger due to the direct interaction of the acoustic jet-like streaming with the gas bubbles; ii) in vicinity of the transducer and in the direction of the acoustic jet like streaming due to large accumulation of kinetic energy in these regions. Comparing the VP-sonicator and HP-sonicator contours also demonstrated that more regions in the HP-sonicator were potential for higher gas-liquid mass transfer coefficient. The opposite was observed in the stirred vessel.



(a)



(b)



(c)

Figure 4.23: Gas-liquid mass transfer coefficient within the a) Vertical sonicator, b) Horizontal sonicator, c) Mechanically stirrer (Sajjadi et al., 2017).

The volumetric mass transfer coefficient (k_La) simulated under 12 different operating conditions, at different positions above the sparger, middle of the reactor and close to the free surface, is demonstrated in Figure 4.23. The exact and averaged values of both the CFD and experimental results are reported and validated in Figure 4.24. It should be noted that only regions in which gas bubbles exist can contribute to the transfer phenomenon. Therefore, the area with zero value of k_La demonstrated no presence of gas bubbles. Generally, the volumetric mass transfer coefficient in the sonicators almost doubled that in the mechanically stirred system. Similar result was reported by Coleman and Roy in their study on mass transfer under ultrasound irradiation who reported that agitation provided by ultrasound significantly increased the mass transfer rate by about 10 times (Coleman and Roy, 2014). Although gas hold-up in the stirred vessel was greater than in the sonicators, the volumetric and overall mass transfer rate were prominently less than that in both the sonicators due to lower turbulent kinetic energy. Between the sonicators, a slight increment was observed in mass transfer value in the HP-sonicator. Generally the results predicted by CFD simulation confirm the results obtained by experimental tests, except in one case (b2). This difference was caused by the low value of gas hold-up predicted by CFD simulation due to weak and incomplete circulation in the system in this case. Experimental analysis of gas volume fraction due to especial geometrical properties of contactors in this study was not possible. However, the authors clearly observed that the flow pattern predicted by CFD simulation agreed well with those in experimental tests which confirm the results predicted by CFD simulation. The other possible reason may be related to the bubbles size distribution. In mass transfer analysis, computationally or experimentally, bubble size distribution and turbulent intensity are the keys which affect the mass transfer results. The other obvious underestimation was observed in case a2. Since, cases of a2 and b2 are accompanied by

higher ultrasound power compared to other cases, the reason of under estimations more likely caused by deviation in bubble size analysis.

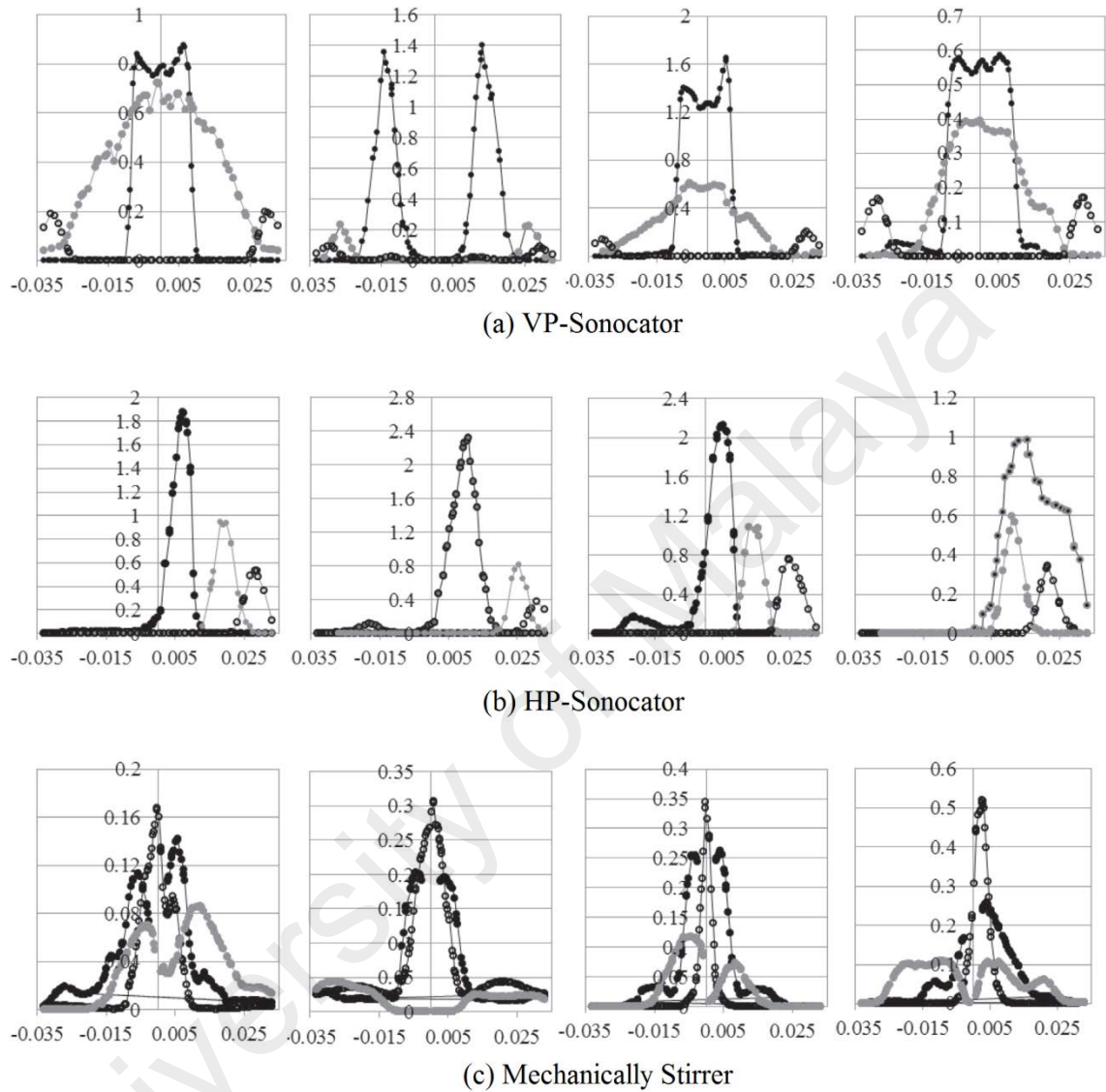


Figure 4.24: Volumetric mass transfer coefficient within the a) VP-Sonocation, b) HP-Sonocation, c) mechanically stirring. ●: Above sparger, ●: Middle of the reactor, ○: Close to the free surface.

The influence of superficial gas velocity, liquid viscosity and ultrasound power amplitude upon the overall mass transfer are also shown Figure 4.24. The simulation and experimental results depicted an increase in the overall mass transfer with the superficial gas velocity. This effect was mostly due to an increase in the gas volume

fraction. Higher viscosity inhibited the mass transfer because of its significant reducing effect on deploying turbulent kinetic energy, which led to a decrease in the mass transfer coefficient and overall mass transfer. Besides, higher viscosity produced another negative effect upon the mass transfer rate since it slightly increased the bubble size distribution. It also reduced the value of gas diffusivity in the liquid phase (Gómez-Díaz et al., 2009).

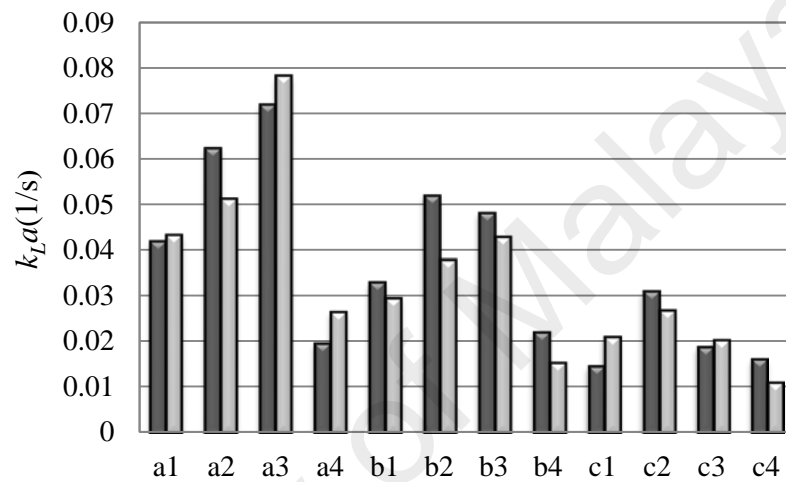


Figure 4.25: Volumetric mass transfer coefficient within the a) VP-Sonocation, b) HP-Sonocation, c) mechanically stirring.

Generally, the effect of liquid viscosity and ultrasound power amplitude upon the mass transfer value was mostly related to the turbulent kinetic energy, while the influence of superficial gas velocity was more related to the gas volume fraction. In the stirred vessel, the rotating rate of impellers affected both the turbulent kinetic energy and gas volume fraction within the liquid. However, in the stirred vessel with an impeller rotating speed of 180 RPM, it was observed that most of the bubbles rose with low dispersion or were almost undisturbed throughout the central area. In the sonicators, turbulent fluid motion that assisted the general gas-liquid mixing caused by acoustic jet streaming increased with ultrasound power amplitude and enhanced the distribution of

the entrapped gas bubbles. Experimentally, increased ultrasound power amplitude reduced the average size of bubbles. In this study, the overall mass transfer coefficient (k_La) increased by about 18.3% and 28.3% with a corresponding increase in the power amplitude by about 200 W in the VP- and HP-sonicators, respectively. Similar observation was found in the literature (Kumar et al., 2005), indicating the linear increment of k_La with the power dissipated per unit volume.

4.1.5 Empirical Correlations for Gas-Liquid Mass Transfer

Many correlations were developed in the last decades in order to predict mass transfer based on operating parameters. Table 4.6 shows some of the most significant correlations for k_La in sonochemical reactors and stirred vessels. The most commonly used correlations in the existing literatures are valid for watery mediums with a viscosity of 1 cP. The influence of viscosity on k_La under ultrasonic irradiations is not considered in any of the sonochemical reactor's correlations, as shown in Table 4.6. The following correlations obtained based on the results from this study for sonochemical reactor with vertical ultrasonic horn, horizontal ultrasonic horn and 4-blade propeller stirred vessel, respectively.

$$k_La = 0.019 \times \left(\frac{P}{V}\right)^{1.18} V_g^{0.25} \mu^{-0.31} \quad (4.5)$$

$$k_La = 0.028 \times \left(\frac{P}{V}\right)^{0.88} V_g^{0.27} \mu^{-0.21} \quad (4.6)$$

$$k_La = 4.4 \times 10^{-3} \left(\frac{P}{V}\right)^{0.6} V_g^{0.73} \mu^{-0.15} \quad (4.7)$$

Where k_La is in s^{-1} , (P/V) is in W/m^3 , V_g is in m/s and μ is in cP . In the first two correlations in Table 4.6, k_La is only the function of ultrasonic power per liquid volume and the superficial gas velocity is not considered. This could be one of the main reasons for big error percentage between their results and the result of this study.

Table 4.6: k_La correlations based on the different operational parameters.

| Type of Reactor | Operating Parameters | Correlation | Error (%) | Remarks | Ref. |
|----------------------|--|---|-----------|--|--------------------------|
| Sonochemical reactor | P (W) V (m ³) | $k_La = 2.9 \times 10^{-10} \frac{P^2}{V}$ | 26.3 | <ul style="list-style-type: none">• Ultrasonic horn• For high ultrasonic power• The superficial gas velocity is not considered | (Gondrexon et al., 1997) |
| Sonochemical reactor | P (W) V (m ³) | $k_La = 4.2 \times 10^{-7} \left(\frac{P}{V}\right)^{1.05}$ | 28.1 | <ul style="list-style-type: none">• Ultrasonic horn tip is located just above the liquid surface• 22 kHz, 150-420 W | (Kumar et al., 2005) |
| Sonochemical reactor | P (W) V (mL) V _g (m/s) | $k_La = 0.029 \left(\frac{P}{V}\right)^{0.17} V_g^{0.37}$ | 18.24 | <ul style="list-style-type: none">• Ultrasonic horn• 20 kHz• Maximum power rating of 65 W• Liquid volume of 500 mL | (Kumar et al., 2004) |
| Sonochemical reactor | P (W) V (mL) V _g (m/s) | $k_La = 0.0039 \left(\frac{P}{V}\right)^{0.4} V_g^{0.6}$ | 16.66 | <ul style="list-style-type: none">• Ultrasonic bath• 20 kHz• Three ultrasonic transducers with power of 120 W• Liquid volume of 1-2.5 L | (Kumar et al., 2004) |
| Stirred vessel | P (W) V (m ³) V _g (m/s) | $k_La = 0.046 \left(\frac{P}{V}\right)^{0.47} V_g^{0.67}$ | 19.33 | <ul style="list-style-type: none">• Six-bladed disc turbine• T=0.60 m, D=T/3 | (Hickman, 1988) |

Table 4.6: Continued

| | | | | | |
|----------------|---|---|-------|---|----------------------------|
| Stirred vessel | P (W) V (m3) Vg (m/s) | $k_La = 0.0149 \left(\frac{P}{V}\right)^{0.59} V_g^{0.55}$ | 15.81 | <ul style="list-style-type: none"> • Four six-bladed rushton turbines • T = 0.23 m • D= T/3 | (Nocentini et al., 1993) |
| Stirred vessel | P (W) Vg (m/s) μ (cP) | $k_La \sim P^{0.62} V_g^{0.4} \left(\frac{\mu}{\mu_W}\right)^{-1.17}$ | 16.48 | <ul style="list-style-type: none"> • Four six-bladed rushton turbines • T = 0.23 m • D= T/3 | (Nocentini et al., 1993) |
| Stirred vessel | P (W) V (m3) Vg (m/s) | $k_La = 6.46 \times 10^{-3} \left(\frac{P}{V}\right)^{0.675} V_g^{0.494}$ | 8.33 | <ul style="list-style-type: none"> • Four rushton turbines • T = 0.19 m, H/D=4 D=T/3 • Vg = 0.00212–0.00848ms⁻¹ | (Linek et al., 1996) |
| Stirred vessel | P (W) V (m3) Vg (m/s) | $k_La = 8.16 \times 10^{-4} \left(\frac{P}{V}\right)^{0.68} V_g^{0.4}$ | 9.1 | <ul style="list-style-type: none"> • For aqueous CMC solution | (Arjunwadkar et al., 1998) |
| Stirred vessel | P (W) V (m3) Vg (m/s) μ (cP) | $k_La = 1.3 \times 10^{-3} \left(\frac{P_g}{V}\right)^{0.57} V_g^{0.54} \left(\frac{\mu}{\mu_W}\right)^{-0.84}$ | 7.23 | <ul style="list-style-type: none"> • Carboxymethyl cellulose (CMC) used for increasing viscosity | (Puthli et al., 2005) |
| Stirred vessel | P (W) V (m3) Vg (m/s) | $k_La = 0.04 \left(\frac{P}{V}\right)^{0.47} V_g^{0.6}$ | 10.15 | <ul style="list-style-type: none"> • T = 0.211 m • 1 < Qg < 15 L/min • 6.67 < N < 13.33 rev s⁻¹ | (Kapic and Heindel, 2006) |

Table 4.6: Continued

| | | | | | |
|----------------------|---|--|------|--|------------|
| Sonochemical reactor | P (W) V (mL) V _g (m/s) μ (cP) | $k_L a = 0.019 \times \left(\frac{P}{V}\right)^{1.18} V_g^{0.25} \mu^{-0.31}$ | 1.23 | <ul style="list-style-type: none"> • Vertical ultrasonic horn • 24 kHz | This study |
| Sonochemical reactor | P (W) V (mL) V _g (m/s) μ (cP) | $k_L a = 0.028 \times \left(\frac{P}{V}\right)^{0.88} V_g^{0.27} \mu^{-0.21}$ | 1.59 | <ul style="list-style-type: none"> • Horizontal ultrasonic horn • 24 kHz | This study |
| Stirred vessel | P (W) V (mL) V _g (m/s) μ (cP) | $k_L a = 4.4 \times 10^{-3} \left(\frac{P}{V}\right)^{0.6} V_g^{0.73} \mu^{-0.15}$ | 2.13 | <ul style="list-style-type: none"> • 4-blade propeller | This study |

Moreover, the difference between operating parameters such as tank size and ultrasonic frequency could be the other reason for the errors. According to Table 4.6, the exponent over P/V in the sonochemical reactors is generally higher compared to the stirred vessels. This is attributed to the fact that ultrasound can provides sufficient mechanical energy for mixing which combined with micro-mixing caused by acoustic cavitation. In addition, the sonochemical reactor with vertical horn from this study has the highest exponent of P/V among these correlations which represent the effective utilization of the ultrasonic power in this reactor. Less dependency of k_La on the V_g for sonochemical reactors of this study can be attributed to position of the gas sparger. Since the gas sparger is very near the ultrasonic horn, all the introduced gas affected by the ultrasonic transducers.

The experimental data obtained in this study are compared with the estimations of correlations proposed in this study (Eqns. 4.5 to 4.7) and those estimated using a few selected correlations in the literature in Figs. 4.25, 4.26 and 4.27 for vertical ultrasonic horn, horizontal ultrasonic horn, and stirred vessel, respectively. Fig. 4.25 and 4.26 demonstrate that the estimations of our correlations and those of Kumar et al. (Kumar et al., 2004) agree well with our experimental data for the sonochemical reactors due to the similarity in operating conditions and superficial gas velocity. Kumar et al.'s correlation is based on the maximum power rating of 65 W and liquid volume of 500 mL. However, the estimations of other correlations do not match well with our experimental data because they do not take the superficial gas velocity into consideration. The k_La values estimated using Kumar et al.'s correlation are higher than our experimental k_La values for the system with vertical ultrasonic horn except at high ultrasonic power of 400 W (Fig.4.25). However, the k_La values estimated using their correlation for horizontal ultrasonic horn are very close to our experimental k_La values (Fig. 4.26).

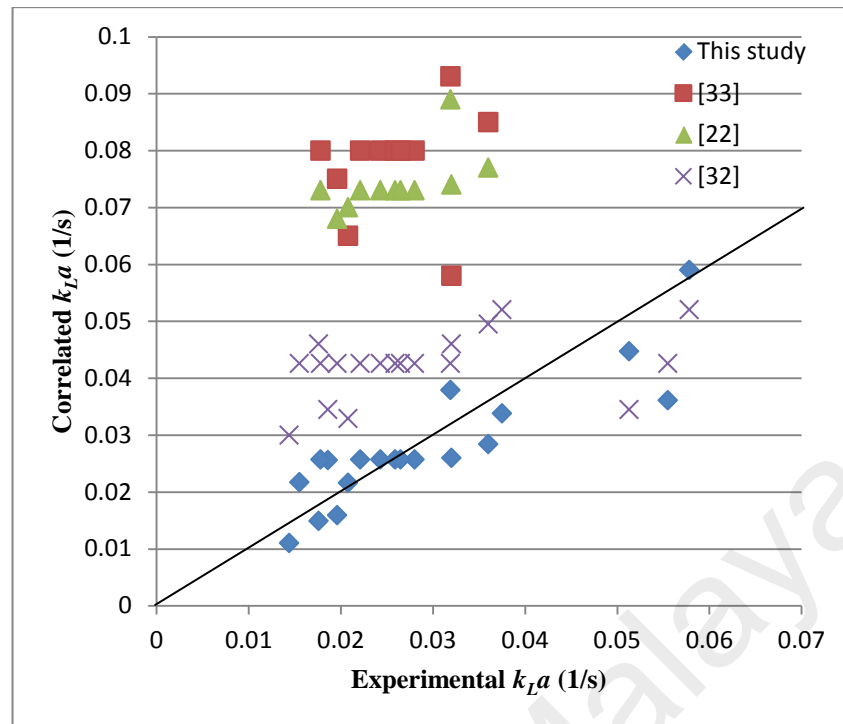


Figure 4.26: The correlated k_La versus k_La obtained from vertical ultrasonic horn experimental work

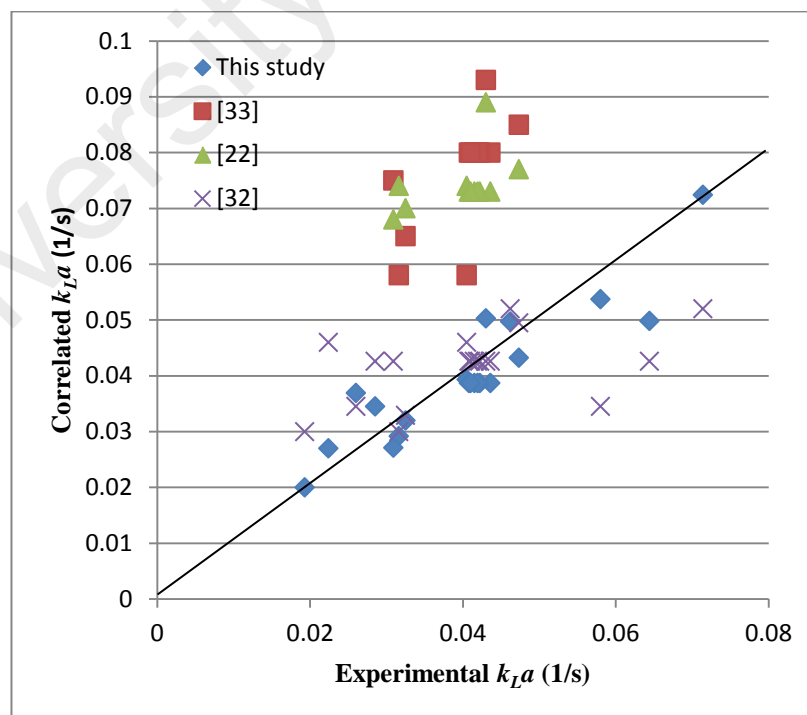


Figure 4.27: The correlated k_La versus k_La obtained from horizontal ultrasonic horn experimental work

The k_La data shown in Fig. 4.27 indicate the estimations of our correlation (Eqn. 4.7) and those of literature correlations vary from the experimental values especially for high k_La values. The variations can be attributed to the differences in vessel size, type and speed of the impeller, liquid viscosity, and superficial gas velocity used in these studies. The estimations of our correlation are close to those of Puthli et al. (Puthli et al., 2005), because it considers the effect of liquid viscosity on k_La . It should be mentioned that the correlations obtained in this study cannot be generalized for all the vessels and sonoreactors. In fact, the equations proposed in this work are quantitative descriptions about the individual and interactive effect of each parameter for different positions of ultrasound transducer compared to that under mechanical mixing.

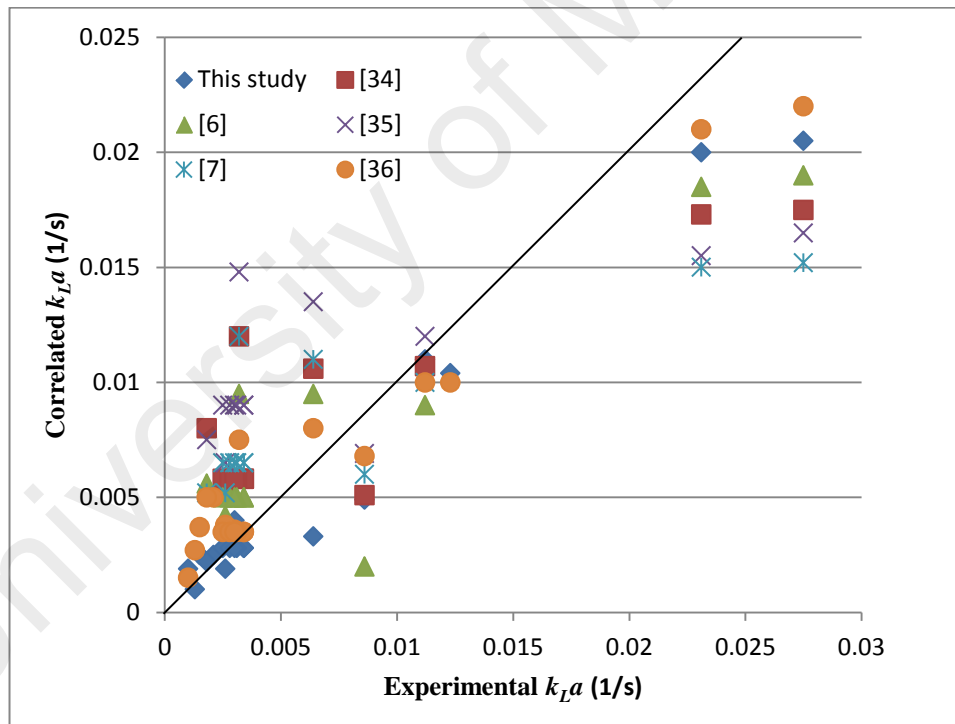


Figure 4.28: The correlated k_La versus k_La obtained from stirred vessel experimental work.

4.2 Experimental Analysis of Ultrasound Effects on Liquid-Liquid System

4.2.1 Effect of Operating Parameters on Transesterification Reaction

The following sets of experiments were designed to analyze the influence of each operating parameters on transesterification reaction of *J. curcas* oil and the effect of each parameter on biodiesel yield and reaction conversion under sonication was studied. The employed design matrix of the experiments with obtained biodiesel yield and conversion rate is presented in Table 4.7.

Table 4.7: Experimental design matrix and response results of biodiesel yield and conversion rate for transesterification reaction.

| Run | Type | Reaction Time | Catalyst Conc. | Methanol to Oil Molar Ratio | Reaction Temp | US Power | Yield % | Conversion % |
|-----|-----------|---------------|----------------|-----------------------------|---------------|----------|---------|--------------|
| 1 | Factorial | 10 | 1 | 6:1 | 30 | 200 | 83.11 | 87.89 |
| 2 | Factorial | 50 | 1 | 6:1 | 30 | 200 | 85.9 | 90.83 |
| 3 | Factorial | 10 | 2 | 6:1 | 30 | 200 | 86.21 | 91.5 |
| 4 | Factorial | 50 | 2 | 6:1 | 30 | 200 | 88.64 | 94.36 |
| 5 | Factorial | 10 | 1 | 12:1 | 30 | 200 | 86.34 | 90.84 |
| 6 | Factorial | 50 | 1 | 12:1 | 30 | 200 | 88.55 | 93.51 |
| 7 | Factorial | 10 | 2 | 12:1 | 30 | 200 | 89.32 | 93.82 |
| 8 | Factorial | 50 | 2 | 12:1 | 30 | 200 | 90.04 | 93.16 |
| 9 | Factorial | 10 | 1 | 6:1 | 50 | 200 | 86.65 | 90.57 |
| 10 | Factorial | 50 | 1 | 6:1 | 50 | 200 | 88.5 | 94.31 |
| 11 | Factorial | 10 | 2 | 6:1 | 50 | 200 | 89.23 | 95.03 |
| 12 | Factorial | 50 | 2 | 6:1 | 50 | 200 | 91.46 | 98.21 |
| 13 | Factorial | 10 | 1 | 12:1 | 50 | 200 | 88.7 | 92.68 |
| 14 | Factorial | 50 | 1 | 12:1 | 50 | 200 | 89.54 | 95.53 |
| 15 | Factorial | 10 | 2 | 12:1 | 50 | 200 | 90.17 | 94.97 |
| 16 | Factorial | 50 | 2 | 12:1 | 50 | 200 | 91.3 | 96.1 |
| 17 | Factorial | 10 | 1 | 6:1 | 30 | 400 | 86.7 | 92.05 |
| 18 | Factorial | 50 | 1 | 6:1 | 30 | 400 | 87.83 | 94.03 |
| 19 | Factorial | 10 | 2 | 6:1 | 30 | 400 | 88.02 | 93.93 |
| 20 | Factorial | 50 | 2 | 6:1 | 30 | 400 | 88.28 | 95.35 |
| 21 | Factorial | 10 | 1 | 12:1 | 30 | 400 | 89.55 | 93.53 |
| 22 | Factorial | 50 | 1 | 12:1 | 30 | 400 | 91.07 | 94.89 |
| 23 | Factorial | 10 | 2 | 12:1 | 30 | 400 | 92.55 | 96.67 |
| 24 | Factorial | 50 | 2 | 12:1 | 30 | 400 | 91.61 | 97.04 |

| | | | | | | | | |
|----|-----------|----|-----|------|----|-----|-------|-------|
| 25 | Factorial | 10 | 1 | 6:1 | 50 | 400 | 90.06 | 94.5 |
| 26 | Factorial | 50 | 1 | 6:1 | 50 | 400 | 92.19 | 96.31 |
| 27 | Factorial | 10 | 2 | 6:1 | 50 | 400 | 92.64 | 97.16 |
| 28 | Factorial | 50 | 2 | 6:1 | 50 | 400 | 94.23 | 98.54 |
| 29 | Factorial | 10 | 1 | 12:1 | 50 | 400 | 90.06 | 94.36 |
| 30 | Factorial | 50 | 1 | 12:1 | 50 | 400 | 92 | 97.15 |
| 31 | Factorial | 10 | 2 | 12:1 | 50 | 400 | 91.85 | 96.64 |
| 32 | Factorial | 50 | 2 | 12:1 | 50 | 400 | 94.51 | 98.85 |
| 33 | Axial | 10 | 1.5 | 9:1 | 40 | 300 | 88.19 | 89.62 |
| 34 | Axial | 50 | 1.5 | 9:1 | 40 | 300 | 90.75 | 94.85 |
| 35 | Axial | 30 | 1 | 9:1 | 40 | 300 | 89.73 | 93.83 |
| 36 | Axial | 30 | 2 | 9:1 | 40 | 300 | 91.06 | 95.16 |

Table 4.7: Continued

| | | | | | | | | |
|----|--------|----|-----|------|----|-----|-------|-------|
| 37 | Axial | 30 | 1.5 | 6:1 | 40 | 300 | 88.46 | 92.56 |
| 38 | Axial | 30 | 1.5 | 12:1 | 40 | 300 | 91.47 | 95.57 |
| 39 | Axial | 30 | 1.5 | 9:1 | 30 | 300 | 88.95 | 92.3 |
| 40 | Axial | 30 | 1.5 | 9:1 | 50 | 300 | 93.96 | 98.5 |
| 41 | Axial | 30 | 1.5 | 9:1 | 40 | 200 | 89.75 | 93.85 |
| 42 | Axial | 30 | 1.5 | 9:1 | 40 | 400 | 90.76 | 94.86 |
| 43 | Centre | 30 | 1.5 | 9:1 | 40 | 300 | 89.75 | 93.85 |
| 44 | Centre | 30 | 1.5 | 9:1 | 40 | 300 | 90.24 | 94.34 |
| 45 | Centre | 30 | 1.5 | 9:1 | 40 | 300 | 90.7 | 94.8 |
| 46 | Centre | 30 | 1.5 | 9:1 | 40 | 300 | 89.68 | 93.78 |
| 47 | Centre | 30 | 1.5 | 9:1 | 40 | 300 | 90.32 | 94.42 |
| 48 | Centre | 30 | 1.5 | 9:1 | 40 | 300 | 88.96 | 93.06 |
| 49 | Centre | 30 | 1.5 | 9:1 | 40 | 300 | 90.24 | 94.34 |
| 50 | Centre | 30 | 1.5 | 9:1 | 40 | 300 | 89.6 | 93.7 |

4.2.1.1 Reaction Temperature

The effects of reaction temperature on biodiesel yield and conversion rate of transesterification process are illustrated in Figure 4.28a and 4.28b, respectively. The graphs are with the catalyst concentration of 1.5 wt%, reaction time of 30 min and power of 300 W.

It was found that biodiesel yield and conversion rate increase with increase of reaction temperature (or bulk temperature). At the methanol to oil molar ratio of 6,

improvements of 3.1 % in biodiesel yield and 1.9 % in conversion rate were observed with temperature increase from 30 to 50 °C when all other parameters were kept at their average values. However, these enhancements were 1.2 % and 1.3 % at the methanol concentration of 12 for both biodiesel yield and conversion rate, respectively. If the other parameters were kept at their minimum values, the biodiesel yield and conversion rate increase were 0.88 % and 1.71 % in methanol to oil molar ratio of 6, but 1.59 % and 1.35 % for methanol to oil molar ratio of 12 for, respectively. By further increasing the other operational parameters to their maximum value, the role of temperature was almost the same as explained.

The reaction under ultrasonication, in molecular scale, is accomplished in a very high temperature because of over-heated regions. It means that the real temperature in these regions is much higher than reported temperature or bulk temperature. However, heating still increases the formation and collapse of micro-bubbles followed by enhancement in mass transfer and also improvement in both biodiesel yield and conversion rate consequently.

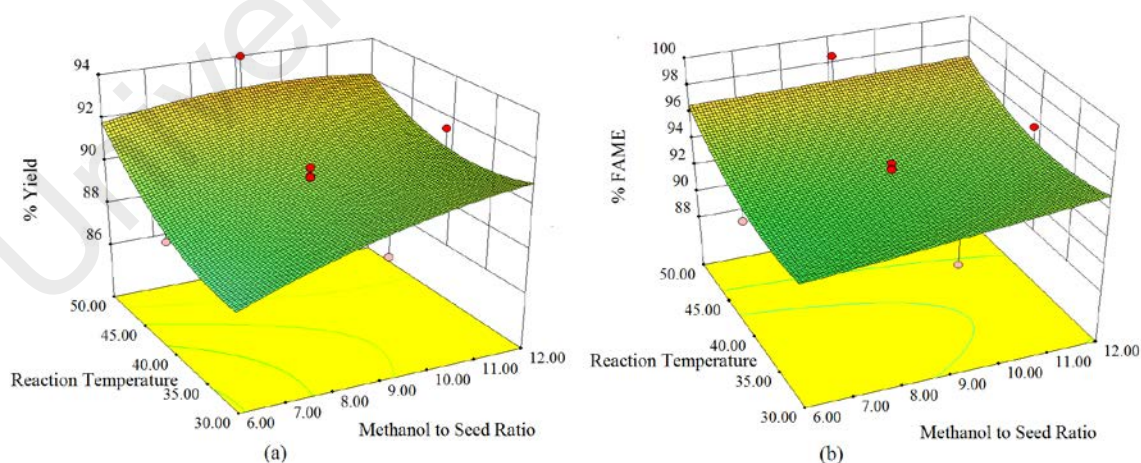


Figure 4.29: Response surface plots showing the effects of reaction temperature and methanol to oil molar ratio on a) product yield, b) conversion rate.

4.2.1.2 Methanol to Oil Ratio

Although the minimum methanol to oil molar ratio of 3:1 is necessary for transesterification process, extra alcohol quantity can accelerate the reaction. However, the problem is the reaction is reversible and the forward reversible reactions can be speed up by increase in the amount of alcohol. In this research, the influence of methanol to oil molar ratios of 6:1 to 12:1 on transesterification reaction was investigated.

Based on the Figure 4.28, the biodiesel yield increased from 88.3 % to 90.8 % at 30 °C by increasing the molar ratio of alcohol under ultrasound irradiation. However, the enhancement of biodiesel yield is not significant at the temperature of 50 °C when the amount of methanol was increasing from 6:1 to 10:1. It was even observed that the yield slightly reduced by further increasing the alcohol concentration from 10:1 to 12:1. Therefore, the optimum range of methanol to oil molar ratio for biodiesel yield was found to be between 9.5:1 to 10.5:1.

It should be justified that increasing the amount of alcohol causes an increase in cavitation activity, formation of smaller drop sizes (higher emulsion quality) and provision of extra areas for mass transfer which finally enhance the yield. At the same time, excessive alcohol in high temperature reduced the concentrations of reactant and catalyst which retarded the reaction. In addition, it was observed that the conversion rate just slightly increased by increasing of methanol to oil molar ratio within the range of 6:1 to 12:1 from 94 % to 94.9 % at 30 °C and from 96.1 % to 96.9 % at 50 °C.

4.2.1.3 Catalyst Concentration

The influence of catalyst concentration (based on the weight of *J.curcas* oil) on biodiesel yield and conversion rate of transesterification reaction is presented in Figure

4.29a and 4.29b, respectively, with the methanol to oil molar ratio of 9:1, reaction time of 30 min and ultrasound power of 300 W.

As shown in Figure 4.28, biodiesel yield and conversion rate increase with increase of catalyst concentration. At the reaction temperature range within 30 °C to 50 °C, improvements of 1.8 % in biodiesel yield and 1.3 % in conversion rate were observed with catalyst concentration increase from 1 wt% to 2 wt% when all other parameters were kept at their average values. Higher influence of catalyst on biodiesel yield was also observed at the maximum value of other parameters and the optimum value of methanol to oil molar ratio. As a result, the transesterification process under ultrasonication still has the potential to reach the higher yield values.

There was another significant observation for conversion rate at the maximum ultrasound power and methanol to oil molar ratio when the other parameters kept at their average values. Initially, insufficient amount of catalyst led to incomplete conversion and increasing the catalyst concentration greatly affected the reaction. In addition, the reaction conversion was not considerable above 30 min by increasing catalyst concentration. The observation can be attributed to the activation of side reactions, especially at higher temperatures.

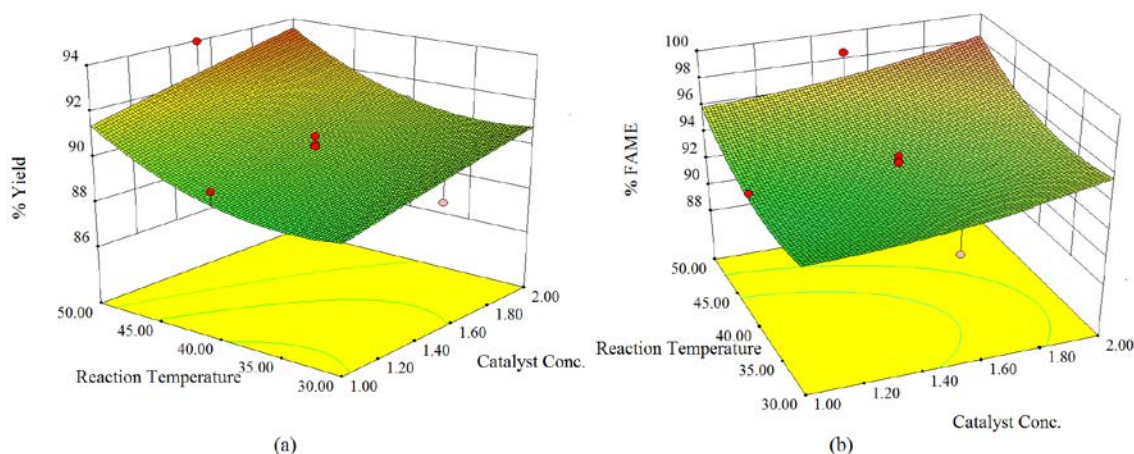


Figure 4.30: Response surface plots showing the effects of reaction temperature and catalyst concentration on a) product yield, b) conversion rate.

4.2.1.4 Ultrasound Power

The influence of micromixing caused by ultrasonic power on biodiesel yield and conversion rate is shown in Figure 4.30a and 4.30b, respectively, when the other parameters were kept at their average value. It was found that the effects of ultrasound power on both biodiesel yield and conversion rate are almost the same and there were an enhancement on transesterification yield and rate by increasing the ultrasound power. It is due to the effect of intensity of ultrasonic waves on critical size of the cavitation bubbles. Consequently, the surface area, the transport activities across the cavitation bubbles interface and the localized heating are speed up. The overall influence is generation of fine micro emulsification that improves transesterification yield and rate.

For biodiesel yield, increase of ultrasound power causes enhancement in the number of cavitation bubbles and their growth and collapse rate. However, this increment continued until a certain value. Further increase of it does not enhance the emulsion quality and biodiesel yield in sequence (Santos et al., 2009). The similar results have been observed by other researchers in sonochemical reactors with high ultrasound power (Okitsu et al., 2010; Thanh et al., 2010).

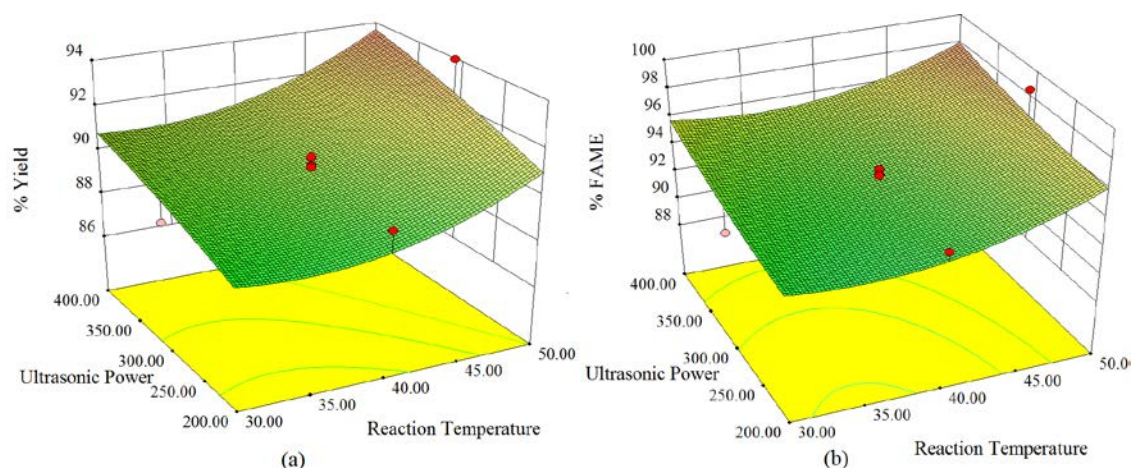


Figure 4.31: Response surface plots showing the effects of reaction temperature and ultrasonic power on a) product yield, b) conversion rate.

4.2.1.5 Reaction Time

The influences of reaction time on biodiesel yield and conversion rate are presented in Figures 4.31a and 4.31b. On the middle value of all other parameters, ultrasound assisted transesterification of *J. curcas* oil within 10 min could achieve the yield of 88.19 % and conversion rate of 89.62 %. These values could also increase until 91.9 % and 93.66 % within 10 min for biodiesel yield and conversion rate, respectively, when other parameters kept at their maximum values.

It was also observed that the biodiesel reaction yield quickly increased within the first 30 min and afterward, increased slowly. This result shows that reaction have almost achieved equilibrium. This phenomenon was repeated at the maximum time and temperature as well.

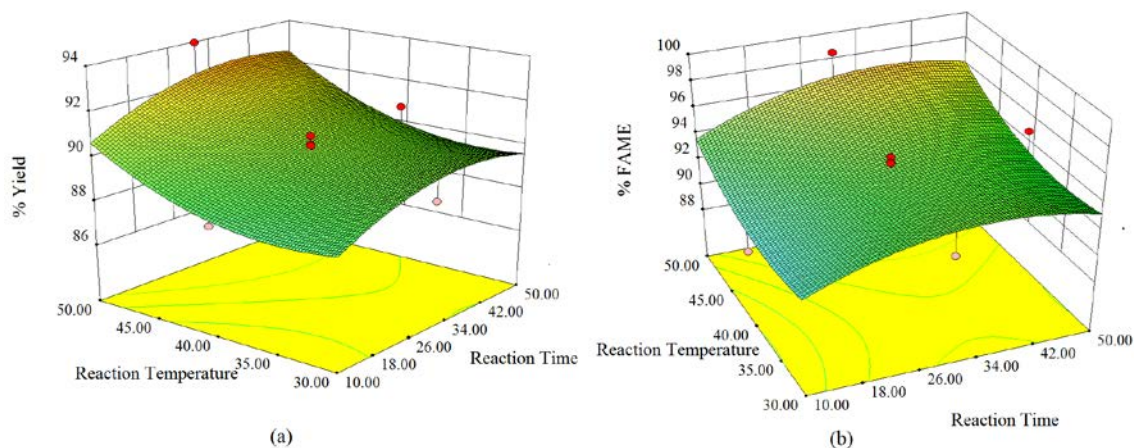


Figure 4.32: Response surface plots showing the effects of reaction temperature and reaction time on a) product yield, b) conversion rate.

4.2.2 Transesterification Process Using Mechanical Stirring

Experimental design matrix and response results for transesterification reaction under mechanical mixing are reported in Table 4.8. In addition, the comparison results of transesterification yield and conversion rate under ultrasound irradiation and mechanical stirring are provided in Figure 4.32. This figure demonstrates that biodiesel yield and conversion rate are higher under ultrasonic irradiation compared to the mechanical stirring within the same reaction time. In other words, the reaction completed faster in the sonochemical reactor, compared to conventional stirred vessel.

Table 4.8: Experimental design matrix and response results for mechanical mixing.

| Run | Reaction Time | Catalyst Concentration | Methanol to oil molar Ratio | Reaction Temperature | Mixing Intensity | Yield % | Conversion % |
|-----|---------------|------------------------|-----------------------------|----------------------|------------------|---------|--------------|
| 1 | 30 | 1.5 | 9:1 | 40 | 100 | 56.33 | 61.3 |
| 2 | 30 | 1.5 | 9:1 | 40 | 250 | 64.8 | 65.85 |
| 3 | 30 | 1.5 | 9:1 | 40 | 400 | 70.54 | 74.68 |
| 4 | 30 | 1.5 | 9:1 | 40 | 550 | 74.11 | 77.59 |
| 5 | 30 | 1.5 | 9:1 | 40 | 700 | 76.52 | 80.88 |

Higher biodiesel yield and conversion rate under sonication is due to the ability of ultrasound irradiation in enhancing mass transfer between the immiscible reactants together with generates vacuum micro-regions in the liquid called “sonoluminescence bubble” that are filled with reactants vapors. The phenomenon of acoustic cavitation also assists the system to generate fine micro emulsion through generation of micro streams, micro turbulent eddies and shock waves. Besides, the collapse is extremely energetic, resulting in generation of highly pressurized and over-heated regions called “hot spots” which induce the reaction (Sajjadi et al., 2015a).

However, the rate of enhancement in biodiesel yield and conversion rate by increasing the ultrasonic power is not as prominent as by increasing the mechanical mixing intensity. It can be justified that, the number of cavitation bubbles and their growth and collapse rate in sonochemical reactor can only increase until a certain value and further increase of it cannot enhance the reaction yield (Santos et al., 2009). In this study, the ultrasound power above 200 W has a slight influence on biodiesel yield and conversion rate while the reaction could potentially enhance by further increasing mixing speed in macro mixing along with conventional heating.

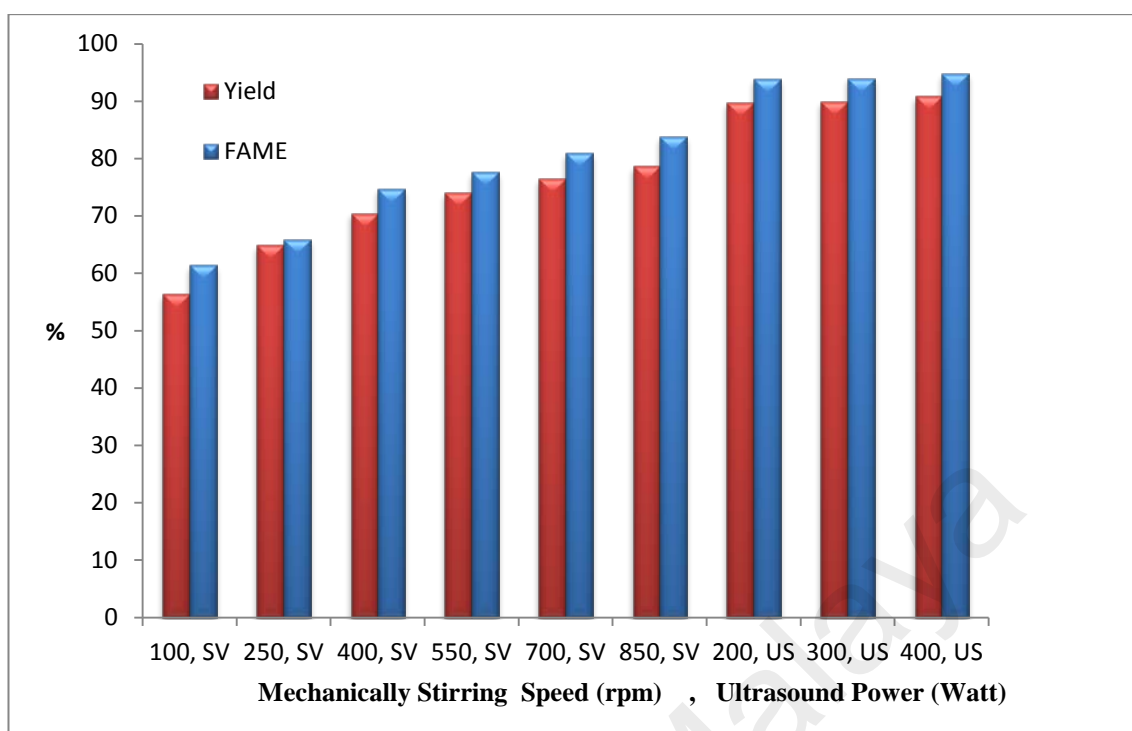


Figure 4.33: Percentages of biodiesel yield and conversion rate versus stirrer speed and ultrasound power. Methanol to oil molar ratio: 9:1, NaOH concentration: 1.5% wt, reaction time: 30 min and reaction temperature: 40 °C.

Sajjadi et al. (Sajjadi et al., 2015b) carried out a comparative study on fluid flow pattern between a sonoreactor and a mechanical stirred vessel. Figure 4.33 and 4.34 show the predicted flow pattern in the vertical slices in ultrasonicator and stirred vessel systems, respectively. As observed, only one fluid loop was generated under ultrasound irradiation that pushed the fluid downward and then upward. However, there were two circulation loops in the stirred vessel, one above the impeller and the other below it. In other words, a downward flow was generated in the center/below the impeller and an upward flow along the vessel walls. By following the path-lines illustrated in Figure 34, it is observed that the two circulation loops appeared like a vertical infinity symbol, in which the upper loop had a smaller diameter than the lower one. It was attributed to higher suction flow rate above the impeller than the discharge flow rate below.

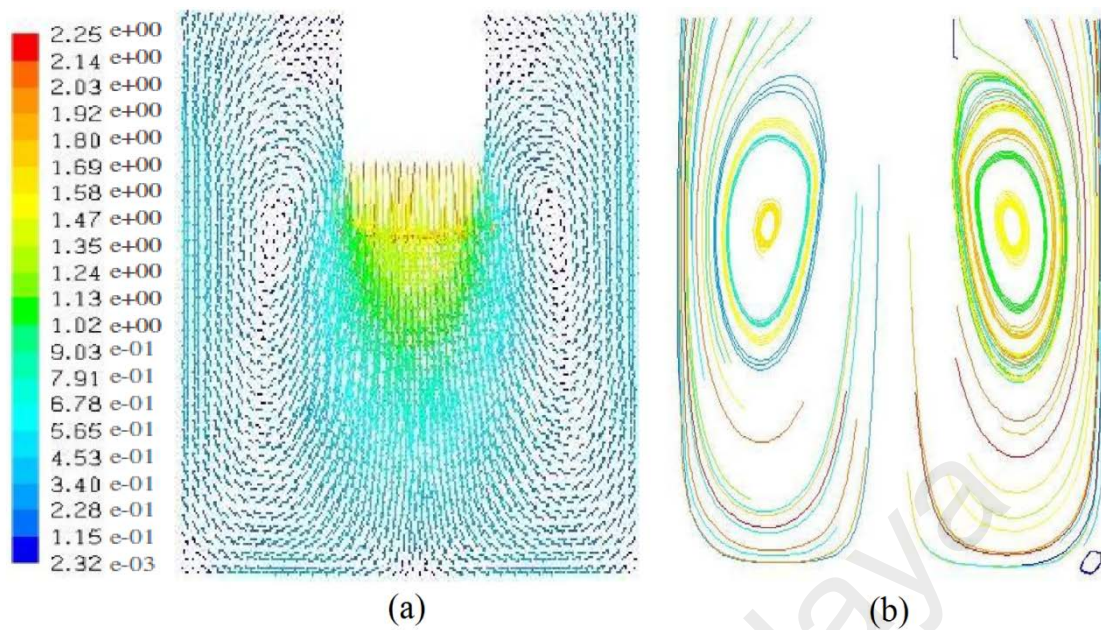


Figure 4.34: Vertical fluid flow pattern induced by ultrasound irradiation with power of 400W (a) presented by velocity vectors (b) presented by pathlines (Sajjadi et al., 2015b).

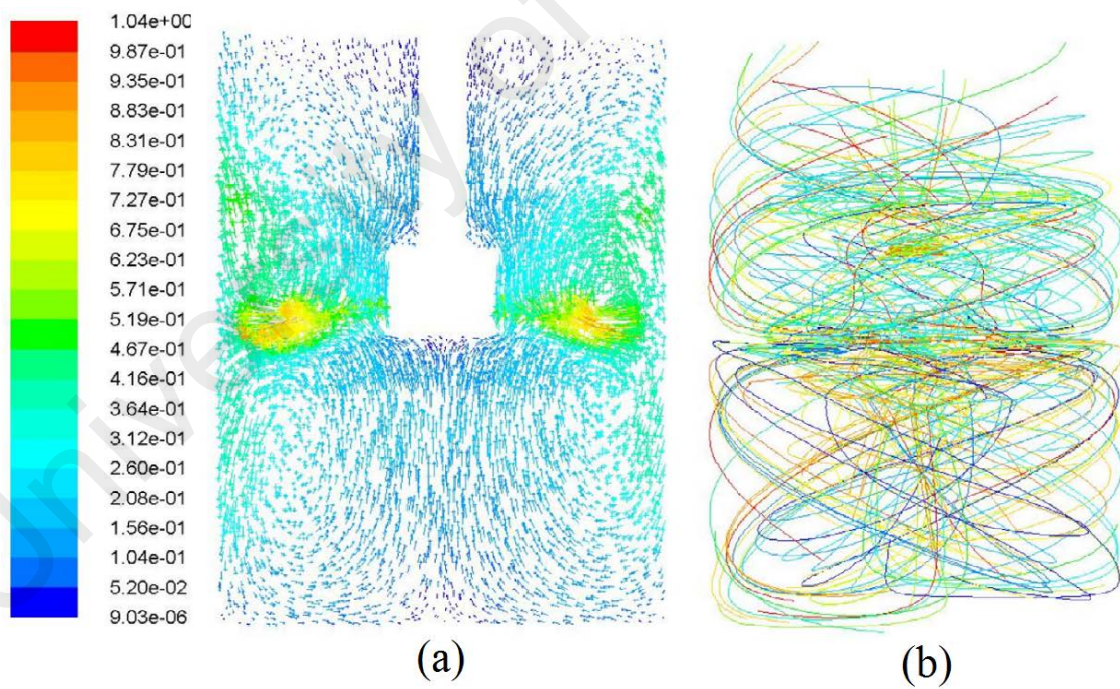


Figure 4.35: Vertical fluid flow pattern induced by stirred vessel with impeller velocity of 600 RPM (a) presented by velocity vectors (b) presented by pathlines (Sajjadi et al., 2015b).

On the other hand, an axial flow was created in the sonoreactor in a downward direction from the transducer toward the top of the tank. Liquid flow pattern under ultrasound irradiation is severely affected by the direction and power of jet-like acoustic streaming. Therefore, different flow patterns are generated depends on these two factors. In other words, jet-like acoustic streaming acts as an input energy and motivating force. It induces the liquid to move and guides its motion within the system starting from the surface of the transducer.

In their study, the probe was introduced from the top of the vessel into the liquid media which pushed the liquid to circulate from the top towards the bottom of the vessel. Accordingly, a uniform fluid circulation that covered all regions was generated by jet-like acoustic streaming in this study. This type of flow pattern is the most suitable for mixing of liquids with different densities as it prevents accumulation of denser liquid at the bottom or less dense liquid at the top (Figure 4.33).

As observed in Figure 4.34, the flow was discharged both axially and radially in the stirred vessel. It was found that the flow moved away from the blades at about 45° due to the angle of the blades. The flow was constrained in this system due to small radius of the vessel, resulting in incomplete liquid circulation and generation of two small circulation loops. Moreover, the flow pattern in both systems did not vary significantly when the power input (in sonoreactor) or impeller speed (in stirred vessel) increased. Therefore, both systems generated a stable flow pattern. This characteristic can considerably decrease the mixing time, especially in sonoreactors which generate only one circulation loop.

4.2.3 Development of Regression Model

4.2.3.1 Biodiesel Yield

The relationship between product yield and five independent parameters under ultrasonication were investigated through CCD. Eight runs were carried out at the centre point, as it shown in Table 4.7, to determine the experimental inaccuracies. The following model was developed in terms of coded factors for prediction of biodiesel production yield (%):

$$\text{Yield (\%)} = 74.18 + 0.21X_1 + 3.59X_2 + 2.26X_3 - 0.57X_4 + 0.02X_5 - 0.02X_3X_4 + 0.01X_4^2 \quad (4.8)$$

The positive and negatives term indicate synergistic and antagonistic effects, respectively (Ahmad et al., 2009). High R-squared value of 0.9237 indicates a good agreement between the predicted and experimental values. The sufficiency of the obtained model was justified through Analysis of Variance (ANOVA). The results of P-value for reaction time (X_1), catalyst concentration (X_2), methanol to oil molar ratio (X_3), reaction temperature (X_4), ultrasonic power (X_5), the interaction effects of methanol to oil molar ratio and reaction temperature (X_3X_4) and the quadratic effect of reaction temperature (X_4^2) (P-value less than 0.05) indicate that they significantly affected the biodiesel production yield. High equation coefficients of X_2 and X_3 demonstrate that catalyst concentration and methanol to oil molar ratio are the most significant parameters on product yield as it was shown in Figure 4.19 and 4.20 as well.

4.2.3.2 Conversion Rate

The relationship between conversion rate and five independent parameters is presented in equation (4.9). R-squared value for obtained model was 0.8954.

$$FAME (\%) = 93.59 + 0.37X_1 - 0.79X_2 + 0.96X_3 - 0.86X_4 + 4.24E^{-3}X_5 - 0.01X_3X_4 - 4.44X_1^2 + 0.01X_4^2 \quad (4.9)$$

The results of P-value depict that the parameters that significantly influenced on conversion rate were reaction time (X_1), catalyst concentration (X_2), methanol to seed ratio (X_3), reaction temperature (X_4), ultrasonic power (X_5), the interaction effects of methanol to oil molar ratio and reaction temperature (X_3X_4) and the quadratic effects of reaction temperature (X_4^2) (P-value less than 0.05).

4.3 Experimental Analysis of Ultrasound Effects on Solid-Liquid System

4.3.1 *J. curcas* Characterisation

The *J. curcas* seed contains two parts; the kernel and the shell. Fat (54%) and protein (25%) constitute the main part of kernel, while the main component in shell is fiber (87%) (Achten et al., 2008). Since, the *in situ* transesterification was performed using the *J. curcas* kernel, the characterization was also carried out only for kernel.

The Soxhlet extraction apparatus was used in order to determine the amount of oil content in the kernel. The oil content in the *J. curcas* kernel was $35.0 \pm 0.5\%$, which was 5% less than that obtained by Azam et al. (Azam et al., 2005). The difference in the oil content could be due to many factors, such as soil characteristics, fertilizers, irrigation and annual rainfall (Achten et al., 2008; Srivastava et al., 2011; Behera et al., 2010). The moisture content was $7.8 \pm 0.5\%$ which need to be reduced before *in situ* transesterification process.

In addition, based on the literature, the free fatty acid (FFA) content in the *J. curcas* oil is 0.18-3.40 % (kg/kg*100) (Becker and Makkar, 2008; Achten et al., 2008). Alkaline catalysts will react with the FFA to produce soap and glycerol, decreasing the amount of catalyst available, or even consuming it altogether. Furthermore, soap acts to emulsify

the product, rendering the separation of alkyl esters from glycerol more difficult. However, the amount of FFA in *J. curcas* oil and as a result, the saponification in this reaction is negligible.

4.3.2 Effect of Operating Parameters on *In Situ* Transesterification

The following sets of experiments were designed to analyze the gradual increasing effect of each operating parameters on *in situ* transesterification individually. The influence of each parameter on biodiesel yield and reaction conversion under sonication with ultrasonic power of 300 W was studied, while the other parameters kept at their center point level. Table 4.9 presents the experimental design matrix and response results for individual increasing of each parameter under ultrasonic power of 300 W.

Table 4.9: Experimental design matrix and response results under ultrasonic power of 300 W

| Run | Type | Reaction Time (min) | Catalyst Concentration (mol/L) | Methanol to seed Ratio (v/w) | Reaction Temperature (°C) | Yield % | Conversion % |
|-----|--------------------|---------------------|--------------------------------|------------------------------|---------------------------|---------|--------------|
| 1 | Catalyst Increment | 30 | 0.025 | 9:1 | 40 | 39.71 | 44.2 |
| 2 | Catalyst Increment | 30 | 0.05 | 9:1 | 40 | 74.24 | 84.31 |
| 3 | Catalyst Increment | 30 | 0.075 | 9:1 | 40 | 85.33 | 90.77 |
| 4 | Catalyst Increment | 30 | 0.1 | 9:1 | 40 | 85.4 | 93.525 |
| 5 | Catalyst Increment | 30 | 0.125 | 9:1 | 40 | 86.95 | 96.5 |
| 6 | Catalyst Increment | 30 | 0.15 | 9:1 | 40 | 86.24 | 95.45 |
| 7 | Catalyst Increment | 30 | 0.175 | 9:1 | 40 | 82.11 | 95.18 |
| 8 | Time Increment | 10 | 0.1 | 9:1 | 40 | 83.28 | 93.41 |
| 9 | Time Increment | 20 | 0.1 | 9:1 | 40 | 84.2 | 93.5 |
| 10 | Time Increment | 30 | 0.1 | 9:1 | 40 | 85.4 | 93.525 |
| 11 | Time Increment | 40 | 0.1 | 9:1 | 40 | 87.9 | 94.3 |
| 12 | Time Increment | 50 | 0.1 | 9:1 | 40 | 89.14 | 95.2 |
| 13 | Time Increment | 60 | 0.1 | 9:1 | 40 | 89.2 | 95 |
| 14 | Time Increment | 70 | 0.1 | 9:1 | 40 | 89.1 | 95.15 |

| | | | | | | | |
|----|----------------------------|----|-----|--------|----|-------|--------|
| 15 | Methanol:seed Increment | 30 | 0.1 | 6:1 | 40 | 82.3 | 91.66 |
| 16 | Methanol:seed Increment | 30 | 0.1 | 7.5:1 | 40 | 84.04 | 92.11 |
| 17 | Methanol:seed Increment | 30 | 0.1 | 9:1 | 40 | 85.4 | 93.525 |
| 18 | Methanol:seed Increment | 30 | 0.1 | 10.5:1 | 40 | 87.1 | 95.05 |
| 19 | Methanol:seed Increment | 30 | 0.1 | 12:1 | 40 | 87.51 | 94.44 |
| 20 | Methanol:seed Increment | 30 | 0.1 | 13.5:1 | 40 | 87.9 | 92.41 |
| 21 | Temperature Increment | 30 | 0.1 | 9:1 | 20 | 81.3 | 91.12 |

Table 4.9: Continued

| | | | | | | | |
|----|--------------------------|----|-----|-----|----|-------|--------|
| 22 | Temperature Increment | 30 | 0.1 | 9:1 | 30 | 83.12 | 92.68 |
| 23 | Temperature Increment | 30 | 0.1 | 9:1 | 40 | 85.4 | 93.525 |
| 24 | Temperature Increment | 30 | 0.1 | 9:1 | 50 | 86.94 | 95.95 |
| 25 | Temperature Increment | 30 | 0.1 | 9:1 | 60 | 86.3 | 96.22 |

4.3.2.1 Catalyst Concentration

The influence of catalyst concentration on product yield and FAME content are shown in Figure 4.35. Increase in concentration of catalyst from 0.025 to 0.1 mol/L improved the reaction conversion from 44.2 to 93.525% and it then reached a plateau by further increasing of catalyst concentration. However, the concentration of NaOH from 0.025 to 0.125 mol/L did not significantly affect the product yield but further overloading led to decrease in yield of reaction due to formation of emulsion.

This emulsion presumably comes from the saponification reaction which is a competing reaction in transesterification process with alkali catalyst (Canakci and Van Gerpen, 1999). Similar results were also reported by Barekati-Goudarzi et al. (Barekati-Goudarzi

et al., 2016) for microwave-assisted *in situ* transesterification of Chinese tallow tree seeds.

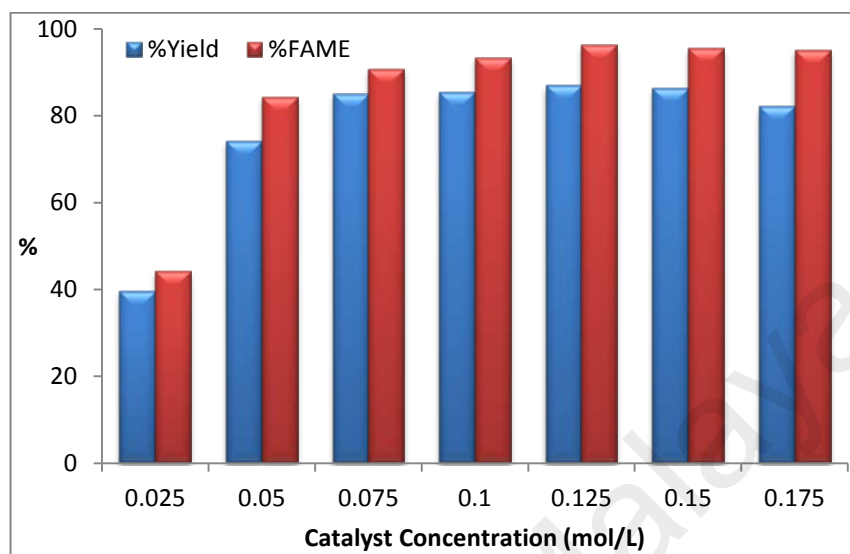


Figure 4.36: Plotted data for the effect of catalyst concentration on *in situ* transesterification of *J. curcas*. Ultrasound power = 300W; methanol to seed ratio = 9:1; reaction temperature = 40°C; reaction time = 30 min.

4.3.2.2 Reaction Time

The effect of reaction time on *in situ* transesterification is given in Figure 4.36. As observed, product yield gradually increased with the reaction time. However, the influence of reaction time on conversion efficiency is negligible. According to the experimental results, the maximum yield of 89.2% was achieved under sonication power of 300 W within 50 minutes.

A comparison to similar works from literature (Amalia Kartika et al., 2013; Shuit et al., 2010) shows that *in situ* transesterification of *J. curcas* seed under ultrasonic irradiation needs less time to be proceed. Shorter reaction time under higher ultrasound power confirmed the principal role of ultrasound in elimination of mass transfer resistance.

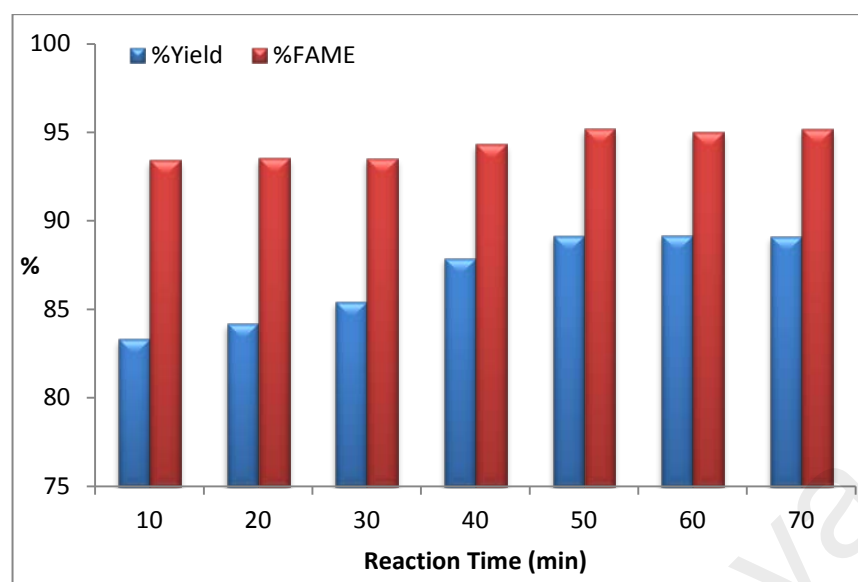


Figure 4.37: Plotted data for the effect of catalyst concentration on *in situ* transesterification of *J. curcas*. Ultrasound power = 300W; methanol to seed ratio = 9:1; NaOH concentration = 0.1N; reaction temperature = 40°C.

4.3.2.3 Methanol to Seed Ratio

Methanol to seed ratio, as shown in Figure 4.37, is significantly effective on both product yield and FAME content. Biodiesel yield increased steadily by increasing the ratio while the conversion rate decreased by passing an optimum amount of alcohol to seed ratio. The observed results are in agreement with the study by Ren et al. (Ren et al., 2010) where they reported that high amount of methanol is needed for penetration of alkaline methanol into the seed.

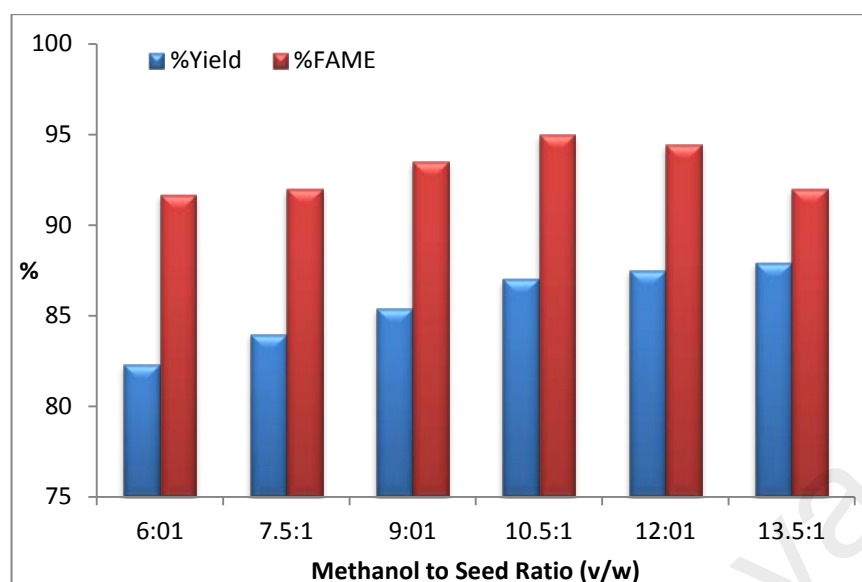


Figure 4.38: Plotted data for the effect of catalyst concentration on *in situ* transesterification of *J. curcas*. Ultrasound power = 300W; NaOH concentration = 0.1N; reaction temperature = 40°C; reaction time = 30 min.

4.3.2.4 Reaction Temperature

The influence of reaction temperature on biodiesel yield and FAME conversion is also shown in Figure 4.38. Five different temperatures (20, 30, 40, 50 and 60 °C) were chosen to investigate the effect of temperature and similar trend with reaction time was obtained. The observed results for reaction time and temperature is slightly in contrast with the published work by Kasim and Harvey (Kasim and Harvey, 2011) where they reported the negligible effects of reaction time and temperature on reactive extraction yield and methyl esters content. The observed contrast is could be due to different mixing method in their work and also the effect of sonication on *in situ* transesterification in the present work.

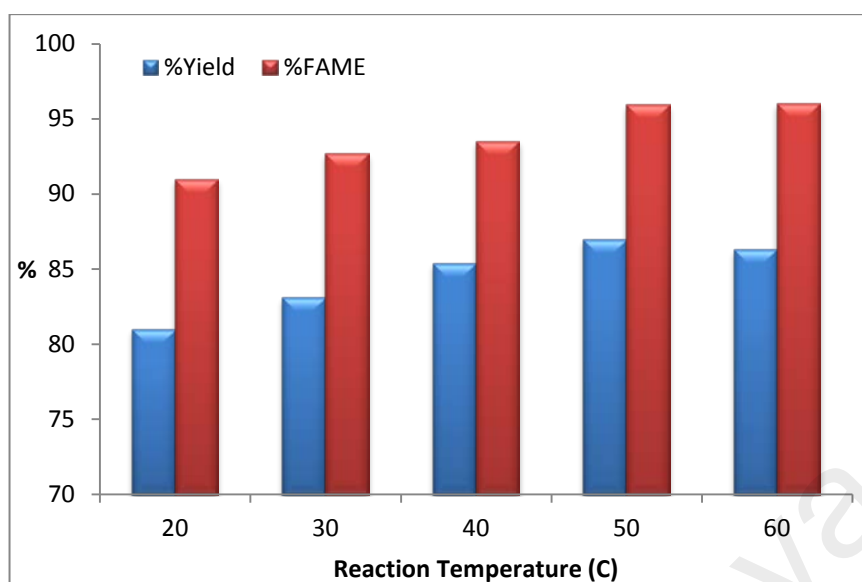


Figure 4.39: Plotted data for the effect of catalyst concentration on *in situ* transesterification of *J. curcas*. Ultrasound power = 300W; methanol to seed ratio = 9:1; NaOH concentration = 0.1N; reaction time = 30 min.

4.3.3 Interaction of Operating Parameters on *In Situ* Transesterification

The interaction between different parameters and their mutual effects on product yield and reaction conversion investigated in the next step using the response surface plots.

4.3.3.1 Biodiesel Yield

The employed design matrix of the experiments with obtained biodiesel yield is reported in Table 4.10. The effect of ultrasonic power and methanol to seed ratio on biodiesel yield at a constant catalyst concentration, reaction time and temperature is shown in Figure 4.39. Continuous increase in product yield was observed by increasing the ultrasonic power and methanol to seed ratio. However, the effect of ultrasonic power in higher amount of methanol is more significant. Higher ratio of methanol to seed leads to an increase in cavitation intensity, formation of smaller bubbles size, more spaces for mass transfer and consequently higher product yield.

Table 4.10: Experimental design matrix and response results of biodiesel yield for *in situ* transesterification.

| Run | Type | Reaction Time | Catalyst Conc. | Methanol to seed Ratio | Reaction Temperature | Ultrasonic Power | Yield % |
|-----|-----------|---------------|----------------|------------------------|----------------------|------------------|---------|
| 1 | Factorial | 10 | 0.05 | 6:1 | 30 | 200 | 73.03 |
| 2 | Factorial | 50 | 0.05 | 6:1 | 30 | 200 | 79.18 |
| 3 | Factorial | 10 | 0.15 | 6:1 | 30 | 200 | 73.41 |
| 4 | Factorial | 50 | 0.15 | 6:1 | 30 | 200 | 75.83 |
| 5 | Factorial | 10 | 0.05 | 12:1 | 30 | 200 | 78.1 |
| 6 | Factorial | 50 | 0.05 | 12:1 | 30 | 200 | 83.98 |
| 7 | Factorial | 10 | 0.15 | 12:1 | 30 | 200 | 78.51 |
| 8 | Factorial | 50 | 0.15 | 12:1 | 30 | 200 | 81.03 |
| 9 | Factorial | 10 | 0.05 | 6:1 | 50 | 200 | 74.32 |
| 10 | Factorial | 50 | 0.05 | 6:1 | 50 | 200 | 80.12 |
| 11 | Factorial | 10 | 0.15 | 6:1 | 50 | 200 | 76.98 |
| 12 | Factorial | 50 | 0.15 | 6:1 | 50 | 200 | 80.7 |
| 13 | Factorial | 10 | 0.05 | 12:1 | 50 | 200 | 78.9 |
| 14 | Factorial | 50 | 0.05 | 12:1 | 50 | 200 | 81.5 |
| 15 | Factorial | 10 | 0.15 | 12:1 | 50 | 200 | 82.34 |
| 16 | Factorial | 50 | 0.15 | 12:1 | 50 | 200 | 83.61 |
| 17 | Factorial | 10 | 0.05 | 6:1 | 30 | 400 | 76.53 |
| 18 | Factorial | 50 | 0.05 | 6:1 | 30 | 400 | 79.42 |
| 19 | Factorial | 10 | 0.15 | 6:1 | 30 | 400 | 76.88 |
| 20 | Factorial | 50 | 0.15 | 6:1 | 30 | 400 | 79.14 |
| 21 | Factorial | 10 | 0.05 | 12:1 | 30 | 400 | 82.9 |
| 22 | Factorial | 50 | 0.05 | 12:1 | 30 | 400 | 86.1 |
| 23 | Factorial | 10 | 0.15 | 12:1 | 30 | 400 | 83.06 |
| 24 | Factorial | 50 | 0.15 | 12:1 | 30 | 400 | 85.49 |
| 25 | Factorial | 10 | 0.05 | 6:1 | 50 | 400 | 81.4 |
| 26 | Factorial | 50 | 0.05 | 6:1 | 50 | 400 | 86.07 |
| 27 | Factorial | 10 | 0.15 | 6:1 | 50 | 400 | 82.11 |
| 28 | Factorial | 50 | 0.15 | 6:1 | 50 | 400 | 87.19 |
| 29 | Factorial | 10 | 0.05 | 12:1 | 50 | 400 | 87.41 |
| 30 | Factorial | 50 | 0.05 | 12:1 | 50 | 400 | 93.08 |
| 31 | Factorial | 10 | 0.15 | 12:1 | 50 | 400 | 88.71 |
| 32 | Factorial | 50 | 0.15 | 12:1 | 50 | 400 | 93.45 |
| 33 | Axial | 10 | 0.1 | 9:1 | 40 | 300 | 83.28 |
| 34 | Axial | 50 | 0.1 | 9:1 | 40 | 300 | 89.14 |
| 35 | Axial | 30 | 0.05 | 9:1 | 40 | 300 | 85.1 |
| 36 | Axial | 30 | 0.15 | 9:1 | 40 | 300 | 86.24 |
| 37 | Axial | 30 | 0.1 | 6:1 | 40 | 300 | 82.3 |

Table 4.10: Continued

| | | | | | | | |
|----|--------|----|-----|------|----|-----|-------|
| 38 | Axial | 30 | 0.1 | 12:1 | 40 | 300 | 87.51 |
| 39 | Axial | 30 | 0.1 | 9:1 | 30 | 300 | 83.12 |
| 40 | Axial | 30 | 0.1 | 9:1 | 50 | 300 | 86.94 |
| 41 | Axial | 30 | 0.1 | 9:1 | 40 | 200 | 81.36 |
| 42 | Axial | 30 | 0.1 | 9:1 | 40 | 400 | 90.12 |
| 43 | Centre | 30 | 0.1 | 9:1 | 40 | 300 | 85.76 |
| 44 | Centre | 30 | 0.1 | 9:1 | 40 | 300 | 85.34 |
| 45 | Centre | 30 | 0.1 | 9:1 | 40 | 300 | 85.94 |
| 46 | Centre | 30 | 0.1 | 9:1 | 40 | 300 | 85.54 |
| 47 | Centre | 30 | 0.1 | 9:1 | 40 | 300 | 84.14 |
| 48 | Centre | 30 | 0.1 | 9:1 | 40 | 300 | 85.67 |
| 49 | Centre | 30 | 0.1 | 9:1 | 40 | 300 | 85.37 |
| 50 | Centre | 30 | 0.1 | 9:1 | 40 | 300 | 85.51 |

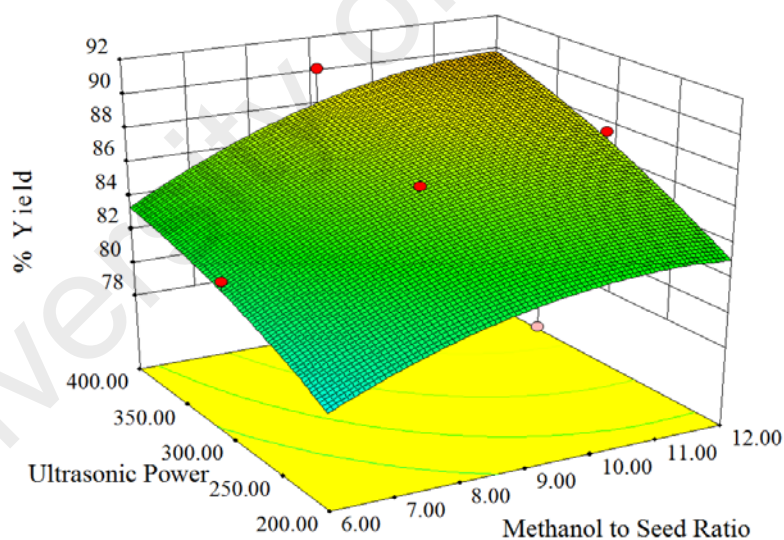
**Figure 4.40:** Response surface plots showing the mutual effects of ultrasonic power and methanol to seed ratio on product yield.

Figure 4.40 presents product yield as a function of catalyst concentration and reaction time while the other parameters are constant at their middle values. Product yield increases constantly by increasing reaction time, however the effect of catalyst

concentration is negligible in low reaction time of 10 min but more significant when reaction time increases to 50 min.

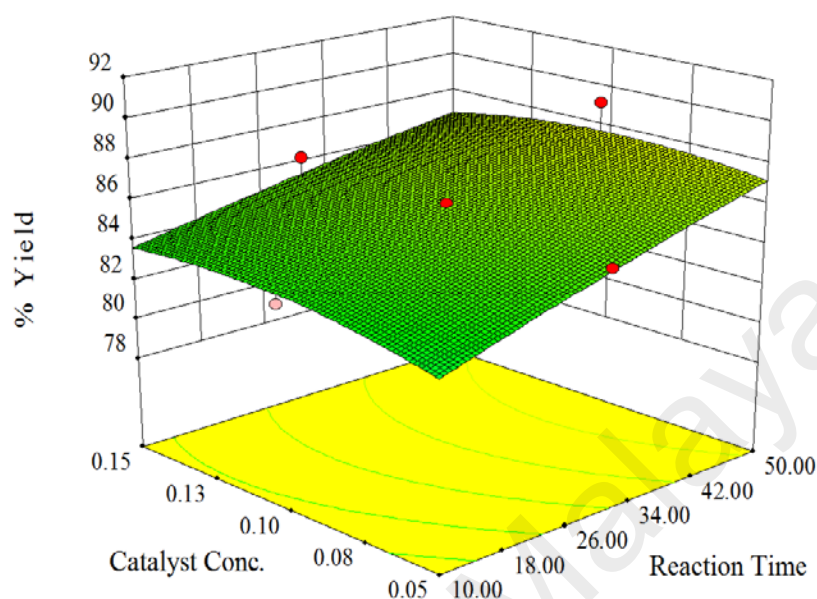


Figure 4.41: Response surface plots showing the mutual effects of catalyst concentration and reaction time on product yield.

The interaction effects of methanol to seed ratio with catalyst concentration on biodiesel yield are illustrated in Figure 4.41. Increasing the ratio of methanol to seed has a positive influence on product yield due to increasing the cavitation intensity. However, further increase in this ratio cannot effect on yield significantly due to solubility. The effect of catalyst concentration on product yield was not very considerable and also there is no remarkable interaction between methanol to seed ratio and catalyst concentration.

Figure 4.42 depicts the effects of ultrasonic power, reaction temperature and their combined interaction on product yield. Product yield increases by increasing ultrasonic power and reaction temperature, however the sonication is more effective at higher

temperature due to the influence of reaction temperature on cavitational activity and mass transfer.

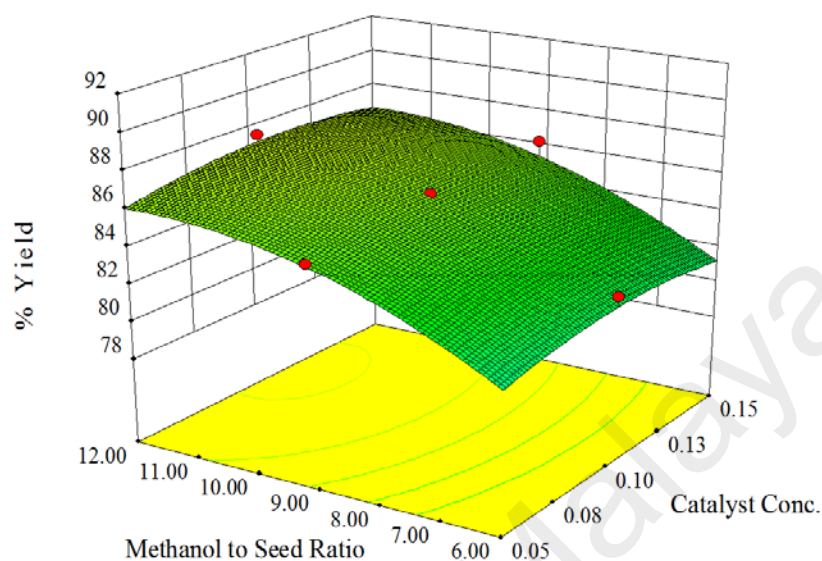


Figure 4.42: Response surface plots showing the mutual effects of catalyst concentration and methanol to seed ratio on product yield.

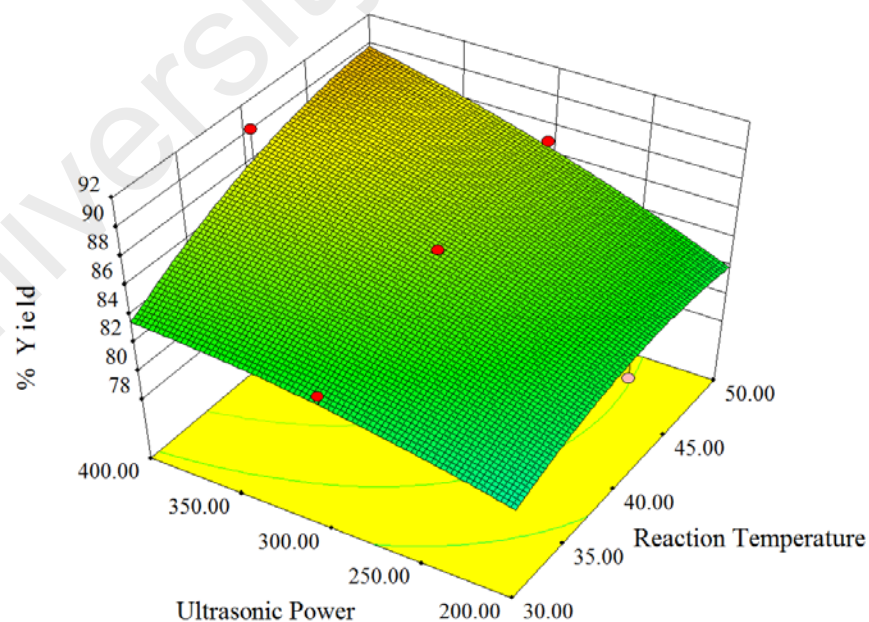


Figure 4.43: Response surface plots showing the mutual effects of ultrasonic power and reaction temperature on product yield.

4.3.3.2 Conversion Rate

The employed design matrix of the experiments with obtained biodiesel yield is reported in Table 4.11.

Table 4.11: Experimental design matrix and response results of conversion rate for *in situ* transesterification.

| Run | Type | Reaction Time | Catalyst Conc. | Methanol to seed Ratio | Reaction Temperature | Ultrasonic Power | Conversion % |
|-----|-----------|---------------|----------------|------------------------|----------------------|------------------|--------------|
| 1 | Factorial | 10 | 0.05 | 6:1 | 30 | 200 | 82.4 |
| 2 | Factorial | 50 | 0.05 | 6:1 | 30 | 200 | 84.33 |
| 3 | Factorial | 10 | 0.15 | 6:1 | 30 | 200 | 87.5 |
| 4 | Factorial | 50 | 0.15 | 6:1 | 30 | 200 | 89.1 |
| 5 | Factorial | 10 | 0.05 | 12:1 | 30 | 200 | 84.9 |
| 6 | Factorial | 50 | 0.05 | 12:1 | 30 | 200 | 85.44 |
| 7 | Factorial | 10 | 0.15 | 12:1 | 30 | 200 | 94.2 |
| 8 | Factorial | 50 | 0.15 | 12:1 | 30 | 200 | 94.95 |
| 9 | Factorial | 10 | 0.05 | 6:1 | 50 | 200 | 83.1 |
| 10 | Factorial | 50 | 0.05 | 6:1 | 50 | 200 | 83.85 |
| 11 | Factorial | 10 | 0.15 | 6:1 | 50 | 200 | 93.5 |
| 12 | Factorial | 50 | 0.15 | 6:1 | 50 | 200 | 93.9 |
| 13 | Factorial | 10 | 0.05 | 12:1 | 50 | 200 | 85.22 |
| 14 | Factorial | 50 | 0.05 | 12:1 | 50 | 200 | 85.9 |
| 15 | Factorial | 10 | 0.15 | 12:1 | 50 | 200 | 94.12 |
| 16 | Factorial | 50 | 0.15 | 12:1 | 50 | 200 | 95.2 |
| 17 | Factorial | 10 | 0.05 | 6:1 | 30 | 400 | 84.4 |
| 18 | Factorial | 50 | 0.05 | 6:1 | 30 | 400 | 85.76 |
| 19 | Factorial | 10 | 0.15 | 6:1 | 30 | 400 | 91.5 |
| 20 | Factorial | 50 | 0.15 | 6:1 | 30 | 400 | 93.1 |
| 21 | Factorial | 10 | 0.05 | 12:1 | 30 | 400 | 86.3 |
| 22 | Factorial | 50 | 0.05 | 12:1 | 30 | 400 | 86.98 |
| 23 | Factorial | 10 | 0.15 | 12:1 | 30 | 400 | 98.1 |
| 24 | Factorial | 50 | 0.15 | 12:1 | 30 | 400 | 98.25 |
| 25 | Factorial | 10 | 0.05 | 6:1 | 50 | 400 | 86.62 |
| 26 | Factorial | 50 | 0.05 | 6:1 | 50 | 400 | 87.04 |
| 27 | Factorial | 10 | 0.15 | 6:1 | 50 | 400 | 96.44 |
| 28 | Factorial | 50 | 0.15 | 6:1 | 50 | 400 | 97.24 |
| 29 | Factorial | 10 | 0.05 | 12:1 | 50 | 400 | 87.61 |
| 30 | Factorial | 50 | 0.05 | 12:1 | 50 | 400 | 88.08 |
| 31 | Factorial | 10 | 0.15 | 12:1 | 50 | 400 | 98.6 |

Table 4.11: Continued

| | | | | | | | |
|----|-----------|----|------|------|----|-----|-------|
| 32 | Factorial | 50 | 0.15 | 12:1 | 50 | 400 | 99.05 |
| 33 | Axial | 10 | 0.1 | 9:1 | 40 | 300 | 93.41 |
| 34 | Axial | 50 | 0.1 | 9:1 | 40 | 300 | 95.2 |
| 35 | Axial | 30 | 0.05 | 9:1 | 40 | 300 | 84.31 |
| 36 | Axial | 30 | 0.15 | 9:1 | 40 | 300 | 95.4 |
| 37 | Axial | 30 | 0.1 | 6:1 | 40 | 300 | 91.66 |
| 38 | Axial | 30 | 0.1 | 12:1 | 40 | 300 | 94.44 |
| 39 | Axial | 30 | 0.1 | 9:1 | 30 | 300 | 92.68 |
| 40 | Axial | 30 | 0.1 | 9:1 | 50 | 300 | 95.95 |
| 41 | Axial | 30 | 0.1 | 9:1 | 40 | 200 | 93.67 |
| 42 | Axial | 30 | 0.1 | 9:1 | 40 | 400 | 98.31 |
| 43 | Centre | 30 | 0.1 | 9:1 | 40 | 300 | 93.48 |
| 44 | Centre | 30 | 0.1 | 9:1 | 40 | 300 | 93.6 |
| 45 | Centre | 30 | 0.1 | 9:1 | 40 | 300 | 93.66 |
| 46 | Centre | 30 | 0.1 | 9:1 | 40 | 300 | 93.26 |
| 47 | Centre | 30 | 0.1 | 9:1 | 40 | 300 | 93.83 |
| 48 | Centre | 30 | 0.1 | 9:1 | 40 | 300 | 93.58 |
| 49 | Centre | 30 | 0.1 | 9:1 | 40 | 300 | 93.09 |
| 50 | Centre | 30 | 0.1 | 9:1 | 40 | 300 | 93.7 |

Response surface plots of conversion rate on combined variables are shown in Figure 4.43, 4.44, 4.45 and 4.46. A comparison between surface plots of product yield and conversion rate (Figure 4.39 to 4.46) demonstrates that some parameters like methanol to seed ratio, temperature and time are more effective on product yield but not on FAME content. However, the effect of catalyst concentration on conversion efficiency is more remarkable compared with biodiesel yield. The transesterification process cannot take place at all without using catalyst.

Kasim and Harvey (Kasim and Harvey, 2011) conducted a comparison between *in situ* transesterification with and without catalyst and reported that solvent extraction with alcohol carried out some extract, but no FAME was observed in the product. Effect of sonication on conversion efficiency also is not very remarkable. Figure 4.43 to 4.46

demonstrate that high percentage of FAME content can be achieved in a short reaction time of 10 min under ultrasonic irradiation, however more time is required in order to obtain a meaningful yield of product.

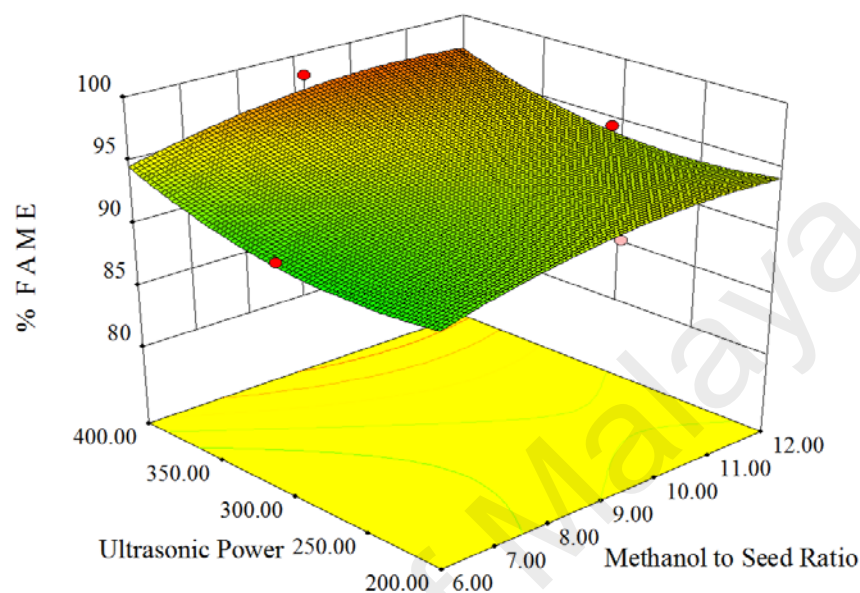


Figure 4.44: Response surface plots showing the mutual effects of ultrasonic power and methanol to seed ratio on conversion rate.

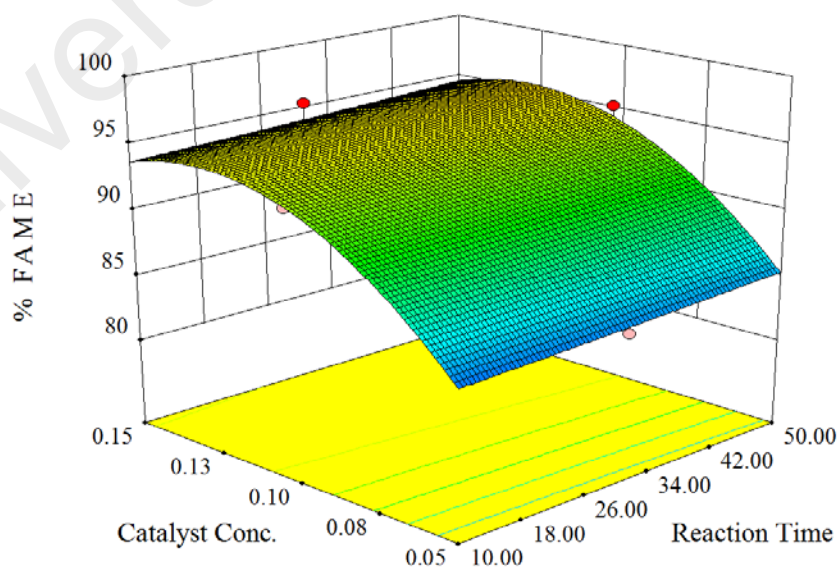


Figure 4.45: Response surface plots showing the mutual effects of catalyst concentration and reaction time on conversion rate.

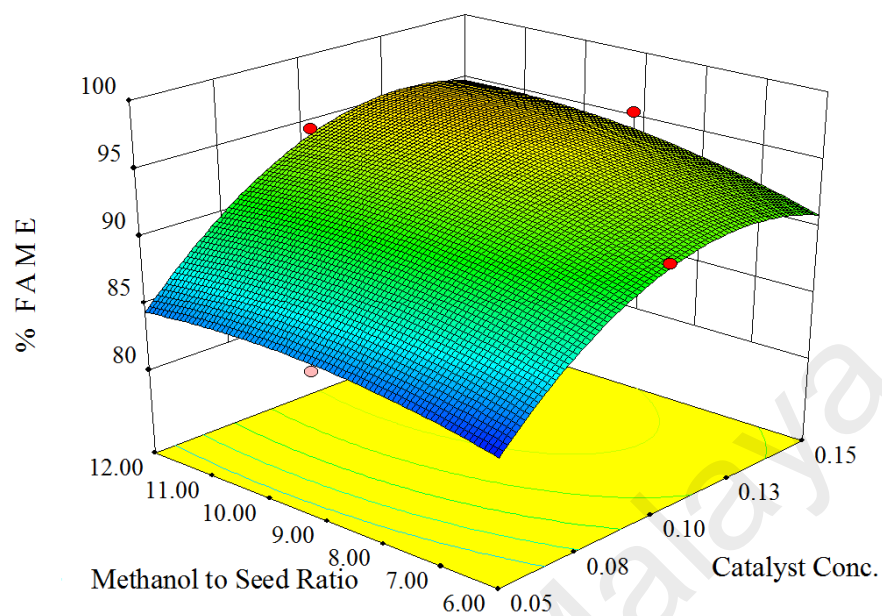


Figure 4.46: Response surface plots showing the mutual effects of catalyst concentration and methanol to seed ratio on conversion rate.

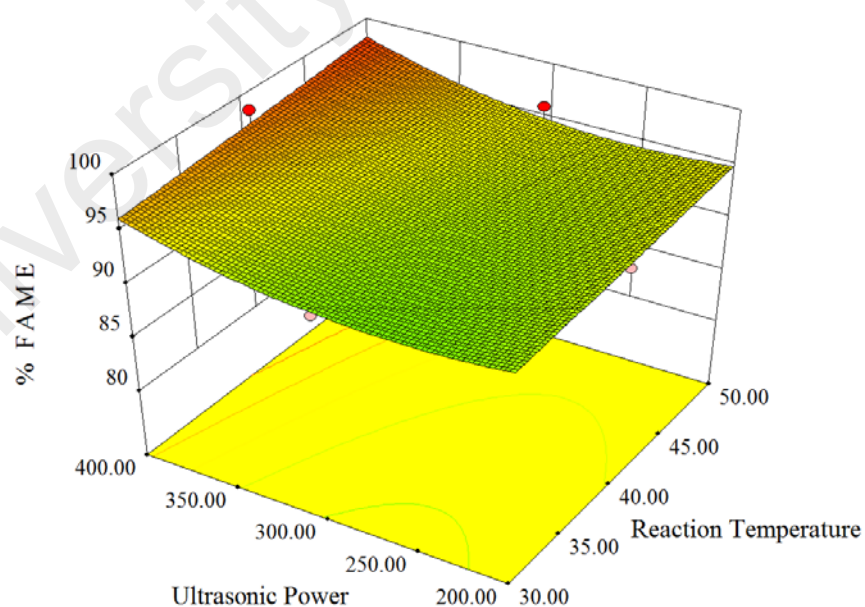


Figure 4.47: Response surface plots showing the mutual effects of ultrasonic power and reaction temperature on conversion rate.

4.3.4 *In Situ* Transesterification Process Using Mechanical Stirring

The comparison results of *in situ* transesterification yield and conversion under ultrasound irradiation and mechanical stirring are provided in Figure 4.47. This figure demonstrates that biodiesel yield and conversion gradually increased by increasing the stirrer speed till they reached a maximum value. However, further increasing in stirrer speed after 400 RPM cannot make a considerable effect on biodiesel yield and FAME content in the short reaction time of 30 min.

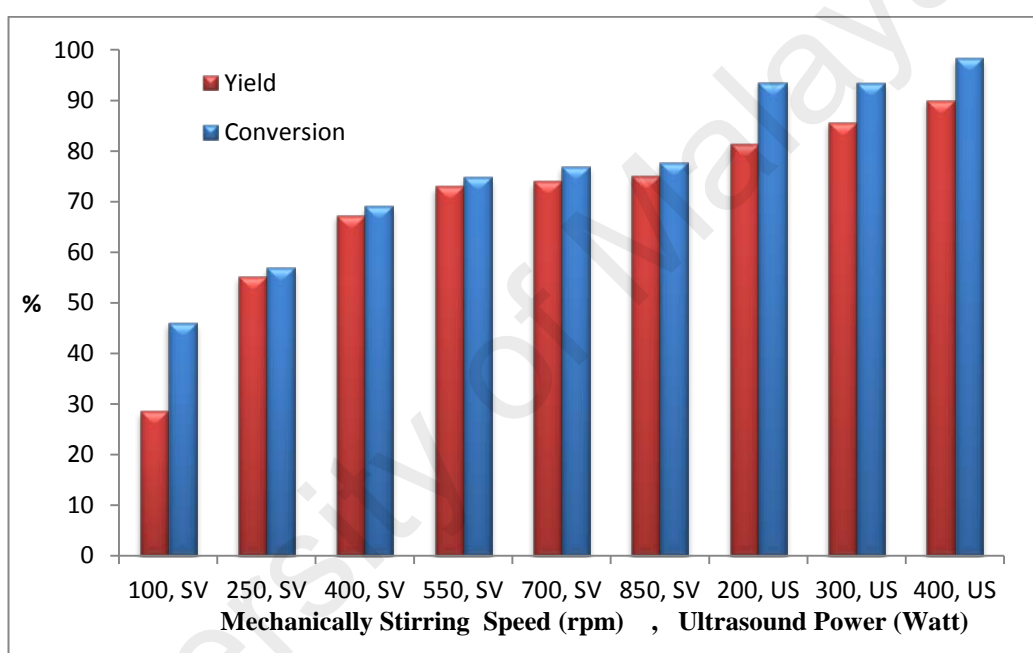


Figure 4.48: Percentages of biodiesel yield and conversion rate versus stirrer speed and ultrasound power. Methanol to seed ratio: 9:1, NaOH concentration: 0.1 mol/L, reaction time: 30 min and reaction temperature: 40 °C.

Similar results were also observed in the works of other researchers (Kasim and Harvey, 2011; Amalia Kartika et al., 2013). However, higher amounts of product yield and FAME conversion were obtained in their works by increasing some operating parameters such as reaction time and temperature and modifying other parameters such as alcohol to seed ratio and catalyst concentration. However, ultrasound irradiation

could increase the reaction yield/conversion by about 20.11% (as the average value) at the same operating conditions confirming the ability of ultrasound energy on overcoming the mass transfer limitations. Experimental design matrix and response results for *in situ* transesterification under mechanical mixing are reported in Table 4.12.

Table 4.12: Experimental design matrix and response results for mechanical mixing.

| Run | Reaction Time | Catalyst Concentration | Methanol to seed Ratio | Reaction Temperature | Mixing Intensity | Yield % | Conversion % |
|-----|---------------|------------------------|------------------------|----------------------|------------------|---------|--------------|
| 1 | 30 | 0.1 | 9:1 | 40 | 100 | 28.5 | 46 |
| 2 | 30 | 0.1 | 9:1 | 40 | 250 | 55.2 | 57 |
| 3 | 30 | 0.1 | 9:1 | 40 | 400 | 67.38 | 69 |
| 4 | 30 | 0.1 | 9:1 | 40 | 550 | 73 | 74.82 |
| 5 | 30 | 0.1 | 9:1 | 40 | 700 | 74 | 76.9 |
| 6 | 30 | 0.1 | 9:1 | 40 | 850 | 75 | 77.75 |

Table 4.13 presents the composition of FAME produced in *in situ* transesterification of *J. curcas* under ultrasonic irradiation and mechanical stirring. It can be concluded from this results that the mass transfer caused by mechanical stirring is not enough to conduct a proper transesterification process in a short reaction time and applying a more suitable mass transfer pattern can reduce the cost of other operating parameters.

Table 4.13: FAME profiles of produced biodiesel under ultrasonication and mechanical stirring.

| Process | Fatty acid methyl esters | | | | | | |
|---------------------------|--------------------------|-------|-------|-------|-------|-------|-------|
| | C16:0 | C16:1 | C17:0 | C18:0 | C18:1 | C18:2 | C18:3 |
| Mechanical stirring (rpm) | | | | | | | |
| 100 | 13.6 | 0.4 | - | 12.9 | 17.7 | 1.0 | 0.4 |
| 250 | 18.4 | 0.5 | - | 15.8 | 20.9 | 1.0 | 0.4 |
| 400 | 24.2 | 0.5 | - | 17.4 | 25.3 | 1.1 | 0.5 |
| 550 | 26 | 0.6 | - | 19.1 | 27.6 | 1.0 | 0.5 |
| 700 | 26.6 | 0.7 | - | 19.7 | 28.4 | 1.1 | 0.6 |
| 850 | 27.1 | 0.7 | - | 19.8 | 28.7 | 1.2 | 0.6 |
| Ultrasonication (W) | | | | | | | |
| 200 | 33.2 | 0.7 | 0.4 | 19.4 | 38.1 | 1.3 | 0.5 |
| 300 | 33.1 | 0.7 | 0.4 | 19.6 | 37.9 | 1.3 | 0.5 |
| 400 | 33 | 0.9 | 0.5 | 20.2 | 41.5 | 1.6 | 0.6 |

4.3.5 Development of Regression Model

4.3.5.1 Biodiesel Yield

The relationship between product yield and five independent parameters under ultrasonication were investigated through CCD. Eight runs were carried out at the centre point, as it shown in Table 4.9, to determine the experimental inaccuracies. The following model was developed in terms of coded factors for prediction of biodiesel production yield (%):

$$Yield (\%) = 85.89 + 1.98X_1 + 2.68X_3 + 2.03X_4 + 2.83X_5 - 0.39X_1X_2 + 0.57X_2X_4 + 0.53X_3X_5 + 1.08X_4X_5 - 1.46X_3^2 \quad (4.10)$$

The positive and negatives term indicate synergistic and antagonistic effects, respectively (Ahmad et al., 2009). High R-squared value of 0.9505 indicates a good

agreement between the predicted and experimental values. The sufficiency of the obtained model was justified through Analysis of Variance (ANOVA). The results of P-value for reaction time (X_1), methanol to seed ratio (X_3), reaction temperature (X_4), ultrasonic power (X_5), the interaction effects of reaction time and catalyst concentration (X_1X_2), catalyst concentration and reaction temperature (X_2X_4), methanol to seed ratio and ultrasonic power (X_3X_5), reaction temperature and ultrasonic power (X_4X_5) and the quadratic effect of methanol to seed ratio (X_3^2) (P-value less than 0.05) indicate that they significantly affected the biodiesel production yield. High equation coefficients of X_3 and X_5 demonstrate that methanol to seed ratio and ultrasonic power are the most significant parameters on product yield as it was shown in Figure 4.32 to 4.35 as well.

4.3.5.2 Conversion Rate

The relationship between conversion rate and five independent parameters is presented in equation (4.11). R-squared value for obtained model was 0.9697.

$$FAME (\%) = 93.89 + 0.45X_1 + 4.64X_2 + 1.35X_3 + 0.93X_4 + 1.53X_5 + 0.54X_2X_3 + 0.45X_2X_4 + 0.38X_2X_5 - 0.59X_3X_4 - 4.41X_2^2 - 1.21X_3^2 + 1.73X_5^2 \quad (4.11)$$

The results of P-value depict that the parameters that significantly influenced on conversion rate were reaction time (X_1), catalyst concentration (X_2), methanol to seed ratio (X_3), reaction temperature (X_4), ultrasonic power (X_5), the interaction effects of catalyst concentration and methanol to seed ratio (X_2X_3), catalyst concentration and reaction temperature (X_2X_4), catalyst concentration and ultrasonic power (X_2X_5), methanol to seed ratio and ultrasonic power (X_3X_4) and the quadratic effects of catalyst concentration (X_2^2), methanol to seed ratio (X_3^2) and ultrasonic power (X_5^2) (P-value less than 0.05). As presented in equation (4), catalyst concentration has the highest equation coefficient which is in agreement with the results of Figure 4.32 to 4.35.

4.3.6 Process Optimization

In order to identify the conditions at which ultrasound *in situ* transesterification can demonstrate its highest biodiesel production yield while is more efficient, optimization of operational factor levels was performed based on the experiments done for both transesterification yield and its conversion and the quadratic models obtained. Accordingly, three different optimizations were considered.

The selected criteria to achieve the maximum desirability were as “maximize” for reaction yield/conversion and 1) “within the range” for catalyst, alcohol concentrations, reaction temperature, reaction time and ultrasound power. 2) “within the range” for catalyst, alcohol concentrations, reaction temperature and “minimize” for reaction time and ultrasound power.

Among 20 proposed solutions for each category, the one with the highest desirability was selected and three additional tests were conducted to evaluate the validity of the procedure. The identified optimum conditions along with the values of the predicted and experimentally obtained transesterification yield and conversion with the value of discrepancy among them are summarized in Table 4.14.

Table 4.14: Predicted and experimental values of the studied responses at optimum conditions.

| Response | | | | | Predicted Values (%) | | Experimental Results (%) | | Error (%) | |
|----------------|----------------|----------------|----------------|----------------|-------------------------|-------|-----------------------------|-------|-----------|------|
| X ₁ | X ₂ | X ₃ | X ₄ | X ₅ | Yield | FAME | Yield | FAME | Yield | FAME |
| 50 | 0.112 | 11.8 | 50 | 400 | 93.3 | 99.30 | 93.45 | 99.26 | 1.37 | 0.68 |
| 10 | 0.129 | 11.1 | 46 | 200 | 81.4 | 95.73 | 83.33 | 96.8 | 2.25 | 1.11 |

As observed, the maximum deviation between the predicted and experimental values was 2.25% which confirmed the validity of the obtained regression model. It is also observed that under the optimum condition of catalyst: 0.129 mol/L in methanol, ultrasound power: 200 W, methanol:seed: 11.14:1 (v/w), reaction temperature: 46 °C and reaction time of 10 min, ultrasound *in situ* transesterification can reach to the maximum product yield and conversion of 83.33% and 96.8%, respectively. Furthermore, product yield and conversion rate can be improved to 93.45 and 99.26, by increasing the ultrasonic power and reaction time to 400 W and 50 min, respectively.

4.4 Summary of Results and Discussion

The effects of ultrasound irradiation on intensification of different operations in gas-liquid, liquid-liquid and solid-liquid systems were studied in this chapter and compared with the results obtained from mechanical stirring. In gas-liquid system, it was found that additional turbulence created by ultrasonication plays the most significant role on intensifying the mass transfer phenomena compared to that in stirred vessel. The obtained results by CFD simulation also presented that the higher mass transfer observed under sonication were due to the high ability of ultrasound in increasing the interfacial surface and turbulent intensity. On the other hand, increasing mixing intensity and superficial gas velocity posed synergistic effects on mass transfer while viscosity presented an antagonistic effect. Higher liquid viscosity did not only reduce the turbulent intensity in the system but also limit the breakage of gas bubbles, reducing the mass transfer phenomenon. In addition, the mass transfer improvement in case the horizontal sonicator was not as significant as in the vertical sonicator, implying the importance of propagation quality of kinetic energy within the system. The CFD simulation was carried out only for gas-liquid operation, due to the insufficient storage capacity and speed of computer used in this research. However, the results of gas-liquid

system can also be a good representative for the behaviours of fluid flow in liquid-liquid and solid-liquid systems.

In liquid-liquid operation, it was found that ultrasonication effects the reaction both physically and chemically. The physical effect refers to formation of fine emulsion that eliminates the mass transfer resistance in the reaction media. Meanwhile, acceleration of the reaction within the cavitation bubbles, due to generation of hot spots (maximum temperature and pressure of 876 K and 679 bar respectively) or generation of situation similar to supercritical situations, is the chemical effect. Among the key operational parameters in transesterification process, ultrasound power was found to be the most significant parameter in intensification of reaction yield and conversion rate due to increasing the bubble radius in liquid phase as well as its internal temperature and pressure.

In solid-liquid operation also the effects of ultrasound irradiation on intensifying the reaction yield and conversion rate of *in situ* transesterification process was significant. Similar to liquid-liquid system, cavitation bubbles generated under ultrasound irradiation grew up to almost ten times of their initial radius till the moment of compression. The bubbles reached to greater radius as the ultrasound power rose. It attributed to the expansion rate of the cavitation bubble which is more prominent at higher power. On the other hand, penetration of ultrasound waves into the solid phase can intensify the process of oil extraction from the seeds during the *in situ* transesterification.

The obtained results in this study are helpful for understanding the role of ultrasound as an energy source and acoustic streaming as one of the most important features of ultrasound waves on intensifying dual-phase operations and can be a breakthrough in the design procedure as no similar study was found in the existing literature.

CHAPTER 5: CONCLUSIONS AND FURTHER WORKS

This chapter comprised of all the individual results obtained from all the experimental studies conducted, evaluation of comparative studies on the effect of ultrasonic irradiation on different dual-phase system including gas-liquid, liquid-liquid and solid-liquid systems and also the results obtained from mechanical mixing. The main conclusions and observations for this research together with recommendation for future studies are as follows:

5.1 Conclusions

The effect of ultrasound irradiation on gas-liquid mass transfer in different liquid volumes was studied in the first set of experiments and it was found that in a suitable selected liquid volume, ultrasonication could considerably intensify the volumetric gas-liquid mass transfer coefficient. Three parameters were then investigated in liquid volume of 2 L: ultrasonic power, gas flow rate and temperature. The maximum value of k_La was found to be 0.0128 s^{-1} but the influence of ultrasonication was not significant due to the high ratio of liquid volume to provided ultrasonic power. However, gas flow rate was found to be the most effective parameter under this experimental setup. A quadratic model with an R-squared value of 0.985 was obtained based on RSM modeling which proved the validation of the experimental data.

Therefore, a smaller tank was selected in order to the effect of ultrasonic irradiation on mass transfer in higher accuracy. Three set of experiments were carried out in 200 mL liquid volume with different situation. Two main situations for ultrasonic horn position were examined and results were then compared with results of same experiments in a mechanically agitated vessel. The effect of ultrasonic horn position on k_La was found to be very significant due to influence of direction and distance of ultrasonic irradiation on sparged gas. In addition, effect of operational parameters such as viscosity, superficial

gas velocity and ultrasonic intensity were studied in all of these experiments. The maximum value of k_La was found to be 0.0714 s^{-1} in vertical ultrasonic horn and it was found that generally, k_La increases with increase of ultrasonic power and superficial gas velocity and decreases with increase of viscosity. Moreover, three empirical correlations were developed to predict k_La in different situations and close results were obtained with correlations from the literature.

The effects of acoustic jet-like streaming on the gas-liquid mass transfer enhancement in macro-scale sonoreactors were also investigated using 3D CFD simulation and the results were then compared with that of a stirred vessel. A significant enhancement in the mass transfer was observed in ultrasonicators, which was attributed to the kinetic energy imposed on the system by acoustic streaming. It was also found that the rheological properties in liquid phase played a dominant role in deciding the residence time of gas bubbles and dissipation of turbulent kinetic energy. This issue was more critical in sonoreactors, which showed the effect of viscosity on reducing the propagation depth of acoustic jet-like streaming.

The CFD simulation was conducted only for gas-liquid system, because the storage capacity and the speed of computer which was applied in this study were not sufficient to enable efficient calculation of reactions in the liquid-liquid and solid-liquid systems. However, the hydrodynamic results obtained from gas-liquid system can also represent the behaviours of fluid flow in liquid-liquid and solid-liquid systems.

In the next step, the intensification of liquid-liquid operation in a sonochemical reactor was investigated. The transesterification of *J. curcas* oil into biodiesel under ultrasound irradiation was studied and the effects of reaction time, catalyst concentration, methanol to oil molar ratio, reaction temperature and ultrasonic power on product yield and conversion rate were determined. A high yield (90.76 %) and reaction conversion

(94.86 %) of *J. curcas* oil to biodiesel were observed under ultrasound irradiation while traditional transesterification could only achieve the maximum product yield of 78.65 % and FAME conversion of 83.9 % within the same duration. In addition, the highest biodiesel yield and conversion rate of 94.23 % and 98.54 % were obtained from the transesterification of *J. curcas* oil under ultrasonication, respectively.

For solid-liquid system experiments, the *J. curcas* seed as solid phase was characterized first and it was shown that it contained 35% oil and 7.8% moisture. *In situ* transesterification of *J. curcas* seed into fatty acid methyl esters (FAME) under ultrasound irradiation was then investigated and various sets of experiments were accomplished to analyze the graduate increasing effect of each variable, evaluate the individual and interactive effects of each parameter, develop regression model and optimize the *in situ* transesterification process. The effects of methanol to seed ratio and ultrasonic power on product yield were found to be more than other operating parameters while catalyst concentration was the most significant parameter on conversion rate. The highest biodiesel yield of 93.45% and conversion rate of 99.26% were achieved with a reaction time of 50 min, NaOH catalyst concentration of 0.112 mol/L in methanol, a methanol to seed ratio of 11.8:1 (v/w), a reaction temperature of 50 °C and an ultrasonic power of 400 W. Furthermore, ultrasonic technology achieved the yield of 83.33% and conversion rate of 96.8% under optimum conditions within only 10 minutes.

A comparison between *in situ* transesterification of *J. curcas* under ultrasonication and mechanical stirring was also carried out and it was found that higher yield and quality of biodiesel in a shorter reaction time can be obtained under ultrasound irradiation. The maximum biodiesel yield of 75% and conversion rate of 77.75% were observed from *in situ* transesterification under mechanical stirring, while ultrasound-assisted *in situ*

transesterification could achieve the product yield of 90.12% and conversion rate of 98.31% within the same duration.

Generally, the results of this research show that using ultrasound irradiation in dual-phase operations can be an appropriate alternative for conventional stirred vessels. The phenomenon of acoustic cavitation, as the origin of sonochemistry, can cause a dramatic increase in temperature and pressure near the ultrasonic transducer which can lead to a great amount of process intensification. A significant increment was observed in gas-liquid system in terms of volumetric mass transfer coefficient. In the other systems also it was proved that sonochemical reactor can successfully increase the yield of reaction and reduces the overall capital cost by intensifying mixing levels and mass transfer between the reactants. In addition, high biodiesel yield and conversion rate can be obtained within a short reaction time using transesterification and *in situ* transesterification method together with ultrasonic technology.

5.2 Further works

Using ultrasound irradiation for process intensification is a promising method and there are still many aspects of the technology which need to be further developed in the near future. Following are some recommendations for future works:

1. An investigation on the effects of ultrasound irradiation in a continuous sonochemical reactor can be carried out in order to apply the advantages of ultrasound energy on continuous systems.
2. To design a control system based on optimum process conditions in order to investigate the various aspects of continuous system under ultrasound irradiation.
3. Mechanical mixing can be applied together with ultrasound irradiation in order to combine macro and micromixing. The reason is that mechanical stirrer can mix the

reactants in the first step of reaction. As a result, the ultrasonic energy will be saved only for micromixing and the energy consumption of the ultrasound may decrease further.

4. For synthesis of biodiesel under ultrasound irradiation, various kinds of catalyst, especially heterogeneous, can be analyzed in order to reduce the cost of purification steps and obtain optimum operating conditions to produce high quality biodiesel.

5. In order to obtain more robust results, the CFD simulation must be performed in a real system of biodiesel synthesis by transesterification in both a stirred vessel as well as ultrasonicator. As a result, the real mixing time and mixing power can be estimated. Therefore, optimum time and power can be employed to decrease the energy consumption in the system.

REFERENCES

- Abolhasani M, Rahimi M, Dehbani M, et al. (2012) CFD modeling of heat transfer by 1.7 MHz ultrasound waves. *Numerical Heat Transfer, Part A: Applications* 62: 822-841.
- Achten W, Verchot L, Franken YJ, et al. (2008) Jatropha bio-diesel production and use. *Biomass and Bioenergy* 32: 1063-1084.
- Adewuyi YG. (2001) Sonochemistry: environmental science and engineering applications. *Industrial & Engineering Chemistry Research* 40: 4681-4715.
- Adrian RJ. (1991) Particle-imaging techniques for experimental fluid mechanics. *Annual review of fluid mechanics* 23: 261-304.
- Afshar Ghotli R, Abdul Aziz AR, Ibrahim S, et al. (2013) Study of various curved-blade impeller geometries on power consumption in stirred vessel using response surface methodology. *Journal of the Taiwan Institute of Chemical Engineers*.
- Agarwal AK and Das L. (2001) Biodiesel development and characterization for use as a fuel in compression ignition engines. *Journal of engineering for gas turbines and power* 123: 440-447.
- Ahmad A, Hameed B and Ahmad A. (2009) Removal of disperse dye from aqueous solution using waste-derived activated carbon: Optimization study. *Journal of Hazardous materials* 170: 612-619.
- Amalia Kartika I, Yani M, Ariono D, et al. (2013) Biodiesel production from jatropha seeds: Solvent extraction and in situ transesterification in a single step. *Fuel* 106: 111-117.
- Arami-Niya A, Wan Daud WMA, S Mjalli F, et al. (2012) Production of microporous palm shell based activated carbon for methane adsorption: modeling and optimization using response surface methodology. *Chemical Engineering Research and Design* 90: 776-784.
- Arjunwadkar S, Sarvanan K, Kulkarni P, et al. (1998) Gas-liquid mass transfer in dual impeller bioreactor. *Biochemical Engineering Journal* 1: 99-106.
- Ashokkumar M and Mason TJ. (2007) Sonochemistry. *Kirk-Othmer Encyclopedia of Chemical Technology*.
- Azam MM, Waris A and Nahar N. (2005) Prospects and potential of fatty acid methyl esters of some non-traditional seed oils for use as biodiesel in India. *Biomass and Bioenergy* 29: 293-302.
- Badday AS, Abdullah AZ, Lee KT, et al. (2012) Intensification of biodiesel production via ultrasonic-assisted process: A critical review on fundamentals and recent development. *Renewable and Sustainable Energy Reviews* 16: 4574-4587.

- Bakłdyga J, Podgorska W and Pohorecki R. (1995) Mixing-precipitation model with application to double feed semibatch precipitation. *Chemical engineering science* 50: 1281-1300.
- Baldyga J, Bourne J and Gholap R. (1995) The influence of viscosity on mixing in jet reactors. *Chemical engineering science* 50: 1877-1880.
- Banerji R, Chowdhury A, Misra G, et al. (1985) Jatropha seed oils for energy. *Biomass* 8: 277-282.
- Barati AH, Mokhtari-Dizaji M, Mozdarani H, et al. (2007) Effect of exposure parameters on cavitation induced by low-level dual-frequency ultrasound. *Ultrasonics Sonochemistry* 14: 783-789.
- Barekati-Goudarzi M, Boldor D and Nde DB. (2016) In-situ transesterification of seeds of invasive Chinese tallow trees (*Triadica sebifera* L.) in a microwave batch system (GREEN 3) using hexane as co-solvent: Biodiesel production and process optimization. *Bioresource technology* 201: 97-104.
- Becker K and Makkar H. (2008) Jatropha curcas: a potential source for tomorrow's oil and biodiesel. *Lipid Technology* 20: 104-107.
- Beckett MA and Hua I. (2001) Impact of ultrasonic frequency on aqueous sonoluminescence and sonochemistry. *The Journal of Physical Chemistry A* 105: 3796-3802.
- Behera SK, Srivastava P, Tripathi R, et al. (2010) Evaluation of plant performance of Jatropha curcas L. under different agro-practices for optimizing biomass—a case study. *Biomass and Bioenergy* 34: 30-41.
- Bhirud US, Gogate PR, Wilhelm AM, et al. (2004) Ultrasonic bath with longitudinal vibrations: a novel configuration for efficient wastewater treatment. *Ultrasonics Sonochemistry* 11: 143-147.
- Birnbaum Y, Luo H, Nagai T, et al. (1998) Noninvasive in vivo clot dissolution without a thrombolytic drug recanalization of thrombosed iliofemoral arteries by transcutaneous ultrasound combined with intravenous infusion of microbubbles. *Circulation* 97: 130-134.
- Bong EY, Eshtiaghi N, Wu J, et al. (2015) Optimum solids concentration for solids suspension and solid-liquid mass transfer in agitated vessels. *Chemical Engineering Research and Design*.
- Boocock DG, Konar SK, Mao V, et al. (1996) Fast one-phase oil-rich processes for the preparation of vegetable oil methyl esters. *Biomass and Bioenergy* 11: 43-50.
- Bouyatiotis B and Thornton J. (1967) Liquid-liquid extraction studies in stirred tanks. Part I Droplet size and hold-up measurements in a seven-inch diameter baffled vessel. *Inst. Chem. Eng. Symp. Ser.* 43-51.
- Cachaza EM, Díaz ME, Montes FJ, et al. (2009) Simultaneous Computational Fluid Dynamics (CFD) simulation of the hydrodynamics and mass transfer in a

partially aerated bubble column. *Industrial & Engineering Chemistry Research* 48: 8685-8696.

Cadwell M and Fogler H. (1971) Ultrasonic gas absorption and acoustic streaming observations. *Chemical Engineering Progress Symposium Series*. 1224-1127.

Cai J, Huai X, Yan R, et al. (2009) Numerical simulation on enhancement of natural convection heat transfer by acoustic cavitation in a square enclosure. *Applied Thermal Engineering* 29: 1973-1982.

Canakci M and Van Gerpen J. (1999) Biodiesel production via acid catalysis. *Transactions of the ASAE* 42: 1203.

Canizares-Macias M, García-Mesa JA and Luque de Castro M. (2004) Fast ultrasound-assisted method for the determination of the oxidative stability of virgin olive oil. *Analytica chimica acta* 502: 161-166.

Capelo J, Dos Reis C, Maduro C, et al. (2004) Tandem focused ultrasound (TFU) combined with fast furnace analysis as an improved methodology for total mercury determination in human urine by electrothermal-atomic absorption spectrometry. *Talanta* 64: 217-223.

Chhetri AB, Tango MS, Budge SM, et al. (2008) Non-edible plant oils as new sources for biodiesel production. *International Journal of Molecular Sciences* 9: 169-180.

Chitra S, Paramasivan K, Sinha P, et al. (2004) Ultrasonic treatment of liquid waste containing EDTA. *Journal of cleaner production* 12: 429-435.

Chivate M and Pandit A. (1995) Quantification of cavitation intensity in fluid bulk. *Ultrasonics Sonochemistry* 2: S19-S25.

Choudhury HA, Malani RS and Moholkar VS. (2013) Acid catalyzed biodiesel synthesis from Jatropha oil: Mechanistic aspects of ultrasonic intensification. *Chemical Engineering Journal* 231: 262-272.

Chouvellon M, Largillier A, Fournel T, et al. (2000) Velocity study in an ultrasonic reactor. *Ultrasonics Sonochemistry* 7: 207-211.

Chu S, Hong C-S, Rattner BA, et al. (2003) Methodological refinements in the determination of 146 polychlorinated biphenyls, including non-ortho- and mono-ortho-substituted PCBs, and 26 organochlorine pesticides as demonstrated in heron eggs. *Analytical chemistry* 75: 1058-1066.

Coleman S and Roy S. (2014) Effect of ultrasound on mass transfer during electrodeposition for electrodes separated by a narrow gap. *Chemical engineering science* 113: 35-44.

Contamine RF, Wilhelm A, Berlan J, et al. (1995) Power measurement in sonochemistry. *Ultrasonics Sonochemistry* 2: S43-S47.

Core J. (2005) New method simplifies biodiesel production. *Agricultural research*.

- Csoka L, Katekhaye SN and Gogate PR. (2011) Comparison of cavitation activity in different configurations of sonochemical reactors using model reaction supported with theoretical simulations. *Chemical Engineering Journal* 178: 384-390.
- Dahlem O, Reisse J and Halluin V. (1999) The radially vibrating horn: A scaling-up possibility for sonochemical reactions. *Chemical engineering science* 54: 2829-2838.
- Dahnke S and Keil F. (1999) Modeling of linear pressure fields in sonochemical reactors considering an inhomogeneous density distribution of cavitation bubbles. *Chemical engineering science* 54: 2865-2872.
- de Oliveira JS, Leite PM, de Souza LB, et al. (2009) Characteristics and composition of *Jatropha gossypifolia* and *Jatropha curcas* L. oils and application for biodiesel production. *Biomass and Bioenergy* 33: 449-453.
- Deshpande SS, Joshi JB, Kumar VR, et al. (2008) Identification and characterization of flow structures in chemical process equipment using multiresolution techniques. *Chemical engineering science* 63: 5330-5346.
- Ding J, Wang X, Zhou X-F, et al. (2010) CFD optimization of continuous stirred-tank (CSTR) reactor for biohydrogen production. *Bioresource technology* 101: 7005-7013.
- Dufreche S, Hernandez R, French T, et al. (2007) Extraction of lipids from municipal wastewater plant microorganisms for production of biodiesel. *Journal of the American Oil Chemists' Society* 84: 181-187.
- Faïd F, Contamine F, Wilhelm A, et al. (1998) Comparison of ultrasound effects in different reactors at 20kHz. *Ultrasonics Sonochemistry* 5: 119-124.
- Fargione J, Hill J, Tilman D, et al. (2008) Land clearing and the biofuel carbon debt. *Science* 319: 1235-1238.
- Feng R, Zhao Y, Zhu C, et al. (2002) Enhancement of ultrasonic cavitation yield by multi-frequency sonication. *Ultrasonics Sonochemistry* 9: 231-236.
- Foidl N, Foidl G, Sanchez M, et al. (1996) *Jatropha curcas* L. as a source for the production of biofuel in Nicaragua. *Bioresource technology* 58: 77-82.
- Francis G, Edinger R and Becker K. (2005) A concept for simultaneous wasteland reclamation, fuel production, and socio-economic development in degraded areas in India: Need, potential and perspectives of *Jatropha* plantations. *Natural Resources Forum*. Wiley Online Library, 12-24.
- Freedman B, Pryde E and Mounts T. (1984) Variables affecting the yields of fatty esters from transesterified vegetable oils. *Journal of the American Oil Chemists Society* 61: 1638-1643.

- Frenkel V, Gurka R, Liberzon A, et al. (2001) Preliminary investigations of ultrasound induced acoustic streaming using particle image velocimetry. *Ultrasonics* 39: 153-156.
- Gallego-Juárez JA, Elvira-Segura L and Rodríguez-Corral G. (2003) A power ultrasonic technology for deliquoring. *Ultrasonics* 41: 255-259.
- Georgogianni K, Kontominas M, Pomonis P, et al. (2008a) Alkaline conventional and in situ transesterification of cottonseed oil for the production of biodiesel. *Energy & fuels* 22: 2110-2115.
- Georgogianni K, Kontominas M, Pomonis P, et al. (2008b) Conventional and in situ transesterification of sunflower seed oil for the production of biodiesel. *Fuel Processing Technology* 89: 503-509.
- Ghotli RA, Aziz AA, Ibrahim S, et al. (2013) Study of various curved-blade impeller geometries on power consumption in stirred vessel using response surface methodology. *Journal of the Taiwan Institute of Chemical Engineers* 44: 192-201.
- Gogate PR. (2002) Cavitation: an auxiliary technique in wastewater treatment schemes. *Advances in Environmental Research* 6: 335-358.
- Gogate PR. (2008) Cavitational reactors for process intensification of chemical processing applications: a critical review. *Chemical Engineering and Processing: Process Intensification* 47: 515-527.
- Gogate PR and Katekhaye SN. (2012) A comparison of the degree of intensification due to the use of additives in ultrasonic horn and ultrasonic bath. *Chemical Engineering and Processing: Process Intensification* 61: 23-29.
- Gogate PR, Mujumdar S and Pandit AB. (2003a) Large-scale sonochemical reactors for process intensification: design and experimental validation. *Journal of Chemical Technology and Biotechnology* 78: 685-693.
- Gogate PR, Mujumdar S and Pandit AB. (2003b) Sonochemical reactors for waste water treatment: comparison using formic acid degradation as a model reaction. *Advances in Environmental Research* 7: 283-299.
- Gogate PR and Pandit AB. (1999) Survey of measurement techniques for gas-liquid mass transfer coefficient in bioreactors. *Biochemical Engineering Journal* 4: 7-15.
- Gogate PR and Pandit AB. (2004) Sonochemical reactors: scale up aspects. *Ultrasonics Sonochemistry* 11: 105-117.
- Gogate PR, Sivakumar M and Pandit AB. (2004) Destruction of Rhodamine B using novel sonochemical reactor with capacity of 7.5 l. *Separation and purification technology* 34: 13-24.

- Gogate PR, Sutkar VS and Pandit AB. (2011) Sonochemical reactors: Important design and scale up considerations with a special emphasis on heterogeneous systems. *Chemical Engineering Journal* 166: 1066-1082.
- Gole VL and Gogate PR. (2012a) Intensification of synthesis of biodiesel from nonedible oils using sonochemical reactors. *Industrial & Engineering Chemistry Research* 51: 11866-11874.
- Gole VL and Gogate PR. (2012b) A review on intensification of synthesis of biodiesel from sustainable feed stock using sonochemical reactors. *Chemical Engineering and Processing: Process Intensification* 53: 1-9.
- Gómez-Díaz D, Gomes N, Teixeira JA, et al. (2009) Oxygen mass transfer to emulsions in a bubble column contactor. *Chemical Engineering Journal* 152: 354-360.
- Gondrexon N, Renaudin V, Boldo P, et al. (1997) Degassing effect and gas-liquid transfer in a high frequency sonochemical reactor. *Chemical Engineering Journal* 66: 21-26.
- Gondrexon N, Renaudin V, Petrier C, et al. (1998) Experimental study of the hydrodynamic behaviour of a high frequency ultrasonic reactor. *Ultrasonics Sonochemistry* 5: 1-6.
- González-García J, Sáez V, Tudela I, et al. (2010) Sonochemical treatment of water polluted by chlorinated organocompounds. A review. *Water* 2: 28-74.
- Gonze E, Gonthier Y, Boldo P, et al. (1998) Standing waves in a high frequency sonoreactor: Visualization and effects. *Chemical engineering science* 53: 523-532.
- Goyat MS, Ray S and Ghosh PK. (2011) Innovative application of ultrasonic mixing to produce homogeneously mixed nanoparticulate-epoxy composite of improved physical properties. *Composites Part A: Applied Science and Manufacturing* 42: 1421-1431.
- Guo Z, Jones A, Li N, et al. (2007) High-speed observation of the effects of ultrasound on liquid mixing and agglomerated crystal breakage processes. *Powder technology* 171: 146-153.
- Haas MJ, McAloon AJ, Yee WC, et al. (2006) A process model to estimate biodiesel production costs. *Bioresource technology* 97: 671-678.
- Haas MJ and Scott KM. (2007) Moisture removal substantially improves the efficiency of in situ biodiesel production from soybeans. *Journal of the American Oil Chemists' Society* 84: 197-204.
- Haas MJ, Scott KM, Foglia TA, et al. (2007) The general applicability of in situ transesterification for the production of fatty acid esters from a variety of feedstocks. *Journal of the American Oil Chemists' Society* 84: 963-970.

- Haas MJ, Scott KM, Marmer WN, et al. (2004) In situ alkaline transesterification: an effective method for the production of fatty acid esters from vegetable oils. *Journal of the American Oil Chemists' Society* 81: 83-89.
- Harrington KJ and D'Arcy-Evans C. (1985) Transesterification in situ of sunflower seed oil. *Industrial & Engineering Chemistry Product Research and Development* 24: 314-318.
- Hatanaka S-i, Mitome H, Yasui K, et al. (2006) Multibubble sonoluminescence enhancement by fluid flow. *Ultrasonics* 44, Supplement: e435-e438.
- Henglein A and Gutierrez M. (1990) Chemical effects of continuous and pulsed ultrasound: a comparative study of polymer degradation and iodide oxidation. *Journal of Physical Chemistry* 94: 5169-5172.
- Hickman A. (1988) Gas-liquid oxygen transfer and scale-up. A novel experimental technique with results for mass transfer in aerated agitated vessels. *Proc. 6th European Conf. on Mixing, Pavia, Italy, 1988*.
- Hodnett M, Choi MJ and Zeqiri B. (2007) Towards a reference ultrasonic cavitation vessel. Part 1: Preliminary investigation of the acoustic field distribution in a 25 kHz cylindrical cell. *Ultrasonics Sonochemistry* 14: 29-40.
- Horst C, Chen Y-S, Kunz U, et al. (1996) Design, modeling and performance of a novel sonochemical reactor for heterogeneous reactions. *Chemical engineering science* 51: 1837-1846.
- Houshmand A, Daud WMAW and Shafeeyan MS. (2011) Tailoring the Surface Chemistry of Activated Carbon by Nitric Acid: Study Using Response Surface Method. *Bulletin of the Chemical Society of Japan* 84: 1251-1260.
- Hsiao M-C, Lin C-C, Chang Y-H, et al. (2010) Ultrasonic mixing and closed microwave irradiation-assisted transesterification of soybean oil. *Fuel* 89: 3618-3622.
- Huang J-H, Ilgen G and Matzner E. (2003) Simultaneous extraction of organotin, organolead and organomercury species from soils and litter. *Analytica chimica acta* 493: 23-34.
- Hung H-M and Hoffmann MR. (1999) Kinetics and mechanism of the sonolytic degradation of chlorinated hydrocarbons: frequency effects. *The Journal of Physical Chemistry A* 103: 2734-2739.
- Jamshidi R, Pohl B, Peuker UA, et al. (2012) Numerical investigation of sonochemical reactors considering the effect of inhomogeneous bubble clouds on ultrasonic wave propagation. *Chemical Engineering Journal* 189: 364-375.
- Ji J, Wang J, Li Y, et al. (2006) Preparation of biodiesel with the help of ultrasonic and hydrodynamic cavitation. *Ultrasonics* 44: e411-e414.

- Jiao Q, Tan X and Zhu J. (2014) Numerical simulation of ultrasonic enhancement on mass transfer in liquid–solid reaction by a new computational model. *Ultrasonics Sonochemistry* 21: 535-541.
- Kang J-W, Hung H-M, Lin A, et al. (1999) Sonolytic destruction of methyl tert-butyl ether by ultrasonic irradiation: The role of O₃, H₂O₂, frequency, and power density. *Environmental science & technology* 33: 3199-3205.
- Kapic A and Heindel T. (2006) Correlating gas-liquid mass transfer in a stirred-tank reactor. *Chemical Engineering Research and Design* 84: 239-245.
- Kasim FH and Harvey AP. (2011) Influence of various parameters on reactive extraction of *Jatropha curcas* L. for biodiesel production. *Chemical Engineering Journal* 171: 1373-1378.
- Kildiran G, Yücel SÖ and Türkay S. (1996) In-situ alcoholysis of soybean oil. *Journal of the American Oil Chemists' Society* 73: 225-228.
- Knothe G. (2006) Analyzing biodiesel: standards and other methods. *Journal of the American Oil Chemists' Society* 83: 823-833.
- Koda S, Kimura T, Kondo T, et al. (2003) A standard method to calibrate sonochemical efficiency of an individual reaction system. *Ultrasonics Sonochemistry* 10: 149-156.
- Kojima Y, Asakura Y, Sugiyama G, et al. (2010) The effects of acoustic flow and mechanical flow on the sonochemical efficiency in a rectangular sonochemical reactor. *Ultrasonics Sonochemistry* 17: 978-984.
- Kumar A, Gogate PR and Pandit AB. (2007) Mapping the efficacy of new designs for large scale sonochemical reactors. *Ultrasonics Sonochemistry* 14: 538-544.
- Kumar A, Gogate PR, Pandit AB, et al. (2004) Gas–Liquid Mass Transfer Studies in Sonochemical Reactors. *Industrial & Engineering Chemistry Research* 43: 1812-1819.
- Kumar A, Gogate PR, Pandit AB, et al. (2005) Investigation of induction of air due to ultrasound source in the sonochemical reactors. *Ultrasonics Sonochemistry* 12: 453-460.
- Kumar A, Kumaresan T, Pandit AB, et al. (2006) Characterization of flow phenomena induced by ultrasonic horn. *Chemical engineering science* 61: 7410-7420.
- Kumar G, Kumar D, Johari R, et al. (2011) Enzymatic transesterification of *Jatropha curcas* oil assisted by ultrasonication. *Ultrasonics Sonochemistry* 18: 923-927.
- Kumar MS, Ramesh A and Nagalingam B. (2003) An experimental comparison of methods to use methanol and *Jatropha* oil in a compression ignition engine. *Biomass and Bioenergy* 25: 309-318.
- Laborde J-L, Hita A, Caltagirone J-P, et al. (2000) Fluid dynamics phenomena induced by power ultrasounds. *Ultrasonics* 38: 297-300.

- Laborde JL, Bouyer C, Caltagirone JP, et al. (1998) Acoustic bubble cavitation at low frequencies. *Ultrasonics* 36: 589-594.
- Laugier F, Andriantsiferana C, Wilhelm AM, et al. (2008) Ultrasound in gas-liquid systems: Effects on solubility and mass transfer. *Ultrasonics Sonochemistry* 15: 965-972.
- Lauder BE and Spalding D. (1974) The numerical computation of turbulent flows. *Computer methods in applied mechanics and engineering* 3: 269-289.
- Lee KT, Bhatia S and Mohamed AR. (2006) Optimization of process parameters for the preparation of CaO/CaSO₄/coal fly ash sorbent for sulfur dioxide (SO₂) removal: Part II. *Energy Sources, Part A: Recovery, Utilization, and Environmental Effects* 28: 1251-1258.
- Leighton T. (1994) *The acoustic bubble*: Academic press.
- Leng DE and Calabrese RV. (2004) Immiscible liquid-liquid systems. *Handbook of Industrial Mixing: Science and Practice*: 639-753.
- Li C, Yoshimoto M, Ogata H, et al. (2005) Effects of ultrasonic intensity and reactor scale on kinetics of enzymatic saccharification of various waste papers in continuously irradiated stirred tanks. *Ultrasonics Sonochemistry* 12: 373-384.
- Lifka J, Ondruschka B and Hofmann J. (2003) The use of ultrasound for the degradation of pollutants in water: aquasonolysis—a review. *Engineering in life sciences* 3: 253-262.
- Lighthill SJ. (1978) Acoustic streaming. *Journal of Sound and Vibration* 61: 391-418.
- Lin Y and Farouk B. (2008) Heat transfer in a rectangular chamber with differentially heated horizontal walls: Effects of a vibrating sidewall. *International Journal of Heat and Mass Transfer* 51: 3179-3189.
- Linek V, Moucha T and Sinkule J. (1996) Gas-liquid mass transfer in vessels stirred with multiple impellers—I. Gas-liquid mass transfer characteristics in individual stages. *Chemical engineering science* 51: 3203-3212.
- Linek V, Vacek V and Beneš P. (1987) A critical review and experimental verification of the correct use of the dynamic method for the determination of oxygen transfer in aerated agitated vessels to water, electrolyte solutions and viscous liquids. *The Chemical Engineering Journal* 34: 11-34.
- Liu B and Zhao ZK. (2007) Biodiesel production by direct methanolysis of oleaginous microbial biomass. *Journal of Chemical Technology and Biotechnology* 82: 775-780.
- Liu D, Vorobiev E, Savoie R, et al. (2013a) Comparative study of ultrasound-assisted and conventional stirred dead-end microfiltration of grape pomace extracts. *Ultrasonics Sonochemistry* 20: 708-714.

- Liu R, Liu Y and Liu C-Z. (2013b) Development of an efficient CFD-simulation method to optimize the structure parameters of an airlift sonobioreactor. *Chemical Engineering Research and Design* 91: 211-220.
- Löning J-M, Horst C and Hoffmann U. (2002) Investigations on the energy conversion in sonochemical processes. *Ultrasonics Sonochemistry* 9: 169-179.
- Loranger E, Paquin M, Daneault C, et al. (2011) Comparative study of sonochemical effects in an ultrasonic bath and in a large-scale flow-through sonoreactor. *Chemical Engineering Journal* 178: 359-365.
- Luche J-L. (1998) *Synthetic organic sonochemistry*: Springer.
- Mandroyan A, Doche M, Hihn J, et al. (2009) Modification of the ultrasound induced activity by the presence of an electrode in a sono-reactor working at two low frequencies (20 and 40kHz). Part II: Mapping flow velocities by particle image velocimetry (PIV). *Ultrasonics Sonochemistry* 16: 97-104.
- Mark G, Tauber A, Laupert R, et al. (1998) OH-radical formation by ultrasound in aqueous solution–Part II: Terephthalate and Fricke dosimetry and the influence of various conditions on the sonolytic yield. *Ultrasonics Sonochemistry* 5: 41-52.
- Mason TJ and Phillip J. (2002) *Applied sonochemistry*: Wiley-VCH Weinheim.
- Memoli G, Gélat PN, Hodnett M, et al. (2012) Characterisation and improvement of a reference cylindrical sonoreactor. *Ultrasonics Sonochemistry* 19: 939-952.
- Miege C, Dugay J and Hennion M. (2003) Optimization, validation and comparison of various extraction techniques for the trace determination of polycyclic aromatic hydrocarbons in sewage sludges by liquid chromatography coupled to diode-array and fluorescence detection. *Journal of Chromatography A* 995: 87-97.
- Mondala A, Liang K, Toghiani H, et al. (2009) Biodiesel production by in situ transesterification of municipal primary and secondary sludges. *Bioresource technology* 100: 1203-1210.
- Monnier H, Wilhelm A-M and Delmas H. (1999a) Influence of ultrasound on mixing on the molecular scale for water and viscous liquids. *Ultrasonics Sonochemistry* 6: 67-74.
- Monnier H, Wilhelm A and Delmas H. (1999b) The influence of ultrasound on micromixing in a semi-batch reactor. *Chemical engineering science* 54: 2953-2961.
- Monnier H, Wilhelm A and Delmas H. (2000) Effects of ultrasound on micromixing in flow cell. *Chemical engineering science* 55: 4009-4020.
- Muniyappa PR, Brammer SC and Nouredдини H. (1996) Improved conversion of plant oils and animal fats into biodiesel and co-product. *Bioresource technology* 56: 19-24.

- Myers RH, Khuri AI and Carter WH. (1989) Response surface methodology: 1966–1988. *Technometrics* 31: 137-157.
- Nagata S. (1975) *Mixing: principles and applications*: Kodansha Tokyo, Japan.
- Nanzai B, Okitsu K, Takenaka N, et al. (2009) Effect of reaction vessel diameter on sonochemical efficiency and cavitation dynamics. *Ultrasonics Sonochemistry* 16: 163-168.
- Nocentini M, Fajner D, Pasquali G, et al. (1993) Gas-liquid mass transfer and holdup in vessels stirred with multiple Rushton turbines: water and water-glycerol solutions. *Industrial & Engineering Chemistry Research* 32: 19-26.
- Noureddini H and Zhu D. (1997) Kinetics of transesterification of soybean oil. *Journal of the American Oil Chemists' Society* 74: 1457-1463.
- Ohl C-D, Arora M, Ikink R, et al. (2006) Sonoporation from jetting cavitation bubbles. *Biophysical journal* 91: 4285-4295.
- Okitsu K, Sadanaga Y, Takenaka N, et al. (2010) A two-step continuous ultrasound assisted production of biodiesel fuel from waste cooking oils: a practical and economical approach to produce high quality biodiesel fuel. *Bioresource technology* 101: 5394-5401.
- Osterman A, Dular M and Sirok B. (2009) Numerical simulation of a near-wall bubble collapse in an ultrasonic field. *Journal of Fluid Science and Technology* 4: 210-221.
- Parvizian F, Rahimi M and Azimi N. (2012a) Macro- and micromixing studies on a high frequency continuous tubular sonoreactor. *Chemical Engineering and Processing: Process Intensification* 57–58: 8-15.
- Parvizian F, Rahimi M and Faryadi M. (2011) Macro-and micromixing in a novel sonochemical reactor using high frequency ultrasound. *Chemical Engineering and Processing: Process Intensification* 50: 732-740.
- Parvizian F, Rahimi M, Faryadi M, et al. (2012b) COMPARISON BETWEEN MIXING IN NOVEL HIGH FREQUENCY SONOREACTOR AND STIRRED TANK REACTOR. *Engineering Applications of Computational Fluid Mechanics* 6: 295-306.
- Patel H, Ein-Mozaffari F and Dhib R. (2010) CFD analysis of mixing in thermal polymerization of styrene. *Computers & chemical engineering* 34: 421-429.
- Pejin DJ, Mojović LV, Pejin JD, et al. (2012) Increase in bioethanol production yield from triticale by simultaneous saccharification and fermentation with application of ultrasound. *Journal of Chemical Technology and Biotechnology* 87: 170-176.
- Pétrier C, Combet E and Mason T. (2007) Oxygen-induced concurrent ultrasonic degradation of volatile and non-volatile aromatic compounds. *Ultrasonics Sonochemistry* 14: 117-121.

- Prabhu AV, Gogate PR and Pandit AB. (2004) Optimization of multiple-frequency sonochemical reactors. *Chemical engineering science* 59: 4991-4998.
- Priego-Capote F and Luque de Castro M. (2004) Analytical uses of ultrasound I. Sample preparation. *TrAC Trends in Analytical Chemistry* 23: 644-653.
- Priego-López E and de Castro ML. (2003) Ultrasound-assisted derivatization of phenolic compounds in spiked water samples before pervaporation, gas chromatographic separation, and flame ionization detection. *Chromatographia* 57: 513-518.
- Pugin B. (1987) Qualitative characterization of ultrasound reactors for heterogeneous sonochemistry. *Ultrasonics* 25: 49-55.
- Puthli MS, Rathod VK and Pandit AB. (2005) Gas-liquid mass transfer studies with triple impeller system on a laboratory scale bioreactor. *Biochemical Engineering Journal* 23: 25-30.
- Qian J, Wang F, Liu S, et al. (2008) In situ alkaline transesterification of cottonseed oil for production of biodiesel and nontoxic cottonseed meal. *Bioresource technology* 99: 9009-9012.
- Ramachandran K, Suganya T, Nagendra Gandhi N, et al. (2013) Recent developments for biodiesel production by ultrasonic assist transesterification using different heterogeneous catalyst: A review. *Renewable and Sustainable Energy Reviews* 22: 410-418.
- Ramos MJ, Fernández CM, Casas A, et al. (2009) Influence of fatty acid composition of raw materials on biodiesel properties. *Bioresource technology* 100: 261-268.
- Ranade V and Joshi J. (1990) Flow generated by a disc turbine. II: Mathematical modelling and comparison with experimental data. *Chemical Engineering Research and Design* 68: 34-50.
- Ranade VV, Tayalia Y and Krishnan H. (2002) CFD predictions of flow near impeller blades in baffled stirred vessels: Assessment of computational snapshot approach. *Chemical Engineering Communications* 189: 895-922.
- Rayleigh L. (1945) The Theory of Sound, 1894. *Republished by Dover Publications, New York.*
- Ren Y, Harvey A and Zakaria R. (2010) Biorefining based on biodiesel production: chemical and physical characterisation of reactively extracted rapeseed. *Journal of Biobased Materials and Bioenergy* 4: 79-86.
- Ren Y, Zakaria R and Harvey A. (2009) Towards a Biodiesel-Based Bio Refinery Chemical and Physical Characterization of Reactively Extracted Canola. *International Bio refineries conference (IBC). New York, NY.*
- Romdhane M and Gourdon C. (2002) Investigation in solid-liquid extraction: influence of ultrasound. *Chemical Engineering Journal* 87: 11-19.

- Rooze J, Rebrov EV, Schouten JC, et al. (2012) Dissolved gas and ultrasonic cavitation—a review. *Ultrasonics Sonochemistry*.
- Rostagno MA, Palma M and Barroso CG. (2003) Ultrasound-assisted extraction of soy isoflavones. *Journal of Chromatography A* 1012: 119-128.
- Sahu J, Acharya J and Meikap B. (2009) Response surface modeling and optimization of chromium (VI) removal from aqueous solution using Tamarind wood activated carbon in batch process. *Journal of Hazardous materials* 172: 818-825.
- Sainz Herrán N, Casas López J and Sánchez Pérez J. (2012) Gas–liquid Mass Transfer in Sonicated Bubble Columns. Effect of Reactor Diameter and Liquid Height. *Industrial & Engineering Chemistry Research* 51: 2769-2774.
- Sajjadi B, Asgharzadehahmadi S, Asaithambi P, et al. (2017) Investigation of mass transfer intensification under power ultrasound irradiation using 3D computational simulation: A comparative analysis. *Ultrasonics Sonochemistry* 34: 504-518.
- Sajjadi B, Aziz AA and Ibrahim S. (2015a) Mechanistic analysis of cavitation assisted transesterification on biodiesel characteristics. *Ultrasonics Sonochemistry* 22: 463-473.
- Sajjadi B, Raman AAA and Ibrahim S. (2015b) A comparative fluid flow characterisation in a low frequency/high power sonoreactor and mechanical stirred vessel. *Ultrasonics Sonochemistry* 27: 359-373.
- Sajjadi B, Raman AAA, Shah RSSRE, et al. (2013) Review on applicable breakup/coalescence models in turbulent liquid-liquid flows. *Reviews in Chemical Engineering* 29: 131-158.
- Sakharov DV, Hekkenberg RT and Rijken DC. (2000) Acceleration of fibrinolysis by high-frequency ultrasound: the contribution of acoustic streaming and temperature rise. *Thrombosis research* 100: 333-340.
- Sakkas VA, Islam MA, Stalikas C, et al. (2010) Photocatalytic degradation using design of experiments: a review and example of the Congo red degradation. *Journal of Hazardous materials* 175: 33-44.
- Santos HM, Lodeiro C and Capelo-Martínez JL. (2009) *The power of ultrasound*: WILEYVCH verlag GmbH & Co. KGaA, Weinheim.
- Searchinger T, Heimlich R, Houghton RA, et al. (2008) Use of US croplands for biofuels increases greenhouse gases through emissions from land-use change. *Science* 319: 1238-1240.
- Servant G, Caltagirone JP, Gérard A, et al. (2000) Numerical simulation of cavitation bubble dynamics induced by ultrasound waves in a high frequency reactor. *Ultrasonics Sonochemistry* 7: 217-227.

- Servant G, Laborde J, Hita A, et al. (2003) On the interaction between ultrasound waves and bubble clouds in mono-and dual-frequency sonoreactors. *Ultrasonics Sonochemistry* 10: 347-355.
- Shafeeyan MS, Wan Daud WMA, Houshmand A, et al. (2012) The application of response surface methodology to optimize the amination of activated carbon for the preparation of carbon dioxide adsorbents. *Fuel* 94: 465-472.
- Shuit SH, Lee KT, Kamaruddin AH, et al. (2010) Reactive extraction and in situ esterification of *Jatropha curcas* L. seeds for the production of biodiesel. *Fuel* 89: 527-530.
- Siler-Marinkovic S and Tomasevic A. (1998) Transesterification of sunflower oil in situ. *Fuel* 77: 1389-1391.
- Simon A, Penpenic L, Gondrexon N, et al. (2000) A comparative study between classical stirred and ultrasonically-assisted dead-end ultrafiltration. *Ultrasonics Sonochemistry* 7: 183-186.
- Singh AK, Fernando SD and Hernandez R. (2007) Base-catalyzed fast transesterification of soybean oil using ultrasonication. *Energy & fuels* 21: 1161-1164.
- Sivakumar M and Pandit AB. (2001) Ultrasound enhanced degradation of Rhodamine B: optimization with power density. *Ultrasonics Sonochemistry* 8: 233-240.
- Snyder J, Friedrich J and Christianson D. (1984) Effect of moisture and particle size on the extractability of oils from seeds with supercritical CO₂. *Journal of the American Oil Chemists' Society* 61: 1851-1856.
- Son Y, Lim M, Khim J, et al. (2012) Comparison of calorimetric energy and cavitation energy for the removal of bisphenol-A: The effects of frequency and liquid height. *Chemical Engineering Journal* 183: 39-45.
- Soong Y, Harke F, Gamwo I, et al. (1997) Hydrodynamic study in a slurry-bubble-column reactor. *Catalysis today* 35: 427-434.
- Srivastava P, Behera SK, Gupta J, et al. (2011) Growth performance, variability in yield traits and oil content of selected accessions of *Jatropha curcas* L. growing in a large scale plantation site. *Biomass and Bioenergy* 35: 3936-3942.
- St Slaczka A. (1986) Effect of ultrasound on ammonium leaching of zinc from galmei ore. *Ultrasonics* 24: 53-55.
- Stavarache C, Vinatoru M, Nishimura R, et al. (2005) Fatty acids methyl esters from vegetable oil by means of ultrasonic energy. *Ultrasonics Sonochemistry* 12: 367-372.
- Stolojanu V and Prakash A. (1997) Hydrodynamic measurements in a slurry bubble column using ultrasonic techniques. *Chemical engineering science* 52: 4225-4230.

- Suslick KS. (1989) The chemical effects of ultrasound. *Scientific American* 260: 80-86.
- Suslick KS and Price GJ. (1999) Applications of ultrasound to materials chemistry. *Annual Review of Materials Science* 29: 295-326.
- Sutkar VS and Gogate PR. (2009) Design aspects of sonochemical reactors: techniques for understanding cavitation activity distribution and effect of operating parameters. *Chemical Engineering Journal* 155: 26-36.
- Tatake PA and Pandit AB. (2002) Modelling and experimental investigation into cavity dynamics and cavitation yield: influence of dual frequency ultrasound sources. *Chemical engineering science* 57: 4987-4995.
- Thanh LT, Okitsu K, Sadanaga Y, et al. (2010) Ultrasound-assisted production of biodiesel fuel from vegetable oils in a small scale circulation process. *Bioresource technology* 101: 639-645.
- Thompson L and Doraiswamy L. (1999) Sonochemistry: science and engineering. *Industrial & Engineering Chemistry Research* 38: 1215-1249.
- Van Gerpen J. (2005) Biodiesel processing and production. *Fuel Processing Technology* 86: 1097-1107.
- Van Hoed V. (2010) Phenolic compounds in seed oils. *Lipid Technology* 22: 247-249.
- Vasudevan PT and Briggs M. (2008) Biodiesel production—current state of the art and challenges. *Journal of industrial microbiology & biotechnology* 35: 421-430.
- Vicente G, Martinez M and Aracil J. (2007) Optimisation of integrated biodiesel production. Part I. A study of the biodiesel purity and yield. *Bioresource technology* 98: 1724-1733.
- Vichare NP, Gogate PR, Dindore VY, et al. (2001) Mixing time analysis of a sonochemical reactor. *Ultrasonics Sonochemistry* 8: 23-33.
- VLAEV S, GEORGIEV D, NIKOV I, et al. (2007) The CFD Approach for Shear Analysis of Mixing Reactor: Verification and Examples of Use. *Journal of Engineering Science and Technology* 2: 177-187.
- Wan Q and Kuznetsov A. (2003) Numerical study of the efficiency of acoustic streaming for enhancing heat transfer between two parallel beams. *Flow, turbulence and combustion* 70: 89-114.
- Wang RY, Jarratt JA, Keay PJ, et al. (2000) Development of an automated on-line analysis system using flow injection, ultrasound filtration and CCD detection. *Talanta* 52: 129-139.
- Wang Y, Rao Q, Fan J, et al. (2006) PIV measurements and CFD simulation of viscous fluid flow in a stirred tank agitated by a Rushton turbine. *5th International Conference on CFD in the Process Industries*.

- Wang Z, Li Y, Wang J, et al. (2012) Sonocatalytic damage of bovine serum albumin (BSA) under ultrasonic irradiation with TiO₂/tooth composite. *Journal of Chemical Technology and Biotechnology* 87: 523-529.
- Wayment DG and Casadonte Jr DJ. (2002) Design and calibration of a single-transducer variable-frequency sonication system. *Ultrasonics Sonochemistry* 9: 189-195.
- Whillock G and Harvey B. (1997) Ultrasonically enhanced corrosion of 304L stainless steel II: The effect of frequency, acoustic power and horn to specimen distance. *Ultrasonics Sonochemistry* 4: 33-38.
- Worapun I, Pianthong K and Thaiyasuit P. (2012) Optimization of biodiesel production from crude palm oil using ultrasonic irradiation assistance and response surface methodology. *Journal of Chemical Technology and Biotechnology* 87: 189-197.
- Wu P, Yang Y, Colucci JA, et al. (2007) Effect of ultrasonication on droplet size in biodiesel mixtures. *Journal of the American Oil Chemists' Society* 84: 877-884.
- Xia K-Q, Sun C and Zhou S-Q. (2003) Particle image velocimetry measurement of the velocity field in turbulent thermal convection. *Physical review E* 68: 066303.
- Xu Z, Yasuda K and Koda S. (2013) Numerical simulation of liquid velocity distribution in a sonochemical reactor. *Ultrasonics Sonochemistry* 20: 452-459.
- Yasui K, Tuziuti T and Iida Y. (2005) Dependence of the characteristics of bubbles on types of sonochemical reactors. *Ultrasonics Sonochemistry* 12: 43-51.
- Yebra M, Moreno-Cid A, Cespón R, et al. (2004) Preparation of a soluble solid sample by a continuous ultrasound assisted dissolution system for the flow-injection atomic absorption spectrometric determination of iron in milk powder and infant formula. *Talanta* 62: 403-406.
- Yuan X, Liu J, Zeng G, et al. (2008) Optimization of conversion of waste rapeseed oil with high FFA to biodiesel using response surface methodology. *Renewable Energy* 33: 1678-1684.
- Yusaf TF and Buttsworth DR. (2007) Characterisation of mixing rate due to high power ultrasound. *Ultrasonics Sonochemistry* 14: 266-274.
- Zeng J, Wang X, Zhao B, et al. (2008) Rapid in situ transesterification of sunflower oil. *Industrial & Engineering Chemistry Research* 48: 850-856.
- Zhao Y, Zhu C, Feng R, et al. (2002) Fluorescence enhancement of the aqueous solution of terephthalate ion after bi-frequency sonication. *Ultrasonics Sonochemistry* 9: 241-243.

APPENDIX

LIST OF PUBLICATIONS AND PAPERS PRESENTED

Publications

Asgharzadehahmadi, S., Abdul Aziz, A. R., Parthasarathy, R., Sajjadi, B. (2016). Sonochemical Reactors; Review on Features, Advantages and Limitations. *Renewable and Sustainable Energy Reviews* 63:302-314. (ISI-Cited Publication, **Impact Factor: 6.798**).

Asgharzadehahmadi, S., Davoody, M., Ghotli, R. A., Abdul Aziz, A. R., Parthasarathy, R. (2016). Effect of ultrasonic irradiations on gas-liquid mass transfer coefficient (k_{La}); Experiments and modelling. *Measurement*. 79:119-129 (ISI-Cited Publication, **Impact Factor: 1.742**).

Sajjadi, B., **Asgharzadehahmadi, S.**, Asaithambi, P., Abdul Aziz, A. R., Parthasarathy, R. (2016). Investigation of Mass Transfer Intensification under Power Ultrasound Irradiation Using 3D Computational Simulation: A Comparative Analysis. *Ultrasound SonoChemistry* (ISI-Cited Publication, **Impact Factor: 4.556**).

Asgharzadehahmadi, S., Sajjadi, B., Abdul Aziz, A. R., Parthasarathy, R. (2016). Ultrasound assisted *in situ* transesterification of *Jatropha*: process evaluation and optimization. *Renewable Energy*. (Under Review; ISI-Cited Publication, **Impact Factor: 3.404**).

Asgharzadehahmadi, S., Sajjadi, B., Abdul Aziz, A. R., Parthasarathy, R. (2016). Mechanistical Analysis of Mass Transfer of Newtonian Fluids with Different Viscosity under Low-Frequency, High-Power Ultrasound Irradiation. *Chemical Engineering Communications*. (Under Review; ISI-Cited Publication, **Impact Factor: 1.104**).

Davoody, M., Abdul Aziz, A. R., **Asgharzadehahmadi, S.**, Ibrahim, S., Parthasarathy, R. (2016). Modeling of volumetric mass transfer coefficient for agitated vessels using artificial intelligence techniques. *Measurement*. (*Under Review; ISI-Cited Publication, Impact Factor: 1.742*)

Conference Proceeding

Asgharzadehahmadi, S., Abdul Aziz, A. R., Parthasarathy, R. (2014). Gas-liquid mass transfer study using ultrasonic irradiation assistance and response surface methodology. *International symposium on mixing in industrial processes VIII*, September 15-17, 2014. Melbourne. (*Conference Paper*)

University of Malaya